# COMPARISON OF NANOSECOND AND FEMTOSECOND LASER MASS SPECTROMETRY (FLMS)

Hamdi Sukur Kilic

Department of Physics&Astronomy


Presented as a thesis for the degree of Ph.D.
In the University of Glasgow



ProQuest LLC.
789 East Eisenhower Parkway
P.O. Box 1346
Ann Arbor, MI 48106 – 1346

To my wife and children

# Acknowledgment

I would like to thank the following people:

- my supervisor, Dr. K.W.D. Ledingham for his enthusiasm, advice and encouragement throughout the period of my studies.

- Dr. R.P. Singhal for many helpful discussions on various aspects of my work.

- my fellow research colleagues in LIS group; Dr. Costantine Kosmidis, Dr. A. Marshall, Dr. A. Clark and Shi-Liang Wang for helpful discussions and suggestions, Robert M. Deas for his considerable assistance with the experimental work, Thomas McCanny, Derek J. Smith, Rong-er Zheng, Weixian Peng, Weijie Jia, Colin Scott for helpful discussions and friendship.

- R. Maxwell for his technical support and advice.

- The Turkish Government and The University of Selcuk for financial support.

- Technical staff, A.J. Langley, W. Shaikh and P. Taday, at RAL for their technical supports during the experimental works at RAL.

- Staff at the Department of Physics and Astronomy, The University of Glasgow, who have provided great opportunities for research students.

- Miss C. McIntyre for her secretarial assistance.

Finally, but above all, I would like to thank my parents, Hasan and Behiye, for their constant support and encouragement, my *wee*-wife, Aysegul, for taking over all my family problems and three children without making any difficulty for me during the period of my study and my daughters, Sumeyye, Hatice Kubra and Hilal Melike for their patience during the period of my study in Glasgow.

# PRESENTATIONS

## *Paper Publications*

1) ***A Comparison of Femtosecond and Nanosecond Multiphoton Ionization and Dissociation for Some Nitro-Molecules***

Ledingham, K.W.D., **Kilic, H.S.,** Kosmidis, C., Deas, R.M., Marshall, A., McCanny, T., Singhal, R.P., Langley, A.J. and Shaikh, W. (1995)

Rapid Commun. in Mass Spectrom., **9**, 1522-1527.

2) ***Multiphoton Ionization and Dissociation of $NO_2$ by 50 fs Laser Pulses***

Singhal, R.P., **Kilic, H.S.,** Ledingham, K.W.D., Kosmidis, C, McCanny, T., Langley, A.J. and Shaikh, W. (1996)

Chem. Phys. Lett., **253**, 81-86.

3) ***The Potential of Femtosecond Laser Mass Spectrometry***

Ledingham, K.W.D., Singhal, R.P., **Kilic, H.S.,** McCanny, T., Smith, D.J., Wang, S., Kosmidis, C., Langley, A.J., Shaikh, W. (1996)

Rutherford Appleton Laboratory Annual Report, 1995-1996, pp:165-166.

*4)* ***The Photo-Dissociative Pathways of Nitromethane Using Femtosecond Laser Pulses at 375* nm**

**Kilic, H.S.,** Ledingham, K.W.D., Smith, D.J., Wang, S.L., Kosmidis, C., McCanny, T., Singhal, R.P., Langley, A.J. and Shaikh, W. (1996)

Eight International Resonance Ionization Spectroscopy, at RIS'96, State College, PA, June 30-July 5, 1996, AIP Conference Proceeding **388**, pp:395-398.

5) ***Multiphoton Processes in Organic Molecules Using VUV Laser Photons***

Ledingham, K.W.D., Singhal, R.P., **Kilic, H.S.,** Wang, S., McCanny, T., Smith, D.J., Turcu, I.C.E. and Allott, R. (1996)

Rutherford Appleton Laboratory Annual Report, 1995-1996, p:167.

6) ***Multiphoton Ionization and Dissociation of Nitromethane Using Femtosecond Laser Pulses at 375 and 750* nm**

**Kilic, H.S.,** Ledingham, K.W.D., Kosmidis, C., McCanny, T., Singhal, R.P., Wang, S.L., Smith, D.J., Langley, A.J. and Shaikh, W. (1997)

J. Phys. Chem. A, **101,** 817-823

7) ***On the Dissociation of Nitrobenzene and Nitrotoluenes Induced by Femtosecond Laser at 375 nm***

Kosmidis, C., Ledingham, K.W.D., **Kilic, HS.,** McCanny, T., Singhal, RP., Langley, AJ. And Shaikh, W. (1997)

J. Phys. Chem. A, **101**(12), 2264-2270.

8) **On the Ionization and Dissociation of $NO_2$ by Short Intense Laser Pulses**

Smith, D.J., **Kilic, H.S.,** Ledingham, K.W.D., McCanny, T., Peng, W.X., Singhal, R.P., Langley, A.J., Taday, P.F. and Kosmidis, C. (1997),

Submitted for publication to Chem. Phys. Lett.

9) ***Ionization and Dissociation of Benzaldehyde Using Short Intense Laser pulses***

Smith, D.J., Ledingham, K.W.D., **Kilic, H.S.,** McCanny, T., Peng, W.X., Singhal, R.P., Langley, A.J., Taday, P.F. and Kosmidis, C. (1997),

to be published.

10) ***Aspects of Intense Polarized Femtosecond Laser Ionization of $CS_2$ at 375 nm and 750 nm***

Wang, S., Ledingham, K.W.D., **Kilic, H.S.,** McCanny, T., Smith, D.J., Singhal, R.P., Kosmidis, C., Langley, A.J., Shaikh, W., Couris, S. and Georgia, S. (1997)

to be submitted to "J. Phys. B: Atom, Mol. Opt. Phys."

11) ***Environmental Applications of Femtosecond Laser Mass Spectrometry***

Ledingham, K.W.D., **Kilic, H.S.,** McCanny, T., Peng, W.X., Smith, D.J., A., Singhal, R.P., Kosmidis, C., Langley, A.J. and Taday, P. (1997)

to be published.

## *Poster Presentations*

*1) Spectroscopic Aspects of Resonant Laser Ablation (RLA) of Aluminum (Al)*

**Kilic, H.S.,** Peng, W.X., Deas, R.M., Ledingham, K.W.D. and Singhal, R.P.

Presented at The Royal Society of Chemistry Annual Chemical Congress, Herriot-Watt University, FP20, 10-13 April 1995, Edinburgh, Scotland, UK.

*2) Urban Air Quality-Meeting Challenge with Lasers*

Peng, W.X., **Kilic, H.S.,** Marshall, A., Ledingham, K.W.D. and Singhal, R.P.

Presented at The Royal Society of Chemistry Annual Chemical Congress, Herriot-Watt University, FP17, 10-13 April 1995, Edinburgh, Scotland, UK.

*3) Dissociation Pathways of Nitromethane*

**Kilic, H.S.,** Ledingham, K.W.D., Smith, D.J., Wang, S., McCanny, T., Singhal, R.P., Kosmidis, C., Langley, A.J. and Shaikh, W. (1996).

Presented at the Eight International Symposium on Resonance Ionization Spectroscopy and Its Applications (RIS'96), June 30-July 5, 1996, State College, Pennsylvanian, USA.

*4) The Potential for Femtosecond Laser Mass Spectrometry*

**Kilic, H.S.,** Ledingham, K.W.D., Smith, D.J., Wang, S., McCanny, T., Singhal, R.P., Kosmidis, C., Langley, A.J. and Shaikh, W. (1996).

Presented at the 22nd Annual Meeting of British Mass Spectrometry (BMSS), 8-11 September 1996, Meeting Proceeding, p:146.

*5) The Potential for Femtosecond Laser Mass Spectrometry (FLMS) for Gas Phase Samples*

Smith, D.J., Ledingham, K.W.D., Kosmidis, C., **Kilic, H.S.,** McCanny, T., Singhal, R.P., Wang, S., Langley, A.J. and Shaikh, W. (1996).

Highlights of British Physics Research and R&D Young Physicists and Scientists, Friday, 27 September 1996 at The Royal Society, London, UK..

*6) The Potential for Femtosecond Laser Mass Spectrometry (FLMS) for Gas Phase Samples*

McCanny, T., Ledingham, K.W.D., Smith, D.J., Kosmidis, C., **Kilic, H.S.,** Singhal, R.P., Langley, Peng, W.X., Wang, S.L., A.J. and Shaikh, W. (1996).

Congress 97; The Institute of Physics Annuel Congress; 24-27 March 1997, University of Leeds, UK.

*7) **Advances in Femtosecond Laser Mass Spectrometry (FLMS) Utilizing Time of Flight Techniques***

Smith, D.J., Ledingham, K.W.D., Kosmidis, C., **Kilic, H.S.,** McCanny, T., Singhal, R.P., Wang, S., Langley, A.J. and Shaikh, W. (1997).

4th International Mass Spectrometry Conference (IMSC'97), 25-29 August 1997, Tampere, Finland.

## ***Oral Presentations***

1) "***Dissociation pathways of Nitromethane***"

Kilic, H.S.

Graduate Workshop, Ultrafast Spectroscopy, The University of Manchester, The Department of Chemistry, 26-27 March, 1996.

2) "***The Potential for Femtosecond Laser Mass Spectrometry***"

Kilic, H.S.

At the Aspects of Spectroscopy VI, The University of Strathclyde, The Department of Physics and App. Phys., 22-23rd August, 1996.

# Summary

The work presented in this thesis was carried out with the primary objective of developing a sensitive ultrafast laser based technique for detecting and identifying nitroaromatic compounds. In addition the mechanisms involved in the production of the fragmentation patterns in the mass spectrum were studied. The data presented in this thesis demonstrates the potential of femtosecond laser mass spectrometry (FLMS).

The first chapter discusses the fundamental principles of the interaction between the laser and the atomic/molecular system, where single photon excitation and relaxation processes are described, considering on and off resonance conditions. The second chapter describes the multiphoton interaction, i.e., excitation, dissociation, ionisation and other radiative and radiationless processes. In Chapter 2, a description of the Glasgow rate equation model is also given. The third chapter gives the basic principles and a brief description of the experimental systems and techniques used.

The nanosecond resonance enhanced multiphoton ionisation (REMPI) is briefly described in Chapter 2 and its application to NO from the dissociation of the $NO_2$ molecule is presented in the early part of Chapter 4. In addition in Chapter 4, the femtosecond laser mass spectrometric investigation of the dissociative ionisation of the $NO_2$ molecule is presented. The results using the femtosecond laser is compared with the results obtained using nanosecond laser mass spectrometry. A comparison of the theoretical results of the Glasgow rate equation model and the experimental results for femtosecond and nanosecond laser mass spectrometry is also carried out in Chapter 4.

In Chapters 5 and 6, respectively, the nanosecond and femtosecond mass spectra of nitromethane and nitrobenzene are compared. Efficient production of the parent ion was obtained for both samples and the mass spectra are presented. Morover, the

different dissociative ionisation and fragmentation mechanisms for both samples are identified. In both chapters, the laser intensity dependencies of the parent ion as well as the fragmentation patterns of the mass spectra are presented.

In Chapter 7, the multiphoton dissociative ionisation processes in the three isomers of nitrotoluene, DNT and TNT are investigated and their nanosecond and femtosecond laser induced mass spectra are compared and the performance of femtosecond laser mass spectrometry is demonstrated. Although, a comparison of the mass spectra of three isomers of nitrotoluene and the mass spectra of the o-nitrotoluene, dinitrotoluene (DNT) and trinitrotoluene (TNT) is made, it is shown that the nanosecond laser mass spectra of the nitrotoluene isomers are similar and the distinction between them is very difficult.

On the other hand, a comparison of the femtosecond laser mass spectra of the three isomers of nitrotoluene is made and the fingerprints of these three isomers are determined using three mass spectra. The differences between the mass spectra of the o-nitrotoluene, DNT and TNT are also discussed in detail. The dissociative ionisation and fragmentation patterns as well as their laser intensity dependencies are used to discuss the dissociation pathways in these molecules. The different dissociation-ionisation mechanisms are presented and identified with particular reference to the femtosecond regime.

Finally, in Chapter 8 aspects of the data presented in this thesis are discussed briefly as well as future plans.

# Contents

## LIST OF FIGURES&TABLES

## FIGURES

## TABLES

## DIAGRAMS

# CHAPTER 1

# INTRODUCTION

## Contents

## 1.1 Introduction

In the first chapter of this thesis, an introductory theoretical background will be given to refresh the knowledge. As is well known the laser interaction with matter is the fundamental subject of the quantum physics and mechanics. It was felt that it would be preferable to start with the quantum mechanical background to understand better the phenomenological aspects of laser ionisation spectroscopy. Firstly the theory of the interaction of light with matter (atom or molecule) will be discussed considering a semiclassical two level medium, where the laser field is considered as a monochromatic plane wave and the atom is considered as a quantum mechanical system. The interaction of a weak and intense laser field with matter will be discussed and the transition probabilities between energy levels in a quantum mechanical system will be discussed.

## 1.2 Absorption and Emission Processes

It is well documented in many quantum mechanics text books that the birth of modern quantum mechanics was at the beginning of this century. The radiation consists of quanta which we know to have energy radiation of $nh\nu$ where $\nu$ is the frequency of the associated wave. The electron in an atom behaves like an oscillator and could be found in certain quantum states which could be observed when a light quantum interacts with an atom.

The best and simplest description of the phenomena dealing with the interaction of laser light with matter can be made considering a semiclassical two level system with the assumption that it is in thermal equilibrium. Such a kind of system is shown in fig.1.1 where $N_1$ is the number of particles in the excited state with energy $E_1$ and $N_0$ in the ground state with energy $E_0$. The total population given by the sum ($N=N_1+N_0$) of the populations in the excited and ground sates. The population distribution

between these two levels are usually expressed by the well known Boltzman equation for the thermal equilibrium conditions;

$$N_1/N_0 = e^{-h\nu_{10}/kT} \qquad 1.1$$

Fig. 1.1 shows a model system of the ground and excited states in an atom or molecule where a single photon can excite the system to the excited state. In the interaction of laser light with matter (atom or molecule) there are three processes that can change the state of the system from $E_0$ to $E_1$ or from $E_1$ to $E_0$, which are called *absorption*, *spontaneous* and *stimulated emissions*, as described in fig.1.1.

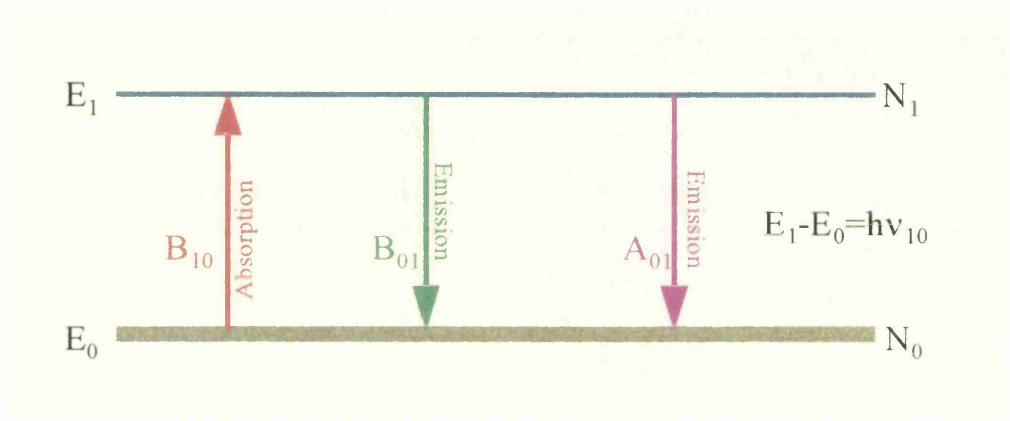


**Figure 1.1:** A model two level system shows possible physical transitions between lower ($N_0$) and upper ($N_1$) level.

The presence of radiation density $\rho_\nu(\nu_{10}) = \varepsilon_0 E^2/2$ of the precise frequency is needed to drive a transition from the ground state to the excited state (Fig. 1.2a) at the rate

$$dN_1/dt = B_{10}\,\rho_\nu(\nu_{10})\,N_0 \qquad 1.2$$

and this transition is known to be absorption of light by the medium (atom or molecule). The coefficient $B_{10}$ is thus a "rate constant" known as the Einstein absorption or Einstein B coefficient. Similarly if the system is already in an excited state, then a photon with an energy of $h\nu_{10}$ can induce the system to make a transition to the ground state. This process is called *stimulated emission*. The rate of *stimulated emission* is given by

$$dN_1/dt = -B_{01}\,\rho_\nu(\nu_{10})\,N_1 \qquad 1.3$$

where $B_{01}$ is the *stimulated emission* coefficient (Fig.1.2b). Finally, if the system in the excited state it can spontaneously emit a photon (Fig.1.2c) at a rate

$$dN_1/dt = -A_{01}\,N_1 \qquad 1.4$$

where $A_{01}$ is the spontaneous emission coefficient. Since the system is in thermal equilibrium, the rate of the population to the excited state induced by the *absorption* must balance the rate of population to the ground state induced by the *stimulated* and *spontaneous emissions*.

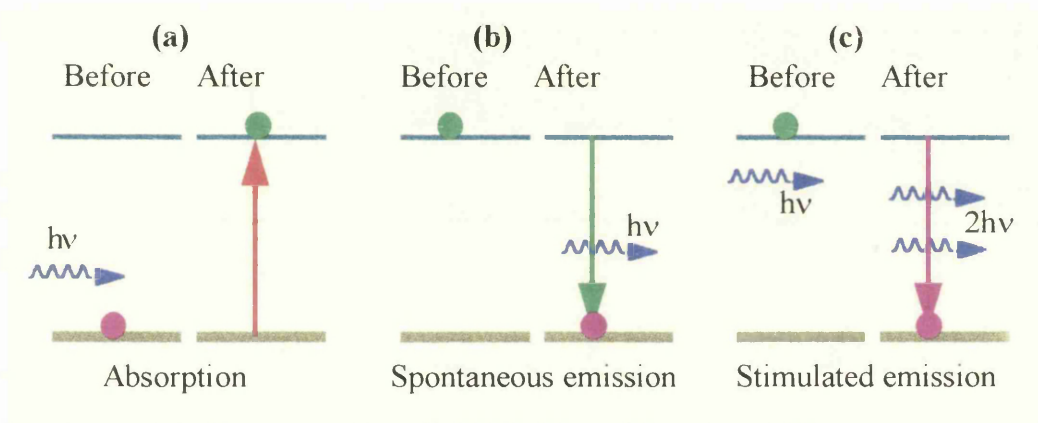


**Figure 1.2:** A schematic presentations of absorption, spontaneous and stimulated emissions.

Considering $A_{01}N_1+B_{01}N_1\,\rho_\nu=B_{10}N_0\,\rho_\nu$, and taking $B_{10} = B_{01}$, (i.e., $B_{10} = B_{01}= B$), the solution of the above equations in terms of black body radiation theory gives the relationship between absorption and emission to be

$$A = A_{01} = (8\pi h\nu^3 / c^3)\,B \qquad 1.5$$

The rate constants for absorption and stimulated emission are identical and the spontaneous emission rate (lifetime of excited state) can be determined from the absorption coefficient $A_{01}$.

## 1.3 Interaction Between Laser Light and Two-Level System

The interaction of laser light with matter can be described by a simple quantum mechanical model two level system as seen in fig.1.3. This kind of system could be described with a time dependent Hamiltonian

$$H(t)=H_0+V(t) \qquad (1.6)$$

In the eq. (1.6), $H_0$ is time independent (unperturbed) part of the Hamiltonian and V(t) is the time dependent part which is the interaction operator between the laser light and the system. The laser field can be assumed to be monochromatic plane wave with frequency ω and can be written in the form of

$$\mathbf{E(t)}=\mathbf{E}_0 e^{i(\mathbf{k}\cdot\mathbf{r}-\omega t)} \qquad 1.7$$

where $\mathbf{E}_0$ is a constant vector and **k** is the wave vector of the field. It is known that the molecular size is about 1 nm, and in the visible laser spectroscopy (in the case of laser wavelength used in this work λ=384-226 nm) λ>>molecular size (1 nm) and therefore the phase of laser light does not change over molecular size (Demproder, 1982). Hence, we can ignore the spatial derivatives of the field amplitude. In the case of the electric dipole interaction between the laser light and the system, assuming the molecule is placed at the origin of the co-ordinate system then $\mathbf{k}\cdot\mathbf{r} \approx 0$, the interaction operator is in the form of atomic dipole (μ) moment as

$$V(t)= -\mu\cdot\mathbf{E(t)} = e\,\mathbf{r}\cdot\mathbf{E}_0\cdot\cos(\omega t) \qquad 1.8$$

where $\mathbf{E}_0$ is the electric field strength created by the laser light. The energy levels of the system can be obtained by the solution of the time-dependent Schrodinger equation for the case of external perturbation

$$H\Psi_n = i\hbar\,(\partial/\partial t)\Psi_n \qquad 1.9$$

where n = 1, 2, 3, ..... . In the model system, the upper level is described by $\Psi_1$ at energy $E_1$ and lower level by $\Psi_0$ at energy $E_0$.

The transition probability from one level to the other is also obtained by solving the time-dependent Schrodinger equation (1.9). In the absence of V(t), two time-dependent solutions of equation are

$$\Psi_0(\mathbf{r},t) = \varphi_0(\mathbf{r})\, e^{-iE_0 t/\hbar} = \varphi_0(\mathbf{r})\, e^{-i\omega_0 t} \qquad 1.10$$

$$\Psi_1(\mathbf{r},t) = \varphi_1(\mathbf{r})\, e^{-iE_1 t/\hbar} = \varphi_1(\mathbf{r})\, e^{-i\omega_1 t} \qquad 1.11$$

The wave function for the perturbed system is given by the linear combination of the complete set of the functions $\psi_0(\mathbf{r},t)$ and $\psi_1(\mathbf{r},t)$.

$$\Psi(\mathbf{r},t) = c_0(t)\, \varphi_0\, e^{-i\omega_0 t} + c_1(t)\, \varphi_1\, e^{-i\omega_1 t} \qquad 1.12$$

where $\omega_i = E_i/\hbar$ and $\varphi_0$ and $\varphi_1$ are the wave functions of the stationary (time-independent) states of the system and $c_0(t)$ and $c_1(t)$ are time dependent coefficients which are the probability amplitudes of the system being in the initial and excited states, respectively.

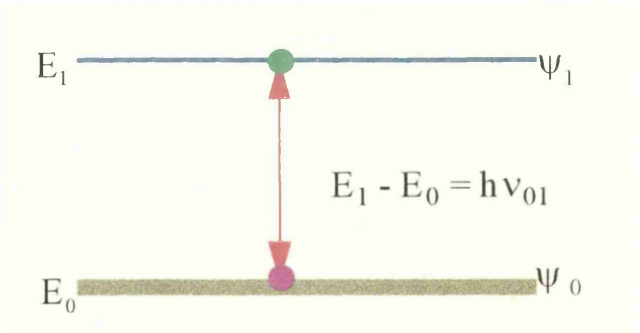


**Figure 1.3:** Two level semiclassical model and energies $E_0$ and $E_1$ and wave functions $\psi_0$ and $\psi_1$, respectively.

The solution of the Schrodinger equation for these time dependent coefficients leads to the equations

$$c`_0 = i\, c_1\, \omega_R\, (e^{-i(\omega_{10} - \omega)t} + e^{-i(\omega_{10} + \omega)t})/2 \qquad 1.13$$

$$c`_1 = i\, c_0\, \omega_R\, (e^{i(\omega_{10} - \omega)t} + e^{i(\omega_{10} + \omega)t})/2 \qquad 1.14$$

for the interaction of the radiation with quantum system. The detuning frequency of the interacting system is given by $\Delta=\omega-\omega_{10}$, and $\Omega=[(\omega_R)^2+\Delta^2]^{1/2}$ is the Rabi frequency and $\omega_R = \mu\cdot\varepsilon/\hbar$ is equal to the Rabi frequency in the particular case of the exact resonance frequency where detuning is zero ($\Delta=\omega-\omega_{10} = 0$) (Letokhov, 1987) and $\mu$ is the interaction dipole moment described above. Based on these two equations a number of particular cases can be discussed.

## 1.4 On and Off-resonance Cases in the Interaction of Radiation with System: Transition Probabilities Between Two-Levels

The $\omega_{10} \approx \omega$ approximation can be made in a particular case where the system oscillates with Bohr frequency $(E_1-E_0)/\hbar=\omega_{10}$ which is in resonance or nearly resonance with the optical angular frequency $\omega=2\pi\nu$ of the incident laser photon. The terms $e^{i(\omega_{10}-\omega)t}$ and $e^{-i(\omega_{10}-\omega)t}$) thus represent slowly varying functions with time compared to the rapidly oscillating nonresonant terms $e^{i(\omega_{10}+\omega)t}$ and $e^{-i(\omega_{10}+\omega)t}$) in eqs.(1.13) and eq.(1.14).

The nonresonant high frequency terms can be neglected because their effect essentially averages to zero since they are rapidly oscillating functions of time. These equations, eq. (1.13) and (1.14) could be rearranged as,

$$c`_0 = i\omega_R (e^{i\Delta t})\, c_1 / 2 \qquad 1.15$$

$$c`_1 = i\omega_R (e^{-i\Delta t})\, c_0 / 2 \qquad 1.16$$

The detuning frequency measures how far the frequency of laser light $\omega$ is tuned from the resonance frequency $\omega_{10}$. The solutions for these first-order differential equations with initial conditions $c_0(0)=1$ and $c_1(0)=0$ for the system initially in the ground state at $t = 0$ is

$$c_0(t) = [\mathrm{Cos}(\Omega t/2) - i\,(\Delta/\Omega)\,\mathrm{Sin}(\Omega t/2)]e^{i(\Delta/2)\,t} \qquad 1.17$$

$$c_1(t) = i\,(\omega_R/\Omega)\,\mathrm{Sin}(\Omega t/2)e^{-i(\Delta/2)\,t} \qquad 1.18$$

Here the absolute square of $c_1(t)$ gives the probability of the finding system in the excited state

$$|c_1(t)|^2 = (\omega_R/\Omega)^2 \mathrm{Sin}^2(\Omega t/2) \qquad 1.19$$

while the time-dependent probability of finding the system in the ground state is given by

$$|c_0(t)|^2 = 1 - |c_1(t)|^2 = 1 - (\omega_R/\Omega)^2 \mathrm{Sin}^2(\Omega t/2) \qquad 1.20$$

At the resonance, since $\omega = \omega_{10}$, $\Delta=0$ and $\Omega = \omega_R$ then in this case

$$|c_1(t)|^2 = \mathrm{Sin}^2(\Omega t/2) \qquad 1.21$$

$$|c_0(t)|^2 = 1 - |c_1(t)|^2 = 1 - \mathrm{Sin}^2(\Omega t/2) = \mathrm{Cos}^2(\Omega t/2) \qquad 1.22$$

The probability, $|c_1(t)|^2$, of finding the system in the excited state for three detuning frequencies; $\Delta=0$, $\Delta= \omega_R$ and $\Delta= 3\omega_R$ are shown in fig.1.4.

The meaning of the Rabi frequency is clear from eq.(1.21) and fig. 1.4. The system is coherently cycled between the ground state and the excited state by the laser light and no significant abrupt changes in the phases and amplitudes of wavefunctions occur during the interaction.

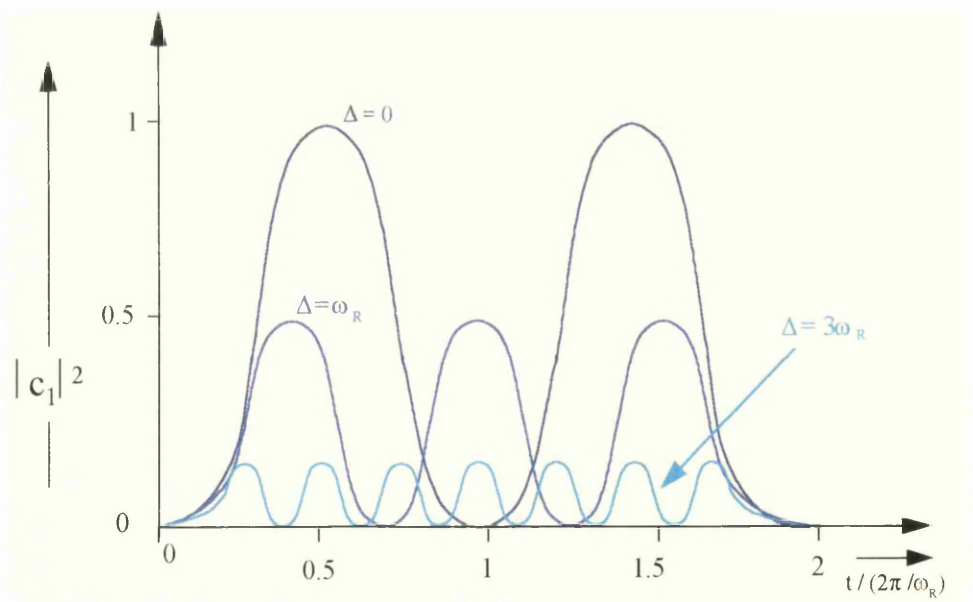


**Figure 1.4:** The probability of finding the system in the excited state for three detuning frequencies: $\Delta=0$, $\Delta= \omega_R$ and $\Delta= 3\omega_R$

The squared probability amplitude $|c_1(t)|^2$, (eq.1.21), is the probability that the two-level particle will be in the upper state at the moment t. The probability of the system being excited to the upper state, $P_{1\leftarrow 0}$ is given by;

$$P_{1\leftarrow 0}=\sin^2[(1/2)\Delta^2+\Omega^2)^{1/2}\, t]\; L(\Delta/\Omega) \qquad 1.23$$

where $L(\Delta/\Omega)$ is the Lorentzian line shape function normalised to unity.

In the case of resonance ($\Delta<<\omega_R$),

$$P_{1\leftarrow 0}=\sin^2[\Omega t/2]= (1-\cos\omega_R t)/2 \qquad 1.24$$

and in the case of off-resonance conditions ($\Delta<<\Omega$);

$$P_{1\leftarrow 0}= (\Omega/\Delta)^2\sin^2[(\Delta/2)t] \;= (\Omega/2\Delta)^2\,(1-\cos\Delta t) \qquad 1.25$$

At the resonance the system is completely inverted after a time $t_\pi=\pi/\omega_R$, while off-resonance there is a reduced probability for finding the system in the excited state.

## 1.5 Loss Mechanisms in the Excited State of the System

In this section, the loss mechanisms from the excited state will be considered briefly. The emission of a photon would break the coherence of the excitation and reset the system to the ground state. These emission processes as described above are known as spontaneous and stimulated (induced) photon emissions. It is also known that the interaction of the system with its surroundings can additionally shorten the lifetime of the excited state. The population relaxation in the equilibrium state is called *longitudinal relaxation* and characterised by the longitudinal relaxation time $T_1$. On the other hand, stimulated emissions may be induced either by the absorption of a photon in the excited state or collisions between atoms. Collisions can also cause relaxation in the system and reset the phase of the atomic or molecular wavefunction without changing any of the populations. This phase changing of collisions also interrupts the coherence cycling of the system. Such a relaxation time is defined to be $T_2$ and the relaxation is generally referred to as the *transverse relaxation*. The phase relaxation has no effect on the populations of levels but it widens the spectral

line of the transition from the ground to the excited state. The homogenous half-width $\Gamma_{hom}$ of a Lorentzian is related to the time $T_2$ by $\Gamma_{hom} = 1/T_2$.

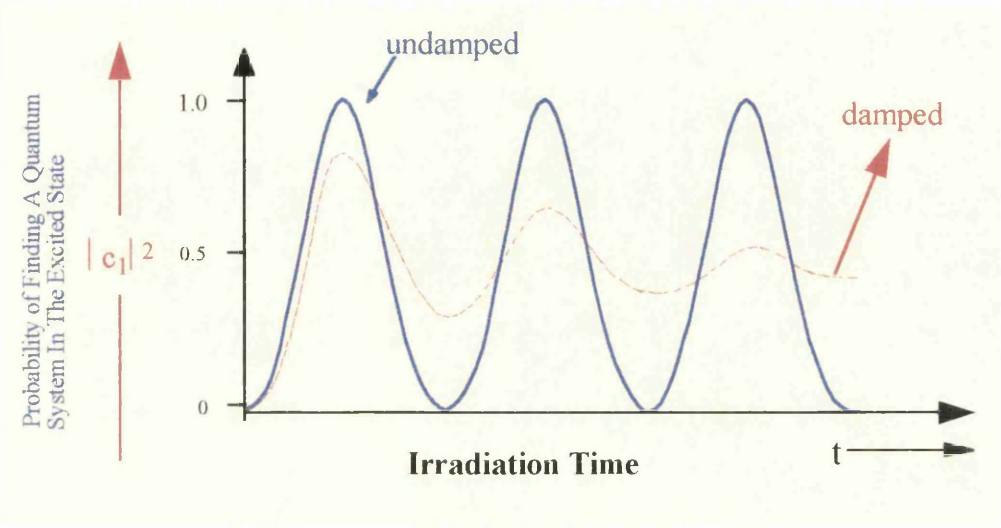


**Figure 1.5:** The driven two level system saturates when relaxation process(damping) are induced.

In this case the population of the states 0 and 1 oscillate with Rabi frequency as shown in fig.1.4 and with blue line (undamped) in fig.1.5. In the infrared and visible region of the spectrum, relaxation processes are much faster and Rabi oscillations are normally damped. For example a real system would oscillate briefly when a strong field is applied suddenly to it, but it soon loses coherence and becomes saturated. When the system is saturated, half of the molecules in the system are in the lower state and half of them in the upper state. The ratio of the stimulated emission(down) matches the rate of the absorption(up).

## 1.6 Interaction of Low Intense Laser Light with System

In the case of a weak electromagnetic field, its interaction with the system is also common and it was the most likely case before the development of the laser (early 1960s). In the weak field case, there is a negligible build-up of population in the excited state, so that $c_1(0)=0$ and $c_0(0)=1$ at $t=0$ while $c_0(t)\approx 1$ and $|c_1(t)|^2 \ll 1$ for all

the irradiation time. So, the probability of finding a system in the excited state after a time t is given by

$$P_{10}=|c_1(t)|^2=(\omega_R/\Delta)^2\mathrm{Sin}^2(\tfrac{\Delta t}{2})=(\mu_{10}E^2/\hbar)\{\mathrm{Sin}^2[(\omega-\omega_{10})t/2]/(\omega-\omega_{10})\} \qquad 1.26$$

This equation (eq.(26)) was produced considering boundary condition where $N_1=0$ and $N=N_0$ at $t=0$. The variation of $|c_1(t)|^2$ is shown in fig.1.6. In fig.1.6, it is indicated that the transition probability is maximum when the laser frequency is tuned to the resonance (zero detuning) with the atomic or molecular transition. As the laser wavelength is varied, the absorption intensity is maximised when the photon energy matches the energy difference between two bound states of the atom or molecule which is the basis of the RIS and REMPI and these will be discussed in later chapters.

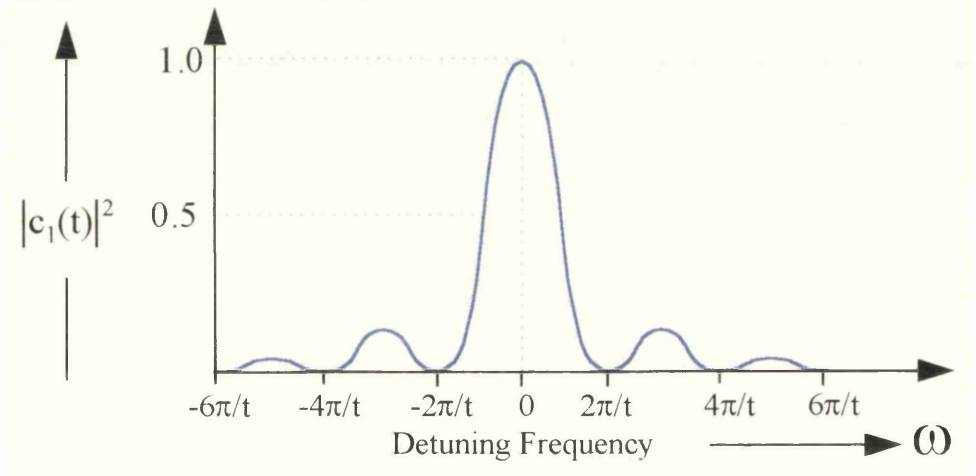


**Figure 1.6:** Transition probability as a function of detuning frequency.

The discussions carried out in this chapter can be found in most of the quantum mechanical text books. The most useful text books, to the author's knowledge, are Lin *et al.*, 1984; Demproder, 1982; Chin and Lambropoulos, 1984; Letokhov, 1987; Mandl, 1992; McMurry, 1994; Yariv, 1997.

# CHAPTER 2

# MULTIPHOTON PROCESSES IN MOLECULES

**Contents**

## 2.1 Introduction

In the first chapter in this thesis, the quantum mechanical description of a simple two level semiclassical model was described and the interaction of the laser light with this system was discussed. In the remaining part of this thesis the processes will be considered and discussed as multiphoton processes where one photon of incident laser light has not sufficient energy to induce an excitation into an excited or ionic state in the molecule.

The multiphoton process was developed and has been applied to atomic spectroscopy over the past 30 years (Voronov and Delon, 1966; Agostini *et al.*, 1968; Chin *et al.*, 1969). After the first experimental observation of the multiphoton ionisation process, developments on laser technology and laser based spectroscopic techniques have been made. Laser based techniques have become widespread and highly selective/sensitive techniques with especially the development of the resonant ionisation spectroscopy (RIS) in the early 1970s. The development of RIS has made the detection of a single atom possible as well as the separation of isotopes (Letokhov *et al.*, 1977; Hurst *et al.*, 1979; Letokhov, 1987; Hurst and Payne, 1988).

After multiphoton ionisation in atoms became reasonably understood the same techniques were applied to molecules (Johnson, 1975a; 1975b; Johnson *et al.*, 1975; Lubman, 1988a; 1988b).

In this thesis, MPI processes in molecules rather than atoms is emphasised. In this chapter, a brief description of molecular energy levels will be made, first. Secondly, the photo-induced phenomena during the interaction of laser beam with molecules will be discussed and the rate equation modelling for dissociative ionisation process in a molecule. Finally a brief introduction to ultrafast laser mass spectrometry will be given.

## 2.2 Energy Levels In Molecules

In order to understand the multiphoton phenomena in molecules, it is important to learn about electronic energy levels in molecules. Electronic energy levels in single and multi-electron atoms are sharply defined while the energy levels in diatomic or polyatomic molecules are broad because of additional vibrational and rotational degrees of freedom available to a molecule. In fig. 2.1a, typical electronic energy levels in a diatomic molecule are shown and it is clear from the figure that each electronic energy levels contain vibrational (horizontal red lines) and rotational (horizontal green lines) sub-energy levels. In the case of most molecules, energy differences between two neighbour vibrational and rotational sub-levels are typically $\approx$1000 $cm^{-1}$ and $\approx$10-100 $cm^{-1}$, respectively.

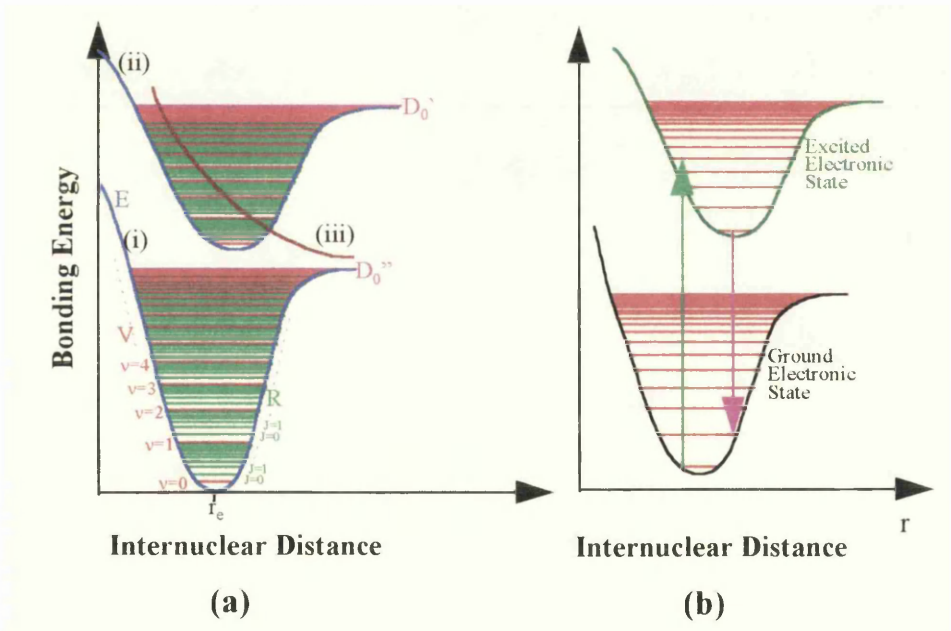


**Figure 2.1:** **(a)** Electronic energy level diagram of diatomic molecule showing dissociation limits for bound ground state ($D_0$"), bound excited state ($D_0$`) and separation between nuclei ($r_e$) in the equilibrium and **(b)** basis of the Franck-Condon principle, showing no change in the internuclear distance during an electronic transition either through absorption or emission. In diagram **(a): (i)** typical bound ground electronic energy state (blue line), **(ii)** bound excited electronic energy state (blue line), **(iii)** unbound excited energy state (brown line), Vibrational (v) and rotational (J) sub-energy levels are also shown.

The bond energy curves in a diatomic molecule are a function of the internuclear separation and are called Morse potentials. They represent a stable state of the molecule when a minimum in the potential energy exists ((i) and (ii) in fig. 2.1a). The minimum in the curve arises due to the balancing of the strong nuclear repulsive forces and the attractive forces arising from the interaction of nuclei with binding electrons.

In the polyatomic molecules, the potential energy curves representing electronic energy state are generally of the same form as the Morse curve shown in fig. 2.1a. In the case of polyatomic molecules in contrast to diatomic molecules, the internuclear separation must be replaced by some generalised co-ordinate, which could be a particular bond length or an angle between two bond etc. Unstable energy states can also arise if the attractive forces are insufficient to overcome the nuclear repulsive forces and in such a state as seen from (iii) in fig. 2.1a, there exists no potential energy minimum. In this case, the molecule does not exist.

An electronic transition in a molecule takes place in a time scale which is shorter than $10^{-15}$s and, therefore, due to the Born-Oppenhimer approximation the nuclei cannot move within this short time scale and hence the internuclear distance remains constant during the electronic transition, i.e., electronic transition in a molecule is always depicted by a vertical line connecting the appropriate states involved in the transitions for both caused by absorption and emission, presented in Fig. 2.1b.

## 2.3 The Photo-processes During The Interaction of Laser Pulses With Molecules

### 2.3.1 Multiphoton Excitation and Ionisation Schemes in Molecules

Several methods based on different excitation and ionisation schemes have been used to investigate several molecules and discussed in some details (Antonov and Letokhov, 1981; Letokhov, 1987; Fisanick *et al.*, 1981; Gadenken *et al.*, 1982; Ashfold and Howe, 1994; Ledingham, 1995). Figure 2.2 shows several

excitation/ionisation schemes for molecules, any one of which may be involved in the process depending on the spectroscopic structure of molecule and the laser wavelength chosen. Each vibrational level also contains rotational levels which are not shown in figure but indicated in fig. 2.1a with horizontal green lines.

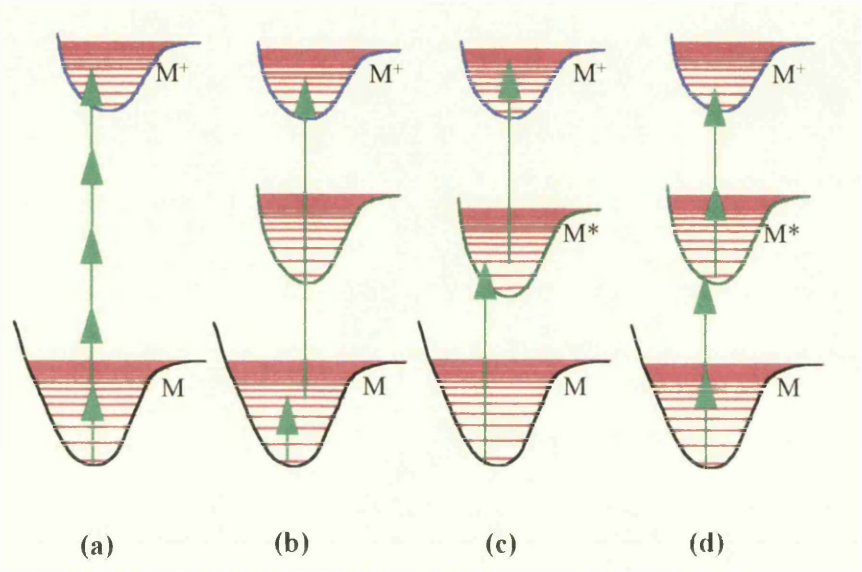


**Figure 2.2:** Possible different excitation/ionisation schemes (Ledingham, 1995).

In fig.2.2, (a) nonresonance multiphoton (5 photon) ionisation, (b) resonant two photon ionisation *via* ground state vibrational level, (c) resonance two photon ionisation *via* excited state vibrational levels, (d) resonance enhanced (2+2) multiphoton ionisation (REMPI).

### 2.3.2 The Fate of Absorbed Energy in Molecules

During the interaction of laser light with molecules, from reagent to products, a number of photoinduced processes are possible such as absorption, ionisation, dissociation, isomerization, luminescence, internal conversion (IC) and intersystem crossing (ISC).

For the mass spectrometric analysis used in this thesis, in general, the detection of positive ions of parent molecule or the ionic fragments is the main purpose.

Therefore, the aim in this work is the detection of parent ion or higher mass fragments because it is believed (Ledingham *et al.*, 1995b; Singhal *et al.*, 1996; Kilic *et al.*, 1997; Kosmidis *et al.*, 1997) that if the molecular parent ion or higher mass ion peaks exist in the mass spectrum, much more structural information is available than the case of the fragmentation pattern which is dominated by small mass ion peaks.

The ionisation efficiency may be reduced by some loss mechanisms which occur in the excited state of the neutral molecule. The loss mechanisms are dissociation, luminescence, internal conversion (IC) and intersystem crossing (ISC). First of all, the ionisation process and latter the other mentioned processes will be discussed briefly.

### 2.3.3 Ionisation Techniques in Molecules

The photoionisation of a neutral substance, M, as a result of the interaction of laser light with a sample, means a subsequent removal of an electron from the neutral (M) parent molecule resulting in the generation of a positive ion $M^+$ and a free electron from the original molecule,

$$M+h\nu \rightarrow M^+ + e^- \qquad (2.1)$$

This process is known as the *photoionisation process*.

In general, all stable neutral organic molecules have an even number of electrons in their highest occupied orbitals which may have bonding or non-bonding structure. Removal of an electron from either a bonding or non-bonding orbital might take place and the molecular ion obtained will subsequently be left with a single electron configuration which does not have a very stable configuration and is called a radical ion ($M^+$).

The ionisation process can be explained for diatomic molecules conveniently and involves two kinds of schemes which are simply described in fig. 2.3. Figure 2.3a shows that the ion obtained is in the lowest vibrational level in its ground state. The

diagram also indicates that the internuclear distance in its ionic ground state is slightly larger than that in a bonding electronic state of neutral molecule. This happens when a non-bonding electron is removed from the molecule by the ionisation process ($\nu`=0 \leftarrow \nu``=0$ transition). In this case the process is called *adiabatic* ionisation. If the internuclear distance in the ionic ground state is much larger than that in the bonding electronic state of the neutral molecule where the transition takes place from the vibrational ground state in the bound state of neutral molecule to the vibrationally excited level of the ion through $\nu`=4 \leftarrow \nu``=0$ transition (for particular presentation in fig. 2.3b) and then this process is called the *vertical ionisation*. This latter case arises as a result of removal of a bonding electron from a neutral molecule. Therefore, the energy required to ionise the molecule through an adiabatic ionisation process is smaller than that in the case of a vertical ionisation process. In both cases, the Franck-Condon principle is valid and the transition strength between two particular vibrational levels is governed by the Frank-Condon factor.

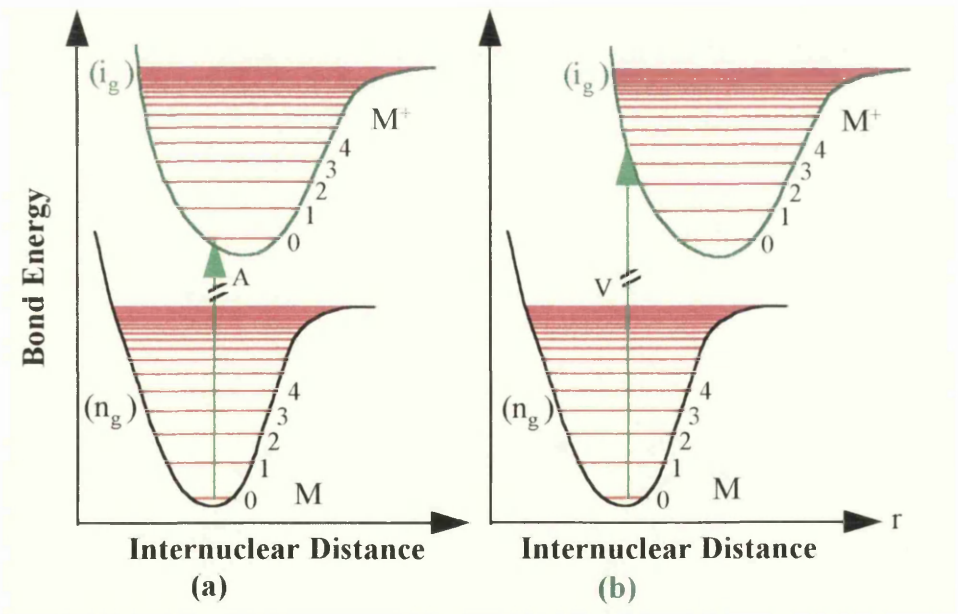


**Figure 2.3:** A schematic presentation of neutral ($n_g$) and ionic ($i_g$) bound ground energy states. In both cases, the ionisation may involve in one of the excitation and ionisation schemes shown in fig.2.2. A indicates adiabatic ionisation process (a) and V is vertical ionisation process (b).

### 2.3.4 Dissociation Processes

The dissociation of molecules is one of the most important chemical processes in photochemistry since it is the first step in a photochemical reaction process which generates radicals and initiates subsequent reactions. If the aim is the detection of photoions, the photodissociation process can be defined as a loss mechanism because a rapid dissociation mechanism reduces the ionisation efficiency of the molecular parent ion but it leads the formation of fragment radical ions with subsequent ionisation of the neutral fragments.

Photodissociation is the break up of a molecule as a result of photon absorption from the laser beam. For a model three atom ABC molecule, the process can be described as

$$ABC + h\nu \rightarrow AB + C \qquad (2.2)$$

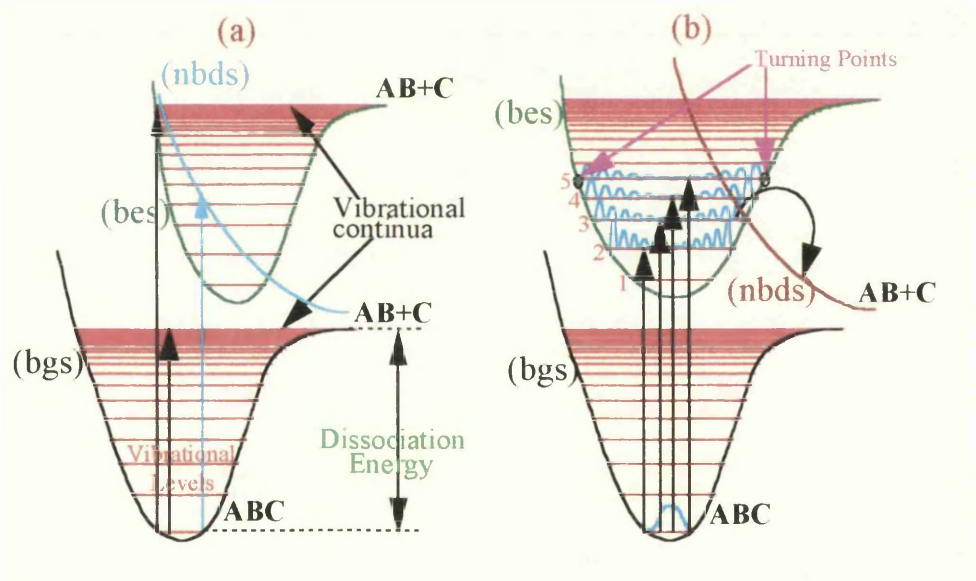


**Figure 2.4:** Diagrams show two kind of dissociation processes; **(a)** photodissociation with dissociation threshold, **(b)** predissociation. In both diagram: **(bgs)**: bound ground state, **(bes)**: bound excited state, **(nbds)**: non-bonding dissociative state

There are two kinds of dissociation processes which are direct dissociation and predissociation as diagramatically shown in fig.2.4 and explained as follows: A molecule may be excited to the vibrational continuum of either the ground electronic

or excited electronic states with absorption of one or more photons as described in fig.2.4a. If the energy of the incident laser photons are chosen properly, the transition from bound ground state to a bound excited state may occur. However, if the photon energy absorbed is sufficiently large, the molecule can be excited into a continuum of rovibrational states where all vibrational/rotational levels are unbound and the subsequent break up of a particular molecular bond takes place (Fig. 2.4a). In another case the molecule can be excited to an unbound excited state (blue arrow and blue (nbds) non-bonding dissociative state), this excitation also results in break-up of the molecule. These two kind of cleavage of a particular bond in molecules is known as *direct dissociation* (Band and Freed, 1975).

On the other hand, the cleavage of a molecular bond may take place indirectly *via* a non-bonding excited state as shown in fig. 2.4b and indicated as (nbds). In this case a transition between two bound electronic state takes place and any or a number (especially in the case of broad band laser sources) of the vibrational levels in the electronic excited state may be populated. In the populated vibrational levels for example $v'=2$, 3, 4 and 5, molecule behaves like a harmonic oscillator obeying Morse potential. In this case the oscillator spends most of its vibration time at the turning points in the potential well and a very small portion is spent about its equilibrium distance. During the vibration of the oscillator in the excited vibrational level of electronic excited state a radiationless transition may occur from that bound vibrational level to an unbound neighbouring state and this results in a break-up of the bond in the molecule. This process is known as *predissociation* (Fig.2.4b).

### 2.3.5 Other Loss Processes

Fig. 2.5 shows absorption and emission processes as well as radiationless transitions in a molecular system. Radiative loss mechanisms in the excited state is, in general term, known as *luminescence* and can arise in two ways, known as *fluorescence* and *phosphorescence*. A molecule undergoes a singlet($S_0$)-singlet ($S_1$) transition absorbing photon(s). In the excited singlet ($S_1$) state a molecule may undergo a radiationless

relaxation through vibrational levels and finally reaches the lowest vibrational level in the excited, $S_1$, electronic state. From the lowest vibrational level in the electronic excited state to a vibrational level in the ground electronic state, a transition takes place by emitting a photon within a time scale of about $10^{-9}$s. This emission process is known as *fluorescence*.

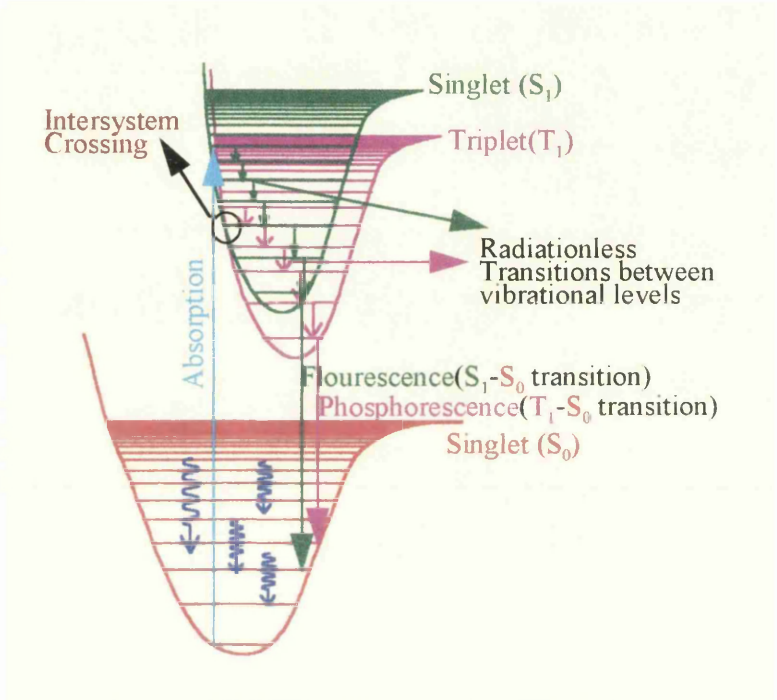


**Figure 2.5:** Radiational and radiationless transition mechanisms are illustrated.

Alternatively, a radiationless transition may take place from a singlet ($S_1$) to a triplet state ($T_1$) and radiationless transitions may continue to occur between vibrational levels in the triplet ($T_1$) state until the system reaches the lowest vibrational level in that state. A transition from the lowest vibrational level in the triplet ($T_1$) state to the ground singlet state($S_0$) may take place by emitting a photon within a time scale about several seconds. This emission process is called *phosphorescence*.

If a radiationless transition take place between states which have different multiplicity (S-T or T-S transitions) the transition is called *inter system crossing* (ISC). If the transition occurs between electronic states which have the same multiplicity (S-S transition) the transition is called *internal conversion* (IC).

### 2.3.6 Isomerisation Process

Isomerisation is one of the important rearrangement processes in organic chemistry, which take place during the interaction of the laser light *prior to* ionisation and dissociation of a molecule. The isomerisation of the molecular ion is also possible. The radiationless transitions IC and ISC have already been discussed in the previous section. A molecule may be involved in a direct crossover from the electronically excited state to a level of a lower lying electronic state (ISC) and is the main process to explain the isomerisation of a molecule (Philips *et al.*, 1968).

For isomerisation to occur, a molecule must be excited to a vibrational level which has a critical energy to initiate this process. The isomer formed in a vibrationally excited energy level may undergo collisional relaxation into its lower or the lowest vibrational level. Additionally, the isomer may absorb further photon(s) and may dissociate or ionise.

When the laser intensity is sufficiently high the molecule may absorb further photons to ionise prior to the dissociation or isomerisation. In the ionisation process, the neutral molecule may absorb photons whose total energy may be greater than the ionisation potential of molecule. This case allows the molecule to have excess energy in its ionic state and this energy of the ion may induce a rearrangement or decomposition of the ion, or alternatively the ion may stay in the vibrationally excited level in its ground electronic state. This excess energy is known as *internal energy* of the ion.

Figure 2.6a shows a sequence of the ionic state where the ion produced has excess energy through photoionisation. Due to its excess energy the ion may fall into one of two energy range where the ion has sufficient energy to decompose (*decomposing ions*) or insufficient energy to decompose (*non-decomposing ions*). In the former case the ion may fragment easily but in the latter case the ion may have either

sufficient energy to excess the isomerisation limit or it may relax into its ground state through a radiationless process to form stable parent ion.

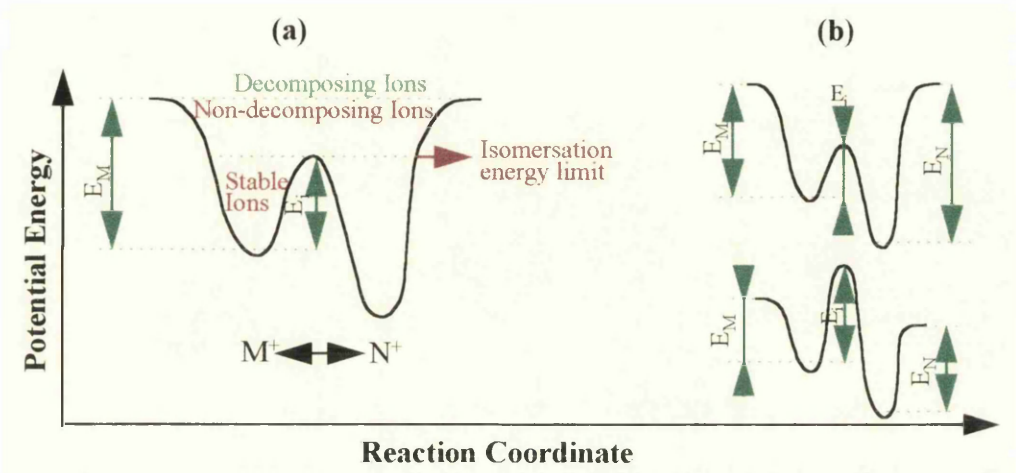


**Figure 2.6:** **(a)** Sequence of the decomposition and isomerisation of ion produced with initial energy. **(b)** different possible energy barrier for isomerisation depending on the constitution of the ion. $\mathbf{M^+}$ indicates the molecular parent ion and $\mathbf{N^+}$ is its isomer. $\mathbf{E_M}$ is decomposition energy for the parent ion, $\mathbf{E_i}$ is isomerisation barrier and $\mathbf{E_N}$ is dissociation energy of a bond in $\mathbf{N^+}$ isomer.

For the ions in the decomposition range, there is competition between fragmentation and isomerisation. In most cases the fragmentation is much faster than the isomerisation, and therefore in this case it is expected that the structural elucidation of the ion is rather simple while the isomerisation complicates it.

In some cases, the isomerisation energy may be either much higher or lower. Fig. 2.6b shows two extreme cases for the isomerisation barrier. (i) In the case of isomerisation barrier which is much lower than the decomposition energy of molecular parent ion (upper diagram in fig 2.6b), i.e., $E_i << E_M$, the isomerisation is possible and as mentioned above the situation is complicated because of the existence of competition between decomposition and isomeration. (ii) In the case of the higher isomerisation barrier (lower diagram in fig.2.6b), $E_i >> E_M$, no isomerisation is possible. In any case, if the internal energy (E) of ion is smaller than the isomerisation energy, i.e., $E < E_i$, the isomerisation is impossible and the ion relaxes into a vibrational level to form a stable ion.

## 2.4 Rate Equation Modelling for $NO_2$ System

The relationships between the laser intensity, the ionisation efficiency, dissociation, etc., are very complex in the multiphoton dissociative ionisation mechanism. In order to investigate this relationship, several mathematical models have been suggested by several groups for atoms (Ackerhalt and Shore, 1977; Singhal *et al.*, 1989) and molecules (Zakheim and Johnson, 1980). Singhal has developed a general solution for the rate equation model to investigate the dissociative ionisation of the molecules (Singhal, 1997) and this rate equation model is used in this work to investigate the dissociative ionisation of the $NO_2$ molecule. The model and relevant approximations made are given below.

The multiphoton dissociative ionisation pathways which the rate equation model considers is shown in fig. 2.7. The diagram at the left hand side shows the multiphoton processes involved in the dissociation/ionisation of a $NO_2$ parent molecule and at the right hand side a neutral, NO, dissociation product.

The rate equation model (Singhal, 1997) used in this work assumes that spontaneous emission is not effective and therefore these effects in either molecules , $NO_2$ and NO, were neglected. For the femtosecond lasers, this assumption is valid and the results under this assumption show very good agreement with the experimental results (Ledingham *et al.*, 1995a; Singhal *et al.*, 1996).

The initial dynamic equations for $NO_2$ molecule in its ground state are

$$n_0' = -a_{01}n_0 + a_{10}n_1 \tag{2.3}$$

$$n_1' = a_{01}n_0 - (a_{12} + a_{10} + k_1)n_1 \tag{2.4}$$

$$n_2' = a_{12}n_1 \tag{2.5}$$

where $n_0' = dn_0/dt$, $n_1' = dn_1/dt$, $n_2' = dn_2/dt$, $n_0$ is the number of $NO_2$ molecule in its ground state, $n_1$ is the number of $NO_2$ molecule in its excited state, $n_2$ is the number of $NO_2^+$ ions produced and $a_{01} = \sigma_{01m_{01}}\Phi_{01}^{m_{01}}$, $a_{10} = \alpha_{10}a_{01}$ and $a_{12} = \sigma_{12m_{12}}\Phi_{12}^{m_{12}}$. In this

model calculation procedure, the statistical weights of each states are taken to be unity and therefore $a_{10} = a_{01}$. $k_1$ is the dissociation rate of the neutral $NO_2$ parent molecule in its excited state, $m_{ij}$ is the number of photon to be absorbed to induce relevant transition and $\Phi$ is the laser flux.

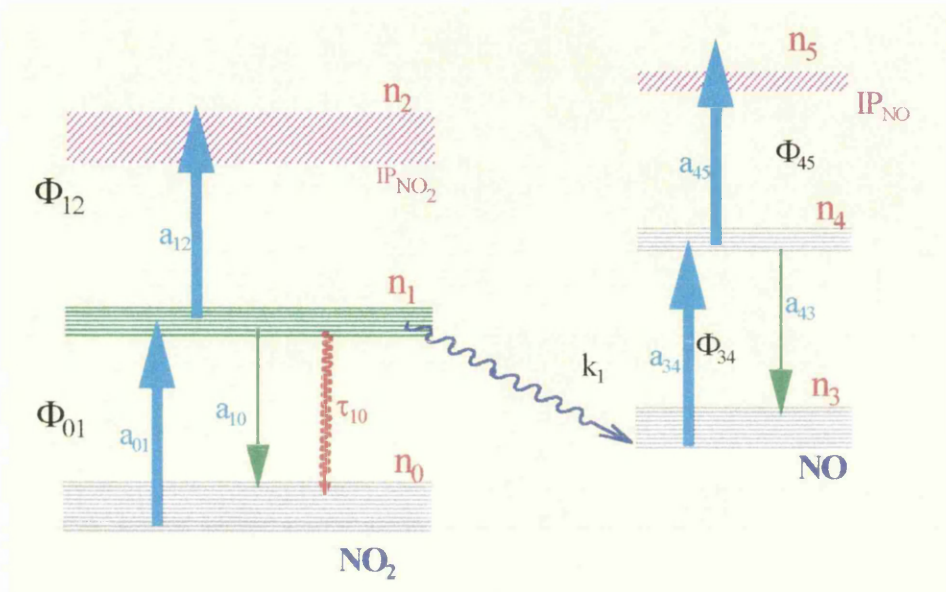


**Figure 2.7:** The energy level diagram and possible transitions considered in the rate equation model are shown.

The initial number of the neutral NO in its ground state is determined by $k_1$ as a result of the dissociative character of the parent molecule in its excited state. Therefore the dynamic equations for the neutral NO can be written as

$$n_3' = k_1 n_1 - a_{34} n_3 + a_{43} n_4 \qquad (2.6)$$

$$n_4' = a_{34} n_3 - a_{43} n_4 - a_{45} n_4 \qquad (2.7)$$

$$n_5' = a_{45} n_4 \qquad (2.8)$$

where $n_3' = dn_3/dt$, $n_4' = dn_4/dt$, $n_5' = dn_5/dt$, $n_3$ is the number of neutral NO in its ground state, $n_4$ is the number of neutral NO in its excited state, $n_5$ is the number of $NO^+$ ions and $a_{34} = \sigma_{34 m_{34}} \Phi_{34}^{m_{34}}$, $a_{43} = \alpha_{43}\, a_{34}$ and $a_{45} = \sigma_{45 m_{45}} \Phi_{45}^{m_{45}}$. The statistical weights of each states are taken to be unity and therefore $a_{34} = a_{43}$.

This model suggests a more complicated but a general solution for the populations of each states. Solutions for this equations were made using the boundary conditions as $n_0 = N_0$, $n_1 = 0$, $n_2 = 0$, $n_3 = 0$, $n_4 = 0$ and $n_5 = 0$ at $t = 0$. The $N_0$ is the initial number of neutral parent molecule in its ground state.

The initial equation set, eqs. (2.3), (2.4), (2.5), for the $NO_2$ parent molecule can be simplified to give a second order differential equation in $n_1$

$$n_1'' + Bn_1' + Cn_1 = 0 \tag{2.9}$$

where $n_1'' = d^2n_1/dt^2$ and $n_1' = dn_1/dt$. This equation, eq.(2.9), has two real positive roots $p_i$ leading to a general solution $n_1(t)$,

$$n_1(t) = \sum_{i=1}^{2} \beta_i \exp(-p_i t) \tag{2.10}$$

which determines the number of excited $NO_2$ molecule. Substitution of eq. (2.10) into eq. (2.5) and integrating it, the number of the $NO_2^+$ ions can be determined by

$$n_2(t) = a_{12} \sum_{i=1}^{2} (\beta_i/p_i)\,[1-\exp(-p_i t)] \tag{2.11}$$

where $p_i$ are determined to be $p_1 = (B-(B^2-4C)^{1/2})/2$ and $p_2 = (B+(B^2-4C)^{1/2})/2$ with $B = a_{01}+a_{10}+k_1+a_{12}$ and $C = a_{01}(a_{12}+k_1)$. $\beta_i$ are determined using initial conditions as $\beta_1 = N_0 a_{01}/(p_2-p_1)$ and $\beta_2 = N_0 a_{01}/(p_1-p_2)$.

The dissociation rate, $k_1$, of the parent molecule determines the number of the dissociation product, NO, in its ground state and the number of neutral NO products, $n_3$, changes as a function of time due to eq. (2.6). The general solution for the equation set, eq. (2.6), (2.7) and (2.8), to calculate the number of $NO^+$ ions is obtained by solving a third order differential equation in $n_5$ following a similar procedure for particular equation

$$n_5'''+Pn_5''+Qn_5'-a_{34}a_{45}k_1n_1=0 \quad (2.12)$$

where $n_5'''=d^3n_5/dt^3$ , $n_5''=d^2n_5/dt^2$ and $n_5'=dn_5/dt$ and $n_1$ is given by eq.(2.10).

The eq. (2.12) can be written as

$$y''+Py'+Qy=\Sigma R_i \exp(-p_it) \quad (2.13)$$

Solving this differential equation,

$$n_5(t)= \sum_{i=1}^{4} (\delta_i/p_i)[1-\exp(-p_it)] \quad (2.14)$$

can be obtained, where $p_i$ are being $p_1$, $p_2$ given above and $p_3 = (P-(P^2-4Q)^{1/2})/2$ and $p_4=(P+(P^2-4Q)^{1/2})/2$ and $P=a_{34}+a_{43}+a_{45}$ and $Q=a_{34}a_{45}$. $\delta_i$ determined using initial conditions as $\delta_1=R_1/(Q-Pp_1+p_1^2)$ with $R_1=a_{34}a_{45}k_1\beta_1$, $\delta_2=R_2/(Q-Pp_2+p_2^2)$ with $R_2=a_{34}a_{45}k_1\beta_2$, $\delta_3=[\delta_1(p_1-p_4)+ \delta_2(p_2-p_4)]/(p_4-p_3)$ and $\delta_4 = -\delta_3-(\delta_1+\delta_2)$. $n_5(t)$, eq.(2.14), is the number of $NO^+$ ion obtained.

Using this rate equation model, the analysis of the dissociative ionisation of the molecule $NO_2$ dealing with a single bond dissociation, the $NO_2^+/ NO^+$ ratio gives a significant information about the competition between the ionisation of the parent molecule and the dissociation through this bond (Ledingham *et al.*, 1995a; Singhal *et al.*, 1996). Therefore, the ratio of $n_2/n_5$ was calculated using eqs. (2.11) and (2.14) and results of this equation model will be discussed in Chapter 4 for $NO_2$ molecule comparing them with experimental results for 10 ns and 90 fs laser pulses.

## 2.5 High Laser intensity and Ultrashort Laser Pulse Dynamics in Multiphoton Dissociative ionisation of Molecules: Ultrafast Laser Mass Spectrometry.

Multiphoton dynamics in a molecular sample were discussed in earlier sections of this chapter. The photon absorption is possible for either neutral or ionic samples within a laser pulse where ions were produced by either the front part of the laser pulse or as a

result of simultaneous absorption of the photons from the intense laser beam by the neutral molecule. A quantitative investigation for large molecules is difficult since a number of molecular bonds may be involved in the fragmentation process in the molecule. Therefore, a qualitative treatment for large molecules is the only way for analytical purpose. In this section a brief discussion will be made distinguishing possible mechanisms involve in the multiphoton dissociative ionisation process depending on the laser pulse width as well as the laser intensity.

In mass spectrometry, the source of information is the fragmentation pattern in the mass spectrum of molecule. The fragmentation pattern could be attributed to two different mechanisms which are an ID (ionisation followed by dissociation) or a DI (dissociation followed by ionisation) processes which take place within a laser pulse from reagent to the fragments (Gedanken *et al.*, 1982; Yang *et al.*, 1983). The fragmentation pattern could be attributed to an ID process when only the fragmentation of the ionised parent molecule occurs. The DI is the case where the subsequent ionisation of the neutral fragments from the dissociation of the neutral parent molecule in its excited state takes place. In the pure DI process however the molecular parent ion cannot be detected. In the both cases, further photon absorption and dissociation-ionisation-fragmentation processes continue until the final products are obtained. These two , ID and DI, processes are in competition depending on the laser parameters as well as the spectroscopic nature of the sample under investigation. In a particular case of the laser intensity, both of these, ID and DI, may be involved in the process, i.e., the process may be a mixture of both mechanisms and elucidation of the spectrum becomes more complicated.

In order to overcome any fast relaxation processes or dissociation in intermediate states, the photon absorption rate must be enhanced by an increasing laser intensity. As the laser intensity increases, the rate of absorption of photons by molecule in the dissociative excited state increases and these two channels, DI and ID, start to compete. It is also known that the competition rate of these two mechanisms strongly

depends on the laser pulse duration saying, i.e., if the laser pulse duration is shorter than the lifetime of the molecule in the dissociative excited state the ID process becomes dominant while the DI may be the dominant process in the case of the longer pulse duration relative to the lifetime of the molecule in the excited state. Therefore it is often concluded that, in the nanosecond laser pulse regime, the DI mechanisms often dominate the process while the ID is often observed when the femtosecond laser pulses were used. A comparison of the nanosecond and femtosecond laser mass spectrometry has been the subject of a number of recent articles (Wei *et al.*, 1992; Mollers *et al.*, 1992; Weinkauf *et al.*, 1994; Aicher *et al.*, 1995; Ledingham *et al.*, 1995b; Grun *et al.*, 1996; Kilic *et al.*, 1997; Kosmidis *et al.*, 1997; Ledingham and Singhal, 1997; Weickhardt *et al.*, 1997; Smith *et al.*, 1997) for a number of molecular samples and the comparison of the nanosecond and femtosecond laser mass spectrometry will be carried out in this thesis for a number of nitro aromatic molecules and will be discussed in the result chapters starting from Chapter 4.

# CHAPTER 3

# INSTRUMENTAL SET-UP AND RELEVANT EXPERIMENTAL TECHNIQUES

## Contents

## 3.1 Introduction

For spectroscopy or spectroscopic applications to be carried out, the first necessities are the source of energy, a spectrometer and a data analysis system. The photochemical application methods have gained considerable interest due to the development and increasing availability of stable and reliable lasers.

For a molecule to be detected using mass spectrometry the molecular ion has to be produced, collected in the detector and finally recorded in a spectrum. The ionisation of large organic molecules, and especially thermally labile molecules, is difficult and powerful lasers are needed for this procedure. The best way to obtain high laser intensities is to use a laser system with ultrashort laser pulses. We carried out a number of experiments using femtosecond laser pulses and compared the results with these of nanosecond laser pulses.

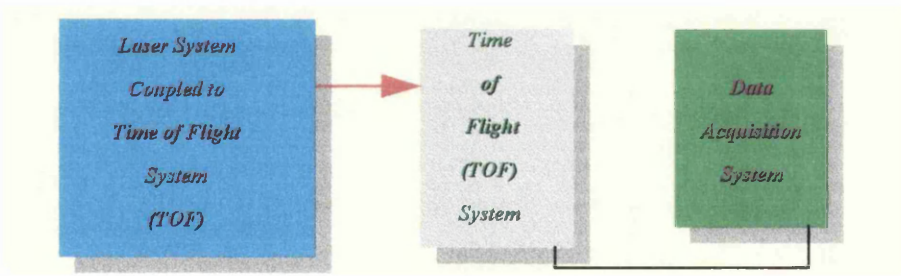


**Figure 3.1:** Outline of experimental set-up which is used to perform this work in this thesis.

A block diagram of the experimental system used in this work is shown in Fig.3.1. This consists of the nanosecond/femtosecond laser system, a detector system (in this case a time of flight mass spectrometer) and a data acquisition system. The same detector and data acquisition systems were used in both nanosecond and femtosecond laser mass spectrometry experiments.

In this chapter, some details of this above mentioned systems will be discussed briefly.

## 3.2 Laser Systems

The laser system consists of a pump and a dye laser. In this work two laser systems have been used which deliver laser pulses at 10 ns and 90 fs durations. The laser system was coupled to a linear time of flight (TOF) system to perform the detection of the ions produced by the laser energy absorbed *via* the multiphoton process as described in Chapter 2 in detail.

The nanosecond laser system is schematically shown in fig.3.2, which consists of a tunable dye laser pumped by a XeCl excimer laser at 308 nm.

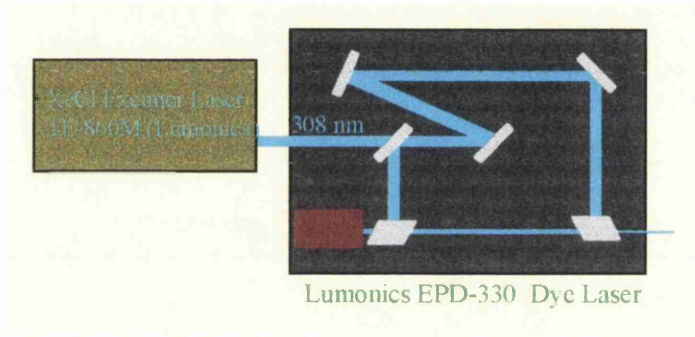


**Figure 3.2:** Diagram of a Lumonics-330 EPD dye laser pumped by a XeCl excimer laser at 308 nm.

The femtosecond laser system with its components is shown in detail in fig.3.3. The femtosecond laser system consists of a cw Ar-ion laser, Q-switched Nd:YAG laser, a mode-locked TISUNAMI and an amplifier laser system. In the femtosecond laser system, the components of the laser system will be described briefly. The detailed description of the femtosecond laser system has been given by Langley *et al.*, 1994.

A description of the XeCl, dye laser and Ti:sapphire laser systems will be given below and some other components and some relevant optical phenomena will also be discussed in this chapter.

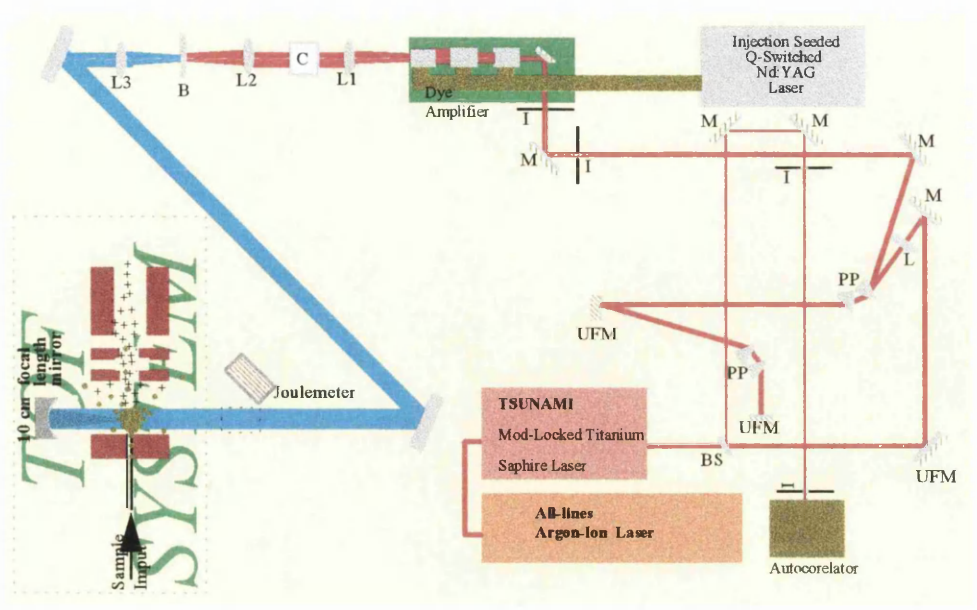


**Figure 3.3:** Components of femtosecond laser system showing lasers; Argon-Ion laser, Titanium sapphire laser, Nd:YAG laser and three stage amplifier dye laser with optical alignment and laser focusing conditions.
In figure; **BS:** Beam spliter, **UFM:** Ultrafast mirror, **M:** Aluminium mirror, **I:** Iris, **L:** Long focal length lens, **PP:** Prism pair, **L2:** 1m focal length lens, **L1:** 0.5 m focal length lens, **L3:** 0.5m focal length lens, **C:** Glass compressor (STF10), **B:** Type 1, BBO (28.7° Brewster angle) crystal.

### 3.2.1 Photochemical Operation of An Excimer Laser System

Generally speaking, excimer lasers are a group of pulsed lasers that incorporate electronic transitions within short lived-molecules. These lasers are usually composed of a combination of a rare gas atom, (Xe), and a halogen atom, (Cl). These lasers are capable of producing high power pulses of ultraviolet/VUV radiation with large beam cross-sections at high repetition rates.

Fig.3.4 shows a schematic energy level diagram of an XeCl excimer laser. This class of molecule has its own characteristics showing a bound structure in the excited state and repulsive/dissociative structure (unbound) in the ground states. This system is therefore unstable in its ground state and dissociates rapidly in a typical time scale of $10^{-12}$-$10^{-13}$s.

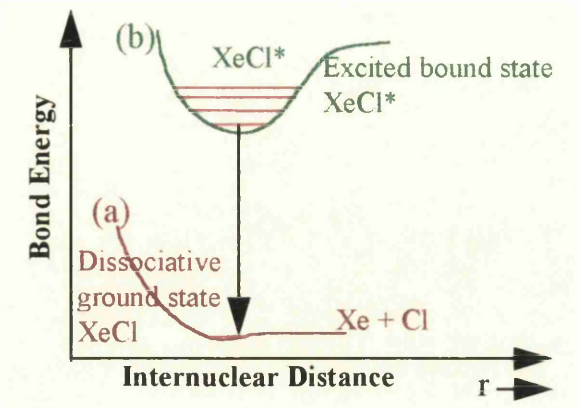


**Figure 3.4:** Energy levels of an excimer molecule (XeCl) showing (a) repulsive ground state, and (b) bound excited state.

This molecule can be formed only in the excited state by a chemical reaction between Xe and Cl ions produced by various special excitation techniques such as an electric discharge. After the excited state is formed, the population rapidly decays to the repulsive ground state and molecule subsequently falls apart. Thus, this molecule exists for only a time duration corresponding to the lifetime of the excited state which is typically 1-5 ns. Since no population is trapped in the ground state, the population inversion is easily achieved and high power pulses of UV radiation are readily available. Transitions between the bound excited state and the repulsive ground state result in the emission of radiation which constitutes the laser output. Typical output parameters of the Lumonics TE 860-3 (XeCl) excimer laser used in this work are given in Table 3.1.

| **Laser Parameters** | **Corresponding values** |
|---|---|
| Wavelength | 308 nm |
| Pulse length | 8-12 ns |
| Beam size | 8 mm x 12 mm |
| Beam divergence | 2.4 x 6 mrad |
| Maximum repetition rate | 70-80 Hz |
| Average pulse energy | 70 mJ |
| Stability (pulse to pulse) | ±5% |

**Table 3.1:** Output characteristics of excimer laser (Lumonics TE-860-3).

### 3.2.2 Photochemical Operation of A Dye Laser System

An energy level diagram for a typical organic dye molecule is shown in fig.3.5a. During the interaction of a pump laser pulse (pulsed pump laser, in this case a XeCl excimer laser) with a dye molecule, the dye molecule is excited from its ground state ($S_0$) to the excited vibrational levels of ($S_1$) state absorbing laser light from the excimer laser beam. The molecule in the excited state ($S_1$) undergoes several radiational and radiationless photoprocesses

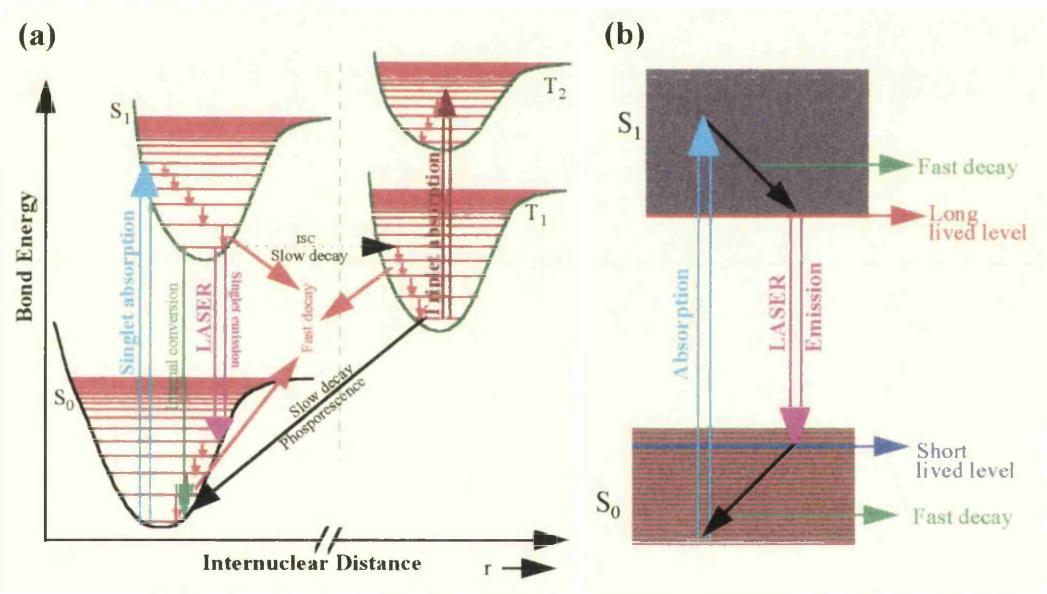


**Figure 3.5:** (a) Electronic energy levels and possible radiational and radiationless transition and absorption phenomena and (b) Ideal working four level laser system are shown.

The photochemical operation of this system can be explained in a similar way to that discussed in Chapter 2 for the fate of absorbed energy in the excited state for gas phase molecules but in this case we are dealing with a liquid sample. In the case of dye lasers, the laser dye is generally dissolved in a solvent such as methanol, ethanol, etc. The concentration of dye molecule in the solvent is very dilute allowing each dye molecule to be isolated from each other and it can therefore be assumed that no interaction between dye molecules takes place. But, on the other hand, dye

molecules can interact with surrounding solvent molecules. Interaction (collisions) between them is strong and vibrationally excited dye molecules thus are rapidly reset to the vibrational ground state of the electronically excited ($S_1$) state. This collisional relaxation process in each state ($S_0$, $S_1$, $T_1$ and $T_2$) is shown by red arrows in fig.3.5a and b and assigned as fast decay process.

The transition from the lowest vibrational level in the excited electronic ($S_1$) state to the highly excited vibrational levels in the ground electronic state of the molecule is the most likely to take place and forms the basis of fluorescence. In this case this transition is induced and so-called *laser* action can be obtained under optical pumping conditions. This laser action can be simply described as an ideal four level lasing system as shown in fig.3.5b.

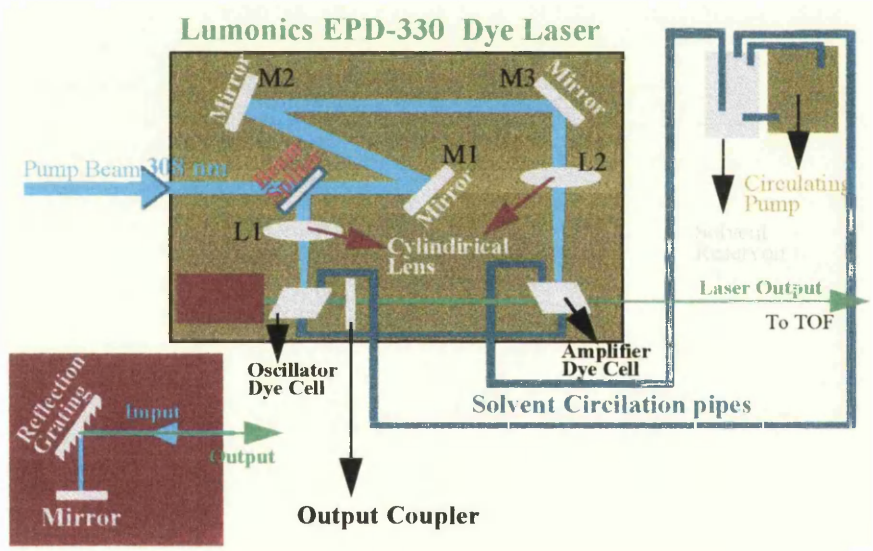


**Figure 3.6:** Components of dye laser system used to perform nanosecond laser experiments for this thesis.

The heating of the solvent by the interaction of the dye and solvent molecules induces radiationless transitions such as intersystem crossing (ISC). The $S_1$-$T_1$ transition can be overcome by circulating the dye solvent continuously by a pump through solvent circulation pipes shown in fig. 3.6. The solvent dye circulation is passed through both the oscillator and dye amplifier cells in order to rapidly remove dye molecules from the $T_1$ state to the lasing volume.

| Laser Parameters | Corresponding values |
|---|---|
| Tuning range | 320-950 nm |
| Pulse length | 6-10 ns |
| Spectral linewidth | <0.02 nm |
| Beam size | 2 mm x 2 mm |
| Beam divergence | <1 mrad |
| Polarisation | %95 vertical |
| Average pulse energy | 10 mJ |
| Stability (pulse to pulse) | ±5% |

**Table 3.2:** Output characteristics of dye laser (Lumonics EPD-330).

A diagram of the dye laser system in which a Lumonics EPD-330 dye laser, pumped by a Lumonics TE-330 excimer (Fig.3.2) is shown in fig. 3.6. The pump beam (at 308 nm) from the excimer (XeCl) laser is passed through a beam spliter and ~10% of the pulse energy is focused into the oscillator cell by a cylindrical lens (L1) and 90% of the pulse energy delayed, travelling *via* mirrors M1, M2 and M3 and focused into a laser amplifier cell by an other cylindrical lens (L2). The oscillator dye cell initiates the laser action. In the amplifier dye cell, the oscillator beam causes further stimulated emission and increases the oscillator power by a factor of ~15. Typical output pulse energies of about 8-10 mJ were easily obtained. Typical dye laser characteristic parameters are given in Table 3.2.

### 3.2.3 Wavelength Tuning System Connected to Dye Laser

Dye lasers are sources of tunable output over a large wavelength range. For a particular operation wavelength to be obtained a proper laser dye should be chosen. The lasing action at a wavelength near the peak of the fluorescence curve can be achieved by aligning the cavity mirrors to this gain region. In lasers with a broad gain bandwith it is often desirable to tune or select any specific laser wavelength over that gain bandwidth without changing the cavity mirrors. A simple means of providing such a wide range of tunability is to install a diffraction grating (or dispersive prisms within the mirrors) as one of the mirrors of the cavity. Tuning the wavelength is accomplished by rotating the grating. This arrangement is shown in

an inset diagram at the left-lower corner in fig. 3.6. The most important advantage of tunable dye lasers over other lasers is the relatively large tuning range and continuous tuning by means of the compuscan.

The EPD-5- motor drive and EPD-60 Compuscan connected to the dye laser allows the control of the wavelength parameters through a keyboard interface. The motor drive consists of a stepping motor and a microstep drive module offering extremely smooth motion. This motor drive unit controls the rotation of a mirror in the optical cavity which alters the angle of the laser beam incident upon the holographic grating.

### 3.2.4 Titanium Sapphire Laser

The titanium sapphire laser ($Ti:Al_2O_3$) is the most widely used tunable solid-state laser pumped by an all line 5 W cw Ar-ion laser (Fig. 3.3). The principles and photochemical operation system of an Ar-ion laser was given elsewhere (Svelto, 1989; Andrews, 1990). Typical operational parameters are given in table 3.3. The pump absorption and laser emission band spectrum and energy level diagram of a Ti:sapphire laser are shown in figs. 3.7a and b.

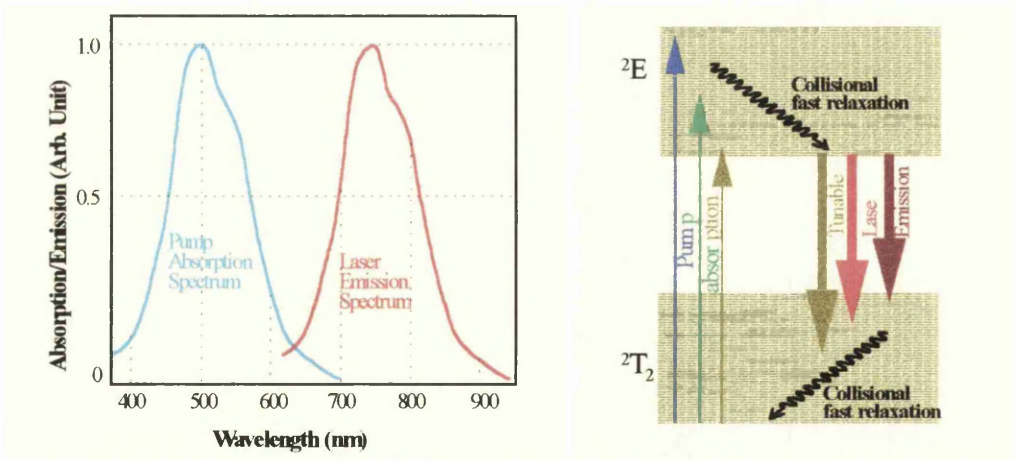


**Figure 3.7:** (a) Absorption and emission spectra of a titanium sapphire laser amplifier rod (in most laser text books), (b) Energy level diagram and lasing action for titanium sapphire laser and.

In the excitation mechanism, the ground state and excited state of a titanium sapphire laser is very similar to that of a typical four level laser system as explained in detail in figs. 3.5a and b, for a real and ideal laser system, respectively.

| Laser Parameters | Corresponding values |
|---|---|
| Wavelength | 750 nm |
| Pulse width | 90 fs |
| Beam diameter at $1/e^2$ points | <2 mm |
| Beam divergence, full angle | <0.6 mrad |
| Maximum repetition rate | 82 MHz |
| Noise | <2% |
| Polarisation | >500:1 vertical |
| Stability (pulse to pulse) | <5% |

**Table 3.3:** Specific parameters of Ti:sapphire laser used in this work.

### 3.2.5 Pulse Evolution

Ultrashort optical pulses (a few ps or fs) allow chemical reactions to be investigated in a time scale of about a vibration or even shorter time. The generation of such ultrashort laser pulses has been made by many groups (Fork *et al.*, 1981; Fujimoto *et al.*, 1984; Norris *et al.*, 1985; Squier *et al.*, 1991; Stingl *et al.*, 1994; Zhou *et al.*, 1994) by using generally mode-locking technique.

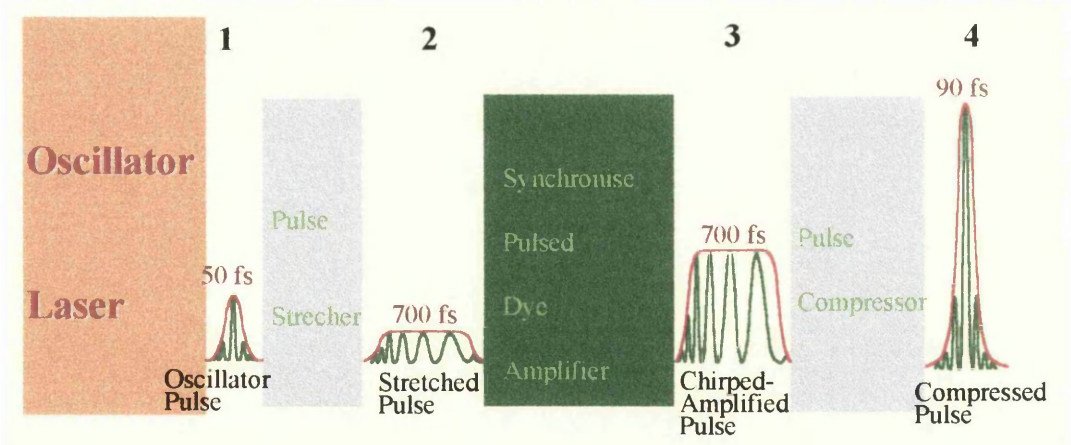


**Figure 3.8:** The pulse evolution stages indicating laser pulse widths for each stage with no accurate scale.

The laser pulse evolution system consists of four steps, as shown schematically in fig.3.8: the generation of ultrashort laser pulse (Fork *et al.*, 1981; Fujimoto *et al.*,

1984; Norris *et al.*, 1985; Squier *et al.*, 1991; Zhou *et al.* 1994; Stingl *et al.*, 1994; Perry and Mouro, 1994), pulse chirping (stretching) (Perry and Mouro, 1994; Yariv, 1997), amplification of chirped pulses (CPA) (Fork *et al.*, 1982; Duling *et al.*, 1985; Fleming, 1986; Knox, 1988; Perry and Mouro, 1994) and re-compression of the chirped-amplified pulses (Shank *et al.*, 1982; Strickland and Mourou, 1985; Fork *et al.*, 1987; Bergman *et al.*, 1994; Perry and Mouro, 1994).

In the case of the amplification of high repetition rate and high intensity laser pulses, the most important undesirable disadvantage is that during the passage of high intensity laser pulses through optics, the optics can be damaged by these high laser intensity effect. This problem can be avoided by stretching the pulses to a longer pulse width prior to amplification. This process reduces the laser intensity in the medium as indicated in fig.3.8.

When a high intensity laser pulse passes through the medium, the refractive index of a non-linear medium changes as a function of laser wavelength and laser intensity (Hutchinson, 1989; Svelto, 1990; Singhal, 1995; Davis, 1996). Thus, such a nonlinear medium disperses the laser beam as a function of the laser wavelength and intensity.

As the pulse travels in a dispersive medium, the shorter wavelength (higher frequency) is dispersed more than the longer wavelength (lower frequency), therefore the lower frequency part of the pulse (red shifted) moves faster than the higher frequency part (blue shifted) of the pulse. In this case the red part of the pulse arrives at the exit of the medium relatively earlier than the blue part of the pulse. This results in a pulse stretching and then the stretched beam has a time-dependent frequency (Fig. 3.8).

In the pulse stretcher system the 100 fs laser pulses was stretched to 700 fs laser pulse duration. The 700 fs laser pulses were amplified using a three stage dye amplifier pumped by a synchronously Q-switched Nd:YAG laser (Fig.3.3). A

simple diagram of the system used is shown in fig. 3.3. Details of the amplification process were given by Langley *et al.*, 1994.

The chirped-amplified laser pulses need to be compressed to obtain shorter laser pulses higher laser intensities. The chirped pulse has a time-dependent frequency distribution as indicated in fig.3.8. When these pulses pass through a nonlinear dispersive material (quartz class in this case) the red-shifted portion of the pulse is slowed down (higher refractive index) and the blue-shifted portion of the pulse is speeded-up (low refractive index). The leading edge of the pulse will arrive at the exit of the medium relatively later than the trailing edge and the process results in a shorter pulse length.

### 3.2.6 Experimental Measurement of Ultrashort Laser Pulse Width Using An Optical Autocorrelation Technique

The direct measurement and monitoring of ultrashort laser pulses is not yet possible because of the slow response of the detectors. In order to measure the width of short laser pulses (fs) the non-collinear second harmonic generation technique has generally been used (Weber, 1967; Fleming, 1985; Singhal, 1995; Yariv, 1997).

In order to measure the laser pulse width, an autocorrelator based on a Michelson interferometer and second harmonic generation technique was used and is schematically shown in fig.3.9. The laser beam enters the autocorrelator and is divided into two arms with a 50% ratio by a beam-spliter (BS). The rotating pair (RM) of parallel mirrors produces a variable delay on arm 1 with respect to the arm 2 as a function of the rotation speed of the shaft (Yasa and Amer, 1981).

A second harmonic signal was produced by focusing these two beams on to the nonlinear rotating crystal. The second harmonic signal was detected using an electron multiplier and displayed on the oscilloscope screen. The intensity of the second harmonic was monitored as a function of the relative delay between the two

arms (Singhal, 1995) and then the FWHM of the second harmonic signal was measured.

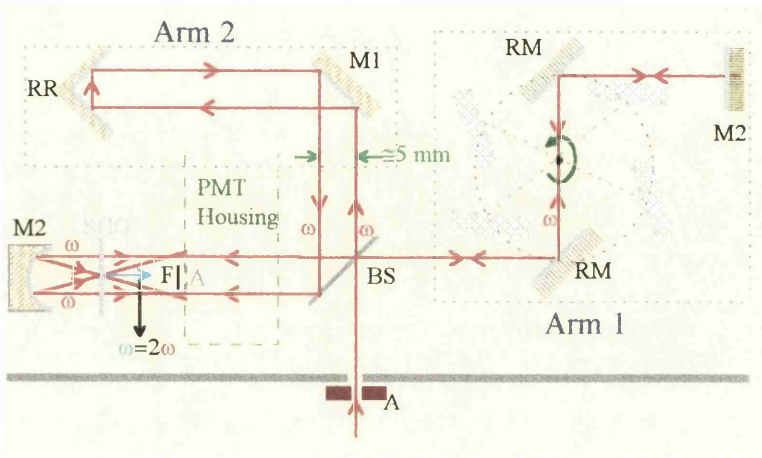


**Figure 3.9:** Configuration of Model FR-103XL Rapid Scanning Autocorrelator used in the experiments. Definitions are; RR: Retroreflector, F: Fundamental Blocking Filter A: Aperture, M1: Mirror, M2: Focus Mirror, RM: Rotating Mirror Pair, BS: Beam Spliter, SHG: Angle Tuned SHG Crystal (BBO)

This configuration of a pair of parallel rotating mirrors (RM) producing a repetitive generation of linear delay makes it possible to continuously monitor the autocorrelation function of the pulses after second harmonic generation. For the monitoring procedure a conventional high impedance oscilloscope synchronised to this rotation and the oscilloscope was triggered with escaped pulses from rotating mirrors.

## 3.3 Detection and Data Acquisition System

### 3.3.1 Time-of-Flight (TOF) Mass Spectrometer and Basic Principles and Operation of Time of Flight (TOF) Mass Spectrometer and Its Components

A time of flight mass spectrometer is a simple and easy to operate system with only an inlet system, an ionisation chamber and an ion acceleration region with an electron multiplier as an ion detector, as shown in fig. 3.10. The time of flight mass spectrometer separates ions of different masses due to their different velocities after

acceleration through a potential (V). A general and detailed consideration of mass spectrometer systems was made in a recent article (Boesl *et al.*, 1994).

The mass spectrometer is based on a Wiley-McLaren (Wiley and McLaren, 1955) design and shown in fig. 3.10. This time of flight (TOF) system has been described in detail elsewhere (Marshall *et al.*, 1992a; 1992b; 1992c; Clark *et al.*, 1993; Ledingham *et al.*, 1995b; Singhal *et al.*, 1996; Kilic *et al.*, 1997; Kosmidis *et al.*, 1997).

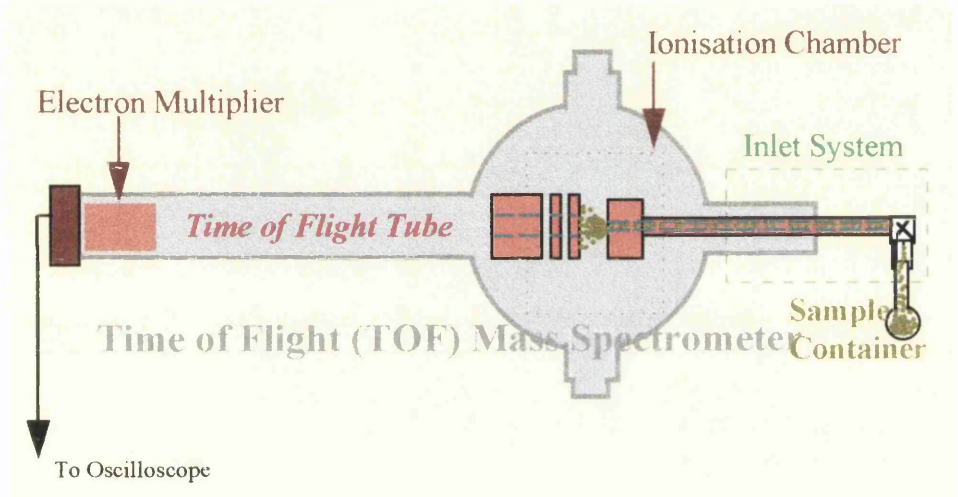


**Figure 3.10:** Time of flight (TOF) mass spectrometer and its parts.

The TOF is a conventional linear system of 1.2 m length pumped by a turbo pump to a base pressure of $10^{-8}$ torr. Optical parameters of the extract optics are based on a Wiley-McLaren design, and the ions were detected by a Thorn EMI electron multiplier. An einzel lens placed immediately after the extract optics increased the ion transmission through the system.

A detailed diagram (Fig. 3.11) shows the ionisation chamber in the mass spectrometer. This consists of a pusher plate, first optic, 2nd optic and an einzel lens, located parallel to each other. These components have different electric potentials to produce an electric field to accelerate the ions (see $V_1>V_2>V_3$ in fig.3.11) and the voltages on these plates were chosen to obtain maximum resolution.

The laser focusing condition is shown in fig. 3.11 indicating the laser spot size at the focal point. Fig. 3.12 is an exaggerated scale to emphasise the interaction volume. The ions are formed in the interaction region at some position in an accelerating electric field. They then gain kinetic energy before being injected into the field free drift region and are then separated due to their mass to charge ratios (m/q). They therefore arrive at the detector (Fig.3.10, an electron multiplier in this case) at different times. The time of flight, t, of an ion of mass m and charge q is given by

$$t = \ell\,[(m/q)/(2eV)]^{1/2} \qquad (3.1)$$

where $\ell$ is the distance travelled by the ions and V is the accelerating potential. In reality the determination of the length, $\ell$, is very difficult since the production of the same mass ions at different positions are possible as indicated in fig.3.12.

In TOF mass spectrometer, the ideal situation arises when ions of the same mass m/q ratio are formed in an infinitesimally thin volume which is perpendicular to the acceleration fields, and with no kinetic energy, the case of A in fig.3.12. In this situation, all ions of the same (m/q) ratio would arrive at the detector at precisely the same time, and the available mass resolution would be defined entirely by the electric characteristics of the ion detector.

However, in reality, the initial spatial, temporal and velocity distributions of the laser produced ions limit the resolving power of the instrument, and all three effects will be discussed below.

The cross sectional area of the ionising laser beam (Fig.3.12) is the sole cause of an initial ion spatial distribution. This limits the resolution due to the variation in flight time for ions of the same m/q ratio which are produced at different points in the laser sample interaction volume as shown in fig.3.12. This may be reduced if beam focusing is employed, although in doing so the actual number of molecules interrogated by the laser beam is reduced due to the reduction in geometrical overlap.

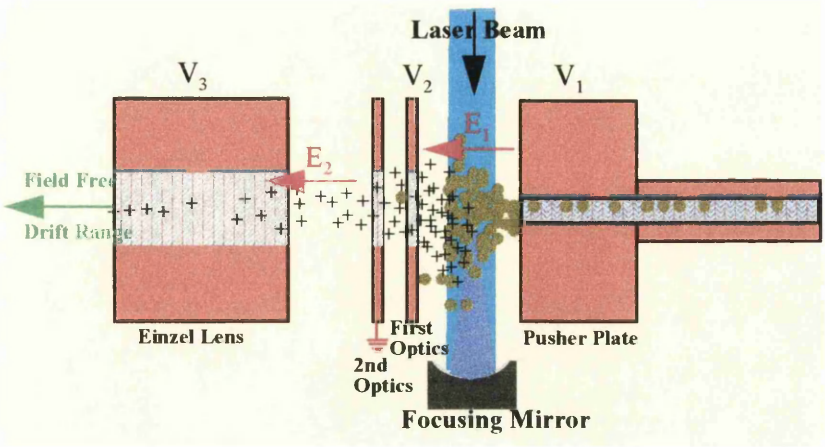


**Figure 3.11:** The ionisation chamber which consists of a conventional double field extraction system with singly charged ions produced as a result of the interaction of focused laser pulses with neutral molecules. The ions produced gain an energy $eV_1$ before entering to the field free time of flight tube (drift region).

The initial temporal distribution is due to only the finite length of the ionising laser pulse (laser pulse length, ~10 ns and 90 fs for nanosecond and femtosecond laser pulse in our cases). Each isomass ion packet will therefore have a temporal spread of at least this value at the detector position, and so this represents an upper limit on the available mass resolution, the case of B in fig.3.12.

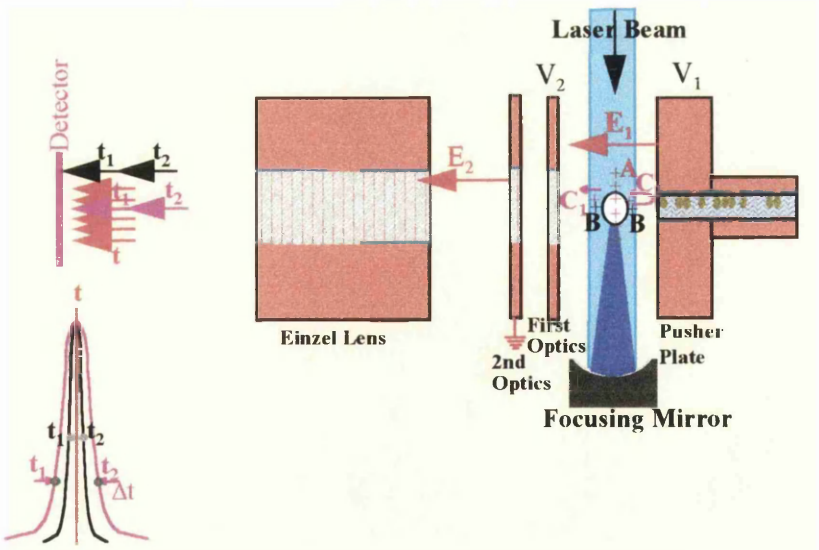


**Figure 3.12:** Diagram shows two extreme case for the positions where same mass ions might be produced and for both case the appearances of a mass ion peak in the mass spectrum.

The mass resolution is also reduced due to the initial velocity distribution of ions formed in the interaction region. In the very worst case, ions of equal mass having the same speed but initially travelling in opposite directions, case of C in fig. 3.12, arrive at the detector with a time difference equal to the turn-around time, $\Delta t$, of the ion moving away from the detector and resulting peak is shown with broad peak in pink colour in fig.3.12.

In the Wiley-Mclaren design, a compromise is met in overcoming the adverse effects of initial spatial and velocity distributions. In the former cases, the potential drop across the ionising laser beam width is kept low so that ions gain most of their kinetic energy from the second acceleration region and therefore the fractional difference in their final energies is smaller. In particular, they showed theoretically that a suitable choice of the voltages $V_1$ and $V_2$ resulted in isomass ions being spatially focused at the detector position. However, to minimise the effects of an initial non-zero ion velocity distribution, it is desirable to have the electric field in the source region as large as possible in order to reduce the turn-around time $\Delta t$. In our experiments, the initial spatial distribution was kept at a minimum by focusing the laser beam, so it is expected that the main source of resolution degradation is from an initial velocity distribution.

### *3.3.2 Electron Multiplier*

The ions produced within a single laser pulse arrive at the detector within a time as a function of the flight path length (eq. (3.1)). In order to detect the ions a Thorn-EMI electron multiplier was connected to a LeCroy 9304 digital oscilloscope. The detector works on the principle that an ion strikes the dynode which then releases a number of electrons for each strike. The liberated electrons are accelerated through an electric field. If each accelerated electron hits a secondary dynode thus resulting a number of electrons being released by dynodes caused by each electron then it continues increasing the number of electrons ejected. The final number of electrons build up an electric current which can be detected and displayed on an oscilloscope

screen. The current produced by this process appears on the screen as a mass spectrum in our application. In this way the electron multiplier behaves like an amplifier.

### 3.3.3 Presentation of A Mass Spectrum

When a molecule absorbs photons it can ionise or fragment to produce smaller ions and neutrals. These in turn can absorb more photons to produce still smaller particles. This results in a mass spectrum being formed.

In the recorded mass spectrum (Fig. 3.13), the vertical axis is a measurement of the number of ions produced for a particular mass and presented as a function of the time of flight indicated by the lower horizontal axis of the spectrum. The m/q is presented as a function of flight time in the upper horizontal axis.

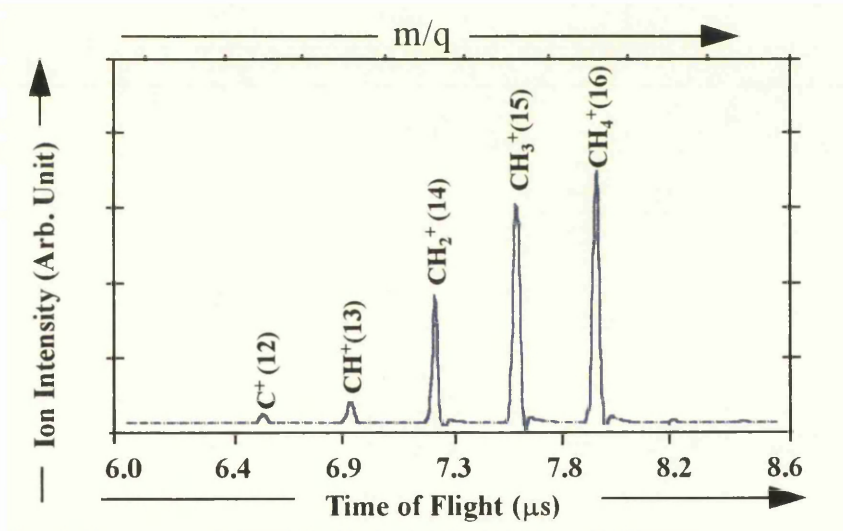


**Figure 3.13:** A typical example for time of flight (TOF) mass spectrum.

In general, neutral molecules have an even number of electrons in their highest occupied molecular orbital. When one of them is removed, the molecule is left with a single electron and the molecular ion could be seen with a single positive charge (q=1) thus the mass ion peak can often be labelled using only mass m instead of m/q ratio because m/q becomes equivalent to the mass, m, of ion.

### 3.3.4 Calibration and Identification of Particular Mass Ion Peaks

The ions arriving at the detector was recorded using a LeCroy 9304 digital oscilloscope and the flight time for each mass ion can be read directly from the oscilloscope in μs. The time of flight calibration was carried out by examining a particular well known small molecular sample. $NO_2$ was considered as the best sample to calibrate the system because it gives only the $NO^+$ and $NO_2^+$ peaks in the spectrum. Once the flight time is calibrated other molecular mass ion peaks can easily be determined using the relationship between flight time and ion mass given by

$$t^2 = ma+b \tag{3.2}$$

The calculation of the a and b constants could be performed choosing two well estimated mass ion peaks, $m_1$ and $m_2$, and using corresponding flight times $t_1$ and $t_2$. Once a and b are calculated the mass for each peak can be determined using the equation

$$m = (t^2-b)/a \tag{3.3}$$

### 3.3.5 Data Acquisition Systems

The data acquisition was performed using a LeCroy 9304 digital oscilloscope. This was a multipurpose oscilloscope and was used for analysis, display and storing waveforms.

Front panel knobs and buttons of the oscilloscope provide easy use. A 550 K memory card has been installed for speed storage and a DOS format floppy disk to extend the storage memory to 1.44 MB without a computer. The data was recorded after performing a summed averaging over a number of laser shots. The maximum number of laser shots can be initially chosen and when the maximum number of sweeps has been reached, the averaging process stops. The oscilloscope is triggered with a portion of laser light from beam spliter *via* a photodiode placed in front of the dye laser. If a suitable and stable trigger is available, the resulting

average has a reduced random noise component compared with the single shot record. In this work the averaging was performed over a few hundred or sometimes thousands of laser shots and a good signal to noise ratio was obtained.

The recorded signal can be plotted using an X-Y plotter. In this work the mass spectra was converted into a PC computer format and the final form of the spectra was obtained. This facilitates ease of manipulation of the data using a computer and puts the spectrum into text format.

## 3.4 Laser Diagnostics

### 3. 4.1 Measurement of Pulse Energy

For the laser pulse energy dependent experiments to be carried out, an accurate measurement of the laser pulse energy is particularly important. The pulse energy measurement is carried out before the laser beam enters the time of flight mass spectrometer just in front of the entrance window. The laser beam is focused down to the size of photosensitive surface of joulemeter to make sure that all photons in the pulse are collected for measurement.

A Molectron J3-09 pyroelectric joulemeter was used for measuring the pulse energy. The operation principles of the joulemeter lie on the photophysical characteristics of a photosensitive lithium tantalate crystal. The crystal rapidly heats after absorbing laser photons and becomes electrically polarised. This polarisation produces a surface charge which is collected, electronically integrated and displayed on the oscilloscope screen in the voltage units. The peak height of the signal is then proportional to the absolute pulse energy with the calibration of our particular model being 1.25 V/mJ. The Joulemeter is designed for operation with pulse widths ranging from picosecond to 250 μs.

### 3.4.2 Optical Attenuation of Laser Pulse Energy

Power dependence experiments were carried out by recording time of flight mass spectrum for different pulse energies. The pulse energy was measured each time using a joulemeter. In the nanosecond experiments, the laser pulse energy was altered using a Newport 935-5 model optical attenuator.

The femtosecond laser pulse energies were altered using neutral density filters and measured using the same joulemeter used to measure the nanosecond laser pulse energies mentioned above.

### 3.4.3 Determination of Spot Size of Focused Laser Beam

The spot size of the focused laser beam can be determined by theoretically using the relationship between the diameter of laser beam before and after the focusing operation and the focal length of optics used. If it is assumed that the laser power distribution is Gaussian shaped then the radius of the focused beam can be calculated (Langley *et al.*, 1995) by

$$w_0 = (1.22\, f\lambda)/\pi D \qquad (3.4)$$

where f is the focal length of optic (a mirror or lens) and D is the diameter of the collimated laser beam before focusing. It can be seen from eq. (3.4) that the spot size of the focused beam is a linear function of the laser wavelength used and the focal length of lens/mirror.

In the experiments carried out in this work, two laser wavelengths 375 nm and 750 nm have been used. In the nanosecond experiments only 375 nm has been performed while both wavelength were used in the femtosecond experiments. In both laser pulse experiments either a 30 cm focal length lens or a 10 cm focal length mirror was used. The diameter of the laser beam on the lens or mirror before focusing was measured as 1 cm. Typical calculated parameters of focused laser beam are given in Table 3.4.

| Laser Wavelength (nm) | 10 cm Focal Length Mirror | | | 30 cm Focal Length Lens | | |
|---|---|---|---|---|---|---|
| | Radius (μm) | Spot Area ($cm^2$) | Intensity ($W/cm^2$) | Radius (μm) | Spot Area ($cm^2$) | Intensity ($W/cm^2$) |
| 375 | 4.575 | $6.59x10^{-7}$ | $1.69x10^{14}$ | 13.73 | $5.93x10^{-6}$ | $1.87x10^{13}$ |
| 750 | 9.15 | $2.63x10^{-6}$ | $1.27x10^{14}$ | - | - | - |

**Table 3.4:** Laser waist, laser spot area and laser intensities at the focal point for 10 cm focal length mirror and 30 cm focal length lens at 375 nm and 750 nm.

### 3.4.4 Calculation of Laser Intensity in the Interaction Region

In our application, the laser pulse energy was measured using a molectron joulemeter in joule and the pulse power was calculated using a relationship, eq.(3.5), between laser pulse energy and laser pulse duration.

$$P\ (W) = E(J)/\tau(s) \tag{3.5}$$

where E is the laser pulse energy and $\tau$ is laser pulse width. Using the result of this equation, the laser intensity was calculated using eq. (3.6)

$$I\ (W/\ cm^2) = P\ (W)/\text{Spot Area}(cm^2) \tag{3.6}$$

The results for laser pulse energies of 10 μJ at 375 nm and 30 μJ at 750 nm at 90 fs laser pulse width are given in Table 3.4.

# CHAPTER 4

# RESONANCE ENHANCED MULTIPHOTON IONISATION (REMPI) AND DISSOCIATION PROCESSES OF NO AND $NO_2$ MOLECULES

## Contents

## 4.1 Introduction

The nitrogen oxides are commonly found as pollutants, because they can be formed during combustion, and generally labelled together as $NO_x$. Nitric oxide is chemically very reactive, and is easily oxidised by oxygen to nitrogen dioxide. Nitrogen dioxide, $NO_2$, is also very reactive with organic molecules, and under atmospheric conditions it is a key factor in producing smog because it combines with unburned hydrocarbon emissions in the exhaust gases of cars. Combustion, production and chemical reaction mechanisms of NO and $NO_2$ have been investigated in detail in a recent article (Warnatz et al, 1996).

The nitric oxide (NO) molecule, which is a heteronuclear diatomic molecule and one of the smallest molecules studied in this thesis as well as one of the simplest molecular structures in chemistry, is one of the first molecules which was investigated using resonance enhanced multiphoton ionisation (REMPI) technique (Johnson *et al.* 1975). Its photophysical and photochemical properties have been extensively studied for many years (Brook and Kaplan, 1954; Gero and Schmid, 1948; Hesser, 1966; Warnatz *et al.*, 1996). The NO molecule is chemically very active and the knowledge of its reactions and structure are of great importance since the molecule participates in many atmospheric, polluting and industrial processes. The absorption, emission and fluorescence spectrum of NO from infrared to ultraviolet range has been analysed since 1920s. The spectroscopic structure and parameters of the NO molecule have been determined and well documented using different methods from discharge to modern laser spectroscopy, by several groups (Leifson, 1926; Gaydon, 1944; Gero and Schmid, 1948; Sutcliffe and Walsh, 1953; Brook and Kaplan, 1954; Barrow and Miescher, 1957; Lagerqvist and Miescher, 1966; Hesser, 1968; Jungen and Miescher, 1968; Suter, 1969; Callear and Pilling, 1970a and 1970b; Miescher, 1971; Brzozowski *et al.*, 1974; Johnson , 1975a).

The electronic excitation and ionisation spectrum of NO can easily be produced over all spectral ranges from far infrared to the vacuum ultraviolet (Zacharias *et al.*, 1980; Zacharias *et al.* 1981; Rottke and Zacharias, 1985; Rudolph *et al.*, 1988; Zakheim and Johnson, 1978) since it is a very stable molecule and has long lived excited states (Benoist D'azy *et al.*, 1975; Brozowski *et al.*, 1974). The $NO^+$ ion is usually formed by the ionisation of the neutral NO molecule produced from the dissociation of a neutral parent molecule containing NO.

While the absorption, emission and ionisation spectra of simple diatomic molecules can easily be analysed, the spectra of molecules with more than two atoms show a complicated structure and to analyse them becomes more difficult. Small polyatomic molecules, such as $NO_2$ commonly possess complex band systems in the visible or ultraviolet regions of the spectrum (Hsu *et al.*, 1978; Okabe, 1978; Calvert and Pitts, 1966). These kinds of molecules were an unsolved problem for a long time. One of the reasons that ultimately lead to the solution of the structure in many complex molecules was the realisation that small polyatomic molecules may change their electronic shape on the electronic excitation. Absorption, excitation, dissociation and ionisation dynamics of the $NO_2$ molecule have been of great interest for scientists (Delon *et al.*, 1995; Jackels and Davidson, 1976a; Jackels and Davidson, 1976b; Gillispie *et al.*, 1975; Merienne *et al.*, 1995; Douglas and Huber, 1965; Stevens *et al.*, 1973; Smalley *et al.*, 1975; Georges *et al.*, 1995a and 1995b; Aoki *et al.*, 1996) and will, in some aspects, be discussed in this and later chapters of this thesis.

## 4.2 Energy Levels in NO and $NO_2$ Molecules

### 4.2.1 Electronic Energy Levels in NO

The ground state of the NO molecule was firmly established as a $^2\Pi$ state. The electronic configuration in the $X^2\Pi$ ground state of the NO has a 15 electron structure with one electron in the anti-bonding valance orbital $\pi^*$. When one of the

electrons from the antibonding orbital is removed, the electronic structure of the remaining 14 electrons has an electronic configuration of the ground state of $NO^+$ which is expressed as $NO^+(X^1\Sigma^+)$.

The absorption spectrum of NO has been well documented and in the literature, the absorption bands from $X^2\Pi$ to the electronic excited states $A^2\Pi$, $B^2\Pi$, $C^2\Pi$ and $D^2\Sigma^+$ are called the $\gamma$, $\beta$, $\delta$ and $\varepsilon$ bands, respectively (Gaydon, 1944). Most of the electronic excited states in NO have high energies and lie just below the ionisation limit (Gilmore, 1966; Lagerqvist and Miescher, 1966; Miescher, 1971; Jungen and Miescher, 1968; Suter, 1969).

For the particular laser wavelengths used in this work, the multiphoton excitation and ionisation processes take place through the $\varepsilon$ band system in the NO molecule. A simple energy diagram of the $\varepsilon$ band system of NO molecule, which is relevant to our work in this thesis at 375 nm and 750 nm, is shown in Fig. 4.1.

### 4.2.2 Energy Levels in $NO_2$ Molecule

The absorption spectrum of $NO_2$ shows a very complex structure and no regularity in the rotational bands. In the ps regime the dynamics of the spectrum shows a chaotic structure, while for shorter times, the dynamics exhibits a regular behaviour and it is suggested that it can be observed with a fs pump-probe experiment (Georges *et al.*, 1995a).

The first excited state of $NO_2$ is $A^2B_2$ and lies above 9737 $cm^{-1}$ (Delon and Jost, 1991a) and is strongly mixed with the vibrationally excited levels of the $X^2A_1$ ground state, which is indicated in Fig. 4.1. The $^2B_1 \leftarrow ^2A_1$ and $^2B_2 \leftarrow ^2A_1$ are allowed, electric dipole transitions, but the $^2A_2 \leftarrow ^2A_1$ transition is weaker (Gangi and Burnelle, 1971; Walsh, 1976). The visible spectrum of $NO_2$ is dominated by the $A^2B_2 \leftarrow X^2A_1$ transition. It is well known that there are some contributions to the absorption spectrum in the visible region coming from the $^2B_1 \leftarrow X^2A_1$ transition.

The electronically excited state, $A^2B_2$, has been the subject of a number of recent articles, and the vibrational and rotational energy levels are mostly identified over an energy range from 9737 $cm^{-1}$ to 23600 $cm^{-1}$ in a series of experimental and theoretical works (Delon and Jost., 1991a; Delon *et al.*, 1991b; Aoki *et al.*, 1993; Georges et al, 1995a; 1995b; Delon *et al.*, 1995; Aoki *et al.*, 1996). To the author's knowledge, there is no information about the vibrational energy levels in this electronic state with energies higher than 23600 $cm^{-1}$ in the literature, but it is known that the strength of the interactions between the higher vibrational states of $X^2A_1$ and $A^2B_2$ increases as the vibrational quantum number, $v$, increases (Miyawaki *et al.*, 1993; Ionov *et al.*, 1993; Rohlfing and Valentini, 1985).

## 4.3 Dissociation and Ionisation Mechanisms In NO and $NO_2$

Resonant enhanced multiphoton ionisation (REMPI) is one of the most sensitive and selective spectroscopic techniques which has proved to be of considerable value in the study of atomic and molecular states ( Johnson and Otis, 1981, Clark *et al.*, 1993; Marshall *et al.*, 1993; 1994a). The sensitivity and selectivity is the main reason that REMPI is used to study trace elements and molecules.

In this work, we have carried out a series of experiments on $NO_2$ molecule using the nanosecond and femtosecond laser mass spectrometry. For this experiments, we have used only one laser wavelength at 375 nm for the nanosecond laser mass spectrometry and two different laser wavelengths at 375 nm and 750 nm for the femtosecond laser mass spectrometry. The results of these experiments are presented and compared with theoretically calculated results of rate equation modelling.

The extensive spectroscopic studies on $NO_2$ suggest that the complex structure of this molecule is due to the strong interactions between the ground state and the low lying electronic excited $A^2B_1$, $A^2B_2$ and $A^2A_2$ states. A simple energy level diagram in fig. 4.1 shows the ground state $X^2A_1$ and the low lying excited $A^2B_2$ and higher

excited $B^2B_2$ state of $NO_2$ which are particularly relevant to the work in this thesis (Gangi and Burnelle, 1971; Aoki *et al.*, 1996; Singhal *et al.*, 1996).

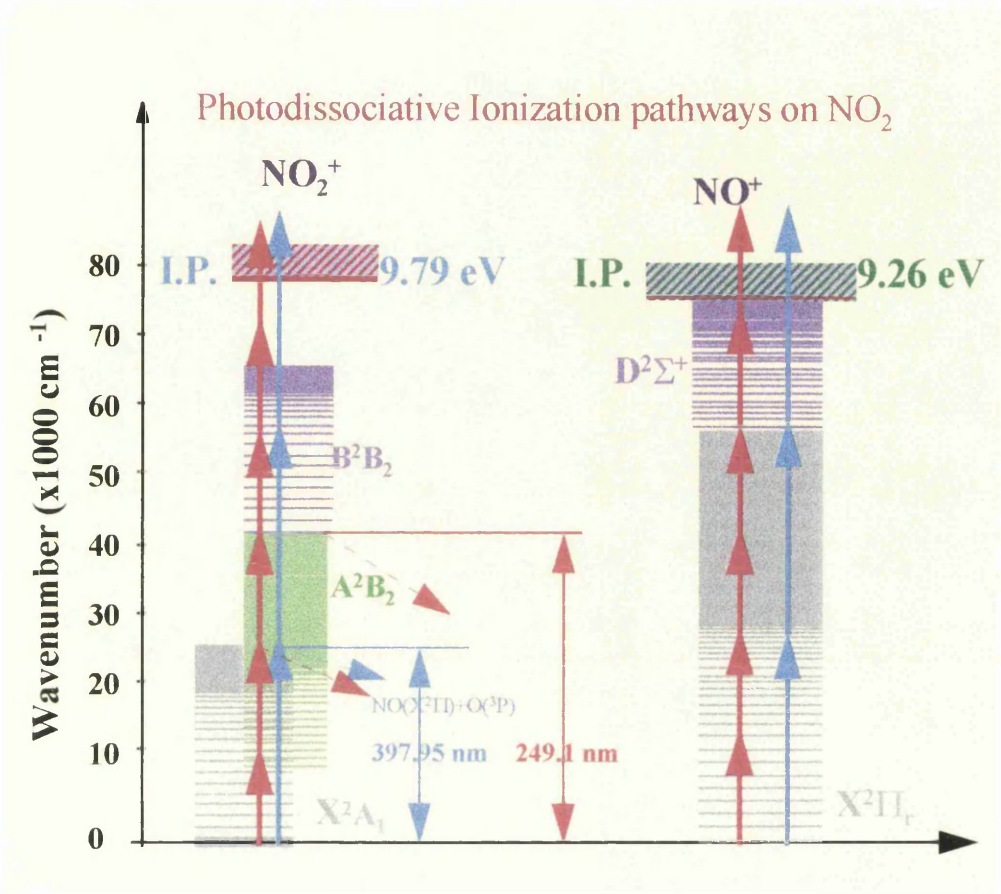


**Figure 4.1:** The dissociation and ionisation pathways of NO and $NO_2$ are shown.

Figure 4.1 shows the dissociation and ionisation routes of NO and $NO_2$ molecules. The dissociative ionisation processes in $NO_2$ have been discussed using different laser wavelengths and laser pulse widths in a number of articles and it is now well known that there are two different dissociation states, as indicated in Fig. 4.1, that have been identified and partially characterised (Hallin and Merer, 1976; Robra *et al.*, 1990; McFarlane *et al.*, 1991; Miyawaki *et al.*, 1991; Kumar et al., 1994; Ledingham *et al.*, 1995a; Jost *et al.*, 1996; Singhal *et al.*, 1996). The first dissociation limit of $NO_2$ was determined some time ago (Chen *et al.*, 1980; Robra *et al.*, 1990) and has been recently confirmed (Jost *et al.*, 1996) and found to be 397.95 nm which is in good agreement with the previous values of 397.92 nm

(Robra *et al.*, 1990) and 397.93 nm (Chen *et al.*, 1980). The second dissociation channel lies just below the $B^2B_2$ electronic excited state (Herzberg, 1966) and the dissociation limit was measured to be 249.1 nm (Hallin and Merer, 1976).

Principally these are two dissociation channels which can be opened to produce $NO(X^2\Pi)$ and $O(^3P_J)$ through eq.(4.1) from the first dissociation limit with energy threshold of 3.11 eV,

$$NO_2(X^2A_1) + h\nu \rightarrow NO(X^2\Pi) + O(^3P_J) \quad (4.1)$$

and $NO(X^2\Pi)$ and $O(^1D_J)$ through eq.(4.2) from the second dissociation limit with an energy barrier 4.977 eV,

$$NO_2\ (X^2A_1) + h\nu \rightarrow NO(X^2\Pi) + O(^1D_J) \quad (4.2)$$

It is also known that the first dissociation channel leaves NO in the lowest vibrational level of the ground electronic state (Miyawaki *et al.*, 1993), $X^2\Pi$, and the second dissociation channel produces NO in the vibrational excited levels of the ground state (McFarlane *et al.*, 1991).

## 4.4 The Mass-Spectrometry of NO and $NO_2$; Dissociation and Resonance Enhanced Multiphoton Ionisation (REMPI) Dynamics

### 4.4.1 Experimental Arrangement

The details of the nanosecond and femtosecond experimental systems as well as detector system were given in chapter 3 and elsewhere (Marshall *et al.*, 1993; 1994b; Kosmidis *et al.*, 1994a; 1994b; Langley *et al.*, 1994; Ledingham *et al.*, 1995b; Singhal *et al.*, 1996; Kilic *et al.*, 1997; Kosmidis *et al.*, 1997).

In a brief description of nanosecond system, it consists of a Lumonics (TE 860-M XeCl) excimer (308 nm) laser pumping a Lumonics dye laser system (EPD 330 Models) with pulse and line widths being nominally 10 ns and 0.01 nm and operated at 10 Hz. The laser dye used in the experiment was TMI whose output covers a

wavelength range from 353 nm to 384 nm with a peak power about 370 nm. The pulse energy was measured using a Molectron Model J3-09 Pyroelectric Joulemeter. The laser pulse energies were a few mJ and the beams were focused using a 30 cm focal length lens to give intensities of $10^{8-9}$ $Wcm^{-2}$.

The femtosecond laser system (Fig.3.3) gives an output of laser light at the wavelength of 750 nm with 90 fs pulse width. The laser light at 375 nm was generated by focusing the fundamental output of the laser to a type 1 BBO crystal (B in Fig.3.3) cut at 28.7 degrees. The experiment at 750 nm was carried out using the fundamental output wavelength of the laser system. The band widths of the laser pulses at 90 fs are about 5 nm and 10 nm for 375 nm and 750 nm, respectively. The laser beam was collimated with a 0.5 m fused silica lens (L3 in Fig.3.3) to give a beam diameter of 1 cm. The femtosecond laser pulses were directed towards the mass spectrometer with UV mirrors. Before entering the TOF mass spectrometer, the 375 nm and 750 nm pulse energies were typically 10 μJ and 40 μJ. The laser beam was tightly focused in the interaction region using a 10 cm focal length mirror, which was placed in the vacuum. The spot size of the focused beam was a function of the wavelength and determined using eq. (3.4). Intensities of about $10^{12-14}$ $W/cm^2$ could be generated (Table 3.4), although smaller pulse intensities were generally used.

A conventional home made time of flight mass spectrometer with a linear system of 1.2 m length (Fig.3.10) were used for both the nanosecond and femtosecond experiments with similar experimental conditions. The spectrometer was pumped by a turbo pump to a base pressure of $10^{-8}$ Torr. The NO and $NO_2$ samples were admitted effusively from the inlet system to the high vacuum system through a needle valve. Typical sample pressure during data taking were a few times $10^{-5}$ Torr. The time-of-flight mass spectra were recorded by taking the electron multiplier output directly into a LeCroy 9304 digital oscilloscope and averaging over hundreds or thousands of laser shots.

The wavelength dependent spectra in nanosecond regime were obtained by scanning the wavelength over the resonance range using a tunable dye laser and compuscan. The ion signal was recorded using a Stanford Research "SR 250" boxcar averager which was interfaced with a Macintosh IIfx computer.

### 4.4.2 Nanosecond Resonance Enhanced Multiphoton Ionisation (REMPI) of NO from the Dissociation of $NO_2$ Molecule

The dissociation and ionisation processes in NO and $NO_2$ has been discussed in previous section. The purpose of this chapter is to describe the experimental application of REMPI to both nitric oxide (NO) and nitrogen dioxide ($NO_2$) with particular emphasis to the $NO^+$ ion, using different laser pulse widths and different REMPI processes. The REMPI process has been used to produce $NO^+$ ion from $NO_2$ over the wavelength range 370-283 nm using nanosecond laser pulses.

In this experiment, a TMI dye molecule was used, whose output covers a wavelength range over 353-384 nm and the fundamental laser light output at the wavelength of 375 nm was used. The wavelength dependence spectrum was produced by scanning the wavelength over a range from 370 nm to 383 nm by means of a compuscan.

For the neutral NO molecule, the resonance $D^2\Sigma^+(v'=0)\leftarrow X^2\Pi(v''=0)$ transition at the wavelength about 187.5 nm can be reached with absorption of two photons of 375 nm (Singhal *et al.* 1996; Ledingham *et al.* 1995b; Kilic *et al.* 1997) with a corresponding excited state energy of 6.605 eV (Heicklen and Cohen, 1968). This transition energy is given elsewhere as 6.67 eV, (theoretical), and 6.61 eV, (experimental), (Delaney *et al.*, 1982). Previous measured dissociation energies of NO were 6.5 eV (Gaydon, 1944) and 6.48 eV (Herzberg, 1950; Brook and Kaplan, 1954). These values are all in agreement and lie just below the electronically excited $D^2\Sigma^+$ level. The ionisation potential for NO is $\approx$ 9.26 eV (Reiser *et al.* 1988) and the molecule can be ionised absorbing three photons of 375 nm from its ground state since the total energy of three photons of 375 nm is $\approx$ 9.92 eV.

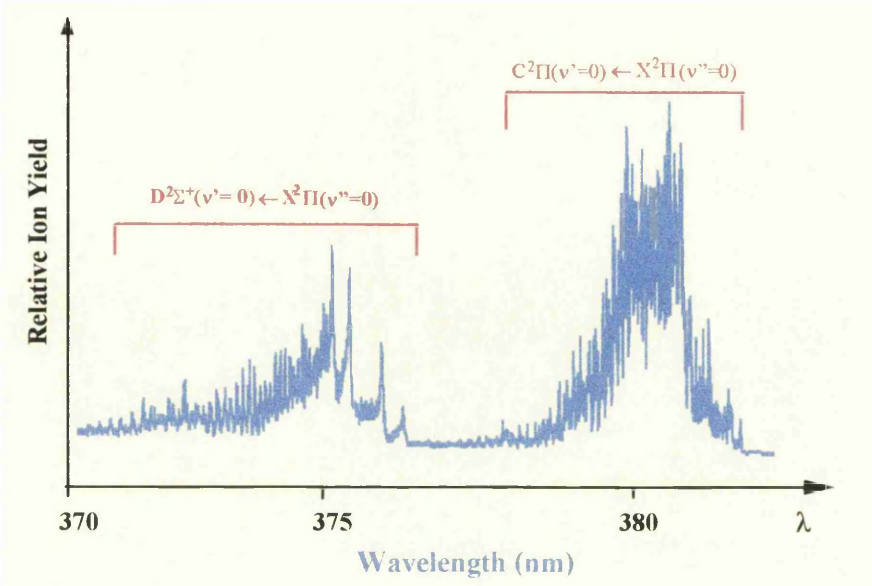


**Figure 4. 2:** The wavelength dependence of $NO^+$ from pure $NO_2$ gas.

The wavelength dependence of $NO^+$ over 370-383 nm at 10 ns is shown in fig.4.2. In this study, the strong wavelength dependent signature of the NO molecule was observed due to the very high enhancement of the ionisation efficiency on the resonant wavelengths. The resonance enhanced multiphoton ionisation of the NO molecule in the relevant range are shown about 375 nm and 382 nm corresponding $D^2\Sigma^+(v'=0) \leftarrow X^2\Pi(v''=0)$ and $C^2\Pi(v'=0) \leftarrow X^2\Pi(v''=0)$ transitions, respectively, *via* a two photon excitation and one photon (2+1) ionisation scheme.

### 4.4.3 The Femtosecond and Nanosecond Laser Mass Spectrometry on $NO_2$ at 375 nm

Multiphoton ionisation and dissociation dynamics for 90 fs and 10 ns laser pulses at 375 nm were carried out. The pulse width dependence of dissociation process changes depending on the lifetime of the sample in the excited state since the lifetime of the $NO_2$ depends on the laser pulse width whether it is femtosecond or nanosecond (Ledingham *et al.*, 1995a).

The multiphoton absorption of $NO_2$ gas and the competition between direct photoionisation to $NO_2^+$ ion and dissociation to NO+O and subsequent multiphoton

absorption and ionisation, has been the subject of recent papers (Fig.4.1) (Ledingham *et al.*, 1995a; Singhal *et al.*, 1996) for a number of different laser pulse widths from nanoseconds to femtoseconds. For the case of 375 nm laser photons, the $NO_2$ molecule reaches the first dissociation limit after absorbing one photon of 375 nm and two more photons are needed for the $NO_2$ molecule to be ionised (Ledingham *et al.*, 1995b; Singhal *et al.*, 1996; Kilic *et al.*, 1997). The experiment was carried out on $NO_2$ gas for different pulse energies at 375 nm for ns and fs laser pulses. The laser pulse energy was changed using a neutral density filter for the femtosecond and a Newport model 935-5 optical attenuator for the nanosecond experiments and measured using a joulemeter. The laser pulse energy dependence of the $NO^+$ and $NO_2^+$ will be discussed with the theoretical results from the rate equation model later in this chapter.

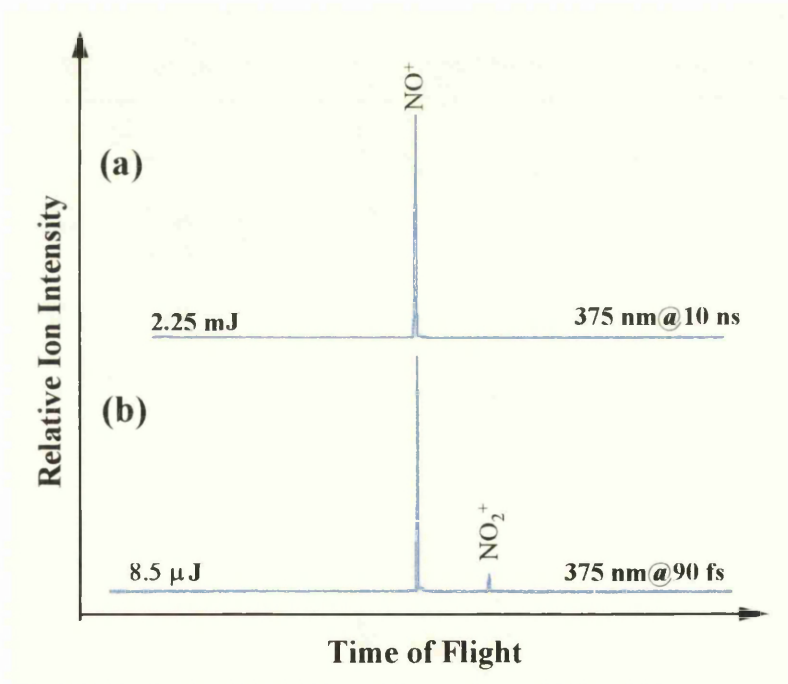


**Figure 4. 3:** A comparison of femtosecond and nanosecond spectra of $NO_2$ is shown. The spectra were taken using a) 10 ns, b) 90 fs width laser pulses at wavelength 375 nm.

The $NO^+$ ion was obtained by ionising the neutral NO molecule which comes from the dissociation of $NO_2$. The result with ns laser pulses shows only one peak appearing at the mass 30 for $NO^+$ (Fig. 4.3a). There were no peaks visible at the

masses 14, 16 and 46 for $N^+$, $O^+$ and $NO_2^+$. In the fs laser mass spectrum (Fig.4.3b), a significant signal is visible at m/q=46 corresponding to the $NO_2^+$ peak and the $NO_2^+$/ $NO^+$ ratio is about 6%-11% in the case of 375 nm for the laser intensities about $10^{12\text{-}14}$ W/cm$^2$ (Fig. 4.3b).

A comparison of the nanosecond and femtosecond laser mass spectra of $NO_2$ molecule is shown in fig.4.3. Both spectra were taken under similar experimental conditions apart from different laser systems used. The laser focusing conditions were also different. The laser was focused using a 10 cm focal length mirror for fs and 30 cm focal length lens for ns laser pulses. The nanosecond laser system gives an output laser pulse width of 10 ns with typical laser intensities about $10^{8\text{-}9}$ W/cm$^2$, but these are 90 fs and $10^{12\text{-}14}$ W/cm$^2$ for femtosecond laser pulses.

### 4.4.4 The Femtosecond Laser Mass Spectrometry on $NO_2$ at 750 nm

An experiment also was carried out on $NO_2$ molecule using 750 nm laser wavelength at 90 fs laser pulse width. A typical time of flight mass spectrum of $NO_2$ is shown in fig. 4.4, which was taken under similar experimental condition of the experiment carried out at 375 nm. Only difference arises from the different laser wavelengths and therefore different laser bandwidths which were mentioned experimental arrangement section in this chapter.

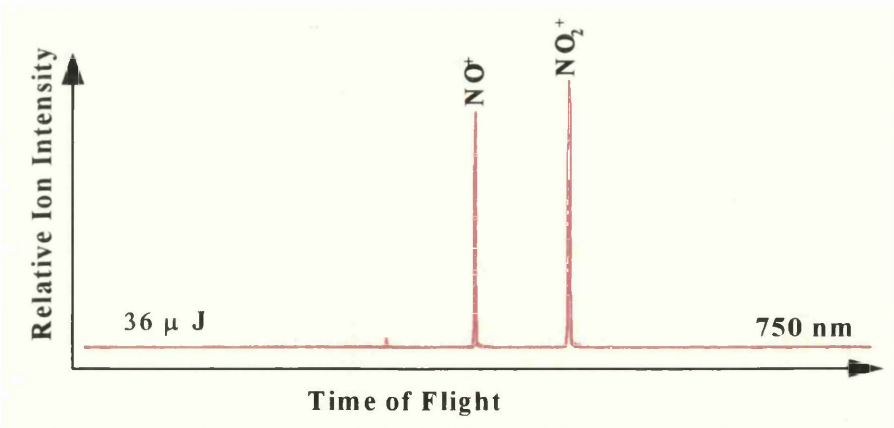


**Figure 4. 4 :** Typical femtosecond laser mass spectrum of $NO_2$ is shown. The spectra was taken using 90 fs laser pulses at the wavelength of 750 nm.

For the 750 nm laser photons, the $NO_2$ molecule can be excited to the first dissociation limit with two photons of 750 nm. The bandwidth of the 90 fs laser pulse at 750 nm covers an excitation region of approximately 400 $cm^{-1}$ and a number of excited states of the molecule are populated. When this effect is considered, the energy of three photons at 750 nm is sufficient to allow $NO_2$ to be excited just above the second dissociation limit. This means that the second dissociation channel of $NO_2$ is opened as well as the first with the absorption of three and two photons at 750 nm, respectively. When both dissociation channels are opened simultaneously, the multiphoton dissociative ionisation processes of $NO_2$ at 750 nm become completely different than that at 375 nm, shown in fig.4.1.

The comparison of the time of flight mass spectra taken using 375 nm at 90 fs (Fig. 4.3b) and 750 nm (Fig. 4.4) shows a significant difference between both spectra. The $NO_2^+/NO^+$ ratio is 100% or even higher when the 750 nm laser wavelength is used and this was 6-11% at 375 nm. This difference in the mass spectra shows that the ionisation efficiency of $NO_2$ at 750 nm is higher than that at 375 nm indicating different multiphoton dissociation-ionisation processes.

## 4.5 Application of the Glasgow Rate Equation Model to the $NO_2$ Molecule at 375 nm

The recent developments of the rate equation model for analysing the dissociation and ionisation efficiencies shows that the rate equation model becomes a reasonable method for the description of the system under examination. The agreement between the experimental results and the results of the rate equation model calculations has been discussed in a number of articles (Ledingham *et al.*, 1995a; Singhal *et al.*, 1996; 1997).

In the visible range of the optical spectrum, the absorption of the $NO_2$ molecule is dominated by the $A^2B_2$ electronic excited state, shown in fig. 4.1. This electronic excited state dissociates to NO + O at the wavelengths shorter than 397.95 nm. The photodissociation rate, k and the lifetimes of the dissociative states in the excitation

region below 400 nm have been determined in a series of recent experiments to have a value $8.5x10^9$ $s^{-1}$ for ns laser pulses (Rohlfing and Valentini, 1985; Miyawaki *et al.*, 1993; 1994; Ionov *et al.*, 1993).

The results of our study of multiphoton ionisation and dissociation of $NO_2$ at the laser wavelength of 375 nm and for a 90 fs and 10 ns laser pulse widths are described in this thesis and presented in a recent article (Singhal *et al.*, 1996) which shows the capability of the Glasgow rate equation model. It is expected that for the ns laser pulses the dissociation rate dominates during the multiphoton process, but for the fs laser pulses, the fast dissociation of $NO_2$ in the shorter lived dissociative excited state is substantially defeated by the multiphoton ionisation (MPI) rates in $NO_2$ and both $NO_2$ and NO ion peaks are expected. A quantitative explanation of such observation is of great importance for understanding the dynamics of photoexcitation and photodissociation of molecules.

It is generally accepted that the rate equations can be used when the coherent effects do not play an important role on the multiphoton process (Ackerhalt and Shore, 1977; Zakheim and Johnson, 1980; Singhal *et al.*, 1996). In the case of $NO_2$ the quantum effects are expected to be small since the molecule is characterised by "chaotic dynamics at ns laser pulses (Georges *et al.*, 1995a) especially in its higher electronic states. Additionally, the bandwidth of the 90 fs laser pulses at 375 nm covers an excitation region approximately 200 $cm^{-1}$ and several eigen states of the molecule are populated. In the case of broad bandwidth, it is not clear how important coherence effects are.

## 4.6 Interpretation of the Results of Rate Equation Model and Comparison of Theoretical and Experimental Results

The dissociation and ionisation pathways which a $NO_2$ molecule may follow after excitation to above the first dissociation threshold having absorbed one photon of 375 nm is shown in fig. 4.1

For the application of the rate equation model, the values for the dissociation rate, k, were used as $2.76x10^{12}$ $s^{-1}$ for the fs and $8.5x10^{9}s^{-1}$ for ns laser pulses, respectively. The lifetime of the second dissociation channel at 248 nm (Hallin and Merer, 1976) was measured to be 42±5 ps for 15 ns laser pulses and we use this value for 10 ns laser pulses at 375 nm for the first dissociation channel. If the lifetime of dissociative state is not longer than 100 ps, the $NO^+$ ion yields at the longer pulse widths are insensitive to the exact value of the lifetime of the dissociative state chosen.

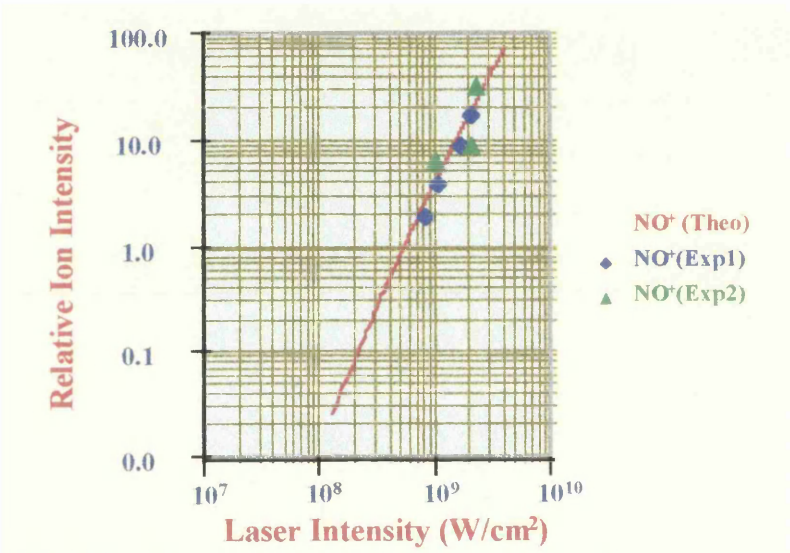


**Figure 4.5:** Experimental and theoretical data shows a good agreement for the nanosecond laser pulses and intensities about $10^{8-10}$ $W/cm^2$.

The values of $\sigma_{exc} = 3.2x10^{-19}$ $cm^2$ for single photon excitation of $NO_2$ (Calvert and Pitts, 1966), $\sigma_{exc} = 4.8x10^{-51}$ $cm^4s$ for two photon excitation of NO (Cremaschi *et al.*, 1978) and $\sigma_{ion} = 9x10^{-18}$ $cm^2$ for one photon ionisation of NO molecule (Watanabe *et al.*, 1967). The two photon ionisation of $NO_2$ is not available in published literature and its value was chosen to reproduce the experimental $NO_2^+/NO^+$ ion yield for the 90 fs laser pulses.

The laser beam spot has a Gaussian intensity profile, and the calculations take into account this intensity profile. Since the experimental ion yield results from a range

of intensities, for comparing experimental data with the results of the calculations, the laser intensity has been used as the variable. In fig. 4.5, the laser intensity dependence of the NO ion yield for the 10 ns pulse duration is presented and seen to be reproduced excellently by the model. For the ns laser pulse widths, the $NO_2$ ion peak was predicted to be $2.5 \times 10^{-5}$ times the NO ion peak. This peak height is below the sensitivity of the mass spectrometer and was not seen even in a high statistics run especially carried out to observe the $NO_2$ ions.

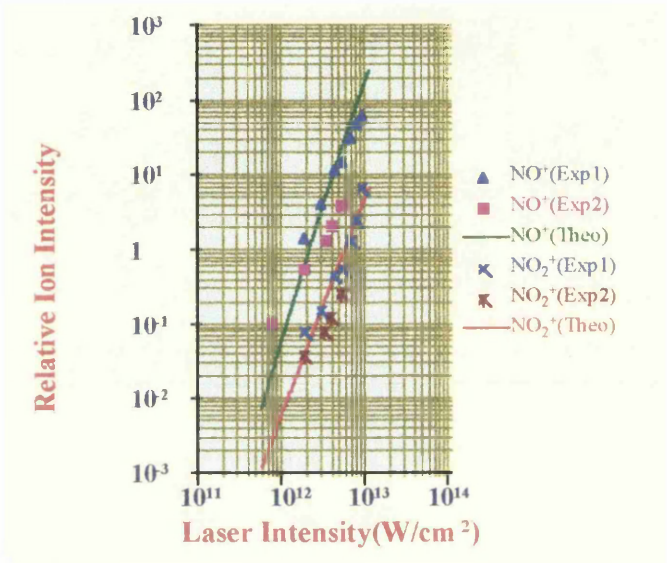


**Figure 4.6 :** A comparison of theoretical and experimental data. The data was taken focusing laser light with a 30 cm focal length lens.

In fig. 4.6, the measured laser intensity dependencies of the $NO^+$ and $NO_2^+$ ion peaks are compared with the predictions of the rate equation model for fs laser pulses. Since the $NO^+$ and $NO_2^+$ ion yields were measured under identical experimental conditions, the same scaling factor was used to compare experimental and theoretical results, and a very good agreement between them is clearly seen from the graph in fig.4.5 and 4.6.

Fig. 4.7 shows the ratios of $NO_2^+$ and $NO^+$ ion yields as a function of laser intensity. While individual points were measured with high statistical accuracy, it is evident from the data that the absolute measurements could only be relied to within a factor

of two to three. This is thought to be due to the different experimental arrangements when the size of the laser focus and its position in the mass spectrometer might be slightly different (Kilic *et al.*, 1997). This experimental data was obtained using a laser intensity between $10^{11\text{-}13}$ W/cm$^2$. In this case, the laser beam was focused using 10 cm focal length mirror. The curve (red line) in fig. 4.7 is the prediction of the rate equation model for the two photon ionisation cross section of $NO_2$ = $10^{-53}$ cm$^4$s.

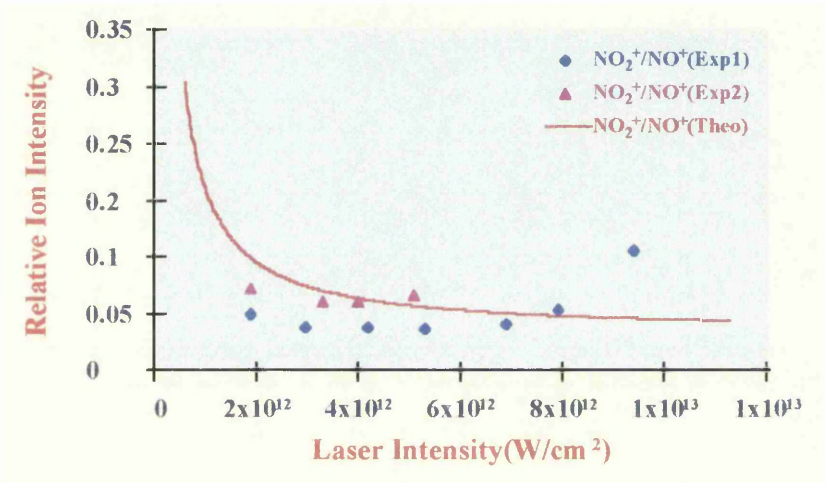


**Figure 4.7** : The ratio of $NO_2^+/NO^+$ is shown. The data was taken irradiating $NO_2$ by 375 nm and 90 fs laser pulses. The curve shows the results obtained using Glasgow rate equation model (Singhal, 1997) and two experimental data series were compared with the theoretically calculated curve.

For the rate equation model calculations, the laser pulse was assumed to have a square shape. For the 90 fs laser pulses and for the laser intensities used, the rate equation model supports our experimental results that a pure multiphoton dissociation and subsequent ionisation processes take place for the $NO_2$ and NO particularly for the intensity range used in our experiment which is about $10^{11\text{-}13}$ W/cm$^2$.

The laser intensity dependencies of NO and $NO_2$ in fig 4.5 support the idea that the multiphoton ionisation process is dominant mechanism indicating some of the excitation steps are saturated due to smaller laser intensity dependence. The two photon ionisation transition of $NO_2$ molecule is unsaturated. The single photon

excitation of $NO_2$ is partially saturated and the overall calculated intensity dependence of $NO_2$ is 2.8. In NO, excitation cross section was determined by the excitation cross section of $NO_2$ as well as by the excitation and ionisation cross sections of NO. All three cross sections are partially saturated and give the overall intensity dependence of about 2.9. For the ns data, the ionisation cross section of NO is saturated and n = 2.2. For the intensity range used for the experiments in this work, the ability of the rate equation model to explain the data for different pulse widths from nanoseconds to femtoseconds suggests that in NO and $NO_2$, the excitation and ionisation dynamics are not dominated by the coherence effects even for very short laser pulse widths.

## 4.7 Conclusions

In Fig. 4.3, a comparison of the mass spectra of $NO_2$ which were taken using 90 fs and 10 ns laser pulses at 375 nm. Typical pulse energies used were 10 μJ and about a few millijoules for fs and ns laser pulses, respectively. The detection of $NO_2$ parent ion is a spectroscopic challenge since its absorption cross section is very small. After absorption of one photon, the dissociation of $NO_2$ to NO+O takes place within a time which might be much shorter than the time required for the further two photon absorption for $NO_2$ to be ionised. It was observed that the $NO_2$ molecule cannot be ionised using nanosecond laser pulses at 375 nm with intensities about $10^{8\text{-}9}$ W/cm$^2$ because the molecule has a dissociative lifetime about a few picoseconds (Ledingham et al, 1995a). But, the femtosecond laser pulses can defeat the lifetime of the dissociative excited state by fast up-pumping with absorption of further photons within the lifetime of the dissociative excited state and the laser pulse width.

We have investigated and observed the dissociation and ionisation dynamics for the $NO_2$ molecule using femtosecond and nanosecond laser mass spectrometry. The $NO_2^+/NO^+$ ratio has been investigated and the results of the present experiment has

been compared with the results of a rate equation model calculation. It has been shown that the results of present experiment is supported by rate equation modelling and agreement between theoretical and experimental results is very good.

It is known that there two observed dissociation thresholds in the $NO_2$ molecule. The measurement of the $NO_2^+/NO^+$ ratio is a favourable way to discuss the relative dynamics for the dissociation-ionisation of both dissociation channels. This ratio has been measured for the first (Singhal *et al.*, 1996) and second (Ledingham *et al.*, 1996) dissociation limits for different wavelengths and pulse widths. We have found that the $NO_2^+/NO^+$ ratio is about 6-11% at 375 nm and 100% or higher at 750 nm for 90 fs laser pulses.

It has been observed that the dissociation-ionisation process differs from 375 nm to 750 nm. It appears that the difference in the ratios for both dissociation thresholds is considerable and can be explained by the different multiphoton processes involved in each case.

# CHAPTER 5

# MULTIPHOTON DISSOCIATIVE IONISATION OF NITROMETHANE AND FRAGMENTATION PROCESS ON NITROMETHANE ION

## Contents

## 5.1 Introduction

Nitro, $NO_2$, containing molecules show significant biological and chemical activity, and contribute to pollution of the atmosphere and serve as essential ingredients in many propellants and explosives. Nitromethane is a simple and prototypical energetic material for organo-nitro compounds and is the simplest nitro explosive molecule and falls in to the class of nitro-alkanes in organic chemistry. Because of its prototypical peculiarities, it is a very attractive molecule for scientists, and therefore a considerable number of papers have been written on nitromethane. Many research groups are still working on it to understand its electronic structure and dissociation/ionisation dynamics. A number of recent articles have shown that it is also an interesting sample to study the multiphoton dissociative ionisation and fragmentation dynamics and is an outstanding example for discussion of ladder climbing and switching processes (Ledingham *et al.,* 1995b; Kilic *et al.,* 1996; Kilic *et al.,* 1997).

Nitromethane is a seven atom molecule and consists of a methyl ($CH_3$) and nitro ($NO_2$) group, which join to each other with a C-N bond to construct $H_3C\text{-}NO_2$ structure. The photophysics and photochemistry of nitromethane is not completely understood despite several experimental (Kandel, 1955; Nicolson, 1961; Napier and Norrish, 1966; Paszyc, 1973; Wodtke *et al.,* 1986; Honda *et al.,* 1969; Nagakura, 1960) and theoretical (McKee, 1985; 1986; 1989a; 1989b; Saxon and Yoshimine, 1991; Marynick *et al.,* 1984; Flicker *et al.,* 1980; Harris, 1973; Rabalais, 1972; McEwan, 1960; Mijoule *et al.,* 1987) studies done to identify its structure.

Absorption and electronic spectra of nitromethane show dominant characteristics of the nitro group but the absorption spectrum of nitromethane is much simpler than that of the $NO_2$. The complicated band system in the visible region is absent, and the near UV spectrum permits assignments with

reasonable certainty. The nitromethane molecule absorbs photons in a broad continuum from 370 nm into the VUV and shows very characteristic absorption dynamics, which consists of three absorption peaks. The weak band peaking at 270 nm has been assigned as a $n \rightarrow \pi^*$ transition and the strong band at about 198 nm has been assigned as $\pi \rightarrow \pi^*$ transition localised on the $NO_2$ moiety. The third absorption peak has a maximum at 281 nm and assigned as a weakly allowed $n^* \rightarrow \pi^*$ transition (Nagakura, 1960; Cundall *et al.,* 1967; Honda *et al.,* 1972; Robin, 1974; Spears and Brugge, 1978; McEwan, 1960; Wagniere, 1969; Balyiss and McRae, 1954; Loos *et al.,* 1968). The observed and calculated transition wavelengths and assigned systems are given in table 5.1

**Table 5.1:** The Transition system, transition wavelengths are shown.

| **Transitions** | **λ(nm) Calc.[a]** | **λ (nm) Observed [b]** |
|---|---|---|
| $\pi \rightarrow \pi^*$ | 214 | 198 |
| $n \rightarrow \pi^*$ | 272 | 270 |
| $n^* \rightarrow \pi^*$ | 281 | - |

[a] McEwan, 1960 [b] Nagakura, 1960

Since they exhibit both diffuse electronic spectra and a propensity for dissociation, direct experimental observation and characterisation of the electronic excited states in nitro containing components is very difficult and the theoretical characterisation of their electronic states have mostly been studied. Some of these excited states have been observed experimentally, but, to the author's knowledge there is little agreement between experiment and theory (Rebbert and Slagg, 1962; Honda *et al.,* 1972; Flicker *et al.,* 1980; Nagakura, 1960; Mijoule *et al.,* 1987).

### 5.1.1 Dissociation Pathways for the Neutral Nitromethane Molecule

Elucidation of the mechanism of the primary processes in photochemical and thermochemical decomposition of the nitromethane molecule has been studied extensively. In the early studies of photochemistry of nitromethane, two primary

dissociation processes were suggested by several research groups, these were eq.(5.1) and eq.(5.2) (Hirschlaff and Norrish, 1936; Brown and Pimentel, 1958). Some of the later experimental works (Nagakura, 1960; Spears and Brugge, 1978; Schoen *et al.,* 1982; Blais, 1983; Butler *et al.,* 1983; Renlund and Trott, 1984; Mialocq and Stephenson, 1986; Lao *et al.,* 1990; Moss *et al.,* 1992) agreed with these pioneering studies that the primary dissociation process at either the absorption maxima is cleavage of the C-N bond to produce $CH_3$ and $NO_2$ radicals. On the dissociation pathway through the rupture of the C-N bond, two possible dissociation channels exist, in agreement in the literature, which are classified as major and minor dissociation channels (Blais , 1983; Butler *et al.,* 1983; Moss *et al.,* 1992). The major dissociation channel leaves the $NO_2$ radical in the $A^2B_2$ excited state (Schoen *et al.,* 1982; Honda *et al.,* 1972; Blais *et al.,* 1983; Butler *et al.,* 1983) which rapidly dissociates to NO + O with a decay rate about $8.5 \times 10^9\ s^{-1}$ (Miyawaki *et al.,* 1993; 1994). The corresponding $CH_3$ radical is produced with a little internal energy. The minor channel produces $NO_2$ in the $X^2A_1$ ground state and it absorbs an extra photon to dissociate to NO + O.

$$CH_3NO_2 + h\nu \rightarrow (CH_3NO_2)^* \rightarrow CH_3 + NO_2 \qquad (5.1)$$

$$CH_3NO_2 + h\nu \rightarrow CH_2O + HNO \qquad (5.2)$$

The dissociation cross section, $\sigma$, of the C-N bond has been measured recently (Blais, 1983) to be $1.7 \times 10^{-17}\ cm^{-2}$ with near unity quantum yield at 193 nm.

The nitromethane molecule has a very fast dissociative character and the $NO_2$ fragment is produced through the reaction of eq.(5.1) within a time scale shorter than 5 ps (Schoen *et al.,* 1982). This result for the dissociative lifetime of the C-N bond in nitromethane shows a good agreement with other measured lifetime for the dissociative state (Mialocq and Stephenson, 1986) which was measured to be 6 ps.

The other important rearrangement process in photo-excited nitromethane molecule is isomerisation to the methyl nitrite ($CH_3ONO$), which was considered

for the first time about 40 years ago (Brown and Pimentel, 1958). It has been concluded that the molecule dissociates first to produce methyl ($CH_3$) and nitrogen dioxide ($NO_2$) radicals through eq. (5.1) and then they undergo a recombination to produce methyl nitrite ($CH_3ONO$) (Brown and Pimentel, 1958; Hirsclaff and Norrish, 1936; Gray *et al.,* 1955b; Napier and Norrish, 1966). Recombination of methyl and nitrogen dioxide will produce methyl nitrite in the excited state of 2.43 eV (Gray *et al.,* 1955a). This excited molecule cannot longer survive and suddenly undergoes some further rearrangements because of deactivation competes with two fragmentation process. These are the reverse reaction of eq. (5.3) or the reaction to produce $CH_3O$ and NO fragments may take place through eq.(5.4). It is argued that eq. (5.4) is dominant because of the weakness of the O-N bond (Gray *et al.,* 1955a) which has a bond energy of about 1.609 eV.

$$CH_3NO_2 + h\nu \rightarrow (CH_3NO_2)^* \rightarrow (CH_3ONO)^* \qquad (5.3)$$

$$(CH_3ONO)^* \rightarrow CH_3O + NO \qquad (5.4)$$

The barrier to the isomerisation of nitromethane to methyl nitrite, eq.(5.3), is low enough to compete with reaction of eq.(5.1) (Dewar *et al.,* 1985; McKee, 1989b; Wotke *et al.,* 1986b). After absorption of one or more photons and rearrangement of nitromethane to methyl nitrite through eq.(5.3), the $CH_3ONO$ should contain enough internal energy (Gray *et al.*, 1955a) to dissociate to $CH_3O$ and NO by itself through eq.(5.4). If $CH_3O^+$ is created during a laser pulse, it spontaneously decomposes to form $HCO^+$ and $H_2$ since it is an unstable radical. Another possible and important dissociation route for the metoxy radical ($CH_3O$) is the formation of the $CH_2O$ and H fragments through the breaking of H-$CH_2O$ bond (Geers *et al.,* 1993).

The opening of the OH loss channel was investigated as a primary dissociation channel with recent article (Zabernick, *et al.,* 1986; Greenblatt *et al.,* 1987). Under collision-free conditions, Zabernick *et al.* has identified that the

observation of the OH radical from nitromethane at 266 nm occurs through the primary dissociation process. But, under the same collisional conditions at 282 nm, Greenblatt *et al.* have observed that the OH production cannot be observed from nitromethane either as a primary or a secondary process product.

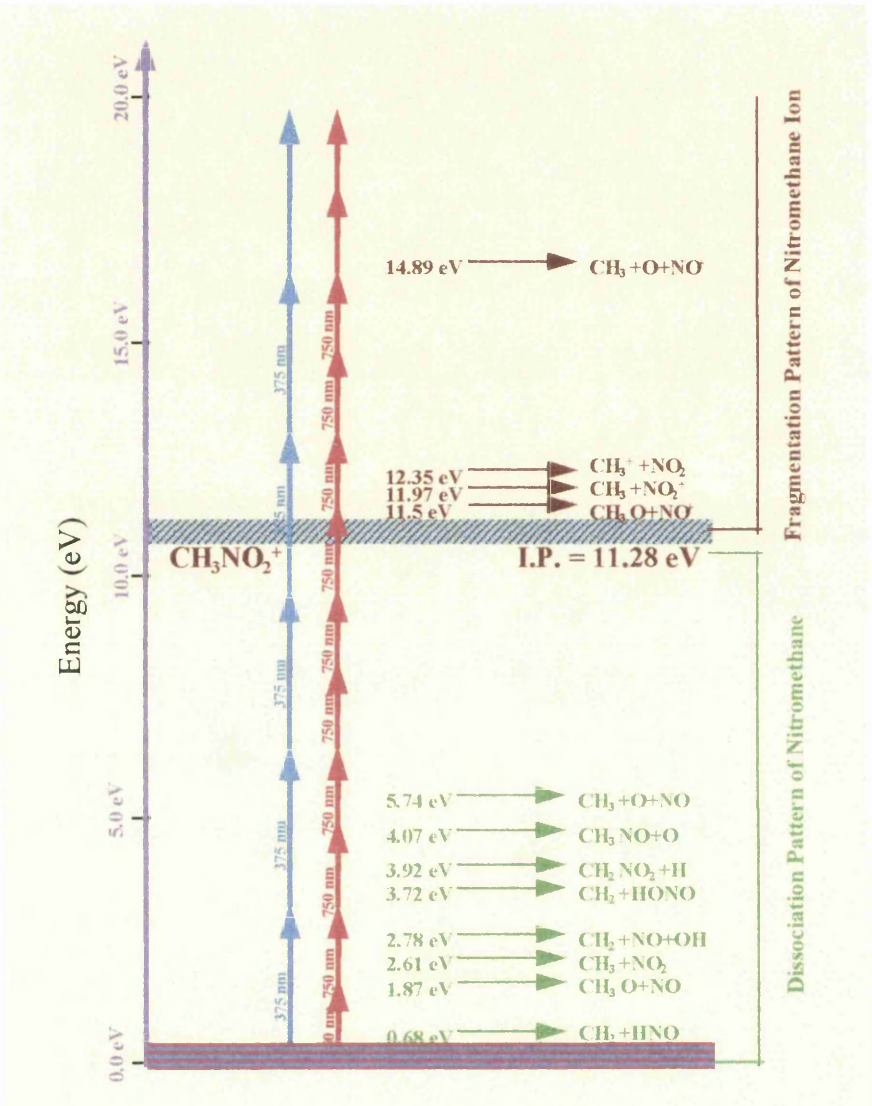


**Figure 5.1:** Energetically allowed and identified fragmentation pathways in the neutral and ionic manifolds of states. The absorption of four photons of 375 nm and seven photons of 750 nm will permit access to the parent ion and the most important ionic dissociative pathways.

The production of the $HNO_2$ fragment from some of the nitro-alkanes has been identified and reported by several authors (Pazycs, 1973; Wodtke *et al.*,1986;

Butler *et al.*, 1983). To the author's knowledge, no significant $HNO_2$ signal from nitromethane was observed.

**Table 5. 2**

| Opened Channel | Required Energy | Method of Detection | Wavelength used |
|---|---|---|---|
| $CH_2O + HNO$ | 0.68 eV | Photolysis<br>Photolysis | 200-300 nm[a]<br>240-360 nm[b] |
| $CH_3O+NO$ | 1.87 eV | Multiphoton Process<br>Flash Photolysis | 266 nm[c]<br>199.9-206.4 nm[d] |
| $CH_3+NO_2$ | 2.61 eV | Photolysis<br>Photolysis<br>Flash Photolysis | 253.7-313 nm[e]<br>313 nm[f]<br>193 nm[g] |
| $CH_2NO+OH$ | 2.78 eV | Pump-Probe | 266 nm[h] |
| $CH_2+HONO$ | 3.72 eV | Emission Spectroscopy | 193 nm[g] |
| $CH_2NO_2+H$ | 3.92 eV | Photolysis | 253.7-313 nm[e] |
| $CH_3NO+O$ | 4.07 eV | Photolysis | 253.7-313 nm[e] |
| $CH_3+NO+O$ | 5.74 eV | Multiphoton Process | 193 nm[i] |

**a** Hirschlaff and Norrish, 1936 **b** Brown and Pimentel, 1958 **c** Kwok *et al.* , 1981
**d** McGarvey and McGrath, 1964 **e** Cundall *et al.*, 1967 **f** Honda *et al.*, 1972
**g** Butler *et al.*, 1983 **h** Zabernick *et al.*, 1986 **i** Moss *et al.*, 1992

The production of nitromethyl, $CH_2NO_2$ has been reported through an H loss channel using a photolysis technique in the vicinity of 313 nm (Cundall *et al.*, 1967). It has been concluded that this channel requires an energy which is more than most of other channels require. The nitromethyl radical dissociates to $CH_2NO+O$ or $CH_2O+NO$ at the wavelengths of 240 nm, 255 nm and 270 nm. In contrast to the nitromethane, the cleavage of C-N bond to give $CH_2+NO_2$ has not been observed at the above mentioned wavelengths (Cry *et al.*, 1993).

Figure 5.1 shows possible dissociation channels and related products for the nitromethane neutral molecule and parent ion. The existing information about the identified and observed dissociation channels, the experimental techniques and related wavelengths used are given in table 5.2.

### 5.1.2 Ionisation of the Neutral Nitromethane Molecule and the Fragmentation Process of the Nitromethane Ion

To the author's knowledge, there is no available information in the literature about the formation of the nitromethane ion using multiphoton processes. There exists valuable information about the formation and rearrangement of the nitromethane ion which was obtained using techniques other than multiphoton processes; such as, electron impact, thermochemical and photoelectron-photoion coincidence techniques (Fields and Meyerson, 1971; Meyerson and Fields; 1974; Weiss and Meisels, 1979; Niwa *et al.,* 1981; Ogden *et al.,* 1983; Gilman *et al.,* 1983; Egsgaard *et al.,* 1986; Qian *et al.,* 1990; Qian *et al.,* 1991).

Figure 5.1 shows some of the energetically allowed dissociation channels (Kilic *et al.,* 1997) for both the neutral nitromethane molecule (Butler *et al.,* 1983) and its ion (Ogden *et al.,* 1983). The ionisation potential of nitromethane is 11.28 eV (Allam *et al.,* 1981), and hence, it takes four photons of 375 nm and seven photons of 750 nm to ionise this molecule. The ultraviolet absorption spectrum of nitromethane (Nagakura, 1960; Loos *et al.,* 1969; Paszyc, 1973) shows that the absorption probability of the nitromethane at 375 nm is very small. Therefore, the absorption of two photons at 375 nm and three or four photons at 750 nm are necessary to permit most of these channels to be opened for the nitromethane neutral molecule with sufficiently high probability.

The primary fragmentation and rearrangement pathways in the nitromethane parent ion have been investigated and it is agreed that the cleavage of the C-N bond is the dominant dissociation channel (Allam *et al.,* 1981; Meyerson and Fields, 1974; Niwa *et al.,* 1981; Gilman *et al.,* 1983). The rearrangement of the nitromethane ion to the methyl nitrite ion through ionic isomerisation was not found to be an important intermediate step in the fragmentation process (Meyerson and Fields, 1974).

## 5.2 Investigation of Multiphoton Dissociative Ionisation (MPD / MPI) Dynamics in Nitromethane and Fragmentation of the Nitromethane Ion Using Different Laser Pulse Widths and Wavelengths

A series of experiments have been carried out on the nitromethane molecule using different laser pulses and wavelengths. The results have been partially discussed in a number of recent articles (Ledingham *et al.,* 1995b; Kilic *et al.,* 1996; Kilic *et al.,* 1997). It has been observed and reported that the excitation, dissociation and ionisation processes show different fingerprint in the time of flight mass spectrum depending on the laser pulse width, laser intensity, laser wavelength and spectroscopic structure of molecular sample used (Herring *et al.*, 1981; Weinkauf *et al.*, 1994; Ledingham *et al.*, 1995a; 1995b; Singhal *et al.*, 1996; Kilic *et al.*, 1997; Kosmidis *et al.*, 1997; Singhal *et al.*, 1997). Mainly, using nanosecond and femtosecond laser pulses, a series of experiments have been carried out and a comparison of the time of flight mass spectra has been made. The nanosecond spectra will be discussed first and then femtosecond spectra. Finally a comparison of the nanosecond and femtosecond spectra will be made

### 5.2.1 Experimental

The application of nanosecond laser mass spectrometry and the resonance enhanced multiphoton ionisation (REMPI) has been carried out. The femtosecond and nanosecond experimental systems used are described in detail in Chapter 3 of this thesis and was described in a number of articles (Marshall *et al.,* 1993; Langley *et al.,* 1994; Kosmidis *et al.,* 1994a; Kosmidis *et al.,* 1994b; Ledingham *et al.,* 1995b; Singhal *et al.,* 1996; Kilic *et al.,* 1997; Kosmidis *et al.,* 1997). Briefly, the femtosecond laser system gives an output of laser light at the wavelength of 750 nm with a 90 fs pulse duration. The laser light at 375 nm were generated through frequency doubling by focusing the fundamental output of the laser to a type 1 BBO crystal cut at 28.7 degrees. Before entering the TOF

mass spectrometer, the pulse energies were measured to be 10 μJ and 40 μJ at the wavelengths of 375 nm and 750 nm, respectively. The laser beam was tightly focused in to the interaction region using a 10 cm focal length mirror, which was placed in the vacuum system. Intensities of about $10^{12\text{-}15}$ $Wcm^{-2}$ could be generated, although smaller pulse intensities were generally used. The pulse intensities were calculated using the radius of the beam spot at the focal point, determined by means of eq.(4.3), to be 4.6 μm for 375 nm and 9.2 μm for 750 nm.

The experimental set-up is also quite similar to the experimental arrangement which was used to carry out experiments on NO and $NO_2$ in Chapter 4. The significant differences will be mentioned below in the text when it is necessary.

### 5.2.2 Femtosecond Time of Flight Mass Spectrometry and A Comparison of Femtosecond and Nanosecond Mass Spectra

The nanosecond resonance enhanced multiphoton ionization (REMPI) process has been applied to the nitromethane molecule over the relevant wavelength range. The laser wavelength was scanned by using a Lumonics EPD 330 tuneable dye laser pumped by Lumonics TEM 860-M excimer laser (at 308 nm) and compuscan. The wavelength dependence of the nitromethane in the nanosecond time scale has been observed and presented that it is due to the NO fragment.

Fig. 5.2 shows the wavelength dependent spectrum of the NO fragment from $CH_3NO_2$ for the wavelength between 373 nm and 384 nm showing the (2+1)[$D^2\Sigma^+(v=0) \leftarrow X^2\Pi(v=0)$] NO transition at 375 nm and (2+1) [$C^2\Pi(v=0) \leftarrow X^2\Pi(v=0)$] NO transition about 382 nm. It takes three photons of both 375 nm and 382 nm to ionise either the ground state $NO_2$ or NO molecules. It has been observed that using nanosecond laser pulses at both 375 nm and 382 nm, no $NO_2^+$ ion could be obtained. For the NO neutral molecule it has been discussed in Chapter 4 of this thesis and presented elsewhere (Kilic *et al.*, 1997) and it can be seen from the wavelength dependent spectrum of nitromethane that the ionisation

efficiency at 382 nm is relatively higher than that at 375 nm despite relatively lower laser energy. For the nanosecond laser experiment, the fundamental laser wavelength directly from the dye laser used was TMI, which gives an output of wavelength between 353 nm and 384 nm. The energy profile of laser output is shown above the wavelength dependent spectrum for the wavelength range used, shown in Fig.5.2.

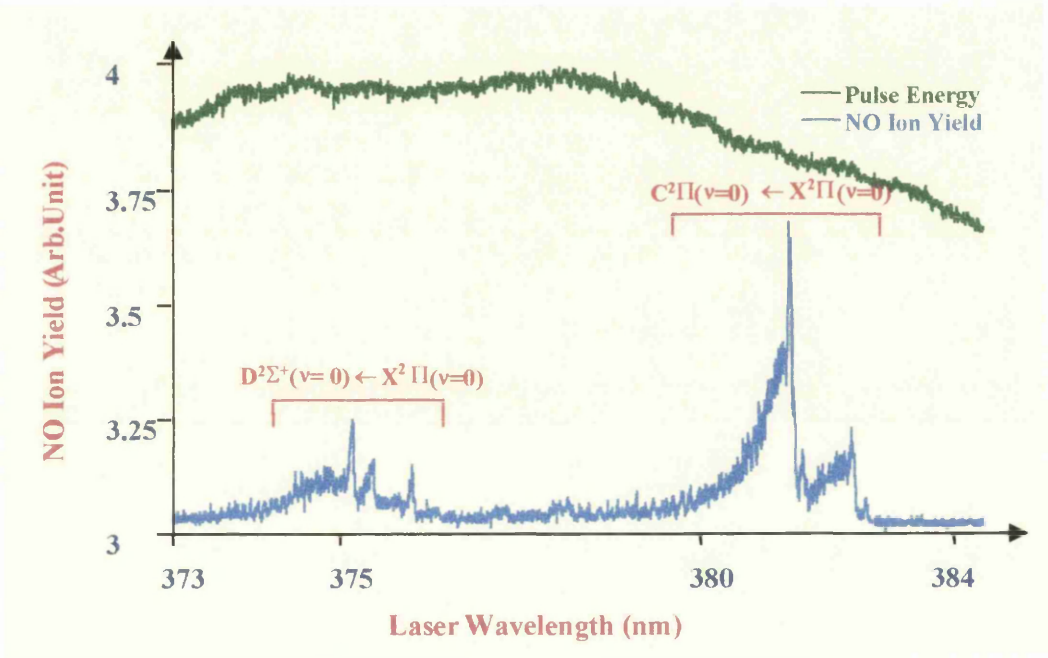


**Figure 5.2:** The wavelength dependence of the NO radical from $CH_3NO_2$ between 373 nm and 384 nm is clearly in a resonance position, about 375 nm and 382 nm.

The typical femtosecond and nanosecond time of flight mass spectra of nitromethane obtained using 90 fs and 10 ns laser pulses at 375 nm is shown in fig. 5.3a and b, respectively. Only one peak at the m/q = 30 (NO) has been observed for the 10 ns laser pulses and there were no other peaks visible. This results from the fact that the fast dissociation occurs within the lifetime of the $CH_3NO_2$ molecule in the excited state which is less than the laser pulse duration. Since, the dissociative excited state has a lifetime shorter than 5 ps (Schoen *et al.*, 1982) which is much shorter than the laser pulse duration, in this case, the

molecule cannot absorb further photons before the dissociation takes place (Ledingham *et al.,* 1995a and b; Singhal *et al.,* 1996; Kilic *et al.,* 1997).

A typical femtosecond time of flight mass spectrum of nitromethane taken using the 90 fs laser pulses at 375 nm is shown in Fig. 5.3a. The pulse energy used for the spectrum were about 8 μJ and the sample pressure was about a few times $10^{-5}$ Torr. The wavelength dependent spectrum cannot be produced for the 90 fs laser pulses, because the bandwidth of the 90 fs laser pulses is very broad and covers several rotational and even vibrational levels. The short pulse laser oscillators generally give an output with a fixed wavelength and it cannot be scanned continuously.

We have observed (Kilic *et al.,* 1997) and discussed in Chap. 3 that the collection efficiency of the ions by the detector changes as a function of the laser beam position in the interaction region. Therefore, before data was taken for the femtosecond spectra, the laser beam position was considered to be optimised when a maximum parent ion peak was obtained.

A comparison of the femtosecond and nanosecond multiphoton ionisation and dissociation for nitromethane at 375 nm can be made by comparing the time of flight mass spectra shown in fig. 5.3a and 5.3b for 90 fs and 10 ns laser pulses, respectively. The time of flight system and experimental conditions for both femtosecond and nanosecond laser experiments were identical. Only differences for both spectra were the laser systems and their parameters, such as the intensities, laser pulse widths and bandwidths are completely different for both laser systems used, which were $10^{8\text{-}10}$ W/cm$^2$, 10 ns and 0.01 nm for the nanosecond laser and $10^{12\text{-}15}$ W/cm$^2$, 90 fs and 5 nm for the femtosecond laser pulses at 375 nm, respectively. The nanosecond laser time of flight mass spectrum shows only one peak at mass 30 (NO) with no parent or any other ion peaks visible. This indicates that with nanosecond laser pulses, apart from the NO ion, neutral fragments are created through the dissociation process but they

cannot be subsequently ionised with the laser fluxes available. Alternatively, the femtosecond spectrum shows a large number of peaks with the principle peaks being m/q = 61 ($CH_3NO_2$), 46 ($NO_2$), 30 (NO) and 15 ($CH_3$). Many other peaks are also visible. While the $NO_2^+$ peak cannot be produced using the nanosecond laser pulses, for the femtosecond laser pulses, a large $NO_2^+$ ion peak is produced and the $NO_2^+/NO^+$ ratio is about 35-45% (in Fig. 5.3a) at 375 nm. The $NO_2^+/NO^+$ ratio for the nitromethane molecule is very much larger than that from the ground state $NO_2$ molecule which is about 6-11% (discussed in Chapter 4) for the 90 fs laser pulses at the wavelength of 375 nm.

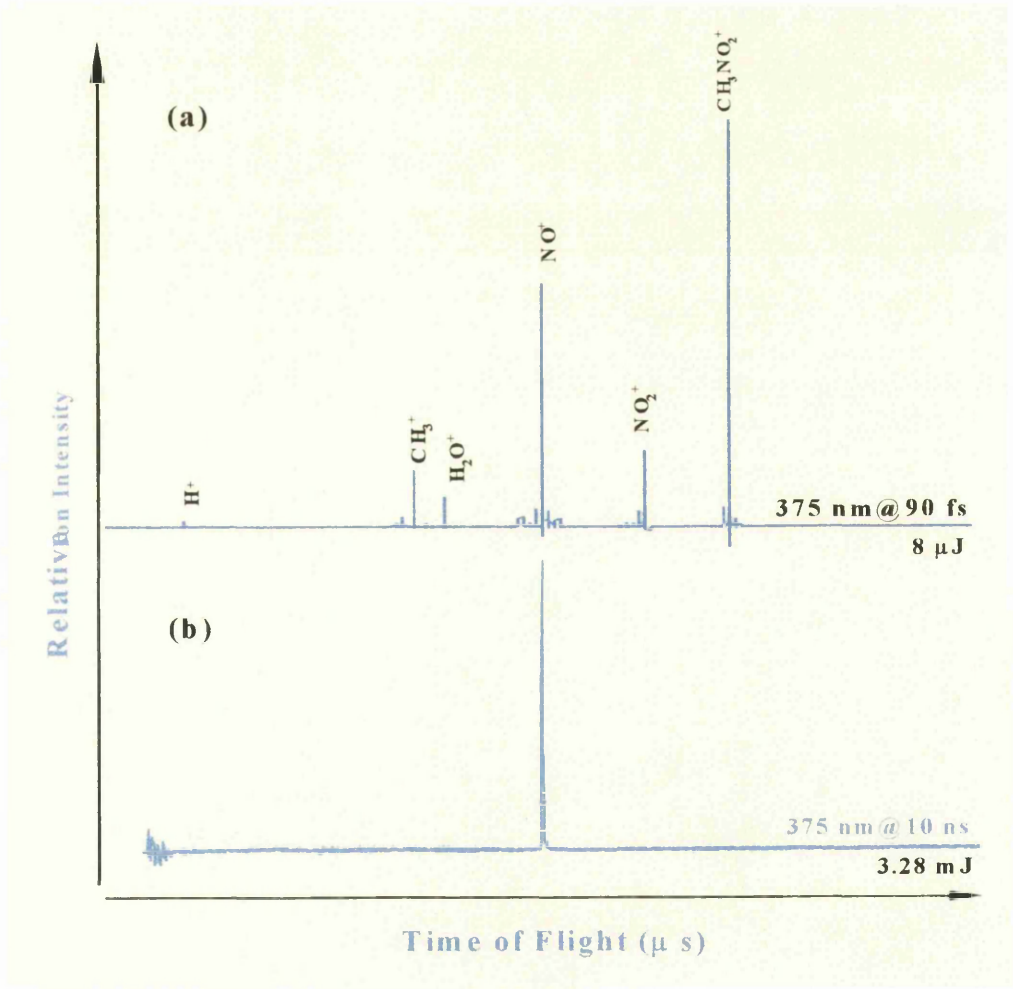


**Figure 5. 3** : Typical time of flight mass spectrum of nitromethane at 375 nm with 90 fs laser pulses.

Figure 5.4 shows the femtosecond laser time of flight mass spectrum of nitromethane at the wavelength of 750 nm with 90 fs laser pulse duration. The laser pulse energies used at 750 nm (in Fig. 5.4) were relatively higher than that was used to produce the spectrum at 375 nm (in Fig. 5.3a). The sample pressures used for the experiment at 375 nm and 750 nm were similar and about $1x10^{-5}$ Torr and $3.3x10^{-5}$ Torr, respectively. The existing number of molecules due to the change of interaction volume are different and the relative ion yield hence is relatively higher for the case of 750 nm than the 375 nm.

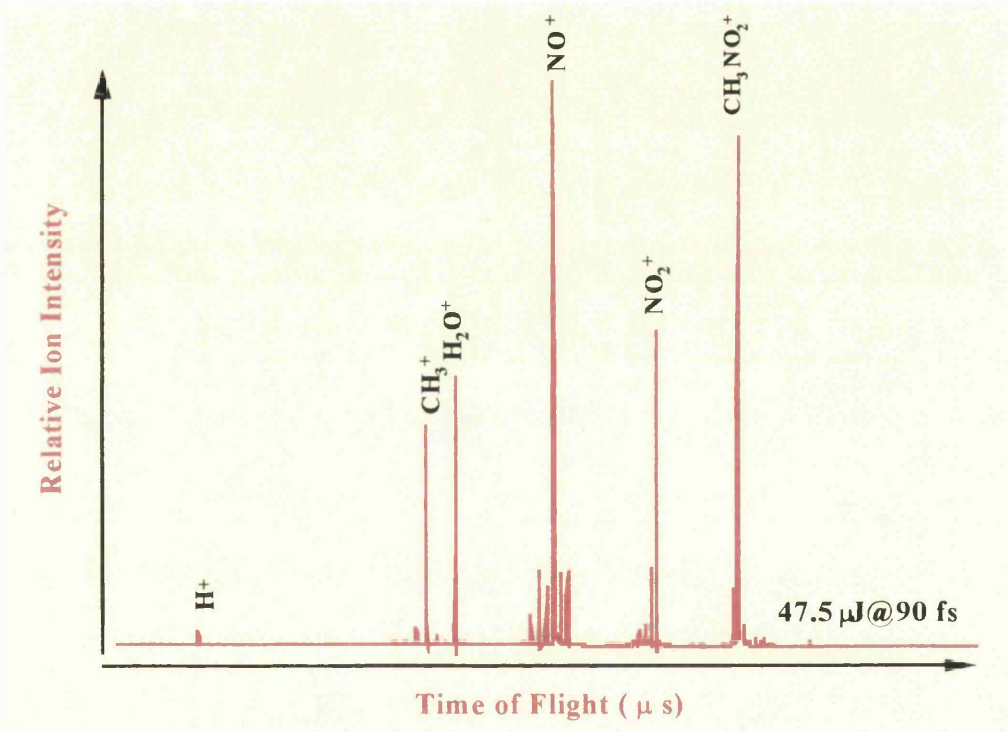


**Figure 5. 4:** Typical time of flight mass spectrum of nitromethane at 750 nm with 90 fs laser pulses.

A comparison of the femtosecond laser time of flight mass spectra of nitromethane for the wavelengths of 375 nm (in Fig. 5.3a) and 750 nm (in Fig. 5.4) shows that both spectra are rather similar, although the fragmentation patterns differ slightly. In the both cases there is a major peak at the m/q = 61 ($CH_3NO_2$) corresponding to the nitromethane parent ion and three major

fragment peaks at m/q = 15 ($CH_3^+$), 30 ($NO^+$) and 46 ($NO_2^+$) with many other weak peaks.

**Table 5.3:** A list of observed fragmentation products from nitromethane is shown with their relative ion intensities, ionisation potentials and the number of photons required to ionise each neutral fragment from their ground state.

| Fragment Products | Mass | I.Intensity at 375 nm | I.Intensity at 750 nm | I.P.(eV) | Photon number 375 nm | 750 nm |
|---|---|---|---|---|---|---|
| $H^+$ | 1 | 2.71 mV | 3.09 mV | 11.25 eV | 4 | 7 |
| $C^+$ | 12 | 1.42 mV | 0.78 mV | 11.25 eV | 4 | 7 |
| $CH^+$ | 13 | 2.26 mV | 0.74 mV | 11.1 eV | 4 | 7 |
| $CH_2^+$ ($N^+$) | 14 | 5.87 mV | 3.84 mV | 11.8(14.5)eV | 4 (5) | 7 (9) |
| $CH_3^+$ or ($NH^+$) | 15 | 27.9 mV | 48.9 mV | 9.8(13.10)eV | 3 (4) | 6 (8) |
| $O^+$ | 16 | 2.1 mV | 1.97 mV | 13.6 eV | 5 | 9 |
| $OH^+$ | 17 | 0.57 mV | 0.43 mV | 13.17 eV | 4 | 8 |
| $H_2O^+$ | 18 | 14.7 mV | 59.8 mV | 12.61 eV | 4 | 8 |
| $CN^+$ | 26 | 1.29 mV | 0.99 mV | 14.4 eV | 5 | 9 |
| $CHN^+$ | 27 | 3.97 mV | 6.63 mV | 13.73 eV | 5 | 9 |
| $CO^+$or ($CH_2N^+$) | 28 | 1.75 mV | 16.25 mV | 14 eV | 5 | 9 |
| $CHO^+$ | 29 | 6.94 mV | 13.15 mV | 10.03 eV | 4 | 7 |
| $NO^+$ or ($CH_2O^+$) | 30 | 77.8 mV | 125.4 mV | 9.25(10.9)eV | 3 | 6 (7) |
| $NOH^+$ or $CH_3O^+$ | 31 | 4.97 mV | 15.98 mV | -----(10.8)eV | 3 (4) | 6 (7) |
| $O_2^+$ | 32 | 1.32 mV | 16.6 mV | 12 eV | 4 | 8 |
| $CNO^+$ | 42 | 0.72 mV | 0.85 mV | | | |
| $CHNO^+$ | 43 | 1.69 mV | 3.36 mV | | | |
| $CH_2NO^+$ | 44 | 1.42 mV | 4.36 mV | | | |
| $CH_3NO^+$ | 45 | 6.84 mV | 16.67 mV | 8.2 eV | 3 | 5 |
| $NO_2^+$ | 46 | 30.8 mV | 70.9 mV | 9.78 eV | 3 | 6 |
| $HNO_2^+$ | 47 | 0.16 mV | 0.58 mV | | | |
| $CH_2NO_2^+$ | 60 | 7.75 mV | 12.34 mV | 7.6 eV | 3 | 5 |
| $CH_3NO_2^+$ | 61 | 98.4 mV | 113.8 mV | 11.28 eV | 4 | 7 |

In the both spectra for both wavelength, an ion peak at m/q $\approx$ 1 corresponding to the $H^+$ ion was detected. This peak may be contributed by several primary and secondary dissociation channels. It is also believed that $H^+$ ion comes directly from ionisation of the neutral H atom from the dissociation of the nitromethane parent ion through the primary fragmentation channel, which is opened to give $CH_2NO_2^+$ + H and some other secondary opened channels. As seen from the femtosecond laser mass spectra the $CH_2NO_2^+$ + H is almost certainly opened, since a large number of $CH_2NO_2^+$ was detected.

Table 5.3 shows a list of mass units for the ions detected from the nitromethane with relative ion yields. The relative ion intensities were read using a LeCroy 9304 oscilloscope with mV units on the screen. Ionisation potentials are given for each neutral radicals to be ionised and the number of photons required to ionise each radical are also given for the case of both wavelengths.

The $H_2O^+$ is one of the major peaks in the spectra taken for the case of both laser wavelengths but it is relatively small in the case of the 375 nm due to the lower pulse energy used. In the previous experiments no significant $H_2O^+$ ion peak has been detected (Kilic *et al.*, 1997) and it is believed that some contributions to this peak may come from water contamination. The efficiency of ionising $H_2O$ molecule at 750 nm is much higher than this at 375 nm which is due to the high laser power available at this wavelength and broader laser bandwidth for 90 fs laser pulses at 750 nm. The $H_2O$ molecule has no excited energy level to be resonantly populated by 375 nm, but the $A(^1B_1)$ electronic excited state with energy of 53800 $cm^{-1}$ and $C^1B_1$ excited state with energy of 80624.8 $cm^{-1}$ in $H_2O$ are in resonance with four and six photons of 750 nm considering broad bandwidth (10 nm) of 90 fs laser pulses. The laser bandwidth at 375 nm for 90 fs laser pulses is not as broad to cover this electronic excitation levels. The resonance excitation to the $C^1B_1$ excited state has been observed and reported in a recent article (Ledingham *et al.*, 1995a) at 248 nm which is in envelope of the bandwidth of three photons of 90 fs laser pulses at 750 nm.

Another important subject in the mass spectra for both wavelength is detection of a peak at m/q = 45 mu corresponds to nitrosomethane ($CH_3NO^+$) fragment ion. This peak appears in the mass spectra over the laser intensity range used in both experiments. For the case of rearrangement of the neutral nitromethane molecule, this peak was observed by several groups (Nappire and Norrish, 1966; Cundal *et al.*, 1967; Honda *et al.*, 1972; Pazyc, 1973) and suggested that the nitromethan molecule undergoes several dissociation and fragmentation processes

to produce neutral methyl and nitric oxide radicals (Fig 5.1 and Table 5.2) and then the $CH_3$ are scavenged by existing nitric oxide in the chamber, i.e., the nitrosomethane ($CH_3NO$) neutral radical can be created through a recombination process *via* eq.(5.5)

$$CH_3+NO \rightarrow CH_3NO \qquad (5.5)$$

In an earlier study, Cundal *et al.* (Cundal *et al.*, 1967) have radiolysed nitromethane positive ion ($CH_3NO_2^+$) and suggested that the nitrosomethane ion ($CH_3NO^+$) could be obtained directly from the dissociation of nitromethane ion through a primary dissociation process of eq. (5.6).

$$CH_3NO_2^+ + e^- \rightarrow CH_3NO^+ + O \qquad (5.6)$$

According to the conclusion made by Cundal *et al.*, the detection of this ion suggests that a dissociation channel of $CH_3NO^+$+O in the nitromethane ion state is opened and most likely it is the source of the $CH_3NO^+$ radical ion appears in the mass spectra, in figs. 5.3a and 5.4.

Fig. 5.5 shows the energy dependence of nitromethane and other four major fragment, $CH_3^+$, $NO^+$, $CH_3NO^+$ and $NO_2^+$ with a number of smaller fragments at 375 nm and 750 nm. The sample pressures for both experiments were very similar and typically $1x10^{-5}$ torr. The pulse energy was changed using a variable neutral density filter and measured using a joulemeter just in front of the entrance window of the time of flight mass spectrometer. The pulse energies for each spectrum are shown at the right end of each spectrum in figs. 5.5a and b for 375 nm and 750 nm, respectively. Before data was taken, the laser beam position was optimized by maximizing parent ion peak. As seen from the fig. 5.5a and b, for the case of both wavelengths, appearances of both spectra are very similar and as laser pulse energy changes from high energy to lower, the fragmentation patterns changes and small mass fragment peaks disappear first and the parent ion is dominant peak for the case of lower laser intensities. This behaviour of the

spectra implies that an ID process is dominating the multiphoton dissociative ionisation process in the nitromethane molecule.

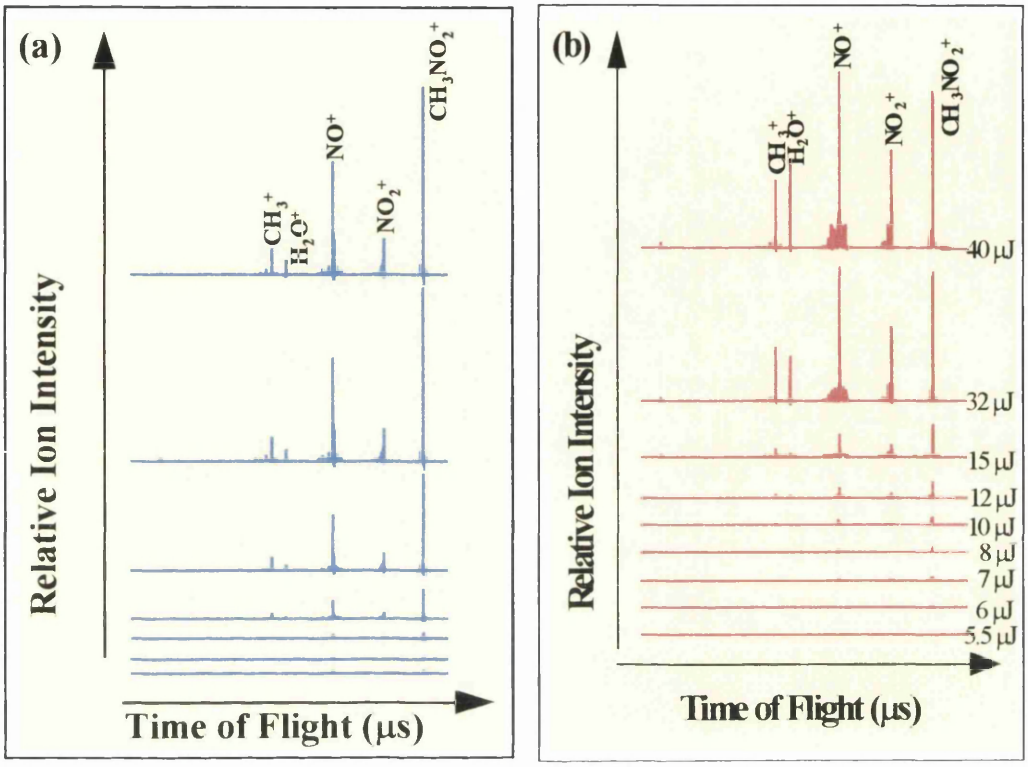


**Figure 5.5:** The energy dependence of the nitromethane parent ion and its fragmentation pattern are shown for 90 fs laser pulses at the wavelengths of **(a)** 375 nm and **(b)** 750 nm.

Fig. 5.6 shows the laser intensity dependencies for the nitromethane parent molecule and some of the most intense fragment ions. The four principal peaks show similar laser intensity dependencies, which are shown in fig. 5.6a and b for the wavelengths of 375 nm and 750 nm, respectively. The relative ion intensities in fig. 5.6 does not show real values for the ion intensities. The ion yields for each fragment have been multiplied by different constants to put them in arbitrary ascending order.

The laser intensity dependencies of the parent ion and other fragments, $NO_2^+$, $CH_3NO^+$, $NO^+$ and $CH_3^+$ ions, are about 3-4 for the 375 nm and 4-5 for the 750 nm, shown in fig. 5.6a and b, respectively, plotted as ion yield versus laser

intensity in a log-log scale. For the same laser intensity range, the difference between the intensity dependencies for the cases of the 375 nm and 750 nm is expected due to the nature of the non-linear chemistry. The ion intensities are a function of the number of photons absorbed. The calculated photon numbers (n) for the case of both laser wavelengths support the conclusion that the multiphoton process dominates the dissociative ionisation dynamics in the nitromethane molecule under the conditions of present experiment. For both case, all fragments shows similar laser intensity dependencies with nitromethane parent ion and this supports the idea that the molecule follows an ID route.

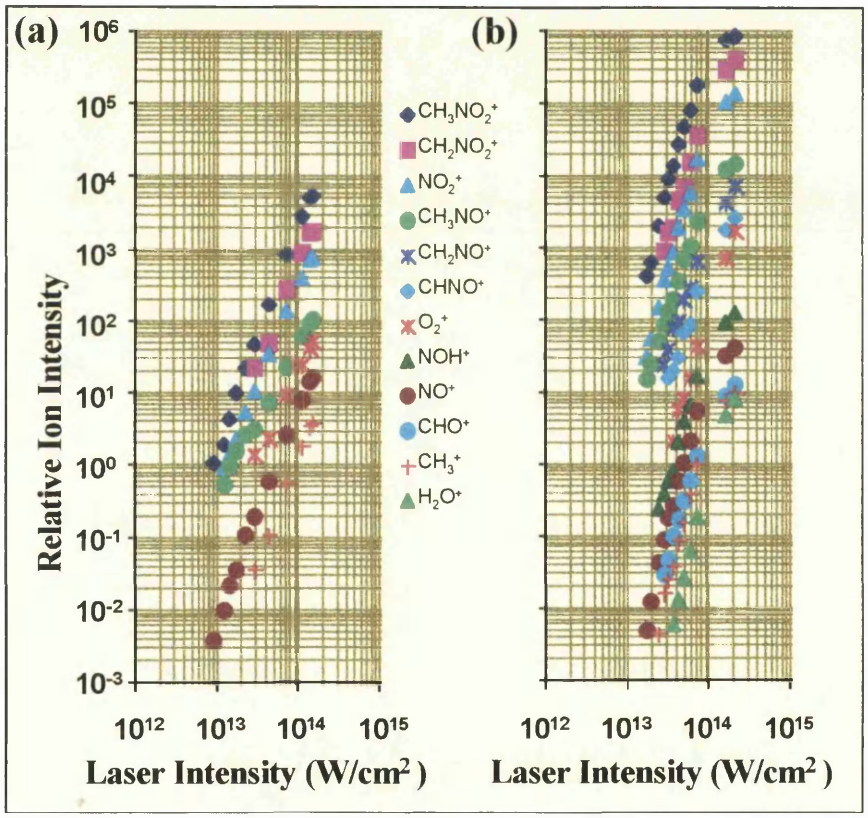


**Figure 5.6:** The laser intensity dependence of the nitromethane parent ion and three other major fragments, $CH_3^+$, $NO^+$ and $NO_2^+$ are shown for 90 fs laser pulses at the wavelengths of **(a)** 375 nm and **(b)** 750 nm.

## 5.3 Conclusion

The multiphoton ionisation and fragmentation of nitromethane at the wavelengths of 375 and 750 nm have been carried out using a time of flight mass spectrometer. The nitromethane molecular parent ion has been obtained, first time in this work, using multiphoton process and earlier observations was presented in a number of recent articles (Ledingham *et al.*, 1995b; Kilic *et al.*, 1996; Kilic *et al.*, 1997). In the nanosecond regime there is only one strong peak at mass m/q=30 (DI). In the case of 90 fs laser pulses, a large number of strong peaks are observed with the principle peaks being m/q=61 ($CH_3NO_2^+$), 46 ($NO_2^+$), 30 ($NO^+$) and 15 ($CH_3^+$). At the laser intensities of $10^{12\text{-}15}$ W/cm$^2$, the parent ion peak shows a laser intensity dependence between n = 3- 4 for the 375 nm and n = 4-5 for the 750 nm, respectively. The small intensity dependencies can be explained by absorption of four photon of 375 nm and seven photons of 750 nm from the ground state assuming one or two of the steps are saturated.

It could be concluded that the ionisation-dissociation (ID) process dominates the multiphoton ionisation process in the nitromethane molecule. The reasons for this conclusion are;

(a) there is a large parent ion peak which is dominant in the time of flight mass spectrum for almost the entire the intensity range used in the experiments,

(b) the laser intensity dependencies of the principal peaks are very similar, suggesting a common parent precursor,

(c) the $NO_2^+/NO^+$ ratio from nitromethane (Fig. 5.5) is very much larger (35-45%) than that from ground state $NO_2$ (6-11%, in Chap.4) for 375 nm and 90 fs, which follows a DI route (Singhal *et al.*, 1996).

The present work has shown that, analytically, multiphoton ionisation in the nanosecond regime has severe limitations for nitromethane because of fast

dissociative states in the neutral excited state manifold. It would have been very instructive if it could have been ascertained whether the nitromethane molecule reached a dissociative state after the absorption of one or more photons at 375 nm and 750 nm, but to the author's knowledge, no detailed information about the dissociative excited states in nitromethane have been identified. Using nanosecond laser pulses, little analytical information could be obtained from the nitromethane since neither the parent ion nor any other ion peak is visible in the spectrum. Alternatively, by application of very short laser pulses, it has been shown in the present work that the dissociative state can largely be bypassed and can produce fragments whose mass spectra again are characteristic of the compound under investigation. Thus, ultrafast laser mass spectroscopy does extend the multiphoton analytical techniques for these difficult molecules.

# CHAPTER 6

# MULTIPHOTON DISSOCIATIVE IONISATION AND FRAGMENTATION PROCESS ON NITROBENZENE;

A Comparison of Time of flight mass spectra of Nitrobenzene at 375 nm and 750 nm using Different Laser Pulse Widths

## Contents

## 6.1 Introduction

In this chapter, the multiphoton dissociation and ionisation dynamics of nitrobenzene are discussed comparing the time of flight mass spectra at different laser wavelengths and laser pulse widths. The photochemistry and photophysics of nitroaromatic molecules have been extensively studied over the years. This group of molecules easily fragments and hence they have ideal structures and properties to study the dissociation pathways. This group of compounds is of great significance in the science of energetic materials and presently have been studied in our and many other laboratories (Kosmidis *et al.*, 1994a; Kosmidis *et al.*, 1997; Marshall *et al.*, 1992a; Marshall *et al.*, 1992b; Kosmidis *et al.*, 1994b; Marshall *et al.*, 1993; Marshall *et al.*, 1992c; Clark *et al.*, 1993; Marshall *et al.*, 1994a; Marshall *et al.*, 1994b; Ledingham *et al.*, 1995b; Abd El-Kader and Ahmed, 1984; Gallowey *et al.*, 1993; Glenevinkel-Meyer and Crim, 1995; Lemire *et al.*, 1993; Rabalais, 1972; Nagakura *et al.*, 1964; Zhu *et al.*, 1990; Rao, 1969).

The electronic absorption spectra of the nitroaromatic molecules have already been reported in the literature and is similar to the aromatic absorption. The absorption bands due to the nitro group are generally hidden under the intense bands due to the $\pi \rightarrow \pi^*$ transitions of the aromatics. Nagakura and co-workers (Nagakura *et al.*, 1964) have examined the electronic absorption spectrum of nitrobenzene in the vapour state down to the vacuum ultraviolet region and have identified a strong band at 164 nm and another band at 193 nm.

In order to present the multiphoton dissociative ionisation of nitrobenzene and the fragmentation of the nitrobenzene ion, the dissociation pathways of the nitrobenzene neutral molecule and the nitrobenzene ion will be summarised in the next section of this chapter. The femtosecond laser mass spectrometric results will be presented and discussed in a later section. Finally, conclusions will be drawn after the presentation of the laser pulse width dependence of the ionisation dynamics of the neutral

nitrobenzene molecule and the dissociation/fragmentation pattern of the nitrobenzene ion have been discussed.

## 6.2 Dissociation and Ionisation Processes of Nitrobenzene ($C_6H_5NO_2$) and the Fragmentation of the Nitrobenzene Ion ($C_6H_5NO_2^+$)

Nitrobenzene is one of the most attractive molecules to investigate the dissociation/fragmentation dynamics for either the neutral or ionic molecular structures and, therefore, the molecule or its ion have been frequently studied using different techniques over the years (Hastings and Matsen, 1948; Benyon *et al.*,1965; Porter and Ward, 1968; Brown, 1970a; 1970b; Mukhtar *et al.*, 1980; Harris *et al.*, 1981; Abd El-Kader and Ahmet, 1983; Panczel and Baer, 1984; Apel and Nogar, 1986; Nishimura *et al.*, 1986; Bunn *et al.*, 1986; Zhu *et al.*, 1990; Marshall *et al.*, 1992a; 1992b; 1992bc; Lemire *et al.*, 1993; Galloway *et al.*, 1993; Clark *et al.*, 1993; Simeonsson *et al.*, 1993; Kosmidis *et al.*, 1994a; Ledingham *et al.*, 1995b; Hwang *et al.*, 1996; Kosmidis *et al.*, 1997).

In this work the nitrobenzene is considered to be a prototypical molecule for nitroaromatic explosives. A knowledge of the photodissociation pathways of this molecule with respect to the characteristics of the fragmenting laser is necessary, since such a fragmentation pattern can be used as a unique fingerprint in the sensitive detection of the molecule. Although nitrobenzene is one of the simplest of the nitroaromatics, it is still complicated and there remain considerable uncertainties about its fragmentation pathways.

Various dissociation pathways of nitrobenzene have been observed using different techniques and reported in the literature (Porter and Ward, 1968; Brown, 1970a; 1970b; Mukhtar *et al.*, 1980; Bunn *et al.*, 1986; Apel and Nogar, 1986; Galloway et al., 1993). It has been proposed that the dissociation of the C-N bond takes place as a primary process to give nitrogen dioxide and phenyl radicals through eq.(6.1)

$$C_6H_5NO_2 \rightarrow C_6H_5 + NO_2 \qquad (6.1)$$

The isomerisation is one of the important processes and complicates the elucidation of the system. The -NO loss dissociation channel detected in nitrobenzene can be more easily explained if a molecular rearrangement takes place prior to the fragmentation. A change of nitrobenzene to the phenylnitrite structure, i.e. a change of C-$NO_2$ to a C-ONO bond, could be such a rearrangement, eq.(6.2). The isomerisation of the nitrobenzene has been studied and presented theoretically in a recent work (Clenewinkel-Meyer and Crim, 1995). It was concluded that phenylnitrite is stable with respect to dissociation into phenoxy ($C_6H_5O$) and nitric oxide (NO) radicals eq. (6.2), and the estimated barrier between the two isomers (nitrobenzene-phenylnitrite) is about 1.13 eV. In this model, after internal conversion of the energy, the excited nitrobenzene molecule undergoes a rearrangement into vibrationally excited phenylnitrite which subsequently dissociates. The NO loss channel giving $C_6H_5O$ has been identified and it is suggested that the $C_6H_5O$ further dissociates to give $C_5H_5$+CO *via* eq.(6.3) which was suggested by Budzikiewicz *et al.*(Budzikiewicz *et al.*, 1967) to explain the fragmentation products in the 70 eV electron impact (EI) mass spectra of nitrobenzene.

$$C_6H_5NO_2 \rightarrow C_6H_5ONO \rightarrow C_6H_5O + NO \qquad (6.2)$$

$$C_6H_5O \rightarrow C_5H_5 + CO \qquad (6.3)$$

The observation of the $C_6H_5NO$ molecule has been made by Hastings and Matsen with an earlier work (Hastings and Matsen, 1948) and they have suggested that it could be detected through an O loss channel *via* eq.(6.4);

$$C_6H_5NO_2 \rightarrow (C_6H_5ONO)^* \rightarrow C_6H_5NO + O \qquad (6.4)$$

These three dissociation channel have been extensively studied and discussed in the literature in a number of articles (Apel and Nogar, 1986; Marshall *et al.*, 1992b; 1992c; Galloway *et al.*, 1993; Lemire *et al.*, 1993; Kosmidis *et al.*, 1994a; Ledingham *et al.*, 1995b). Galloway *et al.* have recently studied the dissociation of the nitrobenzene in the UV range of spectrum and the ionisation of the neutral fragments using VUV laser and have shown evidence for these three channels.

Table 6.1 shows the most probable dissociation channels for the nitrobenzene neutral and ionic molecules with energies required for these channels to be opened. The numbering of reactions in Table 6.1 does not follow these in the text.

**Table 6.1**: Dissociation of Nitrobenzene and its ion with the appearance potentials.

| Neutral Reactions | Appearance Potentials | Eq. | Ionic Reactions | Appearance Potentials | Eq. |
|---|---|---|---|---|---|
| $C_6H_5+NO_2$ | 3.05 eV[a] | (1) | $C_6H_5O^+ +NO$ | 10.89 eV[b] | (4) |
| $C_6H_5O+NO$ | 0.74 eV[a] | (2) | $NO^+ + C_6H_5O$ | 10.89 eV[b] | (5) |
| $C_6H_5NO+O$ | 3.96 eV[a] | (3) | $C_6H_5^+ +NO_2$ | 11.08 eV[b] | (6) |
| | | | $C_6H_5^+ +NO+O$ | 11.08 eV[b] | (7) |
| | | | $C_3H_3^+ +C_2H_2+CO+NO$ | 12.63 eV[b] | (8) |
| | | | $C_4H_3^+ +C_2H_2+NO$ | 15.66 eV[b] | (9) |

[a] Galloway *et al.*, 1993 [b] Nishimura *et al.*, 1986

The dissociation and fragmentation of the nitrobenzene ion have been observed and discussed extensively in a number of previous articles (Brown, 1970a; 1970b; Panczel and Baer, 1984; Bunn *et al.*, 1986; Nishimura *et al.*, 1986; Kosmidis *et al.*, 1994a; Ledingham *et al.*, 1995b; Osterheld *et al.*, 1996; Hwang *et al.*, 1996; Kosmidis *et al.*, 1997). It is generally agreed that $C_6H_5NO_2^+$ can be photofragmented. With respect to the dissociation pathways identified in Table 6.1, three major channels in the nitrobenzene ion have been observed and these specifically are discussed by Bunn *et al.*, Nishimura *et al.*, Osterheld *et al.* and Hwang *et al.*. Osterheld *et al.* have shown that three dissociation channels in the nitrobenzene molecular ion are in competition and this argument has recently been confirmed by Hwang *et al.* who conclude that these are in competition having similar reaction rate constants.

$$\begin{aligned} C_6H_5NO_2^+ &\rightarrow C_6H_5^+ +NO_2 \\ &\rightarrow C_6H_5O+NO^+ \\ &\rightarrow C_6H_5O^+ +NO \\ C_6H_5O^+ &\rightarrow C_6H_5^+ +CO \end{aligned} \qquad (6.5)$$

In addition to these three dissociation channels, the NO and CO neutral fragments produced thorough eq.(6.5) can, however, recombine and produce $CNO_2$ radical *via* eq.(6.6) (Abd El-Kader and Ahmet, 1984), which can subsequently be ionised by absorbing photons from intense laser beam.

$$NO + CO \rightarrow CNO_2 \qquad (6.6)$$

In the present work, the fragmentation of nitrobenzene has been studied at $\lambda$= 375 nm and 750 nm laser light using different laser pulse widths. The dissociation studies with femtosecond lasers can be very useful from many points of view. In the particular case of these molecules it leads to simplified mass spectra compared to those observed using ns laser pulses. In the fs time of flight mass spectra the dissociation channels may be identified with less ambiguity. This is because of the suppression of secondary dissociation and/or ionisation processes which complicate mass spectra measured with longer (nanosecond) laser pulses.

## 6.3 The Dissociative/Ionisation of Nitrobenzene and the Fragmentation of the Molecular Parent Ion at Different Laser Wavelengths and Laser Pulse Widths

### 6.3.1 Experimental

The femtosecond time of flight mass system used has been described in detail in Chapter 3 of this thesis and elsewhere (Langley *et al.*, 1994; Kosmidis *et al.*, 1994a; Ledingham *et al.*, 1995b; Singhal *et al.*, 1996; Kilic *et al.*, 1997; Kosmidis *et al.*, 1997). Briefly, 700 fs at 750 nm laser pulses were re-compressed to the 90 fs using a 4 cm block of SF10 glass. The pulses at $\lambda$ = 375 nm were produced by focusing the output of the laser into a 200 μm thick type 1 BBO crystal. The pulse energy was measured typically 8 μJ and 36 μJ for the 375 nm and 750 nm, respectively, before entering the time-of-flight (TOF) chamber and being focused with 10 cm concave mirror to provide estimated intensities about $10^{12\text{-}15}$ W/cm$^2$. The laser bandwidths at 375 nm and 750 nm are calculated to be 5 nm and 10 nm, respectively.

The nanosecond laser system consists of a XeCl excimer pumped dye laser (Lumonics TEM 860-M and EPD 330) with pulse width about 10 ns. The fundamental output of the TMI dye was used (for $\lambda$ = 375 nm). The mass spectra were recorded with a linear TOF spectrometer of length 1.2 m, based on a Wiley-McLaren design with a

typical mass resolution of 200 at 100 Da. The samples were introduced effusively from the inlet system to the vacuum chamber through a needle valve. The ions were detected by a Thorn EMI electron multiplier connected to a LeCroy 9304 digital oscilloscope.

The same mass spectrometer and signal processing system were used in the experiments with both the femtosecond and nanosecond lasers system. The samples were obtained from the Aldrich Chemical Co and were used as supplied by the manufacturers.

### 6.3.2 Laser Time of Flight Mass Spectrometry on Nitrobenzene

The multiphoton ionisation and dissociation dynamics of benzene ($C_6H_6$) and nitrobenzene ($C_6H_5NO_2$) have been studied and a number of articles have been written about these molecules (Boesl *et al.*, 1990a; 1990b; Weinkauf *et al.*, 1994; Kosmidis et al., 1994a; Ledingham et al., 1995b; Kosmidis et al., 1997). In nitrobenzene, the $NO_2$ group replaces one of the H atoms on the benzene ring. The benzene shows a close shall structure while the nitrobenzene is an open shall molecule. Therefore, as discussed in the previous section of this chapter, the C-N bond is seen to be responsible for the dissociation and fragmentation patterns of either the nitrobenzene neutral molecule or the nitrobenzene molecular ion. The dissociation energy of the C-N bond in nitrobenzene is 3.05 eV and only one photon of 375 nm and two photons of 750 nm are required for the nitrobenzene molecule to be dissociated through the cleavage of this bond. For the case of the nitrobenzene molecular ion only one photon of either wavelength is required for this bond to be broken, Table 6.1.

The ionisation potential (IP) for nitrobenzene has been reported to be 9.86 eV (Matyuk *et al.*, 1979). Therefore, multiphoton ionisation requires at least the absorption of three photons at 375 nm and six photons at 750 nm. The absorption of the first photon ($\lambda$ = 375 nm) is not a resonant step, while the second photon brings the molecules to an excited electronic state (6.6 eV), whose broad one photon

absorption spectrum implies short lifetimes and determined to be less than 10 ps (Takezaki et al., 1997) and thus the existence of very fast non-radiative processes (Nagakura *et al.*, 1964). For the ionisation to take place these non-radiative processes must be "defeated" and it is believed that this can be achieved by using ultra short laser pulses. Although in the case of some small molecules the fragmentation prior to the ionisation has been observed even with ultra short laser pulses, i.e. a DI mechanism (Kumar *et al.*, 1994). However, for polyatomic molecules the dominant mechanism seems to be the ID route when short pulses are used and the fragment ions are generated through a ladder climbing mechanism (Weinkauf *et al.*, 1994; Yang *et al.*, 1983). The latter means that for extremely short laser pulse widths the photon absorption occurs only in the parent molecular ion from which all smaller fragments originate either directly or indirectly.

Fig. 6.1 shows a comparison of the laser induced mass spectra of nitrobenzene with a) $\lambda$= 750 nm and b) $\lambda$ = 375 nm with 90 fs pulse duration and c) $\lambda$ = 375 nm with 10 ns laser pulse duration. All spectra have been recorded using the similar experimental set up. Fig. 6.1d shows the background signal taken before the femtosecond laser experiment carried out on the nitrobenzene. Before nitrobenzene was introduced to the time of flight (TOF) mass spectrometer, the background pressure was about $6x10^{-6}$ torr and in the background spectrum, four peaks have been identified namely, m/q = 18, 19, 28 and 32 corresponding to the $H_2O$, DHO, $N_2$ and $O_2$ ions. In a recent article, Allam *et al.* (Allam *et al.*, 1981) have given a list of the fragment ions from nitrobenzene and $d_5$-nitrobenzene. There was no evidence for the mass 19 and they have not reported this peak in their work. On the other hand, in our laboratory, a number of experiments on nitrobenzene were previously carried out using the same sample which was used for the experiments presented in this work and the peak at m/q=19 effect has never been observed (Ledingham *et al.*, 1995b; Kosmidis *et al.*, 1997). In fig.6.1a, the femtosecond laser time of flight mass spectrum of the nitrobenzene shows a peak corresponds to the mass at m/q=19. It is believed that this peak is due to the $d_2$-nitroethane contamination, since an experiment on $d_2$-

nitroethane was carried out just before the nitrobenzene experiment was initiated and this is a significant peak in its spectrum.

As far as the different dissociation pathways are concerned, it is obvious that their identification is almost impossible from the mass spectrum produced using a ns laser at $\lambda$= 375 nm, because this is dominated by the small mass ion peaks as seen from fig.6.1c. These peaks are generated from the sequential dissociation/ionisation of the daughter fragments, DI. This is due to the long laser pulse duration and the relatively high laser intensities needed for the molecular ionisation (three photon process). In the ns excitation regime at shorter wavelengths, much lower laser intensities are sufficient for the molecular ionisation as discussed in a recent article (Kosmidis *et al.*, 1997). For the case of 246 nm, the molecular ionisation can be achieved *via* a (1+1) excitation process and heavier mass ion peaks have been detected although their intensities are very small (Kosmidis *et al.*, 1994b; Kosmidis *et al.*, 1997). However, for the case of the 375 nm wavelength with 10 ns laser pulse duration (Fig. 6.1c), at least three photons of 375 nm are required to ionise the nitrobenzene molecule and the highest masses observed are $C_4H_n^+$ radical ions with no parent ion. Using a femtosecond laser at $\lambda$ = 375 nm and $\lambda$ = 750 nm, the heavy mass ion peaks become dominant in the mass spectrum (Fig. 6.1a and b). Thus, for the femtosecond laser pulses, the mass spectrum represents more precisely the primary fragmentation pattern of the parent molecule.

A comparison of the femtosecond laser mass spectra taken using 750 nm and 375 nm wavelengths with 90 fs width laser pulses is shown in fig.6.1a and b, respectively. The efficiency of production of either primary or secondary dissociation mass ions as well as parent ion using 750 nm is much higher than this obtained using 375 nm regarding a different number of molecule in the interaction volume. While the highest peak is $C_4H_3^+$ ion peak with a small $C_6H_5O^+$ peak in the 375 nm spectrum, $C_6H_5^+$ ion peak is the dominant with strong parent ion and $C_6H_5O^+$ ion peaks in the 750 nm mass spectrum.

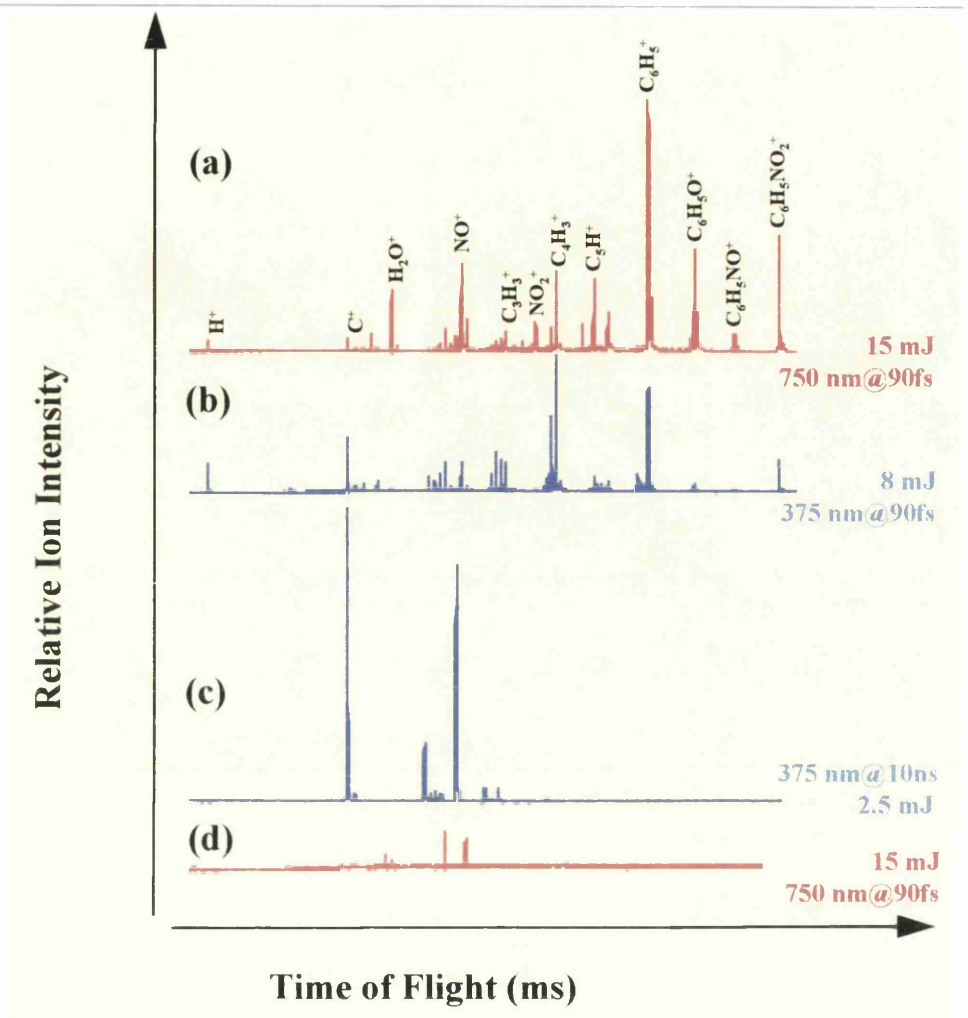


**Figure 6.1:** Laser induced time of flight mass spectra of nitrobenzene. The spectra were taken using (a) 750 nm laser wavelength with 90 fs laser pulses, (b) 375 nm laser wavelength with 90 fs laser pulses, (c) 375 nm laser wavelength with 10 ns laser pulse width and (d) background spectrum was taken before experiment using 90 fs width laser pulses.

A further comparison of the two spectra show three significant differences which can easily be seen from the spectra namely at m/q = 58 and 46 and 15 which correspond to the $CNO_2^+$, $NO_2^+$ and $CH_3^+$, respectively. The peaks for these three radicals exist in the mass spectrum (In Fig. 6.1a) for 750 nm, but in the 375 nm spectrum (in Fig. 6.1b) only a very weak $NO_2^+$ ion peak appears with no $CH_3^+$ and $CNO_2^+$ ion peaks.

The peak at m/q = 58 corresponds to the $CNO_2^+$, and to the author's knowledge, has never been observed before this work using multiphoton processes (Bunn *et al.*, 1986;

Nishimura *et al.*, 1986; Kosmidis *et al.*, 1994a; Marshall *et al.*, 1992a; 1992b; 1992c; Ledingham *et al.*, 1995b; Osterheld *et al.*, 1996; Hwang *et al.*, 1996; Kosmidis *et al.*, 1997). The $CNO_2$ fragment from the nitrobenzene ion was investigated using the kinetic energy release technique (Abd El-Kader and Ahmet, 1983) and it was proposed that the radical ion at m/q=58 can be obtained in the nitrobenzene ion through a -NO loss process followed by recombination of the fragments *via* eq.(6.5) and (6.6) and subsequently ionised by absorbing some photons.

$$CNO_2 + h\nu \rightarrow CNO_2^+ \qquad (6.7)$$

This peak has also been observed in both CID and EI spectra of picric acid. In EI spectrum, it was attributed to the loss of NO+CO neutrals from the TNP (2,4,6-trinitrophenol) molecular parent ion (Zitrin and Yinon, 1978) which has a H atom joined to the C atom in the metha position to the hydroxyl group and hydroxyl group replaced with a methyl group in the TNT structure.

Through the dissociation of either the neutral or ionic nitrobenzene molecule, the $NO_2$ neutral fragment is produced *via* the reactions (1) and (6) in Table 6.1. In the case of the neutral ground state $NO_2$ molecule, the results are dissussed in the 4th chapter of this thesis and it is shown that the $NO_2^+/NO^+$ ratio is about 100% in the case of 750 nm and 10% for the 375 nm. This spectrum shows that the neutral NO molecule produced through a number of possible reactions in Table 6.1. The $NO_2^+/NO^+$ ratio in the femtosecond laser mass spectra of nitrobenzene at both wavelengths is much smaller than what observed from the neutral ground state $NO_2$ molecule. Therefore, the smaller $NO_2^+/NO^+$ ratio in the mass spectra suggests that a considerable contribution to the $NO^+$ ion peak could be made by a number of opened channels apart from the $NO_2$ loss channel.

Panczel and Baer (Panczel and Baer, 1984) concluded that the $-NO_2$ loss occurs from an excited electronic state of the ion by a simple C-N bond cleavage. This implies the preservation of the nitrobenzene structure at least for this reaction and it was the first time that the direct dissociation from an excited state was reported for such a large

ion as nitrobenzene. It should be noted that the $-NO_2$ loss channel and all the other reactions of Table 6.1 are also compatible with the isomerization to phenylnitrite structure by breaking the $C_6H_5$-ONO bond or the $C_6H_5O$-NO bond and so on. The -NO loss channel is favoured in a phenylnitrite structure and can be formed through the vibronic relaxation of electronic excited states of the nitrobenzene ion. This is consistent with the relatively low appearance potential (AP) of the -NO loss channel. The internal conversion of the electronic excitation energy of the ion requires the absence of strongly repulsive excited states, which would cause fast decomposition before much of the electronic energy is degraded. This condition could be satisfied for excitations from molecular orbitals (MO) which are not localised in one particular bond. Such as the $\pi$-MO of the aromatic ring, which are spread all over the ring and therefore their excitation causes a small weakening of all bonds. On the other hand, excitation from a MO localised on one bond results in a drastic weakening of this particular bond, causing the resulting electronic state to be strongly repulsive. It has been proposed for nitrobenzene that the first two IP correspond to excitations from a ring $\pi$-type MO (Rabalais, 1972). Thus, the excitation to these ionic states is likely to be followed by electronic to vibronic energy redistribution and the resulting molecular rearrangement could provide the reasons for the observation of $C_6H_5O^+$ and $NO^+$ ions.

Fig. 6.2a and b show the laser pulse energy dependencies of the nitrobenzene molecule at 375 nm and 750 nm, respectively. The sample pressures for both experiments were typically $10^{-5}$ torr. The laser pulse energy was altered using a neutral density filter and measured with a joulemeter. The pulse energies for each spectrum are shown at the right end of each spectrum (Fig. 6.2a and b).

The dissociation pathways presented in Table 6.1 are verified by the ion peaks which appear in the fs mass spectra (Fig. 6.1a and b). It can be easily seen that the ions produced in reactions 4-9 in Table 6.1 are the ones which are generated first in the fs spectra at the lowest laser intensities. As the intensity increases numerous other peaks become visible almost certainly produced by an ID process. In addition, peaks with

m/q = 27 and m/q = 17 have been observed. The latter is attributed to $OH^+$, while the m/q = 27 peak could be assigned to $HCN^+$ or $C_2H_3$.

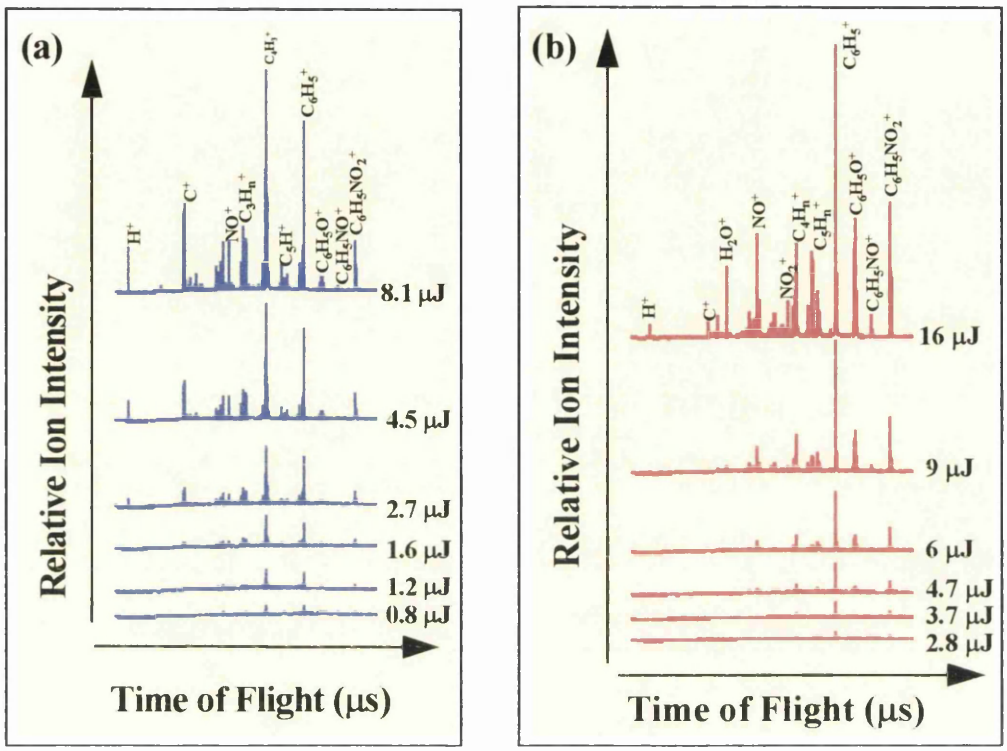


**Figure 6.2:** Laser induced time of flight mass spectra of nitrobenzene. The spectra were taken using (a) 375 nm and (b) 750 nm laser light with 90 fs laser pulse width.

Fig. 6.3a and b show the laser intensity dependencies of the nitrobenzene and related fragments. The ion intensities for each ion were multiplied by a different constant to put them in arbitrary ascending order and plotted as ion yield versus laser intensity in a log-log scale. The laser intensity dependence (Fig. 6.3a) of the parent molecular ion production was found to be about $n \approx 2$ for 375 nm and the gradients of all other fragments are very similar to that of the parent ion suggesting a common parent precursor.

For the case of the wavelength of 750 nm, much higher pulse energies are available and some of the neutral fragments have been ionised, such as $NO_2^+$ and $CNO_2^+$ ions have been observed in the case of 750 nm. The intensity dependence of the nitrobenzene parent ion decreases as the laser intensity increases. In the lower laser

intensity range, the intensity dependence of the nitrobenzene parent ion is about n ≈ 3-4, while in the higher laser intensity range it becomes about n ≈ 1-2. In the lower laser intensity range, the difference between the calculated number of photons absorbed for both wavelengths used is some evidence for the assumption that a non-resonance multiphoton process is responsible for the molecular ionisation. In the case of the weakness of the nitrosobenzene ion peak and the laser intensity dependence of the parent molecular ion support the hypothesis that, the ionisation follows the multiphoton process; a non-resonance molecular excitation and ionisation take place first, followed by fragmentation processes.

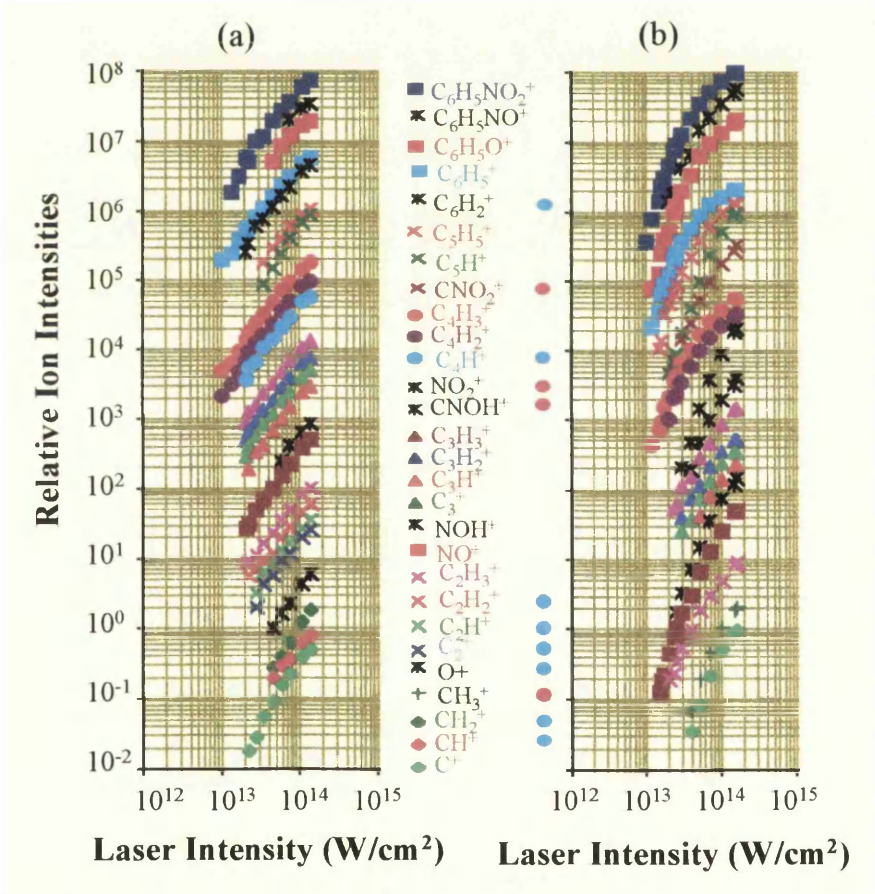


**Figure 6.3:** Laser intensity dependencies of nitrobenzene at the wavelengths of (a) 375 nm and (b) 750 nm. In both case, 90 fs width laser pulses were used. The solid circles at the right hand side of some of the labels indicate that these radicals were observed using only one wavelength but could not observed using other. Blue and red solid circles indicate that the radical were only observed in the spectra using 375 nm and 750 nm wavelengths, respectively.

## 6.4 The Laser Pulse Width Dependence of the Dissociative-Ionisation and Fragmentation Pattern of Nitrobenzene Time of Flight Mass Spectra

Recently, the short pulse laser technology has opened a novel window for scientists to investigate the larger molecules using multiphoton process. The efficiency of the resonance enhanced multophoton ionisation (REMPI) process in large organic molecules cannot be increased by increasing the laser intensity in the interaction region since the photofragmentation rate increases parallel to the laser intensity. In a number of recent studies, it is proposed that the degree of molecular fragmentation depends on the laser intensity, laser wavelength, laser pulse width and the structure of molecule (Weinkauf *et al.*, 1994; Ledingham *et al.*, 1995a; 1995b; Singhal *et al.*, 1996; Kilic *et al.*, 1997; Kosmidis *et al.*, 1997; Singhal *et al.*, 1997). Singhal *et al.* (Singhal *et al.*, 1997) have recently shown that the laser pulse width plays a role on the ionisation-fragmentation dynamics which is much more effective than that the laser intensity plays due to the fact that the $NO_2^+/NO^+$ ratio shows a little change as the laser intensity changes, but this ratio dramatically decreases as the laser pulse width increases.

A comparison of the time of flight mass spectra at 375 nm with 90 fs (in Fig. 6.1b) and 10 ns (in Fig. 6.1c) has already been made in the previous section of this chapter and elsewhere (Ledingham *et al.*, 1995b; Kosmidis *et al.*, 1997). In the nanosecond regime, the time of flight mass spectrum is always dominated by the small mass ion peaks as discussed previously (Kosmidis *et al.*, 1997). It has also been shown that on the ns time scale, the nitrobenzene molecular parent ion is always missing for the case of the 375 nm. In the case of 90 fs laser pulse duration, the molecular parent ion is one of the prominent peaks in the mass spectrum (Fig. 6.1b and 6.2a).

Fig. 6.4 shows femtosecond laser induced time of flight mass spectra of nitrobenzene taken using different laser pulse widths at the wavelength of 750 nm. The laser pulse

energies and relevant laser intensities are shown at the left end of each spectrum and the laser pulse widths at the right end of each spectrum.

A comparison of these three spectra shows a significant dependence on the laser pulse width for the ionisation efficiency and fragmentation patterns of the parent molecule since they have been taken with nearly the same laser intensities. Particularly a comparison of fig.6.4a and 6.4c shows the importance and significance of use of ultra short laser pulses. It is clearly seen that in the case of shorter laser pulses, the mass spectrum shows a dominant parent ion peak with a little fragments (in Fig. 6.4a), but, in the case of longer laser pulses (742 fs in Fig.6.4c), the ionisation efficiency of the parent ion is small and the fragmentation of excited neutral molecule occurs and the neutral fragments are subsequently ionised. In Fig. 6.4c, the $H^+$ and $C^+$ fragment ion peaks are seen with $1.69 \times 10^{13}$ W/cm$^2$ laser intensity. As the laser parameters are changed to shorter pulse widths (from the conditions of Fig. 6.4c to Fig. 6.4b), the number of $H^+$ and $C^+$ ions decreases while the number of parent ion and higher mass fragment ions relatively increase. When the shortest laser pulses are reached (in Fig. 6.4a), no $H^+$ and $C^+$ fragment ions are detected but the parent ion peak becomes much higher.

In the case of 90 fs laser pulses (Fig. 6.4a), there might be significant information about the fragmentation pathways in the nitrobenzene molecular ion. In accordance with a recent conclusion made by Hwang *et al.* (Hwang *et al.*, 1996), the results presented in this work supports the idea that the dissociation rates for the production of $NO^+$, $C_6H_5^+$ and $C_6H_5O^+$ are in competition and the spectra in fig. 6.4a shows an agreement with the previous conclusion since these three products start to appear together in the case of lowest laser intensity and they increase as the laser intensity increases. Using longer laser pulses, it is almost impossible to obtain such structural information about the dissociation pathways of either the neutral or ionic nitrobenzene molecule.

In Table 6.1 the known dissociation channels of nitrobenzene and its molecular ion are presented. In the time of flight mass spectrum of nitrobenzene, shown in fig.6.1a and b for the case of 90 fs laser pulses, a peak appears at the mass 107 and this corresponds to the nitrosobenzene ion ($C_6H_5NO^+$). In the previous experimental studies (Bunn et a., 1986; Nishimura *et al.*, 1986), it was shown that no nitrosobenzene ion peak was observed in the photodissociation of nitrobenzene ion. A conclusion has been made in a recent article (Kosmidis *et al.*, 1997) that the presence of the m/q = 107 peak in the mass spectra of nitrobenzene could be an evidence of a DI route.

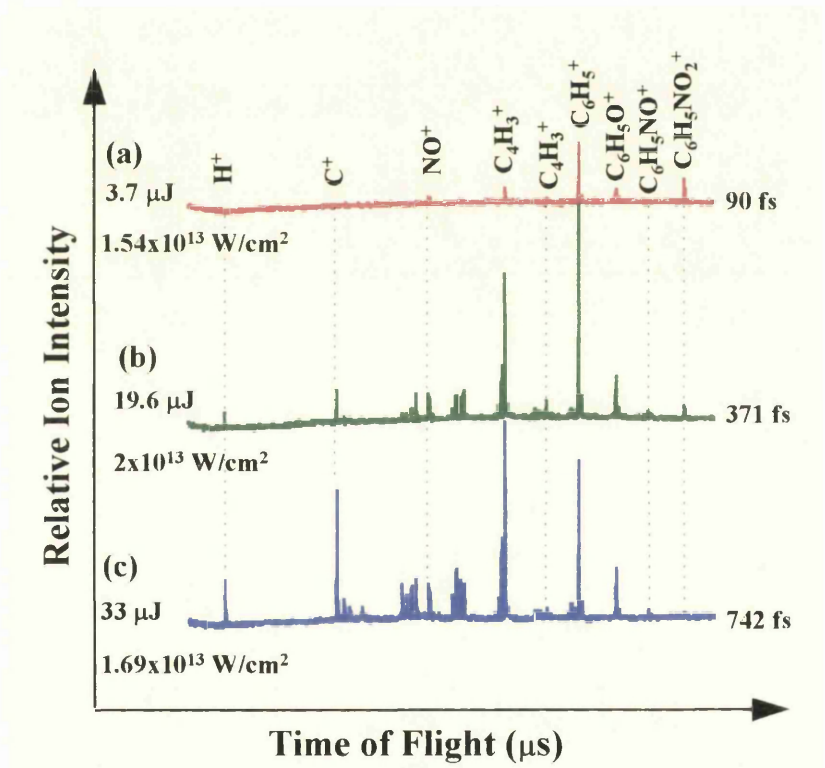


**Figure 6.4:** Laser induced mass spectra of nitrobenzene were taken using (a) 90 fs, (b) 371 fs and (c) 742 fs laser pulse widths. The laser pulse energy and corresponding laser intensities used to illuminate sample are given at the left end of each spectrum.

In fig.6.4, the fragment ion peak at the m/q=107 changes as a function of laser pulse width rather than the laser intensity used. These results support the conclusion made by Singhal *et al.* in a recent article (Singhal *et al.*, 1997). As the laser pulse duration changes from 90 fs (in Fig.6.4a) to 742 fs (in Fig.6.4c) the height of the mass 107

peak increases with increasing pulse width, indicating that the dissociation of the neutral nitrobenzene molecule starts to happen when the laser pulse duration becomes longer. From the results presented in fig 6.4, the conclusion can be made that the production of m/q = 107 peak from a DI route has a higher probability relative to the ID route for longer pulse widths.

The thermochemical threshold for the -O loss channel (reaction 3) is 3.96 eV, and therefore the absorption of two photons of $\lambda$= 375 nm and three photons of $\lambda$= 750 nm are required for this channel to be opened. The absorption of two photons of 375 nm corresponds to the $\pi \rightarrow \pi^*$ transition of benzene (Nagaqura *et al.*, 1964). In the femtosecond laser mass spectrum of nitrobenzene (Fig. 6.1b) at 375 nm, the nitrosobenzene ion is almost absent. For the case of 750 nm, the femtosecond laser mass spectrum of nitrobenzene (Fig.6.1a) shows m/q =107 ion peak which is much stronger than that at the 375 nm mass spectrum but it is still weak compared to other ion peaks. The weak appearance of the m/q=107 peak at 375 nm and 750 nm could be explained by a) the assumption that the radiationless processes are much slower, which has a lifetime of $\leq$10 ps (Takezaki *et al.,* 1997), than the time duration of the laser pulse, and/or b) that the molecular ionisation takes place *via* a non-resonant multiphoton process.

In addition to the preceding concerning the 107 mu ion peak, its laser intensity dependence in fig. 6.3b is rather similar to that of parent ion suggesting that, assuming the conclusion made by Bunn *et al.* and Nishimura *et al.* are true, the ionisation and dissociation process for nitrobenzene at both wavelengths is likely to be a mixture of DI and ID processes.

## 6.5 Conclusions

In this chapter, the photodissociation of the nitrobenzene has been studied using 90 fs laser pulses at $\lambda$ = 375 nm and 750 nm. The laser mass spectra at 90 fs are compared

with those observed with a 10 ns dye laser at the same wavelength using the same experimental set up. The recorded mass spectra are different, as expected. The parent ion and the heavier fragment peaks have been clearly observed only in the spectra with fs laser pulses. The 90 femtosecond mass spectra show a prominent parent ion peak and very large $C_6H_5^+$, $C_4H_3^+$ and $NO^+$ ion peaks for 375 nm while the nanosecond mass spectrum at 375 nm, has only prominent $C_1H_n^+$, $C_2H_n^+$, $C_3H_n^+$ and $NO^+$ ion peaks with a very weak $C_4H_n^+$ group. The large parent and heavy mass peaks are characteristic of ID process where the dissociative below-ionisation states are "defeated" to some degree by the fast up-pumping. The nanosecond nitrobenzene spectrum is very similar (apart from the $NO^+$ peak) to the spectra described by DeWitt and Levis (DeWitt and Levis, 1995) when cyclic aromatic hydrocarbons are ionised and fragmented using a ns laser at 532 nm and fluxes of about $2x10^8$ W/cm$^2$.

On the other hand some fragmentation pathways follow from a molecular rearrangement. The present experiment shows that most of the observed fragmentation takes place from the nitrobenzene structure rather than phenylnitrite.

At the 750 nm, the results being presented in this chapter is very similar to that observed at 375 nm for 90 fs laser pulses and shows very much different process than that at 10 ns. The femtosecond laser mass spectrum at 750 nm is dominated by heavier mass ion peaks with a prominent parent ion. The results shown in fig.6.1a and 6.2b shows a significant large ion peak at m/q=107 corresponding to the $C_6H_5NO^+$ which comes from a rearrangement process of nitrobenzene to phenylenitrite $C_6H_5ONO^+$ and subsequently loss of an oxygen through the dissociation of the N-O bond.

The absence of the 107 mass ion peak from nitrobenzene has already been attributed to a DI process (Bunn *et al.*,1986; Nishimura *et al.*, 1986; Kosmidis *et al.*, 1997) which means that the presence of this peak suggests an ID process. The results being presented shows presence of this peak suggests that a mixture of an ID and DI processes takes place with the laser parameters used.

# CHAPTER 7

# FEMTOSECOND MASS SPECTROMETRY OF MEDIUM SIZE NITRO-AROMATIC EXPLOSIVES

## Contents

## 7.1 Introduction

In this chapter, the multiphoton dissociation and ionisation dynamics of medium mass nitroaromatic explosives; three isomers (*ortho-, metha- and para-)* of nitrotoluene, 2, 4-dinitrotoluene and 2, 4, 6-trinitrotoluene are discussed. The photochemistry and photophysics of this group of compounds is of great significance in the science of energetic materials and have been extensively studied over the years. This group of thermally labile molecules easily fragment through a photorearrangement process prior to ionisation. It is, hence, thought that they have the ideal structure and properties to study the dissociation pathways.

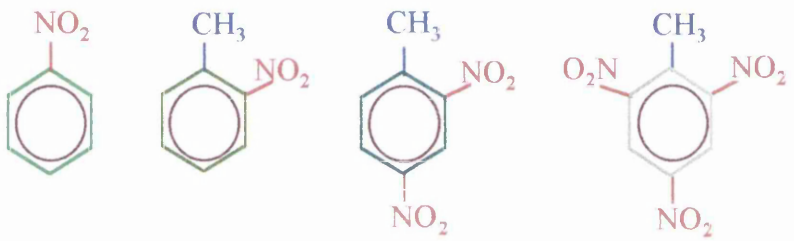


**Figure 7.1:** Geometric structures of (a) nitrobenzene, (b) *o*-nitrotoluene, (c) 2-,4-Dinitrotoluene and (d) 2-, 4-, 6-trinitrotoluene.

Fig. 7.1 shows the geometries of nitrobenzene, *o*-nitrotoluene, dinitrotoluene and trinitrotoluene. The main characteristic structure for this group of molecules are the existence of $NO_2$ and $CH_3$ groups joined to the benzene ring through C-N and C-C bonds, respectively. There is a basic difference between some of these molecules and this difference appears in the mass spectra due to the interaction between the methyl and nitro groups. The difference in the mass spectra is known as the *ortho*-effect which was reviewed and discussed in detail by Schwartz (Schwartz, 1978). The *ortho* effect for nitro-containing molecules has also been discussed in a number of previous articles (Ramana *et al.*, 1990; Konnecke *et al.*, 1980) for some nitro-containing molecules and (Bulusu and Axenrod, 1979; Yinon, 1987; 1988; 1992; Ledingham *et al.*, 1995b; Kosmidis *et al.*, 1997) for nitroaromatic explosives.

In the previous chapter the nitrobenzene molecule was investigated as a prototypical molecule for nitroaromatic explosives with only an $NO_2$ group joined to the benzene ring (Fig.7.1a). The difference between nitrobenzene and other molecules examined in this chapter is existance of an extra $CH_3$ group in the nitrotoluene isomers (Fig.7.1b shows *o*-nitrotoluene), dinitrotoluene (Fig.7.1c) and trinitrotoluene (Fig.7.1d). Dinitrotoluene and trinitrotoluene have also two and three $NO_2$ groups, respectively, which have different localizations with respect to the $CH_3$ group on the benzene ring.

On the other hand, it has already been shown in the literature that there are many similar characteristics between nitrobenzene and three isomers of nitrotoluene. Therefore, it is expected that many common characteristics would appear in their ionisation and photodissociation processes. Hence, the knowledge of the photochemistry of nitrobenzene is essential for understanding that of the nitrotoluene isomers which is also expected to contribute to the understanding of the entire group of nitro-explosives including dinitrotoluene (DNT) and trinitrotoluene (TNT).

This group of molecules has already been investigated by a number of groups using several methods and most of the studies done using laser based techniques were in the nanosecond regime. It is believed that in the nanosecond time scale there exists little useful information in the mass spectrum about dissociation pathways in these molecules or their ions (Marshall *et al.*, 1992a; 1992b; 1992c; 1993; Clark *et al.*, 1993; Lemire *et al.*, 1993; Kosmidis *et al.*, 1994a; 1994b; Marshall *et al.*, 1994a; 1994b; Ledingham *et al.*, 1995b). In order to better understand the mass spectral fragmentation pathways, it is the thought that the femtosecond laser mass spectrometry offers a useful tool and was used to investigate the photoionisation and photofragmentation processes in this class of molecules. Thus femtosecond laser mass spectrometry has been applied and some parts of the data from our experiments have been presented in a number of recent articles (Ledingham *et al.*, 1995b; Kilic *et al.*, 1997; Kosmidis *et al.*, 1997) and will be discussed in greater detail in this chapter.

In this chapter, the nitrotoluene isomers will be discussed first comparing their

nanosecond and femtosecond laser mass spectra. Secondly, nanosecond and femtosecond laser mass spectra of dinitrotoluene and trinitrotoluene will be discussed comparing the mass spectra of *o*-nitrotoluene, dinitrotoluene and trinitrotoluene in either nanosecond or femtosecond regimes. The multiphoton processes in DNT will finally be made in the femtosecond regime.

## 7.2 Femtosecond Laser Mass Spectrometry (FLMS) on the Three Isomers of Nitrotoluene and An Investigation of Multiphoton Processes at 375 nm

### 7.2.1 Experimental Arrangement

The experimental set-up has been described in detail in chapter 3 of this thesis and elsewhere (Langley *et al.*, 1994; Ledingham *et al.*, 1995b; Singhal *et al.*, 1996; Kilic *et al.*, 1997; Kosmidis *et al.*, 1997). Briefly, 700 fs laser pulses were the output of the laser system after the amplifier. The pulses were re-compressed to 90 fs by a 4 cm block of SF10 glass. The pulses at $\lambda$ = 375 nm were produced by focusing the output of the laser into a 200 mm thick type 1 BBO crystal. Before entering the time-of-flight (TOF) chamber the pulse energy was typically 10 $\mu$J at 375 nm before being focused with 30 cm fused silica lens to provide estimated intensities about $10^{11\text{-}13}$ W/cm$^2$.

The nanosecond laser system consists of a XeCl excimer pumped dye laser (Lumonics TEM860-M) with 10 ns pulse duration. The 375 nm fundamental output of TMI dye from a tunable dye laser (Lumonics EPD 330) was used in the experiment. The mass spectra were recorded with a linear TOF spectrometer of length 1.2 m, based on a Wiley-McLaren design with a typical mass resolution of 200 at 100 Da. The samples were introduced effusively from the inlet system to the vacuum chamber through a needle valve. The ions were detected by a Thorn EMI electron multiplier connected to a LeCroy 9304 digital oscilloscope.

The same mass spectrometer and signal processing system were used in the

experiments with both the femtosecond and nanosecond lasers. The samples were obtained from the Aldrich Chemical Co and were used as supplied by the manufacturers. The sample in the sample holder and inlet system was externally heated to obtain sufficient sample pressure in the ionisation chamber from 4-nitrotoluene, dinitrotoluene and trinitrotoluene. For other samples heat was not needed since enough gas pressure could be obtained at room temperature.

### 7.2.2 A comparison of Nanosecond and Femtosecond Laser Induced Mass Spectra of *o*-Nitrotoluene at 375 nm

The photodissociation of the nitrotoluene isomers have been extensively studied using multiphoton process in the nanosecond regime (Marshall *et al.*, 1992c; 1993; 1994a; Kosmidis *et al.*, 1994a; 1994b) and femtosecond regime (Ledingham *et al.*, 1995b; Kosmidis *et al.*, 1997). It was concluded that the dissociation occurs through the multiphoton process and has been interpreted by two main (DI and ID) fragmentation mechanisms. In the first mechanism fragmentation of the neutral molecule is followed by the ionization (DI mechanism (Yang *et al.*, 1983)) of neutral fragments, while in the second the ionization of neutral parent molecule is followed by the dissociation (ID mechanism) of molecular parent ion.

Fig. 7.2 shows a comparison of the fragmentation pattern of *o*-nitrotoluene in the femtosecond (a) and nanosecond (b) laser induced time of flight mass spectra. Sample pressures for both case were about 6-8x$10^{-5}$ torr and other experimental conditions were similar apart from different laser pulse widths and laser pulse energies used in both experiments. The difference between these two spectra is clear and it is seen that in the nanosecond regime small mass ion peaks dominate the mass spectrum while the femtosecond laser induced mass spectrum of *o*-nitrotoluene molecule shows the heavier mass fragments including a strong parent ion, which is one of the strongest peaks in the mass spectrum. It clearly indicates that the femtosecond laser mass spectrum has a much greater potential for analytical and structural interpretation than the nanosecond spectrum.

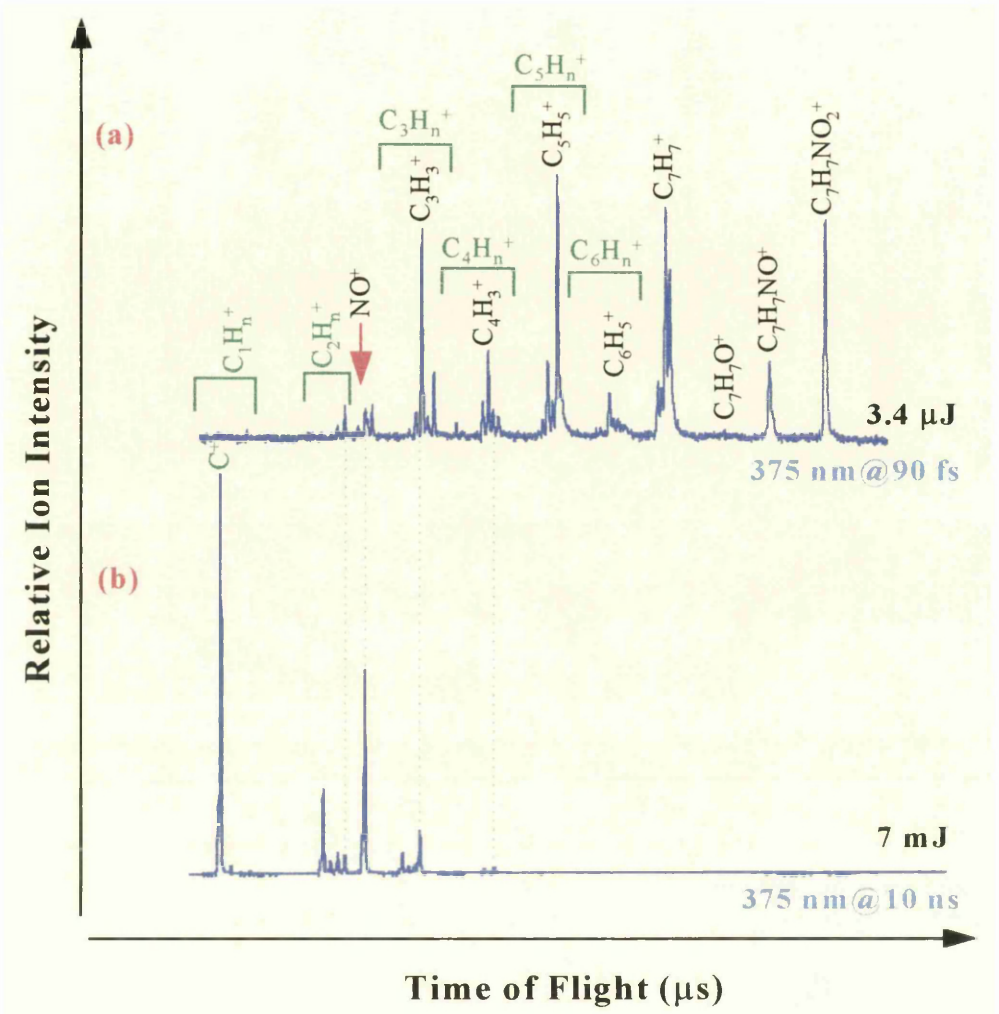


**Figure 7.2:** A comparison of femtosecond (a) and nanosecond (b) laser induced time of flight mass spectra of *o*-nitrotoluene.

In the nanosecond laser induced mass spectrum (Fig. 7.2b), there are two dominant peaks which correspond to $C^+$ and $NO^+$ ions and their ion yields in the mass spectrum are much greater than these in the femtosecond laser induced mass spectrum. It was described in Chapter 4 of this thesis and repeated in a number of articles (Herzberg, 1950; Ledingham *et al.*, 1995b; Singhal *et al.*, 1996; Kilic *et al.*, 1997) that the 375 nm is in resonance with the $D^2\Sigma^+ \leftarrow X^2\Pi$ transition in neutral NO molecule. It can clearly be seen that the resonance enhancement in the nanosecond regime takes place in the neutral NO molecule.

The ionization potentials (IP) for three isomers of nitrotoluene were reported in the

literature to be 9.45 eV, 9.48 eV and 9.4 eV for *o*-, *m*- and *p*-nitrotoluenes (Lias *et al.*, 1988), respectively. One laser photon at 375 nm carries 3.3 eV energy, and therefore, it takes three photons at 375 nm to ionise the three isomers of the nitrotoluene molecule. In off resonance circumstances, it is expected that the gradient of the laser intensity dependent graphs for three isomers of nitrotoluene would have similar gradient due to the power index law ($\propto \sigma I^n$, where n is the number of photons absorbed).

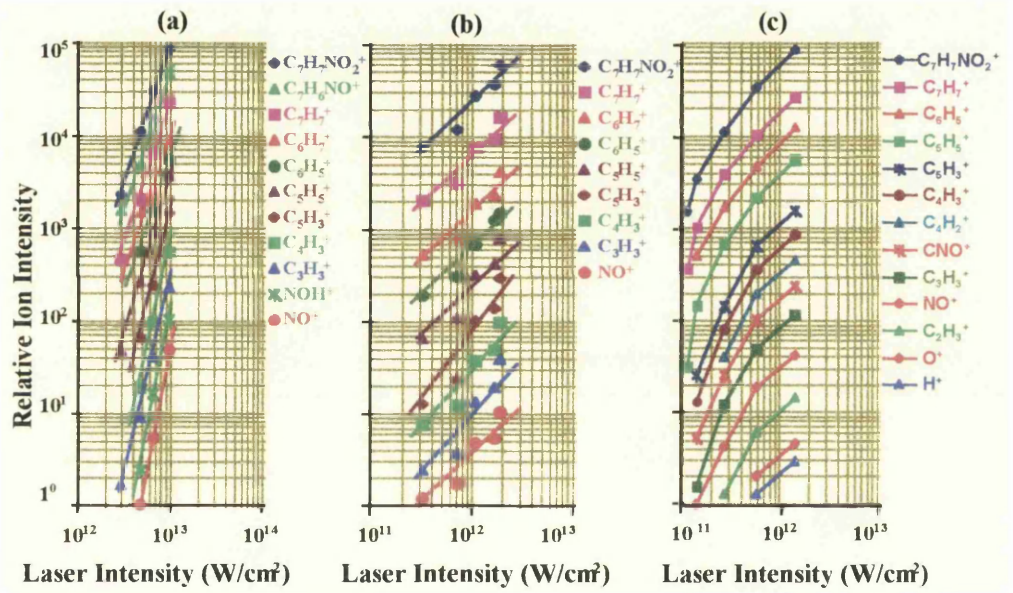


**Figure 7.3:** Laser intensity dependencies of *o*-nitrotoluene (a), *m*- nitrotoluene (b) and *p*-nitrotoluene (c). All three experiments were carried out using 90 fs laser pulses at 375 nm.

Fig. 7.3a, b and c show the laser intensity dependencies for the parent ion peaks and the most prominent fragment ion peaks for *o*-, *m*- and *p*-nitrotoluene. The laser intensity dependencies in this case are about 3 for *o*-nitrotoluene parent ion and fragment ions, but are only between 1 and 2 for the *m*- and *p*-nitrotoluene parent ions and the fragments. The laser intensity dependencies of *m*-nitrotoluene (Fig. 7.3b) and *p*-nitrotoluene (Fig. 7.3c), particularly in the similar intensity range (about $10^{11}$ W/cm$^2$), are very similar but these are different than that observed for *o*-nitrotoluene despite higher laser intensities being used in the *o*-nitrotoluene experiment. These results suggest that the multiphoton excitation, ionization and fragmentation processes in the *o*-nitrotoluene are slightly different than that in the *m*- and *p*-

nitrotoluene. The case of *o*-nitrotoluene suggests a three photon multiphoton excitation and ionization processes with non of the intermediate steps being saturated. In the case of *m*- and *p*-nitrotoluenes, smaller laser intensity dependencies can be explained assuming that one or two of the steps are close to the saturation at these laser intensities.

The laser intensity dependence of the parent ion in the nanosecond regime at the wavelength range of 210-270 nm was investigated by Kosmidis *et al.* (Kosmidis *et al.*, 1994b) and shown that the laser intensity dependence of *m*- nitrotoluene parent molecule was also about 1 whereas the intensity dependence of the NO ion was about 3. Kosmidis *et al.* indicated that there were both DI and ID channels operating in the nanosecond regime. In the present experiment, at the vicinity of 375 nm the laser intensity dependencies of *o*- and *m*- nitrotoluene isomers were carried out using nanosecond laser pulses but no parent ion has been observed in the mass spectra as shown in fig. 7.2b. The laser pulse energy dependence of the fragmentation pattern in the time of flight mass spectra and the laser intensity dependencies for some of the major fragments from the *o*-nitrotoluene are shown in fig. 7.4a and b, respectively. The laser intensity dependencies of the most of the fragment ions are slightly different and this is about 2.6 for $NO^+$ which supports three photon multiphoton excitation and ionization processes in the neutral NO molecule. The similar gradient for the laser intensity dependence of neutral NO molecule was found from the dissociation of neutral $NO_2$ molecule (Singhal *et al.*, 1996) and discussed in chapter 4 of this thesis.

From the laser intensity dependence graph of the major fragment ions in the nanosecond regime (Fig. 7.4b), it is difficult to conclude which is the precursor of most of the fragments. However, in the case of femtosecond laser pulses there exists a dominant parent ion and the slopes of the graphs are very similar for parent ion and the fragment ions in the case of each isomers. This might suggest that an ID route in the multiphoton process is the principal dissociation mechanism in the three isomers of nitrotoluene.

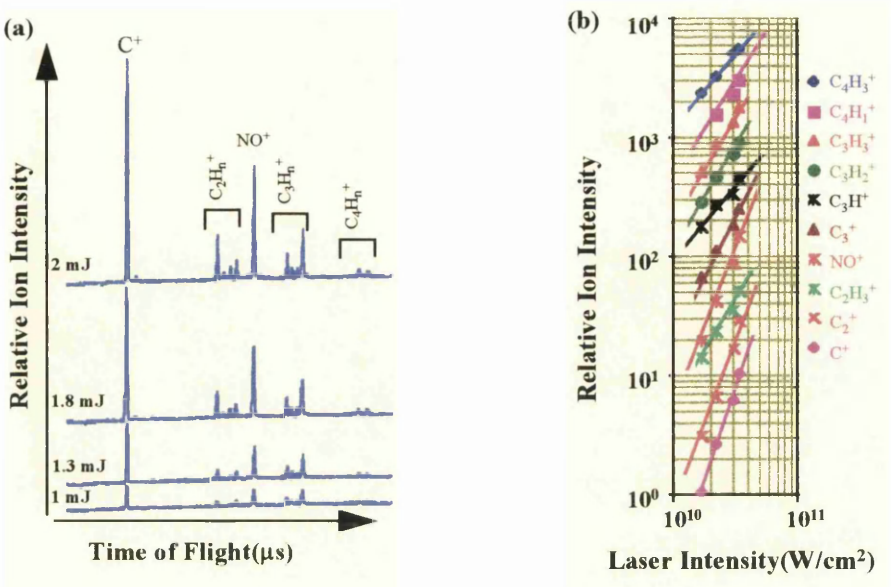


**Figure 7.4:** (a) Laser pulse energy dependence of fragmentation pattern in the mass spectra of *o*-nitrotoluene. (b) The laser intensity dependencies of major fragment ions from neutral *o*-nitrotoluene molecule. Data was taken using 10 ns laser pulses at 375 nm.

### 7.2.3 Identification of Three Isomers (*Ortho-*, *metha-* and *Para-*) of Nitrotoluene at 375 nm

We have carried out a series of experiments on the nitrotoluene isomers using 10 ns and 90 fs laser pulses at 375 nm. The comparison of femtosecond and nanosecond laser induced mass spectra for *o*-nitrotoluene molecule was discussed in section 7.2.2. It has already been shown that there exist very significant differences in the femtosecond and nanosecond laser induced fragmentation pattern of the mass spectra of *o*-nitrotoluene. It should also be mentioned that for the analytical purpose no or little information for the identification of nitrotoluene isomers or the dissociation/fragmentation pathways could be obtained when the nanosecond laser is used to investigate these. For the identification of these molecules, many techniques have been used, including liquid and gas chromatography, ion mobility spectrometry (Yinon and Zitrin, 1993), cyclotron resonance mass spectrometry (Cassady and McElvany, 1993) and laser mass spectrometry (Kosmidis *et al.*, 1994b and 1997). The detection of nitroaromatic explosives and understanding their dissociation and fragmentation mechanisms has gained an increasing interest because of their high strategic importance.

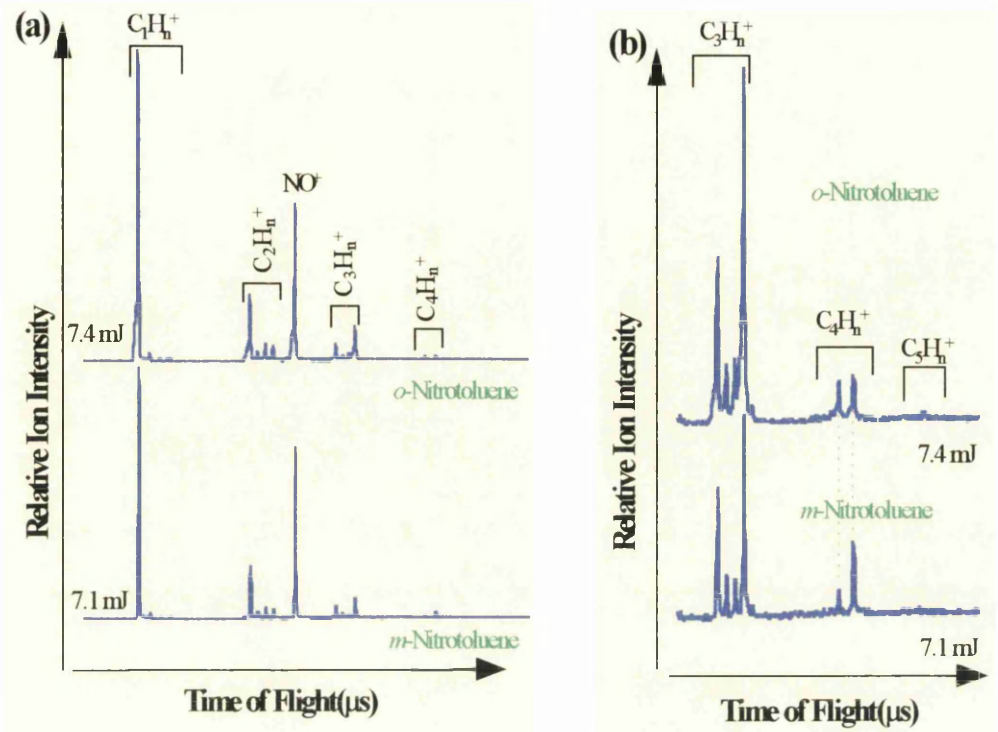


**Figure 7.5:** (a) A comparison of the nanosecond laser induced fragmentation patterns of *o*- and *m*-nitrotoluene molecules. (b) Heavier mass ion part of the spectra in (a).

Fig. 7.5 shows a comparison of the nanosecond laser induced time of flight mass spectra of *o*-nitrotoluene and *m*-nitrotoluene isomers. Since the most of the fragment ion peaks may have some contributions from several dissociation channels, it is very difficult to have a conclusion for the dissociation and fragmentation pathways in the molecules. The comparison of both spectra (Fig. 7.5a) shows that no significant difference between these two spectra exists apart from the relative ion yields. Fig. 7.5b shows the heavier mass ion peaks part of the mass spectra shown in fig. 7.5a. It should be pointed out that no significant difference has been mentioned for the fragmentation patterns of three isomers of nitrotoluene in the literature at the nanosecond regime, apart from some works which investigated above ionization threshold fragmentation pattern (Kosmidis *et al.*, 1994b). The mentioned differences in the work of Kosmidis *et al.* appear in the heavier mass part of the mass spectra.

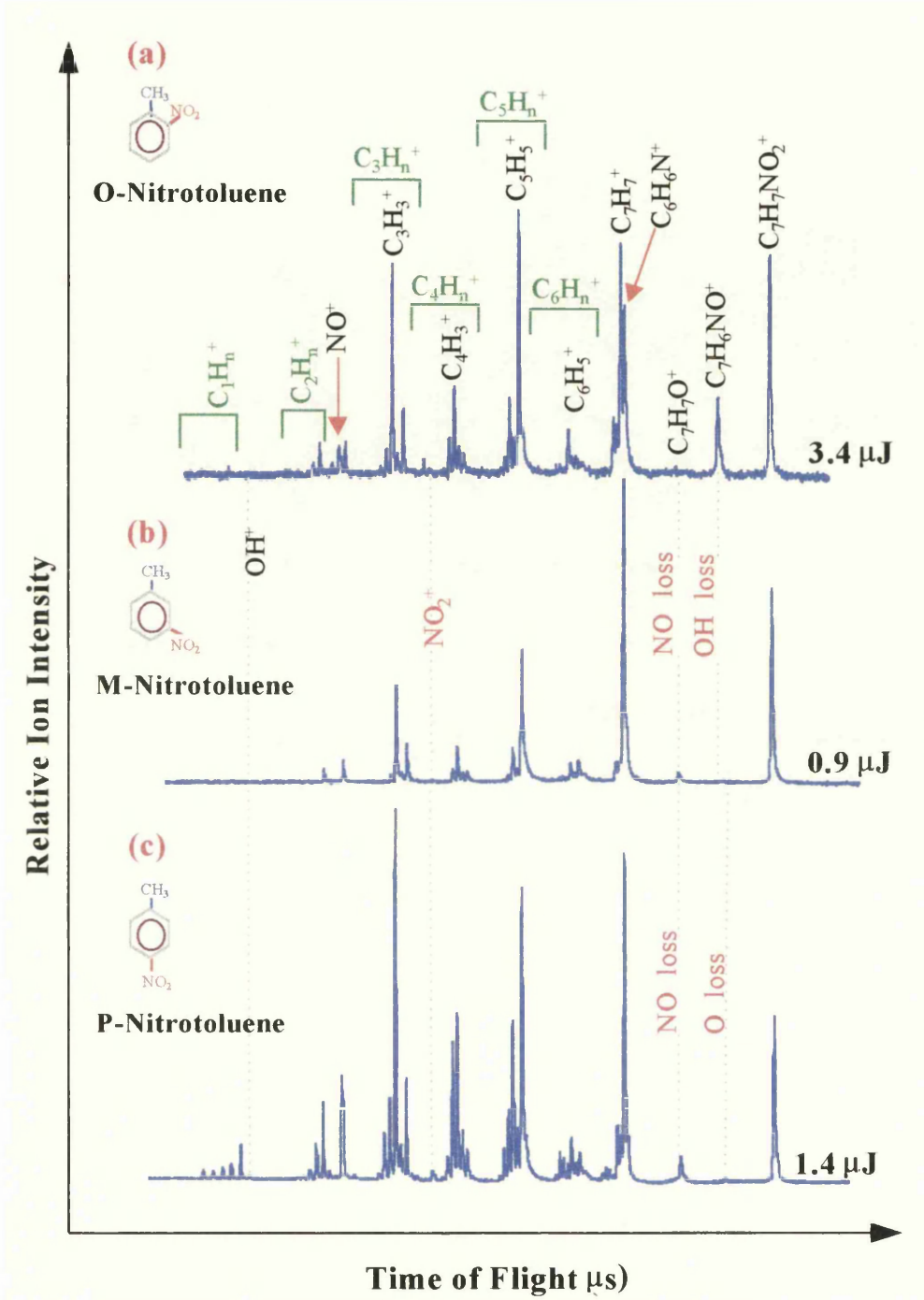


**Figure 7.6:** The femtosecond laser induced mass spectra are shown for (a) *o*-nitrotoluene, (b) *m*-nitrotoluene and (c) *p*-nitrotoluene. Geometry of each isomer is shown at the left hand side of each spectrum.

Fig. 7.6 shows the femtosecond laser induced mass spectra of the three isomers of nitrotoluene at 375 nm. The three spectra in fig. 7.6 have been recorded under

identical experimental conditions apart from the need of heating up the *p*-nitrotoluene isomer to obtain sufficient vapour pressure in the ionization chamber. In the case of 90 fs laser pulses, a strong parent ion peak and a number of heavier mass peaks are clearly recorded for all isomers, while these were missing when nanosecond laser pulses were used at the wavelength of 375 nm as discussed above. It is clearly seen from the comparison of femtosecond laser mass spectra of three isomers of nitrotoluene (Fig. 7.6) that the femtosecond laser mass spectrometry is a powerful technique to elucidate the dissociation and fragmentation pathways of these thermally labile molecules. The differences in the femtosecond laser induced mass spectra of the nitrotoluene isomers facilitate the identification of the three isomers.

In order to detect three isomers of nitrotoluene several techniques have been used as was mentioned above. Most of these studies do not deal with the three isomers of nitrotoluene. There was some work done using multiphoton process in our laboratory which present comprehensive studies on the three isomers of nitrotoluene (Kosmidis *et al.*, 1994b; 1997). In the present work for this thesis a series of experiments were carried out using 90 fs laser pulses at $\lambda$ = 375 nm. It is clear from fig. 7.6 that the time of flight mass spectra of nitrotoluene isomers offer some unique 'fingerprints', which allow their easy distinction taking into account only the four heavier mass ion peaks (m/q= 92 ($C_6H_6N^+$), 107 ($C_7H_7O^+$), 120 ($C_7H_6NO^+$), 121 ($C_7H_7NO^+$)). Thus, apart from the relatively intense parent ion peak in the mass spectra of the isomers, which is very important for analytical purposes, in the mass spectrum of *o*-nitrotoluene (Fig. 7.6a), the peak at m/q= 120 (corresponds to $C_7H_6NO^+$) (-OH loss) with no peak at m/q= 107 ($C_7H_7O^+$) (-NO loss) has been observed. The peaks at m/q= 121 ($C_7H_7NO^+$) (-O loss) and m/q= 107 ($C_7H_7O^+$) (-NO loss) together have been recorded only in *p*-nitrotoluene while in the mass spectrum of *m*-nitrotoluene neither of the peaks at m/q= 120 ($C_7H_6NO^+$) (-OH loss) and 121 ($C_7H_7NO^+$) (-O loss) have been detected and the parent ion peak is accompanied only by the m/q= 107 ($C_7H_7O^+$) (-NO loss) peak. The peak at m/q=92 ($C_6H_6N$) (-$HCO_2$) is a prominent feature only in the *o*-nitrotoluene spectrum and has been seen in nanosecond

fragmentation parent (Kosmidis *et al.*, 1994b). In the femtosecond laser induced spectrum of *o*-nitrotoluene shows a significant peak at m/q=45 corresponds to the $HCO_2^+$ ion peak which is absent in the mass spectra of the other isomers.

### 7.2.4 Multiphoton Dissociative Ionization Processes at 750 nm

Another series of experiments on *o*- and *m*-nitrotoluene were carried out using 90 fs laser pulses at 750 nm. In these experiments, a 10 cm focal length mirror inside the vacuum was used to focus the laser beam to obtain an intensity about $10^{13}$ W/cm$^2$. Fig. 7.7 shows a comparison of *o*-notrotoluene (a) and *m*-nitrotoluene (b) mass spectra at 750 nm. Similar laser pulse energies about 20 μJ were used for both experiment and as seen from fig.7.7, the *o*-nitrotoluene parent ion peak has almost disappeared and the parent ion peak of *m*-nitrotoluene is clearly present. This data indicates that the ionization efficiency in *m*-nitrotoluene is higher than that of the *o*-nitrotoluene. This supports the conclusion made for the three isomers of nitrotoluene at 375 nm that while some of the excitation/ionization steps are close to the saturation in the *m*- and *p*-nitrotoluenes for the laser intensities used, the three photon excitation and ionization processes which takes place in the *o*-nitrotoluene are unsaturated.

In the *o*-nitrotoluene spectrum similar to the multiphoton processes at 375 nm the rearrangement plays an important role and competes with the ionization and fragmentation of the parent molecule. The OH loss peak has grown substantially and, therefore, a small $OH^+$ ion peak visible in the mass spectrum (Fig. 7.7a) of *o*-nitrotoluene. In the mass spectrum of *m*-nitrotoluene, the peak at m/q=107 is also visible but very small which is shown in an enlarged scale (Fig. 7.7b). In the mass spectrum of *o*-nitrotoluene, the peak at m/q=92 ($C_6H_6N^+$) (-$HCO_2$ loss) in the mass spectra taken at 375 nm was smaller than the peak at m/q=91 (-$NO_2$ loss channel) but in the case of 750 nm, the peak at m/q= 92 is larger than 91 peak. This feature of the mass spectrum may suggest that the photorearrangement process at 750 nm is a preferable process relative to that at 375 nm.

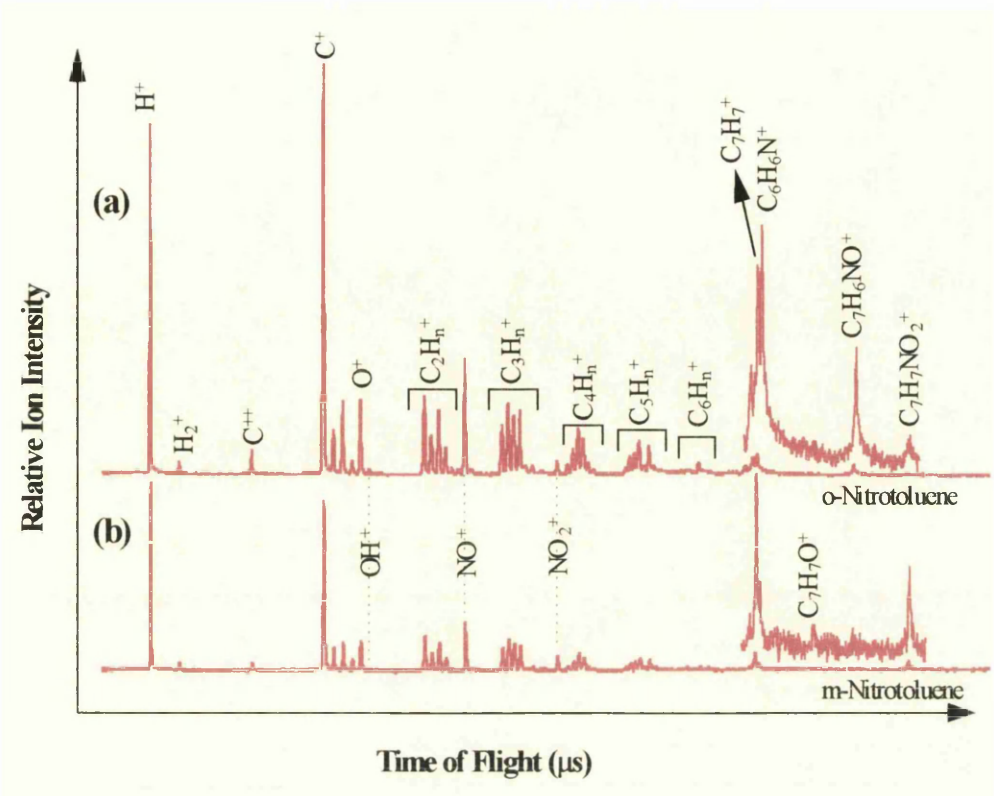


**Figure 7.7:** Femtosecond laser induced mass spectra of (a) *o*-nitrotoluene and (b) *m*-nitrotoluene. Parent ions, and heavier mass fragment ions in an enlarged scale are shown. Data was taken using 90 fs laser pulses at 750 nm. Similar laser pulse energies were used to obtain both spectra and it was about 20 μJ.

Fig.7.8 shows the laser pulse energy dependencies of the fragmentation patterns of *o*- and *m*-nitrotoluene isomers at 750 nm. The spectra were obtained changing the laser pulse energy for each spectrum. The pulse energy was changed using a neutral density filter and measured using a joulemeter just in front of the entrance window of the time of the flight mass spectrometer. The sample pressure was constant during the data taken and about a few times $10^{-5}$ torr. At 750 nm, the fragmentation pattern of *o*-nitrotoluene slightly changed relative to the *m*-nitrotoluene fragmentation pattern. In contrast to the case of mass spectra at the 375 nm, very small parent ion for both isomers are visible. The laser pulse energy dependencies show that, as the laser pulse energy decreases, heavier mass ion peaks starts to disappear first (Fig. 7.8). Across the entire range of energy $H^+$, $C^+$ and $NO^+$ ions are strong peaks in the mass spectrum for the case of both isomers (Fig. 7.8).

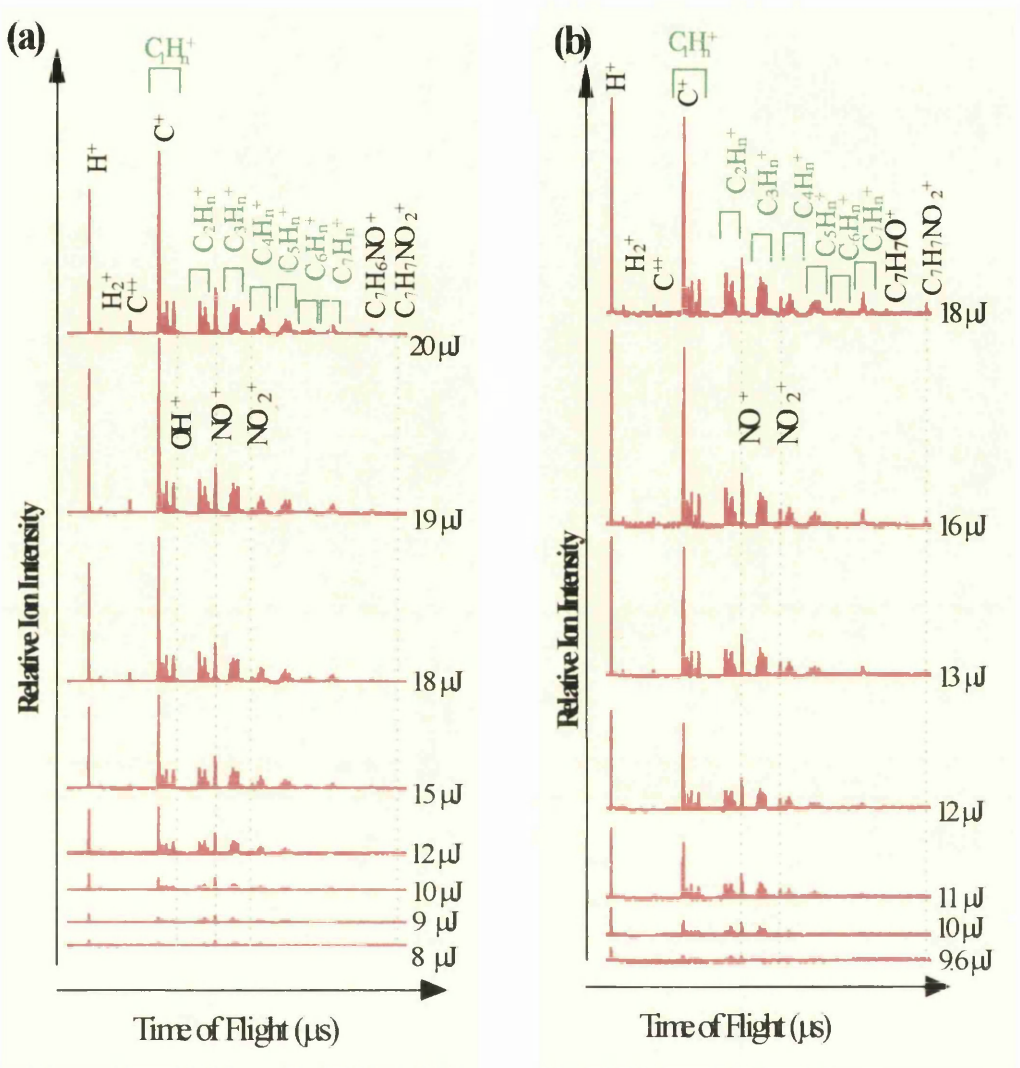


**Figure 7.8:** Laser pulse energy dependencies of the fragmentation patterns of *o*-nitrotoluene and *m*-nitrotoluene isomers. Laser pulse energy used for individual mass spectrum is shown at the right end of each spectrum.

The laser intensities in both experiments seems at about the intensity threshold for the parent molecular ions to be obtained and as laser intensity changes the fragmentation pattern slightly changes. This change of fragmentation pattern in the spectra suggests that at the 750 nm the fragmentation of the neutral molecule and subsequent ionisation of the fragments, i.e., an DI mechanism, is dominating the system in the case of relavant laser pulse energy range which is different than the case of 375 nm, since it was discussed and concluded that an ID process is dominant at the 375 nm over intensity range used in the experiment.

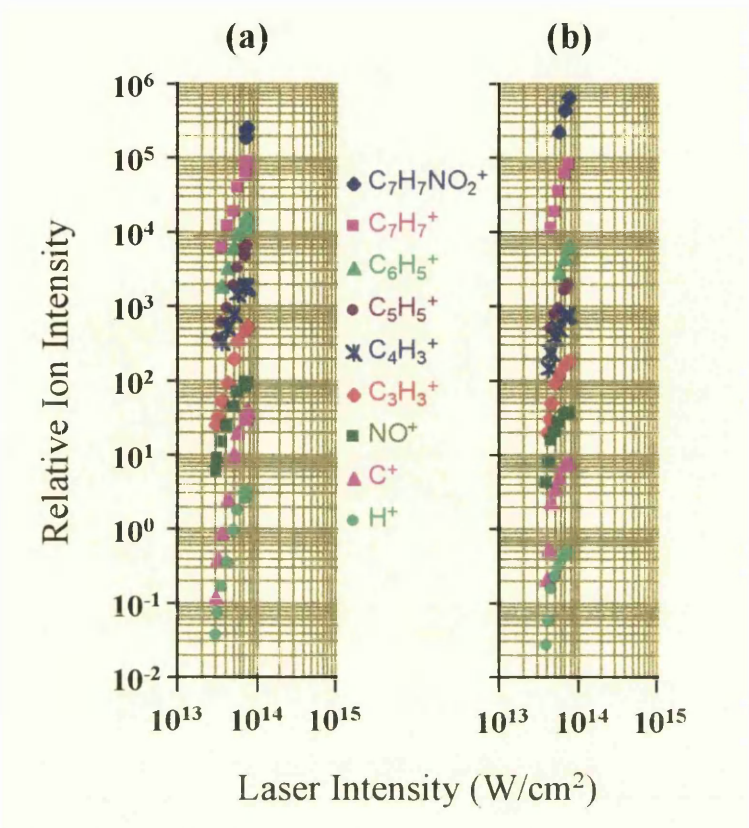


**Figure 7.9 :** Laser intensity dependencies of parent molecule and major fragment ions in the mass spectra of *o*-nitrotoluene (a) and *m*-nitrotoluene (b) at 750 nm.

Fig. 7.9 shows the laser intensity dependencies of both parent and fragment ions from both *o*- and *m*-nitrotoluene. It takes six photons of the 750 nm to ionise nitrotoluene isomers. The parent ion and the most of the fragment ions show similar laser intensity dependencies which are about 4-5. The similar intensity dependencies of the parent ion and the most of the fragment ions suggest an ID route for the fragmentation pattern in relevant laser intensity range.

The data presented in figs. 7.8 and 7.9 suggest that the multiphoton dissociative ionisation of the three isomers of nitrotoluene at 750 nm and in the laser intensity range used is a mixture of the ID and DI processes.

### 7.2.5 General Discussions on The Dissociation/Fragmentation Pathways of The Three Isomers of Nitrotoluene

The irradiation of *o*-nitrotoluene with nanosecond laser pulses in the 210-270 nm wavelength region (Kosmidis *et al.*, 1994b) has shown the existence of some other reactions like the -NO loss, the -O loss and -OH loss channels. Using nanosecond laser pulses, the first two channels were detected also for the other two isomers. The appearance of the -NO loss reaction in the nanosecond laser induced spectra is attributed to a DI route after a rearrangement of the C-$NO_2$ bond to a C-ONO structure (Kosmidis *et al.*, 1994b).

In the present work no peak has been recorded in the mass spectra of *o*-nitrotoluene at m/q= 121 (-O loss) while an extremely weak peak at m/q= 107 (-NO loss) has been observed at 375 nm (Fig. 7.6a) but at 750 nm none of these peaks are visible in the spectrum of *o*-nitrotoluene (Figs.7.7a). Thus, the absence or the near absence of the m/q= 107 ($C_7H_7O^+$) (-NO loss) is again consistent with the conclusion that the fragmentation in this experiment is mainly an above ionization dissociation, precluding the dissociation from a molecular excited electronic state at 375 nm and 750 nm. Since, a significant peak at m/q=107 (-NO loss) could not be detected, on the other hand, the problem within this interpretation seems to be a significant ion peak recorded, in the case of both wavelength, at m/q= 30 ($NO^+$) which is one of the dominant peaks in the mass spectra of *o*- and *m*-nitrotoluene at 750 nm (Fig.7.7) and its size is relatively small in the mass spectrum taken using 375 nm laser wavelength (Fig. 7.6). There are however a number of other dissociation channels in *o*-nitrotoluene which yield $NO^+$ ions and neutrals (Cassady and McElvany, 1993). In addition, the generation of the $NO^+$ ions could come from the fragmentation of $NO_2$ produced by the -$NO_2$ loss channel. The generation of $NO^+$ ions in a number of dissociation mechanisms was the subject of a recent paper (Marshall *et al.*, 1992c) which dealt with the dissociation of the neutral nitrobenzene parent molecule rather than its ion. A very small $NO_2^+$ ion peak has been observed in the mass spectrum of *o*-nitrotoluene (Fig. 7.2a) at 375 nm and shows an agreement with the recent

measurement of photodissociation of $NO_2$ gas by 90 fs laser pulses (Singhal *et al.*, 1996). In the case of 750 nm however the $NO_2^+/NO^+$ ratio from nitrotoluene is in disagreement with what was observed for neutral ground state $NO_2$ molecule, which was presented in chapter 4 of this thesis. The $NO_2^+/NO^+$ ratio was observed with 100% from $NO_2$ at 750 nm but in the case of nitrotoluene it is 10% which suggests that the $NO^+$ ion peak contains contributions from some other channels as well as the dissociation of neutral ground state $NO_2$ radical.

In the femtosecond laser induced mass spectrum of *o*-nitrotoluene, it is clearly seen (Fig. 7.6) that, as discussed above, two peaks at m/q=92 and 120 are the unique fingerprints of the *o*-nitrotoluene isomer. The peak at m/q=120 suggests an additional dissociation channel, related to the -OH loss. This channel can proceed only after a molecular rearrangement and has been studied extensively (Beynon *et al.*, 1965; Meyerson *et al.*, 1966; Herbert *et al.*, 1984; Shao and Bear, 1988) but there still exist some unclear points on the structure of the intermediate species. The observation of the -OH loss reaction (peak at m/q= 120) in the present experiment in conjunction with the results of the study where nanosecond laser pulses were used (Kosmidis *et al.*, 1994b) shows that the -OH loss channel proceeds after the molecular ionization (Kosmidis *et al.*, 1997).

As far as the -OH loss channel in the *o*-nitrotoluene parent ion is concerned, it is found that the OH group is generated by a -H transfer from the $-CH_3$ to the $-NO_2$ group (the *ortho* effect) (Beynon *et al.*, 1965; Meyerson *et al.*, 1966). In a femtosecond pump-probe experiment, Herek *et al.* (Herek *et al.*, 1992) have determined that the time needed for hydrogen atom intramolecular transfer in methyl salicylate is shorter than 60 fs. To the author's knowledge, there is no information in the literature about the time scale for hydrogen transfer in *o*-nitrotoluene. Particularly for *o*-nitrotoluene, Murrey *et al.* have studied the hydrogen transfer from methyl to nitro group and they found that further rearrangement takes place to produce anthranil ($C_7H_5NO$) and water ($H_2O$) (Murrey *et al.*, 1990). In the mass spectra from

our latest experimental work for the case of both laser pulse durations (10 ns and 90 fs) no peak at m/q=18 ($H_2O^+$) or 119 ($C_7H_5NO^+$) have been observed. The OH loss channel was clearly observed showing a small peak at m/q=17 ($OH^+$) and a large peak at m/q= 120 ($C_7H_6NO^+$).

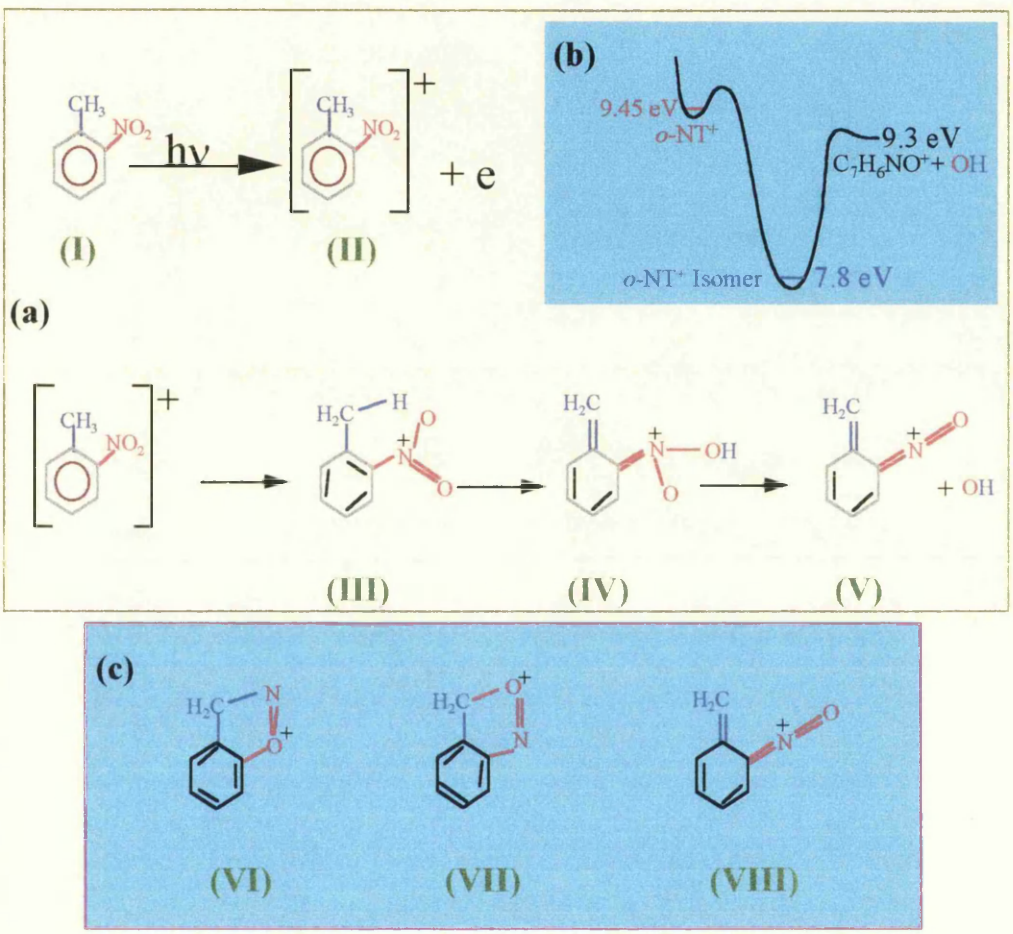


**Figure 7.10:** Proposed mechanisms for the rearrangement and hydrogen transfer in the *o*-nitrotoluene molecular ion (a), the molecular ion has an internal energy to activate to lose OH radical (b) and the proposed structures for the radical detected at m/q=120 (c). Figures are not in exact scale.

Figure 7.10a shows the discrete rearrangement steps in the *o*-nitrotoluene ion after the ionization of the *o*-nitrotoluene neutral molecule and then the -OH loss mechanisms which were suggested by Meyerson *et al.* (Meyerson *et al.*, 1966). Fig.7.10b shows the energy barrier for the dissociation of the *o*-nitrotoluene ion to give the $C_7H_6NO^+$+OH ionic and neutral radicals. The dissociation limit for the OH loss

channel has been calculated by Shao and Baer (Shao and Baer, 1988) to be 9.3±0.1 eV. This value is below the ionization limit and they have calculated that the isomerized parent ion lies in a well of depth 1.5 eV relative to the dissociation limit. The ion peak at m/q=120 has been experimentally observed by Kosmidis *et al.* using 267.5 nm laser wavelength and this observation shows a good agreement with this calculated value since two laser photons at 267.5 nm carry an energy of 9.27 eV (Kosmidis *et al.*, 1994b). The radical ion at m/q=120 has been studied extensively and at least three main structures have been proposed for this radical. Figure 7.10c shows the proposed structures for the $C_7H_6NO^+$ ion (after -OH loss). In fig. 7.10c, VI and VII were suggested by Beynon *et al.* and VIII by Meyerson *et al.* Herbert *et al.* suggested that possibly the best structure for this radical is Fig. 7.10c(VII).

The dissociation/fragmentation of the $C_7H_6NO^+$ fragment ion has been subject of a number of articles (Beynon *et al.*, 1965; Meyerson *et al.*, 1966; Herbert *et al.*, 1984; Shao and Baer, 1988) and it has been suggested that this radical could undergo further dissociation absorbing some more photons to give CO (m/q=28) fragment through the equation (7.1);

$$C_7H_6NO^+ + h\nu \rightarrow C_6H_6N^+ (m/q=92) + CO\ (m/q=28) \qquad (7.1)$$

In the present work at both wavelengths of 375 nm and 750 nm with 90 fs laser pulses, the ion peaks at m/q= 92 and 28 have clearly been observed shown in fig. 7.2a and 7.7a, respectively. The efficiency of the production of the 92 mass peak at 750 nm is greater than that at 375 nm. It can easily be seen from the comparison of the femtosecond laser induced mass spectra of *o*-nitrotoluene at 375 nm (Fig. 7.2a) and 750 nm (Fig. 7.7a) that at the 375 nm peak at m/q=91 ($C_7H_7^+$)(-$NO_2$ loss) is much higher than the peak at m/q=92 ($C_6H_6N^+$)(*M*-OH-CO loss) but this is opposite in the case of the 750 nm, the peak at m/q=92 is much higher than the peak at m/q=91. Therefore it can clearly be said that the rearrangement process in the *o*-nitrotoluene ion at 750 nm has a higher probability than that at 375 nm and the -$NO_2$ loss has less probability.

The spectra of *m*- and *p*- nitrotoluene with respect to the different dissociation pathways are very close to those observed previously using nanosecond laser pulses with the exception of the near absence of the -O loss channel for *m*-nitrotoluene. The absence of the -O loss channel in the *m*-nitrotoluene could be attributed to the different relative position of the $CH_3$ group in the aromatic ring. It is known that in the case of methylpyridines the higher occupied MO is not the same for the three isomers (Kosmidis *et al.*, 1993). It has been demonstrated that for the *o*- and *m*-methylpyridine, the highest occupied MO is a $\pi$-type, while for the *p*-methylpyridine it is an n-type MO. For the case of nitrotoluenes there is no such data available in the literature, but because of the close relation between the type of the MO and the molecular dissociation, a similar explanation might be possible (Kosmidis *et al.*, 1997).

## 7.3. Femtosecond Laser Mass Spectrometry (FLMS) on 2, 4-Dinitrotoluene (DNT) and 2, 4, 6-Trinitrotoluene (TNT)

In the work of this thesis, a systematic study has been carried out using nanosecond and femtosecond laser mass spectrometry and a comparison of the nanosecond and femtosecond laser induced mass spectra has already been carried out for nitrogen dioxide, nitromethane, nitrobenzene, three isomers of nitrotoluene. It is believed that the results discussed in the previous chapters for the above mentioned samples would help us to have some more fundamental understanding about the dissociation and fragmentation processes in larger nitro containing aromatic molecules. In this part of the work, the multiphoton dissociation/fragmentation processes in DNT and TNT will be investigated using femtosecond laser mass spectrometry. The nanosecond laser induced fragmentation patterns of the mass spectra will also be compared with these in the femtosecond regime.

TNT is one of the most dangerous molecular explosives and DNT is used as an intermediate to obtain the TNT molecule. The understanding of the reaction mechanisms in DNT might also help us to better understand and investigate the

reaction mechanisms in the TNT molecule. The dissociation pathways in the DNT and TNT neutral and molecular ions have been investigated using different techniques such as collision induced dissociation (CID) (Yinon, 1987; 1988; 1992), electron impact (EI) (Bulusu and Axenrod, 1979), chemical ionization (Yinon, 1980) and multiphoton process (Apel and Nogar, 1986; Marshall *et al.*, 1994a; Ledingham *et al.*, 1995b). There is agreement in the literature that the main dissociation and fragmentation pathways in the nitroaromatic molecules including the 2,4-dinitrotoluene and 2,4,6-trinitrotoluene are either -$NO_2$ loss or -OH loss through a rearrangement process (the *ortho* effect). Most of the laser based techniques used to investigate the dissociation and fragmentation pathways in these molecules were in the nanosecond regime and it is typical for the nanosecond laser induced mass spectra that the mass spectra are dominated by lighter mass ion peaks (Apel and Nogar, 1986; Marshall *et al.*, 1994a; Ledingham *et al.*, 1995b). Apel and Nogar studied the dissociative ionization of TNT using 248 nm laser wavelength in a one photon resonance excitation and two photon ionisation scheme and they could not observe the molecular ion peak. The laser induced detection and identification of a number of explosive molecules have also been carried out in the nanosecond time scale with some early works from our laboratory (Clark *et al.*, 1993; Marshall *et al.*, 1994a).

In this thesis, the femtosecond laser induced time of flight mass spectra of DNT and TNT will be discussed comparing these with the mass spectrum of *o*-nitrotoluene. In nanosecond fragmentation pattern of *m*-nitrotoluene will be compared to these of DNT and TNT.

### 7.3.1 Experimental

In the detection of some of the medium size nitroaromatic explosives, there exists a problem since the sample must be heated to obtain sufficient vapour pressure in the ionisation chamber. The vapour pressure of a number of explosives including DNT and TNT have been measured by Marshal *et al.* as a function of temperature and given in a recent article (Marshall *et al.*, 1994a). In the case of the TNT molecule, it

would be a very interesting development if any mass spectrometric technique could detect this molecule at a low temperature. The multiphoton dissociation and fragmentation processes were studied in the literature at a temperature of 90 °C which is the lowest temperature until this work. In our experimental set up, the sample source was heated up with an external heater up to 80°C and the temperature of the reagent in the chamber was measured to be 23°C. The sample pressure was typically about $6x10^{-6}$ Torr and it was constant during data taking.

The laser, TOF and data acquisition systems as well as the laser focusing condition were similar to those used in the nitrotoluene experiment carried out at 375 nm.

### 7.3.2 Interpretation of The Laser Induced Time of Flight Mass Spectra of Dinitrotoluene (DNT) and Trinitrotoluene (TNT)

The photofragmentation of these compounds have been studied extensively in the nanosecond regime in a number of recent articles (Lemire *et al.*, 1993; Simeonson *et al.*, 1993; Marshal *et al.*, 1994a; Ledingham *et al.*, 1995b). A significant differences between the nanosecond and femtosecond laser induced mass spectra of medium size nitroaromatic explosives will be discussed in this chapter for *o*- and *m*-nitrotoluene isomers ($C_6H_4CH_3NO_2$), 2,4-dinitrotoluene ($C_6H_3CH_3(NO_2)_2$) and 2,4,6-trinitrotoluene ($C_6H_2CH_3(NO_2)_3$). The fragmentation patterns of the time of flight mass spectra for both nanosecond and femtosecond laser pulses will also be compared. In this section we shall discuss the nanosecond laser mass spectra first and the femtosecond laser mass spectra will be described later. A comparison of the nanosecond and femtosecond laser mass spectra will also be made. Finally the multiphoton processes in DNT and the laser intensity dependence of the fragmentation pattern of the mass spectra of DNT in the femtosecond regime will be discussed.

### *7.3.2.1 Nanosecond Laser Induced Mass Spectra*

We have carried out a series of experiments on *o*- and *m*-nitrotoluene, dinitrotoluene and trinitrotoluene molecules using nanosecond laser pulses at 384 nm, 375 nm and 226 nm laser wavelengths. The nanosecond laser induced time of flight mass spectra of *o*-nitrotoluene and *m*-nitrotoluene at 375 nm were discussed in earlier parts of this chapter. The nanosecond laser induced mass spectra of *m*-nitrotoluene and dinitrotoluene at the laser wavelength of 384 nm as well as the mass spectra of *m*-nitrotoluene, dinitrotoluene and trinitrotoluene at 226 nm will be discussed here. In early parts of this chapter, the nanosecond laser induced mass spectra were compared and it has been shown that the fragmentation patterns in the mass spectra of *o*-nitrotoluene and *m*-nitrotoluene isomers at 375 nm are rather similar. Therefore, it is thought that it would not be inappropriate that we discuss here *m*-nitrotoluene isomer instead of *o*-nitrotoluene for the comparison of nitrotoluene and dinitrotoluene.

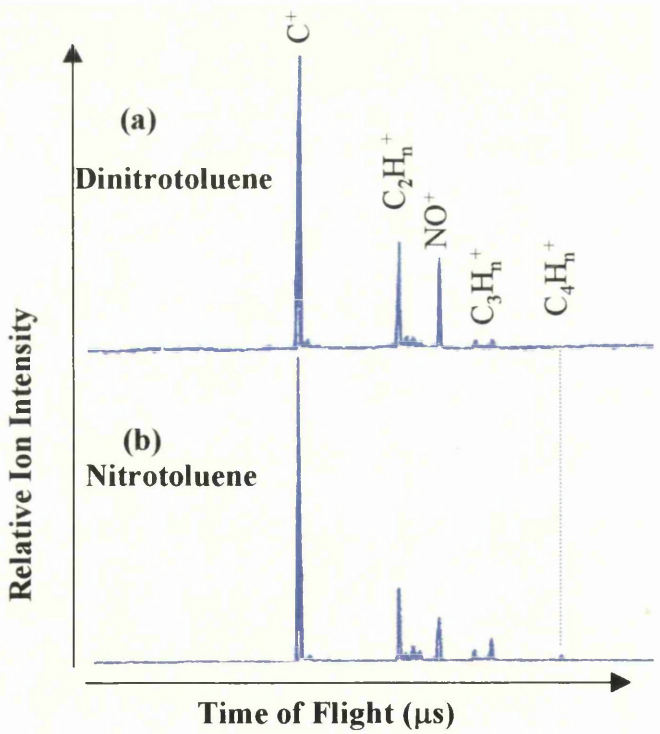


Figure 7.11: The nanosecond laser induced time of flight mass spectra of (a) dinitrotoluene and (b) *m*-nitrotoluene.

Fig. 7.11 shows the nanosecond laser induced time of flight mass spectra of (a) DNT

and (b) *m*-nitrotoluene taken using 10 ns laser pulses at 384 nm. Both spectra were taken using 2 mJ laser pulse energy. The 384 nm laser wavelength is off resonance in the excitation and ionization steps of the ground state neutral NO molecule and it is clear that no resonance enhancement has been observed. Therefore, the $NO^+$ ion peak is small in the mass spectra with no $NO_2^+$ peak. In comparison to the hydrocarbon ion peaks, the $NO^+$ ion peak in the DNT spectrum is larger than this in the *m*-nitrotoluene spectrum. This is due to the increase of the number of the neutral NO molecules in the interaction region.

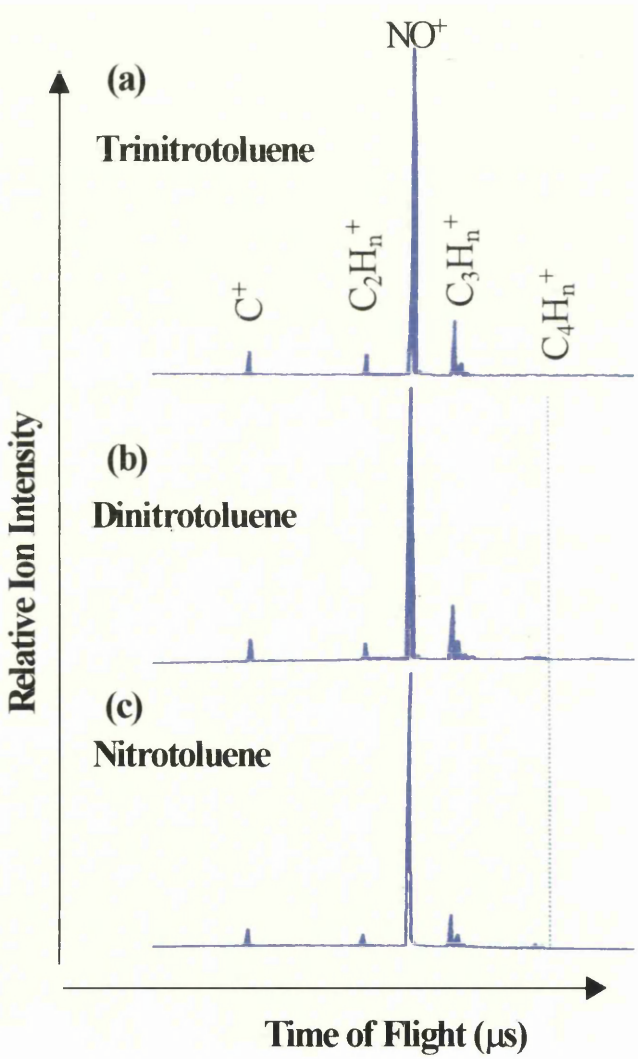


Figure 7.12: The nanosecond laser induced time of flight mass spectra of (a) trinitrotoluene, (b) dinitrotoluene and (c) *m*-nitrotoluene taken at the laser wavelength of 226 nm.

Another series of experiments have been carried out on the *m*-nitrotoluene, DNT and TNT molecules using 10 ns laser pulses at 226 nm and the results are shown in fig. 7.12. The three spectra in the fig.7.12 were taken using 100 μJ laser pulse energy. In the case of 226 nm, the dominant peak in the mass spectra is due to the $NO^+$ ion peak since one photon of laser light at 226 nm carries an energy which is in resonance with the $A^2\Sigma(v=0)$ excited state in the neutral NO molecule and one photon excitation and ionisation (1+1) processes take place *via* a transition of $A^2\Sigma(v=0)\leftarrow X^2\Pi(v=0)$. The resonance enhancement of the $NO^+$ ion peak is clear and, therefore, this peak is dominant in the mass spectra at this wavelength.

The comparison of the nanosecond laser induced mass spectra of *m*-nitrotoluene and dinitrotoluene at 384 nm (Fig. 7.11) and *m*-nitrotoluene, DNT and TNT at 226 nm (Fig. 7.12) shows that the wavelength dependence of the fragmentation patterns shows a major difference which is due to the $NO^+$ peak whether it is excited/ionised *via* a resonance step or not. The common features of the all mass spectra of *m*-nitrotoluene, DNT and TNT at both wavelengths are that the spectra are very similar showing only the $C_1H_n^+$, $C_2H_n^+$and $C_3H_n^+$ ion groups being prominent together with a very strong or a weak $NO^+$ ion peak depending on the existance of a resonance step or not, and very weak $C_4H_n^+$ ion group. It is also seen that the parent and even heavier mass ion peaks of nitrotoluene, DNT and TNT are missing in the nanosecond regime at the relevant wavelength used in this work.

### *7.3.2.2 The Femtosecond Laser Induced Mass Spectra*

The femtosecond and nanosecond laser induced time of flight mass spectra of *o*-nitrotoluene have been discussed in the earlier parts of this chapter. The comparison of the nanosecond laser induced mass spectra was discussed in previous section. This section will focus on the femtosecond laser induced fragmentation patterns of the mass spectra of *o*-NT, DNT and TNT and these will be compared.

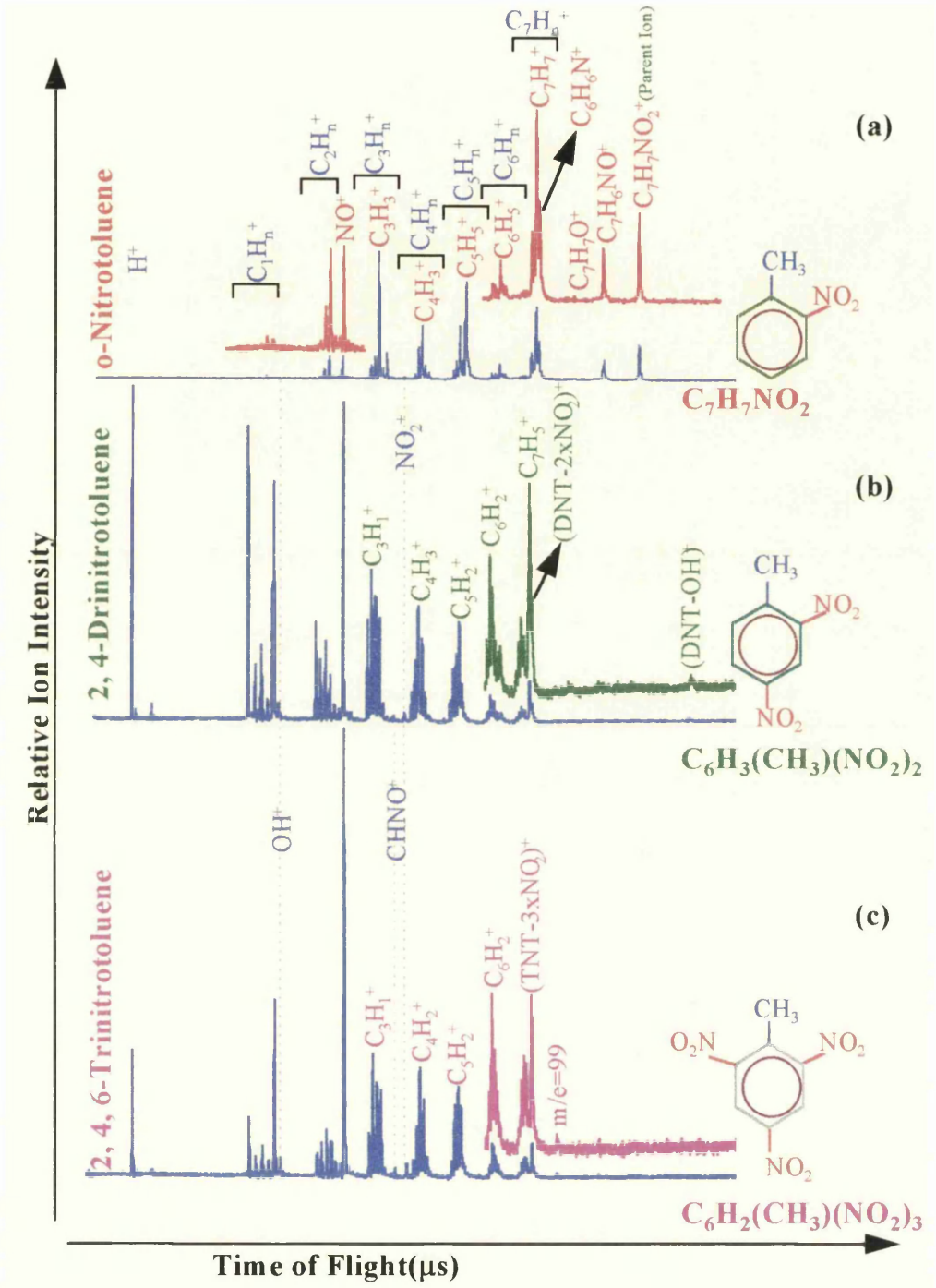


**Figure 7.13:** Femtosecond laser induced time of flight mass spectra of (a) *o*-nitrotoluene, (b) 2, 4-dinitrotoluene and (c) 2, 4, 6-trinitrotoluene. Heavier mass ion part of mass spectra are shown in enlarged scale.

The femtosecond mass spectra of *o*-nitrotoluene, DNT and TNT are shown in fig. 7.13a, b and c, respectively. The spectra of *o*-NT, DNT and TNT have been recorded

using similar laser pulse energies at the wavelength of 375 nm and 90 fs pulses. Sample pressures used in the three experiment were about 9.6, 6 and 7 times $10^{-6}$ torr, respectively. In fig. 7.13, the geometric structures and the chemical formulas for three sample are given and heavier mass ion parts of each spectrum and the $C_1H_n^+$ and $C_2H_n^+$ with $NO^+$ ion part of *o*-nitrotoluene mass spectrum are shown in expanded scale.

It is seen from fig. 7.13a as discussed earlier in this chapter that a strong nitrotoluene parent ion peak at m/q=137 ($C_7H_7NO_2^+$) is one of the strong peaks in the mass spectrum and in the case of DNT and TNT, the ion state of the parent molecule could not be reached under the experimental conditions described above. The comparison of these three spectra shows that the fragmentation pattern in the nitrotoluene mass spectrum is completely different than the fragmentation patterns of the mass spectra of DNT and TNT. While the heavier mass ion peaks and parent ions of DNT and TNT are missing, the smaller mass ion peaks in the nitrotoluene spectrum are absent. The fragmentation patterns in the mass spectra of DNT and TNT are dominated by the $H^+$, $C^+$ and $NO^+$ ion peaks as seen in fig. 7.13b and c, respectively. The most interesting and prominent feature of the fragmentation patterns of these three spectra is that while the $NO^+$ ion peak is very small in the mass spectrum of *o*-nitrotoluene (Fig. 7.13a), it increases substantially in the mass spectra of DNT and TNT. This increase of the $NO^+$ ion yield was expected due to the increasing number of $NO_2$ groups per molecule.

It is also known that in the molecules where the nitro group is *ortho* to the methyl group, one of the major dissociation channels is the OH loss through a rearrangement process. This effect has been observed and discussed in the *o*-nitrotoluene ion in the sections (7.2.3 and 7.2.5) in this chapter (Fig. 7.6) comparing the mass spectra of *o*-nitrotoluene with other isomers of nitrotoluene. The DNT and TNT have one and two nitro groups which are *ortho* to the methyl group shown in fig. 7.1 and in the inset diagrams in fig. 7.13 for each molecule.

The photorearrangement and fragmentation processes in large molecules in their ionic states have been extensively studied and significant information is available at the present (Beynon *et al.*, 1964; Zitrin and Yinon, 1976; Zitrin and Yinon, 1978; Bulusu and Axenrod, 1979; Matyuk *et al.*, 1979; Harris *et al.*, 1981; McLuckey *et al.*, 1985; Yinon, 1987; 1988; 1991; 1992). The above mentioned *ortho* effect is clear for *o*-nitrotoluene molecular parent ion (Figs. 7.13a) showing a dominant peak at m/q=120 ($C_7H_6NO^+$) which corresponds to a OH loss of parent molecular ion and a small $OH^+$ peak is also visible in the mass spectrum (Fig. 7.13a). The photorearrangement and fragmentation mechanisms in DNT molecular ion was investigated in an earlier article (Beynon *et al.*, 1964). Beynon et al have shown that the first steps of rearrangement/fragmentation pathways could be given with eq.(7.2), (7.3) and (7.4), as shown in diagram 7.1.

$$C_7H_6N_2O_4^+ + e^- \rightarrow C_7H_6^+ + N_2O_4 \qquad N_2O_4 \text{ loss channel} \qquad (7.2)$$

$$C_7H_6N_2O_4^+ + e^- \rightarrow C_7H_5N_2O_3^+ + OH \qquad OH \text{ loss channel} \qquad (7.3)$$

$$C_7H_6N_2O_4^+ + e^- \rightarrow C_6H_6NO^+ + CNO_3 \qquad CNO_3 \text{ loss channel} \qquad (7.4)$$

It was well established for dinitrobenzene that one of the prominant fragmentation pathways is due to the loss of a series of neutrals to be DNB-$NO_2$-$NO_2$-H. This structure is very similar to the case of DNT parent ion. In the DNT molecular parent ion, one of the prominent dissociation routes is the loss of 2x$NO_2$ groups which takes place as a single step process with high probability (eq. (7.2)) (Beynon *et al.*, 1964). Other suggested initial fragmentation steps in DNT molecular ion is the loss of an OH and $CNO_3$ neutrals (eqs. (7.3) and (7.4), respectively). The latter dissociation channel, III, (eq. (7.4)) has less probability than other suggested two channels, I and II. The fragmentation route II was also suggested by Yinon and concluded that the major OH loss in the parent ion is followed by the loss of $NO_2$ neutral (Yinon, 1992). This is a parallel suggestion what Beynon et al proposed to produce a fragment ion peak at m/q=119 ($C_7H_5NO^+$) through route II shown in diagram 7.1.

Diagram 7.1 shows the suggested fragmentation channels in the case of DNT parent

molecular ion. In the case of our results being presented here, the mass spectrum suggests that the dissociation of the neutral molecule occurs and the neutral fragments are subsequently ionised which means that a DI route most likely takes place.

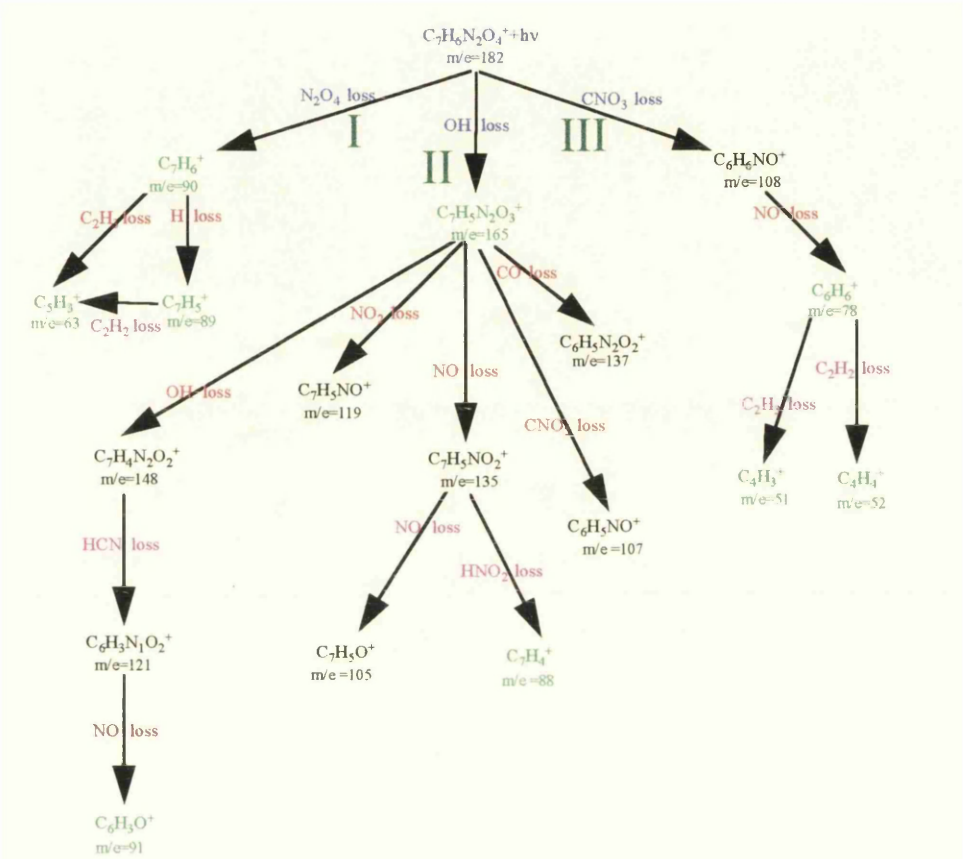


**Diagram 7.1:**
The suggested fragmentation routes in the DNT molecular parent ion

The mass spectrum of DNT shows a number fragment ions and in diagram 7.1 the green coloured fragment ions indicate the fragment ions which were observed from the dissociative ionisation of the neutral DNT molecule in this work. The highest mass fragment ion peak in the mass spectrum of DNT is due to a small peak detected at m/q=165 ($C_7H_5N_2O_3^+$), corresponding to the loss of OH from the neutral parent molecule which is evidence that in the dissociative ionisation process in neutral DNT molecule, the -OH loss channel is opened (Ledingham *et al.*, 1995b). This peak is

clearly visible in Fig. 7.13b and the $OH^+$ ion peak at m/q =17 is also clearly present in the mass spectrum. None of the suggested first step fragmentation products from the fragment of $C_7H_5N_2O_3^+$ (m/q=165) at m/q =107, 119, 135 and 148 were observed in our femtosecond laser induced mass spectrum which was observed from the fragmentation of $C_7H_5N_2O_3^+$ (m/q=165) radical ion reported by Beynon *et al.* Another prominent peak in the mass spectrum is due to the loss of $2xNO_2$ followed by H loss, process I in diagram 7.1 showing a peak at m/q=89 ($C_7H_5^+$). Reaction III is also possible from the peaks corresponding to the $C_6H_n^+$ ion group in the mass spectrum. These major initial step dissociation pathways in neutral DNT seems responsible for the all remaining peaks appear in the mass spectra.

For the TNT molecular ion, it was proposed in the literature that three initial fragmentation steps are dominant in the rearrangement and fragmentation processes (Bulusu and Axenrod, 1979) and all remaining fragments are coming from these peaks appearing at m/q= 211 ($C_6H_2CH_3(N_3O_5)^+$) (-O loss) (eq. (7.5)), m/q=210 ($C_6H_2CH_3(N_3O_5)^+$) (-OH loss) (eq. (7.6)) and m/q=209 ($C_6H_2CH_1(N_3O_5)^+$) (-$H_2O$ loss) (eq. (7.7)). The eq. (7.5) could be an explanation for the $O^+$ peak which is one of the strong peaks in the mass spectrum of TNT (Fig. 7.13c). The initial step fragmentation routes in the TNT molecular parent ion are shown in diagram 7.2 (Bulusu and Axenrod, 1979).

$$C_6H_2CH_3(NO_2)_3^+ + e^- \rightarrow C_6H_2CH_3(N_3O_5)^+ + O \quad \text{-O loss channel} \quad (7.5)$$

$$C_6H_2CH_3(NO_2)_3^+ + e^- \rightarrow C_6H_2CH_2(N_3O_5)^+ + OH \quad \text{-OH loss channel} \quad (7.6)$$

$$C_6H_2CH_3(NO_2)_3^+ + e^- \rightarrow C_6H_2C_1(N_3O_5)^+ + H_2O \quad \text{-}H_2O \text{ loss channel} \quad (7.7)$$

It is also well known from the literature (Bulusu and Axenrod, 1979) that the hydrogen rearrangement-hydroxyl elimination (the *ortho* effect) is the key step in the breakdown of TNT molecule in the EI studies. The TNT has two nitro groups in the *ortho* position to the methyl group and an additional OH group is a major fragmentation process (Yinon, 1987). Therefore, it is expected that the $OH^+$ ion peak might be larger in the mass spectrum (Fig.7.13c) of TNT than it is in the mass

spectrum (Fig.7.13b) of DNT. Yinon observed a peak at m/q=34 corresponding to the double OH loss fragment parent ion $(TNT\text{-}2xOH)^+$ but in the dissociative ionisation mass spectrum of TNT in this work, there is no evidence for this peak (Fig. 7.13c). If a second *ortho* effect existed one would expect the peak at mass 17 for TNT to be twice that of DNT. However, the mass spectra in fig. 7.13b and c indicate that the contribution of the second *ortho* effect is very small.

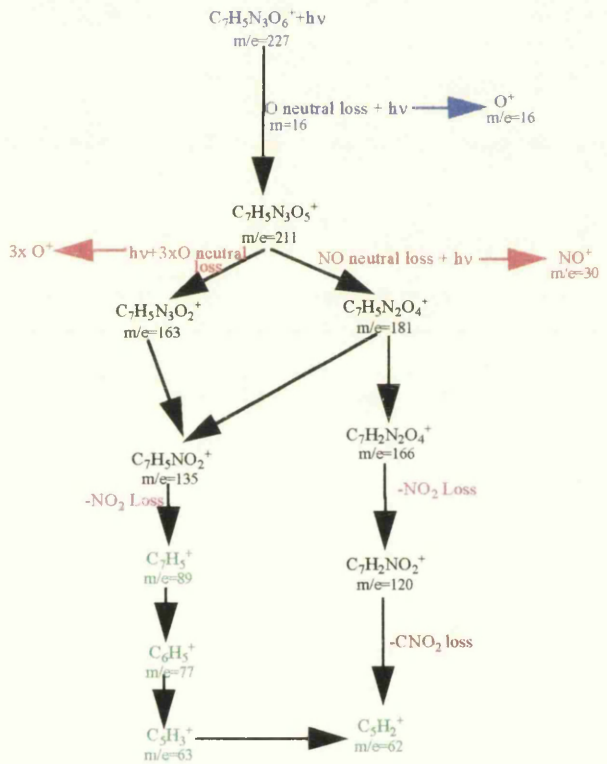


**Diagram 7.2:** One of the suggested fragmentation routes in the TNT molecular parent ion

Fig. 7.14 shows a comparison of the heavier mass ion parts of the three spectra shown in fig. 7.13. The comparison of the mass spectra of these three molecules shows that some fundamental differences appear in the fragmentation patterns of the mass spectra of these molecules. It is well known and as discussed in chapter 5 for nitromethane,

in chapter 6 for nitrobenzene and in the previous sections of this chapter for nitrotoluene isomers that one of the major dissociation channels is the cleavage of the C-$NO_2$ bond either in the neutral molecules or their ions.

It is shown in fig. 7.14 that the $NO_2$ and 3x$NO_2$ losses occur from *o*-NT and TNT showing peaks at m/q=91 ($C_7H_7^+$) and 89 ($C_7H_5^+$), respectvely. The results have already been discussed in detail in the previous sections of this chapter and as shown in fig.7.14a a peak at m/q=91 ($C_7H_7^+$) corresponding to the loss of -$NO_2$ moiety is one of the strong peaks in the mass spectrum of *o*-nitrotoluene. The 2x$NO_2$ loss peak at m/q=90 ($C_7H_6^+$) is very small in the mass spectrum of DNT (Fig. 7.14b), due to the influence of the *ortho* effect and the dominant peak about $C_7H_n^+$ group is due to the $(DNT\text{-}OH\text{-}N_2O_3)^+$ fragment ion peak which appears at m/q=89 ($C_7H_5^+$). This could be attributed to a -NO and -$NO_2$ loss from the peak at m/q=165 ($C_7H_5N_2O_3^+$) (-OH loss) *via* reaction II in diagram 7.1. On the other hand, there may be some possibility that the ion peak at m/q=89 ($C_7H_5^+$) may come from a H loss of $C_7H_6^+$ produced through dissociation route I in diagram 7.1 which indicates an initial -$(NO_2)_2$ loss mechanism in DNT parent molecule.

The mass spectrum of DNT indicates that -$(NO_2)_2$ loss from the DNT molecule takes place due to the presence of the ion peak at m/q=90 ($C_7H_6^+$) but it is small compared the ion peak at m/q=89 ($C_7H_5^+$). In the case of TNT, the dominant ion peak in the vicinity of the $C_7H_n^+$ group is due to the peak appearing at m/q=89 ($C_7H_5^+$), corresponding to the 3x$NO_2$ loss of parent molecule. This ion peak was also observed in the nanosecond pulse experiment at 248 nm in a two photon ionization scheme (Apel and Nogar, 1986). This peak was the highest mass ion peak in their spectrum and is similar to what we have observed with a higher order photon process at 375 nm using 90 fs laser pulses. It is known (Zitrin and Yinon, 1976; Bulusu and Axenrod, 1979) that the major dissociation and fragmentation pathways in the TNT molecular ion is due to the - O loss, -OH loss and - $H_2O$ loss to produce fragment ions at m/q=211 ($C_7H_5N_2O_3^+$) *via* eq.(7.5), 210 ($C_7H_4N_2O_3^+$) *via* eq.(7.6) and 109

($C_7H_3N_2O_3^+$) *via* eq.(7.7) and all fragmentation pattern comes from these major ion peaks. In the dissociative ionisation mechanism in TNT using 90 fs laser pulses at 375 nm, none of the peak at m/q=211, 210 and 209 is present in the mass spectrum. The results in the present work suggest that in the case of the dissociation of the neutral TNT molecule the major fragmentation pathway, under the experimental conditions, due to the $3xNO_2$ loss showing a prominent mass ion peak at m/q=89 ($C_7H_5^+$) as well as a peak at m/q=17, corresponds to the $-OH^+$ loss from the neutral parent molecule and this peak ($-OH^+$ loss) may be contributed by some other channels. For the production of an ion peak at m/q 89 ($C_7H_5^+$) from the molecular parent ion, Bulusu and Axenrod have suggested that the neutral oxygen elimination from the parent ion through the eq.(7.5) takes place as an initial step in the fragmentation process in the TNT shown in diagram 7.2. The intensity of the $NO^+$ ion peak also increases from *o*-nitrotoluene to TNT in respect to the hydrocarbon fragment ion peaks. The $NO_2^+/NO^+$ ratio from the neutral ground state $NO_2$ molecule was investigated in chapter 4 of this thesis and determined to be 6-11%. In the case of *o*-nitrotoluene this ratio is similar to this but in the case of DNT and TNT molecules, this ratio is about 2% and 3%, respectively. These results indicate that the photorearrangement processes in DNT and TNT are more effective than that in *o*-nitrotoluene.

Another prominent feature and fundamental difference in the mass spectra of these three molecule appears in the $C_6H_n^+$ ion group. In this group, the heaviest mass ion peak in the *o*-nitrotoluene spectrum is due to the $C_6H_7^+$ ion peak and this in the DNT spectrum is due to the $C_6H_6^+$ ion peak while it is the $C_6H_5^+$ ion peak in the TNT mass spectrum (Fig. 7.14a, b and c, respectively). The molecular formulas for *o*-NT, DNT and TNT can be written as

$$C_6H_4CH_3NO_2 \quad (7.8)$$

$$C_6H_3CH_3(NO_2)_2 \quad (7.9)$$

$$C_6H_2CH_3(NO_2)_3 \quad (7.10)$$

and hence $C_6H_7^+$, $C_6H_6^+$ and $C_6H_5^+$ correspond to a loss of $-CNO_2$, $-C(NO_2)_2$ and -

$C(NO_2)_3$ from the parents. In the case of nitrobenzene, discussed in chapter 6 of this thesis, a peak at m/q=58 ($CNO_2$) was observed and it was explained that it was obtained by ionising a neutral $CNO_2$ radical after a recombination of CO and NO neutrals from the dissociation of the nitrobenzene parent ion. This peak has also been observed in both CID and EI spectra of picric acid. In EI spectrum, it was attributed to the loss of NO+CO neutrals from the TNP (2,4,6-trinitrophenol) molecular parent ion (Zitrin and Yinon, 1978) which has a H atom joined to the C atom in the metha position to the hydroxyl group and hydroxyl group replaced with a methyl group in the TNT structure.

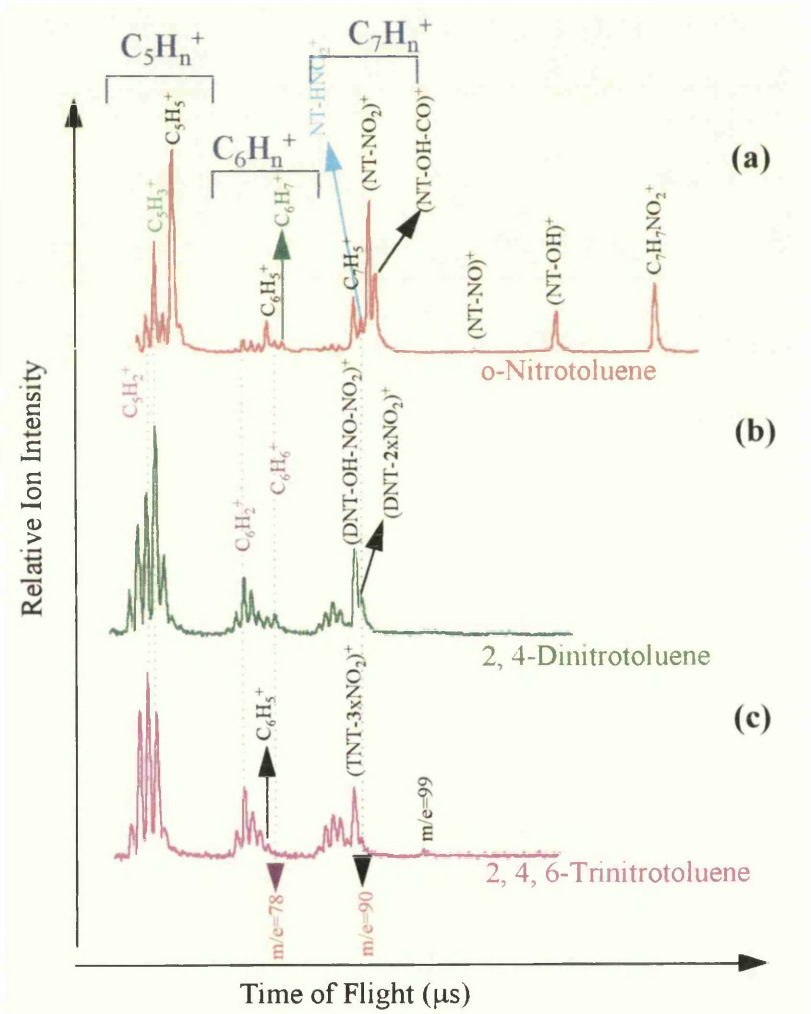


**Figure 7.14:** Heavier mass ion part of mass spectra of *o*-nitrotoluene, DNT and TNT.

In an earlier article on DNT it was indicated that there is a possibility of the loss of a $CNO_2$ neutral from the fragmentation of the $C_7H_5N_2O_3^+$ (m/q=165) fragment ion to give an ion peak at m/q=107 ($C_6H_5NO^+$) (Beynon *et al.*, 1964) (diagram 7.1). None of these peaks appear in the mass spectrum of DNT in the present work (Figs. 7.13b and 7.14b). In the case of TNT molecular ion, Bulusu and Axenrod, (1979) have shown some possible fragmentation pathways and precursors for the production of neutral fragments, indicated in diagram 7.2. But the present results from our femtosecond laser dissociative ionisation experiment show that no peak at the $CNO_2^+$ (m/q=58) nor for $C(NO_2)_2^+$ (m/q=104) and $C(NO_2)_3^+$ (m/q=150) ions have been observed.

In the case of the *o*-nitrotoluene parent ion, a theoretical calculation (Murrey *et al.*, 1990) have shown that there exists the possibility to obtain $H_2O$ loss and detect $C_7H_5NO^+$ (m/q=119). There is evidence for the detection of the $H_2O^+$ ion from the fragmentation of TNT through a rearrangement process (eq. (7.4)) (Bulusu and Axenrod, 1979; Carper et al., 1984; Yinon, 1987). In our experimental results no peaks appear at m/q=164 ($C_7H_3N_2O_3^+$) (-$H_2O$ loss) and m/q=209 ($C_6H_2CHN_3O_5^+$) ($H_2O$ loss) nor at m/q=18 ($H_2O^+$) in the mass spectra of both DNT and TNT, respectively. In addition no peaks were visible at m/q=18 ($H_2O^+$) and 119 ($C_7H_5NO^+$) from the *o*-nitrotoluene molecular parent ion.

### 7.3.3 Multiphoton Dissociation/Ionization Dynamics in DNT at 375 nm and 90 fs Pulse Width

An experiment on DNT was carried out at 375 nm using 90 fs laser pulses to show how the fragmentation pattern varied as the laser intensity changes. The laser pulse energy was varied using a neutral density filter and measured using a joulemeter. The laser beam was focused using a 30 cm focal length lens and the laser intensity was about $10^{13}$ W/cm$^2$.

Figure 7.15a and b show the laser pulse energy dependence of the fragmentation pattern in the mass spectra of the DNT molecule and the laser intensity dependencies

of major fragment ions, respectively. Fig. 7.16 shows the heavier mass ion part of fragmentation pattern as a function of laser pulse energy. It is clearly seen from the figs. 7.15a and 16 that as the laser pulse energy decreases the lighter mass ion peaks start to disappear first and in the case of the lowest laser pulse energy only $NO^+$, $C_3H_3^+$, $C_5H_3^+$ and $C_7H_5^+$ ions are still present and one of the strongest fragment ion peaks is the $C_7H_5^+$ ion peak.

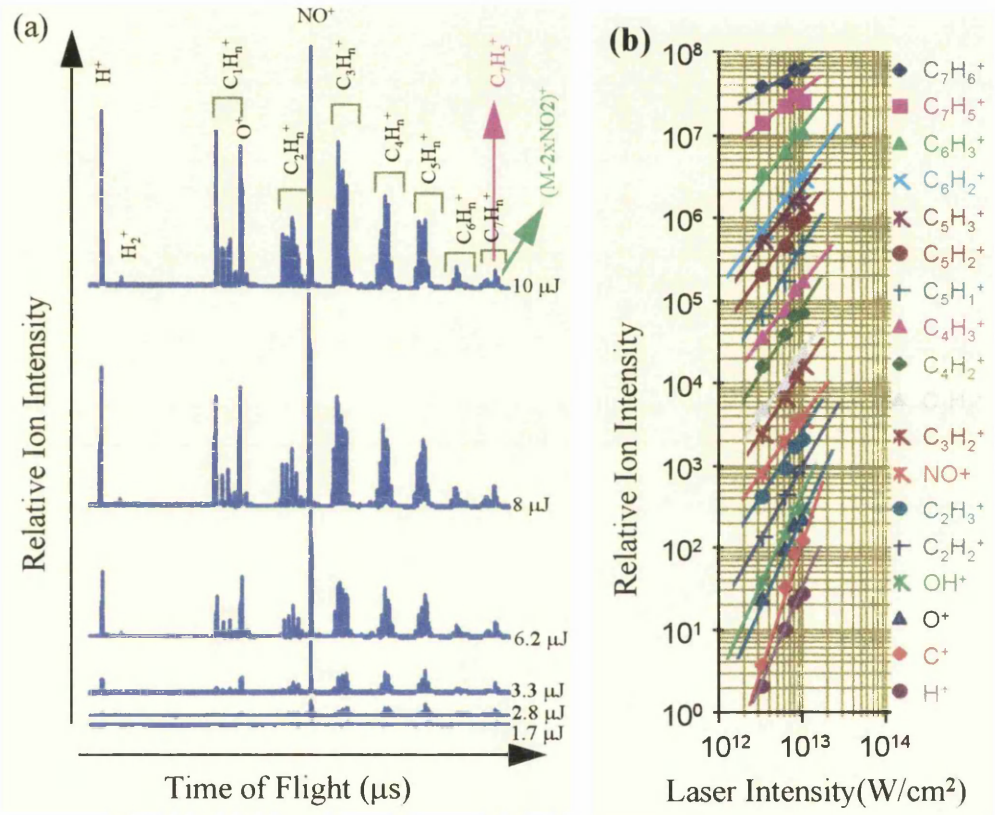


**Figure 7.15:** Laser pulse energy dependence of fragmentation pattern (a) and the laser intensity dependencies of major fragment ions (b) from the dissociation of neutral 2, 4-dinitrotoluene molecule.

Most of the major fragment ions in the mass spectrum of DNT show a laser intensity dependencies between 1.3-2 and the similarity of the gradients (Fig. 7.15b) suggests a common precursor for the fragment ions. This similarity for the gradients of graphs also suggests an ID route for the fragments. As discussed above the ion state in DNT was not visible and, therefore, it is difficult to attribute the fragmentation pattern to the DNT molecular parent ion. Since in the case of the lowest laser pulse energy the

$C_7H_5^+$ or $C_7H_6^+$ peaks still exist and $C_7H_5^+$ peak is one of the strongest peaks in the mass spectrum, this fragment ion might be the precursor for the remaining fragments in the mass spectrum.

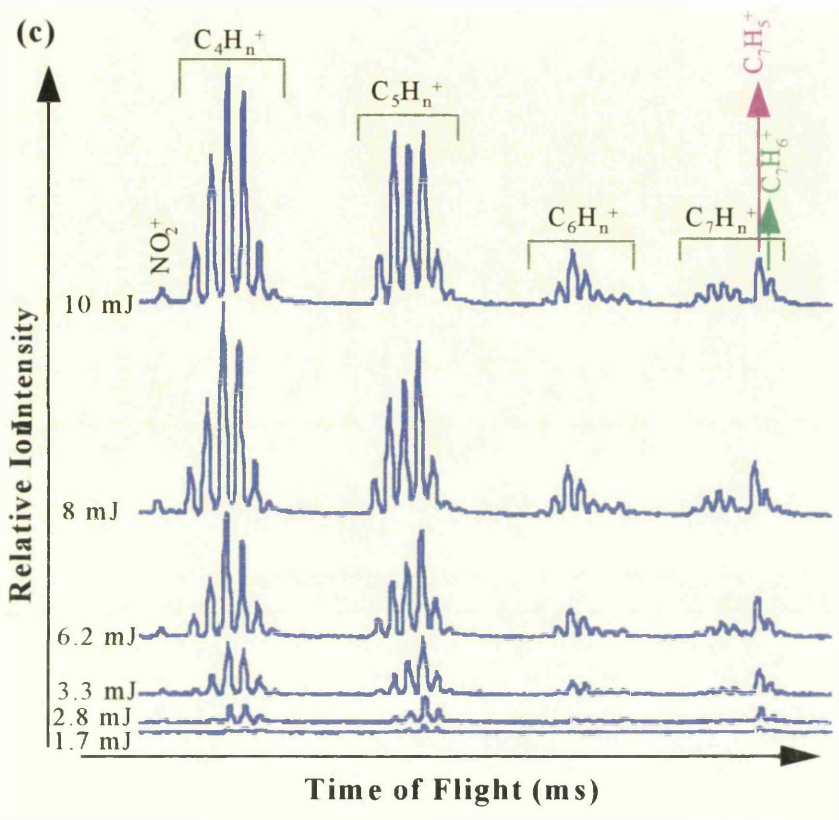


**Figure 7.16**: The laser pulse energy dependencies of the fragmentation pattern of heavier mass ions in the mass spectrum of DNT. The range of detected masses are shown in fig. 7.15a.

## 7.4 Conclusions

Previous UV photolysis experiments in the ns regime for $NO_2$ and the nitro-compounds, have shown that in the mass spectra, the parent peak is invariable missing or at least very small because of fast dissociation after absorption of the first photon. By far the biggest ion peak is always the NO fragment on or off resonance and the hydrocarbon ion production is always small. Although the sensitivity for the detection of a member of this group *via* the $NO^+$ ion peak is high, the lack of strong hydrocarbon ion peaks results in very much reduced selectivity of members within the group. It has been suggested that at shorter photolysis wavelengths, the hydrocarbon

ion yield is increased without markedly reducing the $NO^+$ yield (Simeonssen *et al.*, 1994; Kosmidis *et al.*, 1994b; Weikenhauf *et al.*, 1994; Ledingham *et al.*, 1995b; Kilic *et al.*, 1997; Kosmidis *et al.*, 1997) and this would increase the selectivity.

The present experimental work has shown that when femtosecond excitation is used for the detection of the nitro-compounds, the dissociative states are often "defeated" resulting in a large parent mass ion peak or at least many more high mass ions making the selectivity very much greater. For the nitrotoluene isomers there is a large parent mass ion peak which is completely missing in the mass spectra for nanosecond excitation. For the more energetic compounds like DNT and TNT, although the parent mass is missing, the intensity of the larger mass ion peaks is much greater than for nanosecond excitation. Thus in agreement with the work of Weinkauf *et al.* (1994)., the femtosecond excitation in the present work has been shown to be much more efficient than nanosecond excitation for ion production.

The present work has shown that the potential for femtosecond laser mass spectrometry is considerable, especially for thermally labile molecules. Femtosecond excitation is found to be much more efficient for ion production than nanosecond excitation especially for large molecules (Weikenhauf *et al.*, 1994). The use of ultrafast radiation can also produce large parent mass peaks which is of great use in analytical analysis. Since parent ions are often produced efficiently, FLMS may be of importance for identifying above ionisation fragmentation pathways.

It is known that the mass spectra of thermally labile molecules always contain fragment ions after ns photoexcitation. It is a challenge to produce only parent ions using laser based techniques. The present work was an attempt to this end. However, even with 90 fs pulses, although much higher ion efficiencies were obtained, the parent ion states of DNT and TNT were not obtained.

# CHAPTER 8

# CONCLUSIONS AND FUTURE PLANS

# CONCLUSION AND FUTURE WORK

Recent developments in the laser industry and the applications of ultrashort laser pulses and therefore the developments on the laser based techniques allows us to investigate molecular dynamics on a short time scale of about a vibration time. Mass spectrometry is one of the most powerful technique for analysing chemicals. It has been shown in this thesis that it becomes more powerful technique when it is operated in conjunction with a femtosecond laser system. The same conclusions have been made in a number of articles comparing the nanosecond and femtosecond laser mass spectrometry (FLMS) (Ledingham et al., 1995a; 1995b; Singhal et al., 1996; Kilic et al., 1996; 1997; Kosmidis et al., 1997; Weickhardt et al., 1997; Ledingham and Singhal, 1997).

In the present work, an identification of the dissociative ionisation processes in nitromethane, nitrobenzene, three isomers of nitrotoluene, dinitrotoluene and trinitrotoluene molecules have been carried out and an analytical assessment of the time of flight mass spectra of above mentioned thermally labile molecules has been made. A quantitative treatment of the dissociative ionisation of the $NO_2$ gas has been discussed by means of the Glasgow rate equation model for both nanosecond and femtosecond laser pulses.

In this thesis, the nanosecond and femtosecond time of flight mass spectra of each sample was compared and the multiphoton ionisation and dissociation dynamics have been investigated. The potential of femtosecond laser mass spectrometry (FLMS) for the detection of this difficult group of molecules was presented.

It was pointed out in section 2.5 from the literature that for the ionisation-fragmentation of molecules, one of the two distinct mechanisms may be involved in the multiphoton dissociation-ionisation-fragmentation dynamics from reagent to products, which are termed as DI (dissociation-ionisation) and ID (ionisation-

dissociation) routes. For the efficient production of the parent ion to be obtained, it is often necessary to use short laser pulses, since if the laser pulse width is longer than the lifetime of dissociative excited state, a DI process often dominates the mechanism. This is the general case in the nanosecond regime, but if the laser pulse width is shorter than the lifetime of the dissociative excited state, the ID mechanism dominates the process.

It should be pointed out that one of the most important parameters for production of a large number of parent ions is the laser intensity. The efficiency of REMPI for detecting higher number of molecular parent ion relative to the number of fragments cannot be increased by increasing the laser intensity because as the laser intensity increases the molecular parent ion starts to fragment and fragmentation pattern becomes more pronounced. The fragmentation of the molecular parent ion in an ID process may be decreased by turning the laser intensity down but it may increase the number of neutral fragments from the excited state of the neutral parent molecule and DI mechanism becomes dominant in the process. This can clearly seen in the mass spectrum of nitromethane in fig.5.5b taken at 750 nm where an ID mechanism is the most likely case. In some cases, it has been noticed that the fragmentation pattern with respect to the parent ion is not a function of the laser intensity, but is a function of the laser pulse duration (Ledingham et al., 1995a; Singhal et al., 1996; 1997; Smith et al. 1997). The laser pulse width dependence experiment at 750 nm at 90 fs on nitrobenzene has shown that as the laser pulse width changes to longer duration, the fragment ion peaks become dominant in the spectrum. The parent ion becomes prominent in the shortest laser pulse duration with respect to the fragment ions (Fig. 6.4).

Chapter 4 discussed the multiphoton dissociative ionisation of $NO_2$ molecule where a single bond was probed by both nanosecond and femtosecond laser pulses. For a quantitative investigation of a particular bond, the competition between the dissociation of this particular bond and the ionisation of the neutral ground state

parent molecule has been made using a rate equation model. It was shown that the Glasgow rate equation model is able to reproduce the experimentally obtained results and a comparison of the experimental and theoretical results show that these perfectly fit. The $NO_2^+/NO^+$ ratio is the number which shows how the dissociation competes with the ionisation when a particular bond is broken. It was also shown that this ratio at 375 nm is about 6-11% and no significant change on the ratio takes place as the laser intensity changes about the intensity range of $10^{12-14}$ W/cm$^2$. It has been shown elsewhere (Singhal et al., 1997) that a significant change can be observed as a function of the laser pulse duration and wavelength.

It was shown with the work carried out in this thesis that the nanosecond REMPI fails to overcome the problem of rapidly dissociating states of a molecule which have short lifetimes in the dissociative excited state. In the femtosecond time scale however, the molecular dynamics in the excited state of the neutral molecule are frozen (Grubela and Zewail, 1990). Thus the femtosecond laser mass spectrometry can often "defeat" these dissociative states by fast up-pumping to the parent ion states resulting in a large parent ion peak or at least many higher mass ion fragments which make the interpretation of the mass spectra much less ambiguous.

In the case of the results presented in the chapter 5 and 6 for nitromethane and nitrobenzene, the excited states in the neutral molecules have short lifetime about a few picosecond. When nanosecond laser pulses are used to ionise these molecules the dissociation or fast radiationless relaxation processes in these molecules are dominating the process and the production of the parent ion becomes impossible. The nitromethane dissociates in a time scale which is shorter than 5 ps (Schoen et al., 1982) and in the excited state of nitrobenzene, nonradiative relaxation takes place in a time scale which is less then 10 ps (Takezaki et al., 1997). When a femtosecond laser pulse system is used, the lifetimes for both molecules are long with respect to the femtosecond time scale and the molecular dynamics in the

excited state is frozen. Fast up-pumping become dominant resulting in a large parent ion with higher mass ion peaks in the mass spectrum.

An important experiment was carried out on the nitrobenzene molecule using the similar laser intensities and different laser pulse duration, at 90 fs, 371 fs and 742 fs, to investigate the laser pulse width dependence of the dissociative ionisation process in this molecule. It was shown that as the laser pulse width changes to longer laser pulse duration the fragmentation pattern becomes much obvious (Figs. 6.4b and c) while the prominent peak is the parent ion in the mass spectrum with the shortest laser pulse duration (Fig. 6.4a). It was also observed that the production of $NO^+$, $C_6H_5^+$ and $C_6H_5O^+$ fragments are in competition at the 90 fs in the relevant laser intensity range (Fig. 6.4a). In the results presented in Chapter 6 these three ion peaks increase similar to that of the parent ion as the laser intensity increases.

In Chapter 7, the nanosecond and femtosecond laser mass spectra of nitroaromatics were compared and significant differences between the results were obtained. The mass spectra of *o*-nitrotoluene and *m*-nitrotoluene in the nanosecond regime were compared and it was shown that the mass spectra of these two isomers could not be distinguished. In the femtosecond regime however, a distinction between the three isomers of nitrotoluene was shown and thus the femtosecond laser mass spectrometry is a powerful technique for identification of these molecules. This distinction was supported by the laser intensity dependencies of these three isomers which were different. It was shown that the laser intensity dependencies of the *m*- and *p*-nitrotoluene are rather similar, but are different than the laser intensity dependence of the *o*-nitrotoluene. In the mass spectra of the three isomers (Fig. 7.6), the mass ion peaks appears at m/q=120 ($C_7H_6NO^+$) and m/q=92 ($C_6H_6N^+$) for *o*-nitrotoluene, m/q=121 ($C_7H_7NO^+$) for *p*-nitrotoluene and absence of the above mentioned three peaks for *m*-nitrotoluene were identified as *fingerprints*.

The laser wavelength dependence of the ionisation and fragmentation processes at 375 nm and 750 nm were also observed for nitrotoluene isomers. Prominent parent ions at 375 nm are present in the mass spectra of three nitrotoulene isomers while very small parent ions of the *o*- and *m*-nitrotoluene isomers at 750 nm were present in the spectra despite higher laser intensities being used at 750 nm.

It was also shown in Chapter 7 that in the larger nitroaromatic molecules, DNT and TNT, the ionic state in parent molecules could not be reached with the available laser parameters used. The mechanism involved in the multiphoton dissociation and ionisation process follows a DI route.

In the multiphoton dissociative ionisation of the DNT molecule, the process was attributed to a DI process due to the absence of the parent ion and the lighter mass ions were produced with higher efficiencies. The laser pulse energy dependence of the fragmentation pattern in the mass spectrum of DNT show that as the laser intensity increases the lighter mass ion peaks disappear first and higher mass ion peaks were still present in the mass spectrum. The laser intensity dependencies of the major fragments in the mass spectra were similar indicating a common precursor.

All the data presented in chapters 5, 6 and 7 for nitromethane, nitrobenzene and nitrotoluene isomers and DNT, the laser intensity dependencies of fragments are similar to that of relevant parent ion and this is usually attributed to a common precursor for the fragment ions. The appearance of the same laser intensity dependence curves is the evidence of the ID mechanism which a molecule follows from reagent to the product. In the nanosecond regime (Fig. 7.4b), it was also shown that each fragment ions shows different laser intensity dependence due to their own spectroscopic characteristics and this case was attributed to a DI process.

However, the present experimental work has shown that when femtosecond excitation is used for the detection of the nitro-compounds, the dissociative states are often "defeated" resulting in a large parent mass ion peak or at least many more high mass ions making the selectivity very much greater. This conclusion is especially true for nitromethane and nitrobenzene and the lifetime of the excited states in these molecules are known from the literature. In the case of nitrotoluene there is no available published data, to the author's knowledge, but the result indicated that a similar conclusion can be drawn. For the smaller mass nitro-compounds, nitromethane, nitrobenzene and nitrotoluene there is a large parent mass signal which is completely missing in the mass spectra for nanosecond excitation.

Thus in agreement with the literature (Mollers et al., 1992; Weinkauf *et al.*, 1994; Ledingham et al., 1995b; Grun et al., 1996; Kilic et al., 1997; Kosmidis et al., 1997; Weickhardt et al., 1997; Ledingham and Singhal, 1997), the femtosecond excitation in the present work has been shown to be much more efficient than nanosecond excitation for heavy ion production. However, a large hydrogen production was also often observed in the femtosecond induced fragmentation and ionisation of the nitro-compounds. This was possibly due to the fact that higher laser intensities were used. As the laser intensity is decreased the hydrogen peak disappeared earlier than the higher mass ion peaks in almost every spectrum taken.

As a summary, the present work has shown that the potential for femtosecond laser mass spectrometry is considerable, especially for thermally labile molecules. Three aspects of the work carried out to the present time are especially worth noting. Femtosecond excitation is found to be much more efficient for ion production than nanosecond excitation especially for large molecules which is similar to the conclusion made by Weinkhauf et al (1994). The use of ultrafast radiation can also produce large parent mass peaks which is of great use in analytical techniques.

Since parent ions are often produced efficiently, FLMS may be of especial importance for identifying above ionisation fragmentation pathways.

The applications of the FLMS to a number of aromatic molecules, such as benzene ($C_6H_6$), toluene ($C_7H_8$), naphtalene ($C_{10}H_8$) and anthracene ($C_{14}H_8$) and a number of nitroalkane molecules such as, nitroethane ($C_2H_5NO_2$), nitroprophane ($C_3H_7NO_2$) and nitrobuthane ($C_4H_9NO_2$) will be done to show and further emphasise the potential of the FLMS. In these molecules the multiphoton process as well as the laser pulse width dynamics on the dissociative ionisation processes will be investigated.

# REFERENCES

## References

Abd El-Kader, F.H. and Ahmed, H.M. (1984),
*Dissociative Ionization and Metastable Ions of Nitrobenzene and Nitrobenzene- $d_5$*,
Z. Naturforsch., **39a**, 391-394.

Ackerhalt, J.R. and Shore, B.W. (1977),
*Rate Equations versus Bloch Equations in Multiphoton Ionization*,
Phys. Rev. A, **16**(1), 277-282.

Agostini,P., Barjot, G., Bonnal, J.F., Mainfray, G., Manus, C. and Morellec, J. (1968), *U-5 Multiphoton ionization of Hydrogen and Rare Gases,*
IEEE J. Quantum Electron., **QE-4**(10), 667-669.

Aicher, K.P., Wilhelm, U. and Grotemeyer, J. (1995),
*Multiphoton ionisation of Molecules: A Comparison Between Femtosecond and Nanosecond Laser Pulse Ionization Efficiency*,
J. Am. Soc. Mass Spectrom., **6**, 159-168.

Allam, S.H., Migahed, M.D. and El Khodar, A. (1981),
*Electron Impact Study of Nitrobenzene and Nitromethane*,
Int. J. Mass Spectrom. and Ion Proc., **39**, 117-122.

Andrews, D.L. (1990),
*Lasers in Chemistry*,
2nd *Ed.*, Springer-Verlag berlin Heidelberg New York.

Antonov, V.S. and Letokhov, V.S. (1981),
*Laser Multistep and Multiphoton Ionisation of molecules and Mass Spectrometry*,
App. Phys., **24**, 89-106.

Aoki, K., Nagai, M., Hoshina, K. and Shibuya, K. (1993),
*Rotational Quantum Number and Vibronic Symmetry of $NO_2$ Excited with Visible Light in the Region of 563-566 nm: Optical-Optical Double Resonance Measurement and Spin-Orbit Interaction between $^2B_2$ and $^2A_2$ Vibronic States*,
J. Phys. Chem., **97**, 8889-8894.

Aoki, K., Hoshina, K. and Shibuya, K. (1996),
*Vibronic Analysis of Fluorescence Spectrum of $NO_2$ $D^2B_2(000)$ in the Region of 250-550 nm*,
J. Chem. Phys., **105**(6), 2228-2235.

Apel, E.C. and Nogar, N.S. (1986),
*Multiphoton Photoionization Mass Spectra of Nitrobenzene and 2, 4, 6-Trinitrotoluene,*
Int. J. Mass Spectrom. Ion Proc., **70**, 243-246.

Ashfold, M.N.R. and Howe, J.D. (1994),
*Multiphoton Spectroscopy of Molecular Species,*
Annu. Rev. Phys. Chem., **45**, 57-82.

Band, Y.B. and Freed, K.F. (1975),
*Dissociation process of polyatomic Molecules,*
J. Chem. Phys., **63**(8), 3382-3397.

Barrow, R.F. and Miescher, E. (1957),
*Fine Structure Analysis of NO Absorption Bands in the Schumann Region,*
Proc. Phys. Soc. (London) A, **70**, 352-357.

Bayliss, N.S. and McRae, E.G. (1954),
*Solvent Effects In The Spectra of Aceton, Crotonaldehyde, Nitromethane and Nitrobenzene,*
J. Phys. Chem., **58**, 1006-1011.

Benoist D'azy, O., Lopez-Delgado, R. and Tramer, A. (1975),
*NO Fluorescence Decay from Low-Lying Electronic States Excited into Single Vibronic Levels with Synchrotron Radiation,*
Chem. Phys., **9**, 327-338.

Bergman, K., Haus, H.A., Ippen, E.P. and Shirasaki, M. (19914),
*Squeezing in A Fiber Interferometer with A Gigawatt Pump,*
Opt. Lett., **19**(4), 290-292.

Beynon, J.H.; Saunders, R.A. and Williams, A.E.(1964),
*The Combinated Use of Low and High Resolution Mass Spectrometry: Organic Nitro-Compounds,*
Industrie Chimique Belge., **4**, 311-328.

Beynon, J.H.; Saunders, R.A.; Topham, A. and Williams, A.E.(1965),
*The Dissociation of o-Nitrotoluene Under Electron Impact,*
J.Chem.Soc., 6403-6405.

Blais, N.C. (1983),
*Photofragmentation of Nitromethane in A Molecular Beam at 193 nm,*
J.Chem.Phys., **79,** 1723-1731.

Boesl, U., Weinkauf, R., Walter, K., Weickhardt, C. and Shlag, E.W. (1990a),
*Multiphoton Dissociation of Organic Molecules: Step by Step Investigation*

*with Laser tandem mass Spectrometry*,
Ber. Bunsenges. Phys. Chem., **94,** 1357-1362.

Boesl, U., Weinkauf, R., Walter, K., Weickhardt, C. and Shlag, E.W. (1990b),
*Tandem Time of Flight Techniques and Multiphoton Mass Spectrometry: The Ledder Switching in Benzene*,
J.Phys.Chem. **94,** 8567-8573.

Boesl, U., Weinkauf, R., Weickhardt, C. and Shlag, E.W. (1994),
*Laser Ion Sources for Time-of-Flight Mass Spectrometry*,
Int. J. Mass Spcetrom. Ion proc. **131,** 87-124.

Brook, M. and Kaplan, J. (1954),
*Dissociation Energy of NO and $N_2$*,
Phys. Rev. **96**, 1540-1542.

Brown, H.W. and Pimentel, G.C. (1958),
*Photolysis of Nitromethane and of Methyl Nitrite in an Argon Matrix; Infrared Detection of Nitroxyl, HNO*,
J. Chem. Phys., **29**, 883-888.

Brown, P. (1970a),
*Kinetic Studies in Mass Spectrometry-VII: Competing Cleavage and Rearrangement Processes in Molecular Ion and Decomposition Reactions*,
Org. mass Spectrom., **3**, 1175-1186.

Brown, P. (1970b),
*Kinetic Studies in Mass Spectrometry-IX: Competing (M-$NO_2$) and (M-NO) Reactions in Substituted Nitrobenzenes. Approximate Activation Energies from Ionization and Appearance Potentials*,
Org. mass Spectrom., **4**, 533-544.

Brzozowski, J., Elander, N. and Erman, P. (1974),
*Direct Measurements of Lifetimes of Low-lying Excited Electronic States in Nitric Oxide*,
Physica Scripta, **9**, 99-103.

Budzikiewicz, H., Djerassi, C. and Williams, D.H. (1967),
*Nitro and Related Compounds*
*in* Mass Spectrometry of Organic Compounds, Holden-Day, San Fransisco.

Bulusu, S. and Axenrod, T. (1979),
*Electron Impact Fragmentation mechanisms of 2, 4, 6-Trinitrotoluene Derived From Metastable Transitions and Isotopic Labeling*,
Org. Mass Spectrom., **14**(11), 585-592.

Bunn, T.L., Richard, A.M. and Baer, T. (1986),
*Photodissociation of the Energy Selected Nitrobenzene Ion*,
J. Chem. Phys., **84**(3), 1424-1431.

Butler, L.J., Krajnovich, D., Lee, Y.T., Ondrey, G. and Bersohn, R. (1983),
*The Photodissociation of Nitromethane at 193 nm*,
J.Chem.Phys. **79,** 1708-1722.

Callear, A.B. and Pilling, M.J. (1970a),
*Fluorescence of Nitric* Oxide,
Trans. Faraday Soc., **66**, 1618-1634.

Callear, A.B. and Pilling, M.J. (1970b),
*Fluorescence of Nitric* Oxide,
Trans. Faraday Soc., **66**, 1886-1906.

Calvert, J.G. and Pitts, J.N. (1966),
*Photochemistry*, Wiley, New York.

Carper, W.R., Dorey, R.C., Tomer, K.B. and Crow, F.W. (1984),
*Mass Spectral Fragmentation Pthways in 2,4,6-Trinitrotoluene Derived from a MS/MS Unimolecular and Collisisonally Activated Dissociation Study,*
Org. Mass Spectrom., **19**, 623-626.

Cassady, C.J. and McElvany, S.W. (1993),
*Collison-Induced Dissociation and Photodissociation of Nitroaromatic Molecular Ions: A Unique Isomerization for p-Nitrotoluene and p-Ethylnitrobenzene Ions*,
Org. Mass Spectrom., **28**, 1650-1657.

Chen, C.H., Clark, D.W., Peyne, M.G. and Kramer, S.D. (1980),
*Determination of Dissociative Limit of $NO_2$ and Characteristics of A Molecular Beam by Fluorescence Excitation Spectra*,
Opt. Commun., **32**, 391-395.

Chin, S.L., Isenor, N.R. and Young, M. (1969),
*Multiphoton ionization of Hg and Xe*,
Phys. Rev. **188**, 7-8.

Chin, S.L. and Lambropoulos, P. (1984),
*Multiphoton Ionization of Atoms*,
Academic Press.

Christie, M.I., Gillbert, C. and Voisey, M.A. (1964),
*The Disproportionation of Nitric Oxide: A Reaction of Nitroso-Compounda*,
J. Chem. Soc., 3147-3155.

Clark, A., Kosmidis, C., Deas, R.M., A., Ledingham, K.W.D., Marshall, Sander, J. and Singhal, R.P. (1993),
*Multiphoton Processes in Open Atmosphere in the Wavelength Region 224-238 nm*,
J. Phys. D: Appl. Phys., **26**, 2107-2111.

Cremaschi, P., Johnson, P.M. and Whitten, J.L. (1978),
*Multiphoton Ionization Spectroscopy: A Theoretical Analysis of the NO Spectrum*,
J. Chem. Phys., **69**(10), 4341-4348.

Cry, D.R., Leahy, D.J., Osborn, D.L., Continetti, R.E. and Neumark, D.M. (1993),
*Fast Beam photodissociation of the $CH_2NO_2$ Radical*,
J. Chem. Phys., **99**(11) 8751-8764.

Cundal, R.B., Locke, A.W. and Street, G.C. (1967),
*The Radiolysis and Photolysis of Nitromethane* in *The Chemistry of Ionization and Excitation*,
Eds G.R.A.Johnson and G.Scholes, Taylor Francis Ltd., London,131-140.

Davis, C.C. (1996),
*Lasers and Electro-Optics: Fundamentals and Engineering*,
Cambridge University Press.

Delaney, J.J., Hillier, I.H. and Saunders, V.R. (1982),
*Photoexcitation and Ionization in Nitric Oxide: Theoretical Studies in the Static Exchange Approximation*,
J. Phys. B: Atm. Mol. Phys., **15**, 1477-1486.

Delon, A. and Jost, R. (1991a ),
*Laser Induced Dispersed Fluorescence Spectra of Jet Cooled $NO_2$: The Complete Set of Vibrational Levels up to 10 000 $cm^{-1}$ and The Onset of the $X^2A_1$ - $A^2B_2$ Vibronic Interaction*,
J. Chem. Phys., **95**, 5686-5700.

Delon, A., Jost, R. and Lombardi, M. (1991b),
*$NO_2$ Jet Cooled Visible Excitation Spectrum: Vibronic Caos Induced by the $X^2A_1$ - $A^2B_2$ Interaction*,
J. Chem. Phys., **95**, 5701-5718.

Delon, A., Georges, R.. and Jost, R. (1995),
*The Visible Excitation Spectrum of Jet Cooled $NO_2$: Statistical Analysis of Vibronic Interactions*,
J. Chem. Phys., **103**(18), 7740-7773.

Demproder, W. (1982),

*Laser Spectroscopy*,
Springer-Verlag, Berlin.

Dewar, M.J.S., Ritchie, J.P. and Alster, J. (1985),
*Thermolysis of Molecules Containing $NO_2$ Group*,
J. Org. Chem., **50**, 1031-1036.

DeWitt, M.J. and Levis, R.J. (1995),
*Near-Infrared Femtosecond Photoionization/ Dissociation of Cyclic Aromatic Hydrocarbons*,
J.Chem.Phys. **102,** 8670-8673.

Douglas, A.E. and Huber, K.P. (1965),
*The Absorption Spectrum of NO2 in the 370-460 nm Region*,
Can. J. Phys., **43**, 74-81.

Duling III, I.N., Norris, T., Sizer, T., Bado, P. and Mourou, G.A. (1985),
*Kilohertz Synchronous Amplification of 85-Femtosecond Optical Pulses*,
J. Opt. Soc. Am. B, **2**(4), 616-618.

Egsgaard, H., Carlsen, L. and Elbel, S. (1986),
*Isomerisation of The Nitromethane Radical Cation in The Gas Phase*,
Ber. Bunsengen. Phys. Chem., **90**, 369-374.

Fields, E.K. and Meyerson, S. (1971),
*Mass-Spectral and Ther Reactions of Nitromethane*,
General Papers Sessions on Petrochemicals, American Chemical Society, Los Ange;es Meeting, **March 28- April 2**, B96-B108.

Fisanick. G.J., Gedanken, A., Eichelberger IV, T.S., Kuebler, N.A. and Robin, M.B. (1981),
*Multiphoton Ionisation Spectroscopy of Organometallics: The $Cr(CO)_6$, $Cr(CO)_3C_6H_6$, $Cr(C_6H_6)_2$ Series*,
J. Chem. Phys., **75**(11), 5215-5225.

Fleming, G.R. (1986),
*Chemical Applications of Ultrafast Spectroscopy*,
International Series of Monographs on Chemistry **13**, Oxford Science Publications, New York.

Flicker, W.M., Mosher, O.A. and Kupperman, A. (1980),
*Variable Angle Electron-Impact Excitation of Nitromethane*,
J. Chem. Phys., **72**(4), 2788-2794.

Fork, R.L., Greene, B.I. and Shank, C.V. (1981),
*Generation of Optical Pulses Shorter Than 0.1 psec by Colliding Pulse Mode*,
Appl. Phys. Lett., **38**(9), 671-672.

Fork, R.L., Shank, C.V. and Yen, R.T. (1982),
*Amplification of 70-fs Optical Pulses to Gigawatt Powers*,
Appl. Phys. Lett., **41**(3), 223-225.

Fork, R.L., Cruz, C.H.B., Bercker, P.C. and Shank, C.V. (1987),
*Compression of Optical Pulses to Six Femtoseconds by using Cubic Phase Compensation*,
Oppt. lett., **12**(7), 483-485.

Fujimoto, J.G., Weiner, A.M. and Ippen, E.P. (1984),
*Generation and Measurement of Optical Pulses as Short as 16 fs*,
Appl. Phys. Lett., **44**(9), 832-834.

Galloway, D.B., Bartz, J.A., Huey, L.G. and Crim, F.F. (1993),
*Pathways and Kinetic Energy Disposal in the Photodissociation of Nitrobenzene*,
J. Chem. Phys., **98**(3), 2107-2114.

Gangi, R.A. and Burnelle, L. (1971),
*Electronic Structure and Electronic Spectrom of Nitrogen Dioxide. II. Configuration Interaction and Ossilator Strengths*,
J. Chem. Phys., **55**, 843-850.

Gaydon, A.G. (1944),
*The Spectrum of NO: Rotational Analysis of Epsilon Bands and New Observations on the Beta and Delta Band Systems*,
Phys. Soc., **56**, 160-174.

Gedanken, A., Robin, M.B. and Kuebler, N.A. (1982),
*Nonlinear Photochemistry in Organic, Inorganic, and Organometallic System*,
J. Phys. Chem., **86**, 4096-4107.

Geers, A., Kappert, J., Temps, F. and Wiebrecht, J.W. (1993),
*Direct Measurements of State Specific Unimolecular Dissociation Rate Constants of Highly Excited Single Rotation Vibration Quantum States of $CH_3$) ($X^2E$)*,
J. Chem. Phys., 99(3), 2271-2274.

Georges, R., Delon, A., Bylicki, F., Jost, R., Campargue, A., Charvat, M., Chenevier, M. and Stoeckel, F. (1995a),
*Jet Cooled $NO_2$ Intra Cavity Laser Absorption Spectroscopy (ICLAS) Between 11200 and 16150 $cm^{-1}$*,
Chem. Phys., **190**, 207-229.

Georges, R., Delon, A. and Jost, R. (1995b),
*The Visible Excitation Spectrum of Jet Cooled $NO_2$: The Chaotic Behavior of a*

*Set of $^2B_2$ Vibronic Levels*,
J. Chem. Phys., **103**(5), 1732-1747.

Gero, L. and Schmid, R. (1948),
*Dissociation Energy of the NO* Molecule,
Proc. Phys. Soc. LX-6, **35**, 533-539.

Gillispie, G.D., Khan, U., Walsh, A.C., Hosteny, R.P. and Krauss, M. (1975),
*The Electronic Structure of Nitrogen Dioxide: Multiconfiguration Self-Consistent-Field Calculation of the Low-lying Electronic* States,
J. Chem. Phys., **63**(8), 3425-3444.

Gilman, J.P., Hsieh, T. and Meisels, G.G. (1983),
*Competition Between Isomerisation and Fragmentation of Gasous Ions. II. Nitromethane and Methylnitrite Ions*,
J. Chem. Phys., **78**(3), 1174-1179.

Gilmore, F.R. (1966),
*Potential Energy Curves for $N_2$, NO, $O_2$ and Corresponding Ions*,
Memorandum, RM-4034-1-PR, RAND-Contract No. AF 49(638)-1700.

Glenewinkel-Meyer, T. and Crim, F.F. (1995),
*The Isomerization of Nitrobenzene to Phenylnitrite*,
J. Mol. Struc. (Theochem), **337**, 209-224.

Gray, P., Yoffe, A.D. and Roselaar, L. (1955a),
*Bond Dissociation Energies in Nitrites and Nitro Compounds and The Reaction of Free Radicals with Nitrogen Dioxide*,
Trans. Faraday Soc., **51**, 1367-1374.

Gray, P., Yoffe, A.D. and Roselaar, L. (1955b),
*Thermal Decomposition of The Nitroalkanes*,
Trans. Faraday Soc., **51**, 1489-1496.

Greenblatt, G.D., Zuckermann, H. and Haas, Y. (1987),
*OH Production on the Collision-Free UV Photolysis of Aliphatic Nitrocompounds*,
Chem.Phys.Lett., **134**, 593-599.

Grubela, M. and Zewail, A.H. (1990),
*Ultrafast Reaction Dynamics*,
Phys. Today, **May**, 24-33.

Grun, C., Weickhardt, C. Grotemeyer, J. (1996),
*Multiphoton Ionisation mass Spectrometery of Metal Organic Compounds: Avoiding The Ultrafast Neutral Dissociation Channels by Femtosecond Laser*

*Activities*,
Eur. Mass Spectrom., **2**, 197-202.

Hallin, K.-E. and Merer, A.J. (1976),
*The 249.1 nm band system of $NO_2$. Rotational Structure and Evidence for Predissociation in the Zero-point Level*,
Can. J. Phys., **54**, 1157-1171.

Harris, L.E. (1973),
*The Lower Electronic States of Nitrite and Nitrate Ion, Nitromethane, Nitramide, Nitric Acid, and Nitrate Esters*,
J. Chem. Phys., **58**(12), 5615-5626.

Harris, F.M., Mukhtar, E.S., Griffits, I.W. and Beynon, J.H. (1981),
*Design of A High-Resolution Mass Spectrometry for Studying the Photodissociation of Organic Ions in the Gas Phase*,
Proc. R. Soc. London, **A374**, 461-473.

Hastings, S.H. and Matsen, F.A. (1948),
*The Photodecomposition of Nitrobenzene*,
J. Am. Chem. Soc., **70**, 3514-3515.

Heicklen, J. and Cohen, N. (1968),
*The Role of Nitric Oxide in Photochemistry*, In *Advances in Photochemistry*,
Ed. by Noyes, Jr., W.A., Hammond, G.S. and Pitts, Jr., J.N., **5**, 157-328.

Herbert, C.G., Larka, E.A. and Beynon, J.H. (1984),
*The Elimination of Masses 27 and 28 from the $[M-OH]^+$ Ion of 2-Nitrotoluene*,
Org. Mass Spectrom., **19**(7), 306-310.

Herek, J.L., Pedersen, S., Banares, L., H.Zewail, A. (1992),
*Femtosecond Real-Time Probing of Reactions. IX. Hydrogen-Atom Transfer,*
J.Chem.Phys., **97**, 9046-9061.

Herzberg, G. (1950),
*Molecular Spectra and Molecular Structure: I. Spectra of Diatomic Molecule*,
2nd Ed. and 2nd Printing, D. Van Nostrand Com., Inc.,

Herzberg, G. (1966),
*Molecular Spectra and Molecular Structure : III. Electronic Spectra and Electronic Structure of Poliatomic Molecules*,
Klieger Pub. Com., Florida.

Hesser, J.E. (1966),
*Absolute Transition Probabilities in Ultraviolet Molecular Spectra*,
J. Chem. Phys., **45**, 3149-2535.

Hesser, J.E. (1968),
*Absolute Transition Probabilities in Ultraviolet Molecular Spectra*,
J. Chem. Phys., **48**(6), 2518-2535.

Hirschlaff, E. and Norrish, R.G.W. (1936),
*Primary Photochemical Processes. Part IX. A Preliminary Study of the Decomposition of Nitromethane and Nitroethane*,
J.Chem.Soc., 1580-1585.

Honda, K., Mikuni, H. and Takahasi, M. ((1972),
*Photolysis of Nitromethane in Gas Phase at 313 nm*,
Bull.Chem.Soc.Jap., **45**, 3534-3541.

Hsu, D.K., Monts, D.L. and Zare, R.N. (1978),
*Spectral Atlas of Nitrogen Dioxide*,
Academic Press, New York.

Hurts, G.S., Payne, M.G., Kramer, S.D. and Young, J.P. (1979),
*Resonance Ionisation Spectroscopy and One-Atom Dtection*,
Rev. Mod. Phys., **51**(4), 767-819.

Hurts, G.S. and Payne, M.G. (1988),
*Principles and Applications of Resonance Ionisation Spectroscopy*,
Adam Hilger, Bristol and Philedelphia.

Hutschinson, M.H.R. (1989),
*Terawatt Lasers*,
Contemporary Phys., **30**(5), 355-365.

Hwang, W.G., Kim, M.S. and Choe, J.C. (1996),
*Photodissociation Dynamics of Nitrobenzene Molecular Ion on a Nanosecond Time Scale*,
J. Phys. chem., **100** 9227-9234.

Ionov, S.I., Brucker, G.A., Jaques, C., Chen, Y. and Wittig, C. (1993),
*Probing the $NO_2 \rightarrow NO+O$ Transition State via Time Resolved Unimolecular Decomposition*,
J. Chem. Phys., **99**(5), 3420-3435.

Jackels, C.H. and Davidson, E.R. (1976a),
*The Two Lowest Energy $^2A'$ States of $NO_2$*,
J. Chem. Phys., **64**(7), 2908-2917.

Jackels, C.H. and Davidson, E.R. (1976b),
*An ab Initio Potential-Energy Surface Study of Several Electronic States of $NO_2$*,

J. Chem. Phys., 65(8), 2941-2957.

Johnson, P.M. (1975a),
*Multiphoton Ionization Spectroscopy: A New State of Benzene,*
J. Chem. Phys., **62**(11), 4562-4563.

Johnson, P.M. (1975b),
*Multiphoton Ionization Spectrum of Benzene,*
J. Chem. Phys., **64**(10), 4143-4148.

Johnson, P.M. and Otis, C.E. (1981),
*Molecular Multiphoton Spectroscopy with Ionization detection,*
Ann. Rev. Phys. Chem., **32**, 139-57.

Johnson, P.M., Berman, M.R. and Zekhaim, D. (1975),
*Nonresonant Multiphoton Ionization Spectroscopy: The four Photon Ionization Spectrum of Nitric Oxide,*
J. Chem. Phys., **62**, 6, 2500-2502.

Jost, R., Nygard, J., Pasinski, A. and Delon, A. (1996),
*The Photodissociation Threshold of $NO_2$: Precise Determination of Its Energy and Density of* States,
J. Chem. Phys., **105**(3), 1287-1290.

Jungen, Ch. and Miescher, E. (1968),
*Absorption Spectrum of the NO Molecule. VIII. The Heterogeneous ($^2\Sigma$-$^2\Pi$) Interactions between Excited States,*
Can. J. Phys., **46**, 987-1003.

Kandel, R.J. (1955),
*Appearance Potential Studies. II. Nitromethane,*
J. Chem. Phys., 23(1), 84-87.

Kilic, H.S., Ledingham, K.W.D., Smith, D.J., Wang, S.L., Kosmidis, C., McCanny, T., Singhal, R.P., Langley, A.J. and Shaikh, W. (1996),
*The Photo-Dissociative Pathways of Nitromethane Using Femtosecond Laser Pulses at 375* nm,
Eight International Resonance Ionization Spectroscopy, at RIS'96, State College, PA, June 30-July 5, 1996, AIP Conference Proceeding **388**, pp:395-398.

Kilic, H.S., Ledingham, K.W.D., Kosmidis, C., McCanny, T., Singhal, R.P., Wang, S.L., Smith, D.J., Langley, A.J. and Shaikh, W. (1997),
*Multiphoton Ionization and Dissociation of Nitromethane Using Femtosecond Laser Pulses at 375 and 750* nm,
J. Phys. Chem. A, **101,** 817-823,

Knox, W.H. (1988),
*Femtosecond Optical Pulse Amplification*,
IEEE J. Quantum Electron., **24**(2), 388-397.

Konnecke, A., Lepom, P., Dorre, R., Lippmann, E., Herzschuh, R., Kralj, B., Stanovnik, B. and Tisler, M. (1980),
*Mass Spectrometry of Condensed N-Heterocycles; II-A Novel* Ortho *Effect in the Electron Impact Induced Fragmentation of Some C-(2-Nitrophenyl)-Azoles and -Azoloazines*,
Org. Mass Spectrom., 15(2), 75-77.

Kosmidis, C. Bolovinos, C.; Tsekeris, P. (1993),
*Polarization measurements of the Resonant Multiphoton Ionization Spectrum of the 3s Rydberg States of Monomethylepyridines*,
J.Mol.Spectrosc., **160**, 186-191.

Kosmidis, C., Ledingham, K.W.D., Clark, A., Marshall, A., Jennings, R., Sander, J. and Singhal, R.P. (1994a),
*On the Dissociation Pathways of Nitrobenzene*,
Int. J. Mass Spectrom. Ion Proc., **135**, 229-242.

Kosmidis, C., Marshall, A., Clark, A., Deas, R.M., Ledingham, K.W.D. and Singhal, R.P. (1994b),
*Multiphoton Ionization and Dissociation of Nitromethane Isomers by UV Laser Light*,
Rapid Commun. Mass Spectrom., **8**, 607-614.

Kosmidis, C., Ledingham, K.W.D., Kilic, HS., McCanny, T., Singhal, RP., Langley, AJ. And Shaikh, W. (1997),
*On the Dissociation of Nitrobenzene and Nitrotoluenes Induced by Femtosecond Laser at 375 nm*,
J. Phys. Chem. A, **101**(12), 2264-2270.

Kumar, R.G., Safvan, C.P., Rajgara, F.A. and Mathur, D. (1994),
*Dissociative Ionization of Molecules by Intense Laser Field at 532 nm and* $10^{12}$-$10^{14}$ $Wcm^{-2}$,
J. Phys. B: Atm. Mol. Opt. Phys., **27**, 2981-2991.

Kwok, H.S., He, G.Z., Sparks, R.K. and Lee, Y.T. (1981),
*On the Photodissociation of Nitromethane at 266 nm*,
Int. J. Chem. Kin. 13, 1125-1131.

Lagerqvist, A. and Miescher, E. (1966),
*Absorption Spectrum of The NO Molecule; VI. Band Structures below 1600* $\AA$, *Rydberg States* $C^2\Pi$, $D^2\Sigma^+$, $K^2\Pi$, $M^2\Sigma^+$, $S^2\Sigma^+$, *Non-Rydberg States* $B^2\Pi$, $L^2\Pi$

*and Their Interactions*,
Can. J. Phys., **44**, 1525-1539.

Langley, A.J., (1995),
*private communication.*

Langley, A.J., Noad, W.J., Ross, I.N. and Shaikh, W. (1994),
*High-Brightness Femtosecond Laser Using Titanium-Sapphire Technology and Amplification in Dyes*,
Appl. Opt., **33**, 3875-3880.

Lao, K.Q., Jensen, E., Kash, P.W. and Butler, L.J. (1990),
*Polarized Emission Spectroscopy of Photodissociating Nitromethane at 200 and 218 nm*
J.Chem.Phys. **93**, 3958-3969.

Ledingham, K.W.D. (1995),
*Multiphoton ionisation and Laser Mass Spectrometry*, in An Introduction to Laser Spectroscopy
*Ed.* by Andrews, D.L. and Demidov, A.A., Plenum Press, New York and London, pp.199-227.

Ledingham, K.W.D., Kosmidis, C., Georgiou, S., Couris, S. and Singhal, R.P. (1995a),
*A Comparison of The Femto- Pico- and Nano-second Multiphoton Ionization and Dissociation Processes of $NO_2$ at 248 nm and 496 nm*,
Chem. Phys. Lett., **247**, 555-563.

Ledingham, K.W.D., Kilic, H.S., Kosmidis, C., Deas, R.M., Marshall, A., McCanny, T., Singhal, R.P., Langley, A.J. and Shaikh, W. (1995b),
*A Comparison of Femtosecond and Nanosecond Multiphoton Ionization and Dissociation for Some Nitro-Molecules*,
Rapid Commun. in Mass Spectrom., **9**, 1522-1527.

Ledingham, K.D.W. and Singhal, R.P. (1997),
*High Intensity Laser mass Spectrometry-A Review*,
Int. J. Mass Spectrom. Ion Proc., **163**, 149-168.

Leifson, S.W. (1926),
*Absorption Spectra of Some Gases and Vapours in The Schumann Region*,
Astrophys. J., **63**, 73-89.

Lemire, G.W., Simeonsson, J.B. and Sausa, R.C (1993),
*Monitoring of Vapor-Phase Nitro Compounds Using 226 nm Radiation: Fragmentation with Subsequent NO Resonance-Enhanced Multiphoton Ionization Detection*,

Anal. Chem., **65**, 529-533.

Letokhov, V.S., Mishin, V.I. and Puretzky, A.A. (1977),
*Selective Photoionization of Atoms by Laser and Its Applications*,
J. Prog. Quant. Electr., **5**, 139-203.

Letokhov, V.S. (1987),
*Laser Photoionization Spectroscopy*,
Academic Press Inc., London.

Lias, S.G., Liebman, J.F., Holmes, J.L., Levin, R.D. and Mallard, W.G. (1988),
*Gas-Phase Ion and Neutral Thermochemistry*,
J. Phys. and Chem. Ref. Data, Supp. 1, **V:17**.

Loos, K.R., Wild, U.P. and Guthard, H.H. (1968),
*Ultrviolet Spectra and Electronic Structure of Nitroethylene*,
Spectrchimica Acta, **25A**, 275-281.

Lubman, D.M. (1988a),
*Analitical Multiphoton Ionization Mass Spectrometry. Part I. Theory and Instrumentation*,
Mass Spectrom. Rev., **7**, 535-554.

Lubman, D.M. (1988b),
*Analitical Multiphoton Ionization Mass Spectrometry. Part II. Applications*,
Mass Spectrom. Rev., **7**, 559-592.

Marshall, A., Clark, A., Jennings, R., Ledingham, K.W.D., Sander, J. and Singhal, R.P. (1992a),
*Laser-Induced Fragmentation Processes in Nitrobenzene*,
Inst. Phys. Conf. Ser., **128**(5), at RIS 92, Santa Fe., NM, USA, 24-29, May.

Marshall, A., Clark, A., Jennings, R., Ledingham, K.W.D. and Singhal, R.P. (1992b),
*Wavelength-Dependent Laser-Induced Fragmentation of Nitrobenzene*,
Int. J. Mass Spectrom. Ion proc., **112**, 273-283.

Marshall, A., Clark, A., Jennings, R., Ledingham, K.W.D., Sander, J. and Singhal, R.P. (1992c),
*Laser-Induced Dissociation, Ionization and Fragmentation Processes in Nitroaromatic Molecules*,
Int. J. Mass Spectrom. Ion proc., **116**, 143-156.

Marshall, A., Clark, A., Ledingham, K.W.D., Sander, J. and Singhal, R.P. (1993),
*Laser Ionization Studies of Nitroaromatic and NOx(x=1 or 2) Molecules in the region 224-238* nm,
Int. J. Mass Spectrom. and Ion Proc., **125**, R21-R26.

Marshall, A., Clark, A., Deas, R.M., Kosmidis, C., Ledingham, K.W.D., Peng, W. and Singhal, R.P. (1994a),
*Sensitive Atmospheric Pressure Detection of Nitroaromatic Compounds and NOx(x=1,2) Molecules in an Ionization Chamber Using Resonance-enhanced Multi-photon Ionization*,
Analyst, **119**, 1719-1724.

Marshall, A., Clark, A., Deas, R.M., Ledingham, K.W.D., Sander, J., Singhal, R.P., Kosmidis, C. and Deas, R.M. (1994b),
*Detection and Identification of Explosives Compounds Using Laser Ionization Time-of-Flight Technique*,
Rapid Commun. Mass Spectrom., **8**, 521-526.

Marynick, D.S., Ray, A.K., Fry, J.L. and Kleier, D.A. (1984),
*The Electronic Structure of Nitromethane: A Multiconfiguration Self-Consistent Field Study*,
J. Mol. Structure (Theochem), **108**, 45-48.

Matyuk, V.M., Potapov, V.K. and Prokhode, A.L. (1979),
*Photoexcitation and Photoionization of Nitro-Derivatives of Benzene and Toluene*,
Russ. J. Phys. Chem., **53**(4), 538-541.

McEwan, K.L. (1960),
*Electronic Structures and Spectra of Nitromethane and Nitrogen Dioxide*,
J. Chem. Phys., **32**(6), 1801-1814.

McFarlane, J., Polanyi, J.C. and Shapter, J.G. (1991),
*Photodissociation Dynamics of $NO_2$ at 248 nm*,
J. Photochem. Photobiol. A: Chem., **58**, 139-172.

McKee, M.L. (1986a),
*Isomerisation of Nitromethane and Methyl Nitrite Radical Cations. A Theoretical Study*,
J. Phys. Chem., **90**, 2335-2340.

McKee, M.L. (1986b),
*Ab Initoo Study of Rearrangements of the $CH_3NO_2$ Potential Energy Surface*,
J. Am. Chem. Soc., **108**, 5784-5792.

McKee, M.L. (1989a),
*MCSCF Study of Rearrangements of Nitromethane to Methyl Nitrite*,
J. Phys. Chem., **93**, 7365-7369.

McKee, M.L. (1989b),
*Calculated C-$NO_2$ Bond Dissociation Energies*,

Chem. Phys. Lett., **164**(5), 520-526.

McLuckey. S.A., Glish, G.L. and Carter, J.A. (1985),
*The Analysis of Explosives by Tandem Mass Spectrometry*,
J. Forensic Sci., **30**(3), 773-778.

McMurry, S.M. (1994),
*Quantum Mechanics*,
Addison-Wesley Publishing Company.

Merienne, M.F., Jenouvrier, A. and Coquart, B. (1995),
*The $NO_2$ Absorption Spectrum. I : Absorption Cross Section at Ambient Temperature in the 300-500 nm Region*,
J. Atmosph. Chem., **20**, 281-297.

Meyerson, S., Puskas., I. and Fields, E.K. (1966),
*Organic Ions in the Gas Phase. XVIII. Mass Spectra of Nitroarenes*,
J. Am. Chem. Soc. **88**(21), 4974-4980.

Meyerson, S. and Fields, E.K. (1974),
*Mass Spectrum of Nitromethane*,
Organic Mass Spectrometry, 9, 485-490.

Mialocq, J.C. and Stephenson, J.C. (1986),
*Picosecond Laser-Induced Fluorescence Study of The Collisionless Photodissociation of Nitrocompounds at 266 nm*,
Chem. Phys., **106,** 281-291.

Miescher, E. (1971),
*Absorption Spectrum of The NO Molecule. X. The 3d Rydberg Complex, Its Vibrational Structure, Spin-Orbit Coupling, and Interactions with Non-Rydberg States*,
Can. J. Phys., **49**, 2350-2365.

Mijoule, C., Odiot, S., Fliszar, S. and Schnur, J.M. (1987),
*On the Dissociative Nature of The First Excited States of Nitromethane*,
J. Mol. Structure (Theochem), **149**, 311-321.

Miyawaki, J., Yamanouchi, K. and Tsuchiya, S. (1991),
*Photofragment Excitation Spectrum of $NO_2$ Observed through $O(^3P_J)$ Detection*,
Chem. Phys. Lett., **180**(4), 287-292.

Miyawaki, J., Yamanouchi, K. and Tsuchiya, S. (1993),
*State Specific Unimolecular Reaction of $NO_2$ Just Above the Dissociation Threshold*,

J. Chem. Phys., **99**, 254-264.

Miyawaki, J., Yamanouchi, K. and Tsuchiya, S. (1994),
*Response to "Comment on 'State-Specific Unimolecular Reaction of $NO_2$ Just Above the Dissociation Threshold' "*,
J. Chem. Phys., 100, 4716-4717.

Mollers, R., Terhorst, M., Niehuis, E. and Benninghoven, A. (1992),
*Resonance Photoionisation of Sputtered Organic Molecules by Femtosecond UV Laser Pulses*,
Org. Mass Spectros., **27**, 1393-1395.

Moss, D.B., Trentelman, K.A. and Houston, P.L. (1992),
*193 nm Photodissociation Dynamics of Nitromethane*,
J.Chem.Phys. **96**, 237-247.

Mukhtar, E.S., Griffits, I.W., Harris, F.M. and Beynon, J.H. (1980),
*Photo Dissociation of Positive Molecular Ions of Nitrobenzene*,
Org. Mass Spectrom., **14**(1), 51-52.

Murrey, J.S., Lane, P., Politzer, P., Bolduc, P.R. and McKenney, R.L., Jr. (1990),
*A Computational Analysis of Some Possible Hydrogen Transfer and Intramolecular Ring Formations of O-Nitrotoluene and O-Nitroaniline*,
J. Mol. Struct. (Theo. Chem.), **209**, 349-359.

Nagakura, S. (1960),
*Ultraviolet Absorption Spectra and $\pi$-Electron Structures of Nitromethane and the Nitromethyl Anion*,
Mol. Phys. **3,** 152-162.

Nagakura, S., Kojima, M. and Maruyama, Y. (1964),
*Electronic Spectra and Electronic Structures of Nitrobenzene and Nitromesitylene*,
J. Mol. Spectrosc., **13**, 174-192.

Napier, I.M. and Norrish, R.G.W. (1966),
*The Photolysis and Prolysis of Nitromethane and Methyl Nitrite*,
Proc. Roy. *Soc., A* **299,** 317-336.

Nicholson, A.J. (1961),
*Photolysis of Nitromethane*,
Nature, 190, 143-144.

Nishimura, T., Das, P.R. and Meisels, G.G. (1986),
*On the Dissociation Dynamics of Energy-Selected Nitrobenzene Ion*,
J. Chem. Phys., **84**(11), 6190-6199.

Niwa, Y., Tajima, S. and Tsuchiya, T. (1981),
*Fragmentation of Energy-Selected Nitromethane Ions*,
Int. J. Mass Spectrom. Ion Phys., **40**, 287-293.

Norris, T., Sizer II, T. and Mourou, G. (1985),
*Generation of 85-fsec Pulses by Synchronous Pumping of A Colliding-Pulse Mode-Locked Dye Laser*,
J. Opt. Soc. Am. B **2**(4), 613-614.

Ogden, I.K., Shaw, N., Danby, C.J. and Powis, I. (1983),
*Competing Dissociation Channels of Nitromethane and Mehyle Nitrite Ions and The Role of Electronic and Internal Modes of Excitation*,
Int. J. Mass Spectrom. and Ion Proc., **54**, 41-53.

Okabe, H. (1978),
*Photochemistry of Small Molecules*,
John Wiley&Sons, New York.

Osterheld, T.H., Baer, T. and Brauman, J.I. (1993),
*Infrared Multiple-Photon Dissociation of the Nitrobenzene Radical Cation. A Paradigm for Competitive Reactions*,
J. Am. Chem., Soc., **115**, 6284-6289.

Panczel, M. and Baer, T. (1984),
*A Photoelectron Photoion Coincidence (PEPICO) Study of Fragmentation Rates and Kinetic Energy Release Distribution in Nitrobenzene*,
Int. J. Mass Spectrom. Ion Proc., **58**, 43-61.

Paszyc, S. (1973),
*Photochemistry of Nitroalkanes*,
J. Photochem., **2**, 183-198.

Perry, M.D. and Mourou, G. (1994),
*Terawatt to Petawatt Subpicosecond Lasers*,
Science, **264**, 917-924.

Phillips, D., Lemaire, J., Burton, C. and Noyes, Jr., W. (1968),
*Isomerization as a Route for Radiationless Transitions*,
Ed. by Noyes, Jr., W.A., Hammond, G.S. and Pitts, Jr., J.N., **5**, 329-363.

Porter, G. and Ward, B. (1968),
*The Photolitic Preparation of Cyclopentadienyl and Phenyl Nitrene from Benzene Derivatives*,
Proc. R. Soc. London, **A303**, 139-.156

Qian, K., Shukla, A. and Futrell, J. (1990),

*Observation of Isolated Electronic States in The Collision-Induced Dissociation of Nitromethane Ions*,
Rapid Commun. Mass Spectrom., **4**(6), 222-224.

Qian, K., Shukla, A. and Futrell, J. (1991),
*Electronic Excitation in Lw-Energy Collisions: A Study of The Collision-Induced Dissociation of Nitromethane Ion by Cross-Beam Tandem Mass Spectrometry*,
J. Am. Chem. Soc., **113**, 7121-7129.

Rabalais, J.W. (1972),
*Photoelectron Spectroscopic Investigation of The Electronic Structure of Nitromethane and Nitrobenzene*,
J. Chem. Phys., **57**(2), 960-967.

Ramana, D.V., Sundaram, N. and George, M. (1990),
Ortho *Effects in Organic Molecules on Electron Impacts; Part 22. Competing Oxygen Transfers from the Nitro Group to Sulphur and the Olefinic Double Bond in 2-Nitrophenyl Styryl Sulphides*,
Org. Mass Spectrom., **25**, 161-164.

Rao, C.N.R. (1969),
*Spectroscopy of the Nitro Group*
In The Chemistry of The Nitro- and Notroso- Groups, Part.1, Ed. by H.Feuer, Interscience Publisher, John Wiley&Sons, New York-London.

Rebbert, R.E. and Slagg, N. (1976),
*Primery Processes in the Photochemical Decomposition of Nitroalkanes,*
Bull. Soc. Chem. Belg., **71**, 709-721.

Reiser, G., Habenicht, W., Muller-Dethlefs, K. and Schlag, E.W. (1988),
*The Ionization Energy of Nitric Oxide*,
Chem. Phys. Lett., **152**(3), 119.

Renlund, A.M. and Trott, W.M. (1984),
*ArF Laser-Induced Decomposition of Simple Energetic Molecules*,
Chem. Phys. Lett., **107**, 555-560.

Robin, M.B. (1974),
*Higher Excited States of Poliatomic Molecules*, Vol:2,
Academic Press, New York.

Robra, U., Zacharias, H. and Welge, K.H. (1990),
*Near Threshold Channel Selective Photodissociation of $NO_2$*,
Phys. D : Atoms, Molecules and Clusters, **16**, 175-188.

Rohlfing, E.A. and Valentini, J.J. (1985),
*Structure and Predissociation Dynamics of Electronically Excited Nitrogen Dioxide: A Resonance Raman Study*,
J. Chem. Phys., **83**(2), 521-528.

Rottke, H. and Zacharias, H. (1985),
*Photoionisation of Single Rotational Levels in $B^2\Pi$, $C^2\Pi$ and $D^2\Sigma^+$ States of $^{14}N^{16}O$*,
J. Chem. Phys., **83**(10), 4831-4844.

Rudolph, H., Dixit, S.N., McKoy, V. and Huo, W.M. (1988),
*Ionic Rotational Branching Ratios in Resonant Enhanced Multiphoton Ionization of NO via the $A^2\Sigma^+$ ($3s\sigma$) and $D^2\Sigma^+$ ($3p\sigma$) States*,
J. Chem. Phys., **88**(2), 637-641.

Saxon, R.P. and Yoshimine, M. (1991),
*Theoretical Study of Nitro-Nitrite Rearrangement of $CH_3NO_2$*,
Can. J. Chem., **70**, 572-579.

Schoen, P.E., Marrone, M.J., Schnur, J.M. and Goldberg, L.S. (1982),
*Picosecond UV Photolysis and Laser-Induced Flourescence Probing of Gas-Phase Nitromethane*,
Chem.Phys.Lett. **90**, 272-276.

Schwartz, H. (1978),
*Some Newer Aspects of Mass Spectrometric* Ortho *Effects*,
Top. Curr. Chem., **73**, 231-263.

Shank, C.V., Fork, R.L., Yen, R., Stolen, R.H. and Tomlinson, W.J. (1982),
*Compression of Femtosecond Optical Pulses*,
Appl. Phys. Lett., **40**(9), 761-763.

Shao, H.D. and Baer, T. (1988),
*The Dissociation Dynamics of Energy Selected* o-*Nitrotoluene Ions*,
Int. J. Mass Spectrom. Ion Proc., **86**, 357-367.

Simeonsson, J.B.; Lemire G.W.; Sausa, R.C. (1993),
*Trace Dtection of Nitrocompounds by ArF Laser Photofragmentation and Ionization Spectroscopy*,
Appl. Spectrosc., **98**, 2107

Singhal, R.P., Land, A.P., Ledingham, K.W.D. and Towrie, M. (1989),
*Population Rate Equations Modelling of A Resonant Ionisation Process*,
J. Anal. Atomic Spectrom., **4**, 599-603.

Singhal, R.P. (1995),

*Nonlinear Optics*,
in An Introduction to Laser Spectroscopy *Ed.* by Andrews, D.L. and Demidov, A.A., Plenum Press, New York and London, pp.149-169.

Singhal, R.P., Kilic, H.S., Ledingham, K.W.D., Kosmidis, C, McCanny, T., Langley, A.J. and Shaikh, W. (1996),
*Multiphoton Ionization and Dissociation of $NO_2$ by 50 fs Laser Pulses,*
Chem. Phys. Lett., **253**, 81-86.

Singhal, R.P. (1997),
*Internal report.*

Smalley, R.E., Wharton, L. and Levy, D.H. (1975),
*The Fluorescence Excitation Spectrum of Rotationally Cooled $NO_2$,*
J. Chem. Phys. **63**, 4977-4989.

Smith, D.J., Ledingham, K.W.D., Kilic, H.S., McCanny, T., Peng, W.X., Singhal, R.P., Langley, A.J., Taday, P.F. and Kosmidis, C. (1997),
*Ionization and Dissociation of Benzaldehyde Using Short Intense Laser pulses,*
to be poblished.

Spears, K.G. and Brugge, S.P., (1978),
*Vibrationally Excited $NO_2$ From $CH_3NO_2$ and 2-$C_3H_7NO_2$ Photodissociation,*
Chem.Phys.Lett., 54, 373-377.

Squier, J., Salin, F. and Mourou, G. (1991),
*100-fs Pulse Generation and Amplification in Ti:$Al_2O_3$,*
Opt. Lett., **16**(5), 324-326.

Stevens, C.G., Swagel, M.W., Wallace, R. and Zare, R.N. (1973),
*Analysis of Poliatomic Spectra Using Tunable Laser-Induced Fluorescence: Applications to the $NO_2$ Visible Band System,*
Chem. Phys. Lett., **18**(4), 465-469.

Stingl, A., Spielmann, C. and Krauzs, F. (1994),
*Generation of 11-fsec pulses from a Ti:sapphire Laser without the use of prisms,*
Opt. Lett., **19**(3), 204-206.

Strickland, D. and Mourou, G. (1985),
*Compression of Amplifier Chirped Optical Pulses,*
Opt. Commun., **56**(3), 219-221.

Sutcliffe and Walsh, (1953),
*The Ultraviolet Absorption Spectrum of Nitric Oxide,*
Proc. Phys. Soc.(London), A, **66**, 209-216.

Suter, R. (1969),
*Absorption Spectrum in the Vacuum Ultraviolet and Visible Emission Spectrum of the NO Molecule. The 4d Complex*,
Can. J. Phys., **47**, 881-891.

Svelto, O.( 1989),
*Principles of Lasers*,
3rd ed., Plenum, New York.

Takezaki, M., Hirota, N. and Terazima, M. (1997),
*Nonradiative Relaxation Processes and Electronically Excited States of Nitrobenzene Studied by Picosecond Time-Resolved Transient Grating Method*,
J. Phys. Chem., **101**, 3443-3448.

Voronov, C.S. and Delon, N.B. (1966),
*Many-Photon Ionization of The Xenon Atom by Ruby Laser radiation*,
Sov. Phys. JETP (Eng. Trans.), **23**, 54.

Wagniere, G.H. (1969),
*Theoretical Aspects of The C-NO and C-$NO_2$ Bonds*
In The Chemistry of The Nitro- and Notroso- Groups, Part.1, Ed. by H.Feuer, Interscience Publisher, John Wiley&Sons, New York-London.

Warnatz, J., Maas, U. and Dibble, R.W. (1996),
*Combustion: Physical and Chemical Fundamentals, Modelling and Simulation, Experiments, Pollutant Formation*,
Springer Verlag, Berlin Heidelberg.

Watanabe, K., Matsunaga, F.M. and Sakai, H. (1967),
*Absorption Coefficient and Photoionisation Yield of NO in the Region 58-135 nm*,
Appl. Opt., **6**, 391-396.

Weber, H.P. (1967),
*Method for Pulsewidth Measurement of Ultrashoet Light Pulses Generated by Phase-Locked Lasers Using Nonlinear Optics*,
J. Appl. phys. **38**(5), 2231-2234.

Weickhardt, C., Grun, C., Henicke, R., Meffert, A. and Grotemeyer, J. (1997),
*The Application of Resonant Multiphoton Ionization by Sub-Picosecond Laser Pulses for Analytical Mass Spectrometry*,
Rapid Commun. Mass Spectrom., **11**, 745-748.

Weinkauf, R., Aicher, P., Wesley, G., Grotemeyer, J. and Schlag, E.W. (1994),
*Femtosecond versus Nanosecond Multiphoton Ionization and Dissociation of Large Molecules*,

J.Phys.Chem. **98,** 8381-8391.

Weiss, M.J. and Meisels, G.G. (1979),
*State-Selected Fragmentation of Nitromethane Ions by Threshold Photoelectron Coincident Photoion Mass Spectrometry*,
27th Annual Conf. on Mass Spectrometry and Allied Topics, Seattle, Washington Paper MAMP 20, 104-105.

Wiley, W.C. and McLaren, I.H., (9155),
*Time -of-Flight Mass Spectrometer with Improved Resolution*,
Rev. Sci. Instrum., **26**(12), 1150-1157.

Wodtke, A.M., Hintsa, E.J. and Lee, Y.T. (1986a),
*Infrared Multiphoton Dissociation of Three Nitroalkanes*,
J. Phys. Chem. **90,** 3549-3558.

Wodtke, A.M., Hintsa, E.J. and Lee, Y.T. (1986b),
*The Observation of $CH_3O$ in the Collision Free Multiphoton Dissociation of $CH_3NO_2$*,
J.Chem.Phys. **84,** 1044-1045.

Yang, J.J., Gobeli, D.A., Pandolfi, R.S. and El-Sayed, A. (1983),
*Wavelength Dependence of The Multiphoton Ionization-Fragmentation Mass Spectrometric Pattern of Benzaldehyde*,
J. Phys. Chem., **87**, 2255-2260.

Yariv, A. (1997),
*Optical Electronics in Modern Communications*,
Oxford University Press, Oxford, New York.

Yasa, Z.A. and Amer, N.M. (1981),
*A Rapid Scanning Autocorrelation Scheme for Contunious Monitoring of Picosecond Laser Pulses*,
Opt. Commun., **36**(5), 406-408.

Yinon, J. (1980),
*Direct Exposure Chemical Ionization Mass Spectra of Explosives*,
Org. Mass Spectrom., **15**(12), 637-639.

Yinon, J. (1987),
*Mass Spectral Fragmentation Pathways in 2,4,6-Trinitroaromatic Compounds; A Tandem Mass Spectrometric Collision Induced Dissociation Study*,
Org. Mass Spectrom., **22**, 501-505.

Yinon, J. (1988),
*Mass Spectral Fragmentation Pathways in Redcution Metabolities of 2, 4-*

*Dinitrotoluene and in 2, 4, 6-Trinitroaromatic. A Tandem Mass Spectrometric Collision Induced Dissociation Study*,
Org. Mass Spectrom., **23**, 274-277.

Yinon, J., Fraisse, D. and Dagley, I.J. (1991),
*Electron Impact, Chemical Ionization and Negative Chemical ionization Mass Spectra, and Mass-Analysed Ion Kinetic Energy Spectrometry-Collision-Induced Dissociation Fragmentation Pathways of Some Deuterated 2,4,6-Trinitrotoluene (TNT) Derivatives*,
Org. Mass Spectrom., **26**, 867-874.

Yinon, J. (1992),
*Mass Spectral Fragmentation Pathways in Some Dinitroaromatic Compounds Studied by Collision-induced Dissociation and Tandem Mass Spectrometry*,
Org. Mass Spectrom., **27**, 689-694.

Yinon, J. and Zitrin, S. (1993),
*Modern methods and Applications in the Analysis of Explosives*,
John Wiley, Chichester.

Zabernick, S., Fleming, J.W. and Baronavski, A.P. (1986),
*Production of OH from The Collision-Free Photodissociation of Nitromethane at 266 nm*,
J.Chem.Phys. **85,** 3395-3400.

Zacharias, H., Schmield, R. and Welge, K.H. (1980),
*State Selective Step-Wise Photoionization of NO with Mass Spectrometric Ion Detection*,
App. Phys., **21**, 127-133.

Zacharias, H., Rottke, H. and Welge, K.H. (1981),
*Sensitive and Mass Selectivity of NO by Stepwise Photoionization*,
App. Phys., **24**, 23-28.

Zakheim, D. and Johnson, P.M. (1978),
*Two- and Three-Photon Resonances in the Four-Photon Ionization Spectrum of Nitric Oxide at Low Temperature*,
J. Chem. Phys., 68, 3644-3653.

Zakheim, D. and Johnson, P.M. (1980),
*Rate Equation Modelling of Molecular Multiphoton Ionization Dynamics*,
Chem. Phys., **46**, 263-272.

Zhou, J., Taft, G., Huang, C.P., Murname, M.M., Kapteyn, H.C. and Christov, I.P. (1994),
*Pulse Evolution in A Broad-Bandwidth Ti:Sapphire Laser*,

Opt. Lett., **19**(15), 1149-1151.

Zhu, J., Lustig, D., Sofer, I. and Lubman, D.M. (1990),
*Selective Laser Induced Resonant Two-Photon Ionization and Fragmentation of Substituted Nitrobenzenes at Atmospheric Pressure*,
Anal. Chem., **62**, 2225-2232.

Zitrin, S. and Yinon, J. (1976),
*Chemical Ionization Mass Spectrometry of Explosives*,
Adv. Mass Spectrom. Biochem. and Medicine, **1**, 369-381.

Zitrin, S. and Yinon, J. (1978),
*Mass Spectrometry Studies of Trinitroaromatic Compounds*,
Adv. Mass Spectrom., **7B**, 1457-1464.